REMOVAL OF HEAVY METALS FROM WASTEWATER USING RAW DIATOMITE AND MANGANESE OXIDE-DIATOMITE COMPOSITE

SAMUEL KING'ORI MWANGI

A Thesis Submitted to the Graduate School in Partial Fulfillment of the Requirements for the Award of the Degree of Master of Science in Chemistry of Chuka University.

CHUKA UNIVERSITY

OCTOBER, 2024

DECLARATION AND RECOMMENDATION

Declaration

This thesis is my original work and has not been presented for award of a degree in any other University.

Signature:..... Date..16/10/2024.....
Samuel King ori Mwangi
SM11/29279/17

Recommendation

This thesis has been examined, passed and submitted with our approval as University supervisors.

Signature.....Date..16/10/24.....
Prof. Joel Mwangi Gichumbi, PhD
Chuka University

Signature..... Date.....
Prof. Ochieng Ombaka, PhD
Chuka University

DEDICATION

I proudly dedicate this thesis to my mother, Mary Nyambura Mwangi and my dad, Joseph Mwangi Kariuki. Further, I dedicate this thesis to my wife, Purity Mbithe Kiteme and my sons, Hector Mwangi and Aldrick Kiteme. I also dedicate this thesis to my brother, John Kariuki and sister, Teresia Wanjiku.

ACKNOWLEDGEMENT

My gratitude goes to the almighty God, who has given me the gift of life and good health to be able to undertake my studies. I sincerely appreciate my supervisors, Prof. Joel Mwangi Gichumbi and Prof. Ochieng Ombaka of Department of Physical Sciences, Chuka University for their constant encouragement, constructive advice, corrections, suggestions and guidance throughout the period of study. Their positive criticism and mentorship have been of great help in this research.

I acknowledge the Internal Research Fund, Chuka University for the financial support that enabled me to carry out my research work smoothly.

I am greatly indebted to Mr. Erick Lihanda, Mr. Chrispin Odhiambo and Ms. Juliet Makau, technologist in the Chemistry Laboratory, Chuka University for their technical support during data collection. Their professional advice contributed greatly to the success of this study. I also acknowledge the African Diatomite Industry Limited (ADIL) in Kariandusi, Gilgil, Nakuru County for the material support accorded to me. I also appreciate Mr. Gerald Njiru of Geothermal Development Company (GDC), Nakuru County for his great assistance in XRD analysis.

Finally, my special appreciation goes to my dad, Joseph Mwangi; my mum, Mary Nyambura and my wife, Purity Kiteme for their encouragement and support throughout the course of this study.

ABSTRACT

Access to clean water is a basic human right, however about 43% of the population in Kenya do not have access to clean water mainly due to water pollution. Most industries and wastewater treatment plants in the country discharge their effluents laden with heavy metals such as Cd and Pb into the environment at levels exceeding the maximum limits setup by NEMA. Pb (II) and Cd (II) ions are toxic to humans, therefore, there is a great need to remove them from wastewater before discharge into the environment. Adsorption is an effective method in remediating wastewater laden with heavy metals, but the high cost of adsorbents limits its application in developing countries such as Kenya. This study aimed at synthesizing MnO_2−diatomite composite, characterizing and using both raw diatomite and MnO_2−diatomite composite as low-cost adsorbents for the removal of Pb (II) and Cd (II) ions from aqueous solutions. The raw diatomite obtained from the African Diatomite Industries Limited (ADIL) in Kariandusi, Gilgil, Nakuru County, Kenya was used to prepare MnO_2−diatomite composite by acid reduction of $KMnO_4$−diatomite mixture at room temperature using 6M HCl acid. These adsorbents were characterized using Fourier transform infrared spectroscopy (FTIR), X-ray fluorescence (XRF), X-ray diffraction (XRD), Brunauer-Emmett-Teller (BET) and Barrett-Joyner-Halenda (BJH) techniques. Both raw diatomite and MnO_2−diatomite composite were found to be mainly composed of silica and alumina with hydroxyl (-OH), silanol (Si-OH), siloxane (Si-O-Si) and aluminosilicate (Al-O-Si) functional groups. In addition, the adsorbents were amorphous in nature with BET surface area of 32.29m^2/g for raw diatomite and 30.48m^2/g for MnO_2-diatomite composite. The surface area and porosity of the MnO_2-diatomite composite was lower compared to raw diatomite due to the blocking of pores by MnO_2 particles during the modification process. Batch adsorption experiments were carried out to optimize the effects of pH, initial metal ion concentration, contact time, adsorbent dosage and temperature on the percentage removal of Pb (II) and Cd (II) ions from single ion and binary ion solutions. For single ion studies, the optimal conditions for Pb (II) adsorption were initial metal concentration 10mg/L, contact time 60 minutes, temperature 25 ^oC, pH of 4 (raw diatomite) and pH of 6 (MnO_2-diatomite composite) and dosage of 4g/L (raw diatomite) and 6g/L (MnO_2-diatomite composite). Optimal adsorption conditions for Cd (II) were initial metal concentration 10mg/L, pH of 6, contact time 80 minutes, temperature 65 ^oC, adsorbent dose 6g/L (raw diatomite) and 8g/L (MnO_2-diatomite composite) resulting in 100% removal. Raw diatomite had higher removal efficiency of Pb (II) and Cd (II) ions compared to MnO_2-diatomite composite since it had a larger surface area and porosity, therefore, it was chosen for adsorption of heavy metal ions from Pb-Cd binary mixture. For binary ion studies, optimal conditions were pH of 6, initial metal ion concentration of 10mg/L each, contact time 80 minutes, adsorbent dosage 10g/L and temperature of 65 ^oC. The removal efficiency of the metal ions from binary solutions was lower compared to that of single ion solutions. The order of removal of the heavy metal ions by both adsorbents was Pb (II)>Cd (II) ions. Adsorption kinetics and isotherm analysis of experimental data showed that the adsorption of Pb (II) and Cd (II) ions by the adsorbents was well described by pseudo-second order kinetic model and Langmuir isotherm model respectively. Thermodynamic parameters namely Gibbs free energy ($\Delta G°$), enthalpy change ($\Delta H°$) and entropy change ($\Delta S°$) were evaluated and revealed that the adsorption process was feasible and spontaneous. $\Delta H°$ indicated that Pb (II) ions adsorption was exothermic process while Cd (II) adsorption was an endothermic process. Equilibrium studies demonstrated that both raw diatomite and MnO_2-diatomite composite were efficient in the removal of Pb (II) and Cd (II) ions from aqueous solutions. The results of this study indicate that both raw diatomite and MnO_2-diatomite composite are effective in heavy metal remediation, therefore, they should be employed as low-cost adsorbents in the treatment of industrial effluents laden with heavy metals.

TABLE OF CONTENTS

LIST OF TABLES

LIST OF FIGURES

LIST OF ABBREVIATIONS AND ACRONYMS

AAS	Atomic Absorption Spectroscopy
ADIL	African Diatomite Industries Limited
BET	Brunauer, Emmett and Teller
BHJ	Barrett-Joyner-Halenda
BOD	Biochemical Oxygen Demand
CEC	Cation Exchange Capacity
COD	Chemical Oxygen Demand
EDXRF	Energy Dispersive X-ray Fluorescence
IARC	International Agency for Research in Cancer
FT-IR	Fourier Transform Infrared Spectroscopy
MCL	Maximum Concentration Limit
MF	Microfiltration
MnO_2-diatomite	Manganese oxide diatomite composite
NACOSTI	National Committee of Science, Technology and Innovation
NF	Nanofiltration
NEMA	National Environment Management Authority
PFO	Pseudo-First Order Kinetic Model
PSO	Pseudo-Second Order Kinetic Model
Qe	Equilibrium Sorption Capacity (mg/g)
Qmax	Maximum Sorption Capacity, (mg/g)
RO	Reverse osmosis
TOC	Total Organic Carbon
UF	Ultrafiltration
USEPA	United States Environmental Protection Agency
WDXRF	Wavelength Dispersive X-ray Fluorescence
WHO	World Health Organization
XRD	X-Ray Diffraction
XRF	X-Ray Fluorescence

CHAPTER ONE
INTRODUCTION

1.1 Background Information

Water is a precious resource that sustains all forms of life on earth, economic development and food production. About 75% of the earth's surface is covered with water with 97% of it being saline. The remaining 3% is fresh water; 69% of which is locked up in ice caps, glaciers and permanent snow cover in polar regions. As a consequence, only 31% of the fresh water available on earth is in rivers and ground water (Plessis, 2017). According to WHO, access to clean water is a basic human right and an essential step towards improving the livelihood of people worldwide (WHO, 2014). However, more than a billion people all over the world do not have access to safe drinking water especially in developing countries (Guterres, 2023) mainly due to pollution of water resources. Water pollution degrades the quality of water making it unfit for human and animal consumption, industrial use, fishing, agriculture and leisure activities.

In most developing countries, water pollution is a major problem that poses a huge threat to the state of natural water resources and Kenya is no exception (Kithiia, 2012). In the recent years, water pollution in Kenya has been on the rise and it has been linked directly or indirectly to increasing urbanization and indiscriminate disposal of agrochemicals and industrial effluents (Nzeve *et al.,* 2015; Wafula *et al.,* 2020). Most industries in the country discharge their untreated or semi-treated effluents loaded with harmful organic and inorganic contaminants (Ahenda *et al.,* 2020) such as heavy metals, surfactants, dyes and other organic compounds directly into the receiving water bodies. Consequently, about 43% of the population in the country do not have access to clean water (Francis, 2015) and the situation is worsening with increase in water pollution.

Among the various contaminants, heavy metals pose a great danger to human health due to their toxicity even at low concentrations and their non-biodegradable nature leading to accumulation in organisms and the environment (Burakov *et al.,* 2018). According to Shamim (2018), most of the heavy metals in the environment originate from industrial activities such as mining, battery manufacture, tanneries, metal plating

and smelting, textiles, and paint manufacturing. The most common heavy metals discharged into the environment by these industries include chromium (Cr), lead (Pb), cadmium (Cd), mercury (Hg), zinc (Zn), copper (Cu) nickel (Ni) and Arsenic (As) and are therefore regarded as priority pollutants (He *et al.,* 2013).

Due to poor methods employed in wastewater treatment in Kenya, effluents from industries and wastewater treatment plants released into the environment usually contain heavy metals. Heavy metals such as Cr, Pb, Cd, Zn and Fe have been reported in the effluents of several industries in the country (Nyabaro *et al*., 2013; Munene, 2019; Ahenda *et al*., 2020) at levels exceeding the recommended limits set by WHO and NEMA for discharge into the environment. Miruka (2016), Sewe (2010), Wafula *et al.* (2020) and Sayo *et al*. (2020) have also reported presence the presence of Cd, Pb, Cr, Mn, Cu and Zn in the final treated effluents of Kariobangi, Dandora Export Processing Zone (EPZ) and Embu wastewater treatment plants in the country respectively. The concentrations of these heavy metals were above the WHO permissible levels in wastewater for irrigation.

Since Kenya is a water-scarce country, where most County governments are unable to supply their population with sufficient clean water (Francis, 2015), the presence of heavy metals in effluents of industries and sewage treatment plants is a matter of great concern as they pollute the available freshwater bodies in the country. According to Zhao *et al.* (2019), heavy metals are serious environmental pollutants due to their toxic, carcinogenic and non-biodegradable nature which results in their bioaccumulation in food chains, thereby resulting in long-term toxic effects. In Kenya, researchers have reported the presence of heavy metals in vegetables (Enyogoi *et al.,* 2020) and fish (Nyingi *et al.,* 2016; Omwenga *et al.,* 2014) at levels exceeding the maximum permissible limits stipulated by WHO. Such vegetables and fish pose great health risks when consumed either raw or after processing.

Heavy metals have detrimental effects on human health such as damage to vital organs like kidneys, liver, reproductive system, respiratory system and the central nervous system, DNA damage, cardiovascular diseases, cancer, miscarriage and stillbirths in pregnant women, and in extreme cases, death (Chaltopadhyaga *et al.,* 2014; Akpor *et*

al., 2014). Cd, hexavalent chromium, nickel and their compounds have been classified by the International Agency for Research in Cancer (IARC) as toxic group1 human carcinogens while organic Pd and Hg have been classified as probable human carcinogens (Kamunda *et al.,* 2016; Suvarapu and Baek, 2017). It is therefore essential to treat industrial wastewater laden with heavy metals before discharge into the environment.

A wide range of techniques namely: chemical precipitation, ion exchange, membrane filtration techniques, biological treatment methods and adsorption have been employed for removal of heavy metals from wastewater (Gunatilake, 2015). Among these technologies, adsorption has emerged as a better technique for heavy metal remediation due to its low-cost, simple operation and does not produce heavy metal bearing sludge but the high cost of activated carbon, activated alumina and other commercial adsorbents limits its application in developing countries (Visa *et al.,* 2014; Zhao *et al.,* 2019). Therefore, there is a great need to replace commercial adsorbents with low-cost adsorbents that are abundant in nature, have a large surface area and require little processing before use. The low-cost adsorbents may be of mineral origin, biological biomass such as algae and fungi or industrial and agricultural wastes (Liu, 2015).

This study focused on the use of diatomite mineral as a low-cost adsorbent for the removal of heavy metals. Diatomite also referred to as diatomaceous earth ($SiO_2.nH_2O$) is an inorganic material with a microporous structure containing amorphous silica as the main component (Du *et al*., 2014). Diatomite represents a good adsorbent material for heavy metal removal due to its porous structure, high surface area, chemical stability, good adsorption capability, low cost (ElSayed, 2018; Zhao *et al.,* 2019) and abundance in the country in Nakuru and Baringo Counties. The adsorption capability of diatomite mineral can be increased by chemical modification of the diatomite surface leading to increased surface area.

1.2 Statement of the Problem

Heavy metals are serious environmental pollutants that pose a great danger to human health and the environment due to their toxicity even at low concentration levels. Cadmium and lead ions are prevalent in effluents from most industries and wastewater

treatment plants and are routinely discharged into the environment at levels that surpass the maximum permissible level of 0.01 mg/L setup by NEMA and WHO. This has led to water pollution and bioaccumulation of these heavy metals in plants and animals. Cd and Pb are toxic, non-biodegradable in nature and have also been characterized as human carcinogens among other negative health effects; therefore, it is necessary to remove them from industrial effluents before discharge into the environment. At the industrial level, on site treatment of wastewater laden with heavy metals using technologies such as membrane filtration, ion exchange and chemical precipitation is expensive and requires high capital investment. In addition, the production of heavy metal bearing sludge by chemical precipitation that requires further treatment increases the operational costs. Therefore, these technologies are unsuitable for the small industries in the country. Although wastewater treatment by adsorption technique is relatively cheap, the high cost of adsorbents such as activated carbon, activated alumina and silica gel limits its application in developing countries such as Kenya. Therefore, there is a great need to replace activated carbon and other commercial adsorbents with low-cost adsorbents that are cheap and readily available.

1.3 Objectives

1.3.1 General Objectives

To modify raw diatomite, characterize and use both raw and modified diatomite as adsorbents for heavy metals removal.

1.3.2 Specific Objectives

i. To synthesize and characterize MnO_2-diatomite composite.
ii. To investigate the effects of pH, contact time, adsorbent dose, temperature and initial metal ion concentration on removal of Pb (II) and Cd (II) ions by raw diatomite and MnO_2-diatomite composite.
iii. To determine the isothermal, kinetics and thermodynamic parameters of adsorption of Pb (II) and Cd (II) ions on to raw diatomite and MnO_2-diatomite composite.
iv. To determine the percentage removal of Pb-Cd binary ion system using the adsorbent with highest sorption capacity for Pb (II) and Cd (II) single ions from aqueous solution.

1.4 Research Questions

This study aims at addressing the following research questions.

i. How can MnO_2-diatomite composite be synthesized and characterised?
ii. How do the various sorption parameters such as pH, contact time, adsorbent dose, temperature and initial metal ions concentration affect the removal of Pb (II) and Cd (II) ions by adsorption onto raw diatomite and MnO_2-diatomite composite?
iii. What are the isothermal, kinetics and thermodynamic parameters of adsorption of Pb (II) and Cd (II) ions on to raw diatomite and MnO_2-diatomite composite?
iv. What is the the percentage removal of Pb-Cd binary ion system using the adsorbent with highest sorption capacity for Pb (II) and Cd (II) single ions from aqueous solution?

1.5 Justification of the Study

Due to lack of adequate capacity and technology, treatment of wastewater laden with heavy metals has become a major challenge in developing countries (Pokhrel, 2017), such as Kenya. Inferior wastewater treatment methods employed in the country have resulted in the discharge of heavy metal bearing waste by industries and wastewater treatment plants into the environment at levels beyond the maximum concentration limit (MCL) proposed by regulatory authorities such as NEMA. Cd and Pb are among the most toxic heavy metals yet they are common pollutants present in industrial effluents (Arowojobe *et al.,* 2020; Zhang *et al.,* 2020). Studies by Ahenda *et al.* (2020) and Munene (2019) have shown the presence of Pb and Cd among other heavy metals in the effluents of paint manufacturing industries and several industries in the industrial area in Nairobi County respectively. The concentration of these heavy metals was above the MCL of 0.01mg/L for Pb and Cd that is set by NEMA.

Exposure to these heavy metals has led to negative health effects and death of civilians in the country. For instance, Pb poisoning incident that claimed three lives has been reported in Owino Uhuru slum in Mombasa, Kenya near a former lead smelting industry (Githinji *et al.,* 2019). In addition, bioaccumulation of heavy metals in vegetables due to the use of untreated or semi-treated wastewater for irrigation has been reported in Nakuru and Nairobi Counties (Enyogoi *et al.,* 2020). Similarly, presence of

heavy metals in farmed fish have been reported in Machakos and Kiambu Counties (Omwenga *et al.*, 2014) at levels surpassing the MCL stipulated by WHO and NEMA, thereby, posing great health risks to consumers. Therefore, there is a great need to remove heavy metals from industrial effluents before discharge into the environment.

Adsorption has emerged as a cost-effective technique for heavy metal removal (Tripathi and Ranjan, 2015; Sun *et al.,* 2019) but the high cost of adsorbents such as activated carbon and activated alumina hinders its application (Zhao *et al.,* 2019) especially in developing countries. This study therefore explored the use of diatomite mineral as a low-cost adsorbent for heavy metal removal. Diatomite is cheap, abundantly available, highly porous and has a high surface area (Terracciano *et al.,* 2018) making it a good low-cost adsorbent. Despite the merits, the use of diatomite as a heavy metal adsorbent has not been utilised in Kenya yet there are huge deposits of diatomite in Kariandusi, Gilgil, Nakuru County and Baringo County (Kipsanai, 2017).

Furthermore, studies have shown that diatomite has good adsorption capabilities for heavy metals (Du *et al*., 2014; El Sayed, 2018; Muntean *et al.,* 2023) and dyes (Zhang *et al.,* 2014; Dang *et al.,* 2016) especially when the diatomite surface is coated with metal oxides. In these studies, the focus was on the removal of single heavy metal ions only from wastewater using diatomite and none investigated the removal of binary heavy metal ions from wastewater using diatomite. This study therefore focused on the removal of both single and binary heavy metal ions from wastewater using raw diatomite from Kenya. This will contribute to the search for low-cost adsorbents and also investigate the possibility of utilizing natural deposits of diatomite from Kenya in heavy metal removal.

CHAPTER TWO
LITERATURE REVIEW

2.1 Water Pollution

Water pollution has become a major concern and one of the most significant problems of this century (Ushakumary, 2013). Since only about 3% of the total water on earth is fresh water (Kaur and Mahajan, 2016), water pollution is a threat to the state of natural water resources and also reduces the amount of fresh water available for domestic, industrial and agricultural use. Most developing countries have emphasized on the growth of the industrial and agricultural sectors in the quest of achieving national development goals at the cost of the environment and Kenya is no exception to this phenomenon (Kithiia, 2012). The rapid industrial growth and urbanization has resulted in increased water pollution by organic and inorganic compounds as well as humic substances (Ahogle *et al.,* 2023; Tomno *et al.,* 2020).

Among all the inorganic pollutants, heavy metals pose a great threat to human health and the environment (Zhang, 2014) due to their toxicity and non-biodegradable nature leading to their persistence in the environment (Chaudhary *et al.,* 2016). According to Chege *et al.* (2018), about 1.5 billion people lack safe drinking water globally due to water pollution and at least 5 million deaths occur per year attributed to waterborne diseases (Chege *et al.,* 2018). In Kenya, it is estimated that about 43% of the population in the country do not have access to clean water (Francis, 2015) and the quality of water has been deteriorating with increasing pollution.

2.2 Sources of Heavy Metals

The term "heavy metals" refers to any metal and metalloid elements whose density exceeds 5g/cm³ (Tutic *et al.,* 2015). According to Gautam *et al.* (2014), heavy metals are mostly considered to be the following elements: cadmium (Cd), arsenic (As), chromium (Cr), copper (Cu), zinc (Zn), mercury (Hg), lead (Pb), iron (Fe) and nickel (Ni). Most compounds of these elements are highly toxic, carcinogenic and bioaccumulate in the environment (Gunatilake, 2015; Tomno *et al.,* 2020) therefore, pose significant health threat to humans, animals and aquatic animals.

Heavy metals are natural components of the earth's crust. They are released into the environment by natural activities such as weathering of rocks and volcanic activities (Chowdhury *et al.,* 2018) in combination with anthropogenic activities such as mining, use of agrochemicals, incineration of municipal wastes and discharge of untreated domestic and industrial effluents into the environment (Singh and Gupta, 2016). Among all the anthropogenic sources, heavy metal contamination mainly arises from effluents of industrial units such as smelting, electroplating and metal finishing industries, paint manufacture, tannery, printing and photographic industries, battery manufacture, electronic and soldering, pesticide manufacture and textile industries (Shamim, 2018; Hossain, 2013). Unlike organic pollutants, heavy metals are non-biodegradable and tend to accumulate in the environment therefore pose a great risk to human health and the entire ecosystem (Tomno *et al.,* 2020).

2.3 Heavy Metal Pollution in Kenya

In Kenya, most industries discharge their untreated or semi-treated effluents into the sewer system or directly into the environment (Ahenda *et al.,* 2020). Due to lack of proper monitoring and poor methods employed in wastewater treatment in the country, effluents released into the environment by industries and sewerage treatment plants usually contain heavy metals. Various studies have shown the presence of heavy metals in the effluents of industries and sewage treatment plants in the country at concentrations greater than the values set by WHO and NEMA. For instance, Ahenda *et al*. (2020) reported presence of Cd, Cr and Pb in the effluents of paint manufacturing industries in Nairobi County while Langat (2018) also reported the presence of total Cr in the effluents of several tanneries in Nairobi County. Nyabaro *et al*. (2013) in an assessment of pollution levels of wastewater from a tanning industry in Nakuru County, found out that the effluents contained Cr (0.68-0.945 mg/L) and Pb (4.0-5.5 mg/L) at levels above the permissible limit of 0.05 mg/L for Cr (VI) and 0.01 mg/L for Pb outlined by WHO and NEMA. Munene (2019) reported the presence of Pb, Cr, Zn, Cd and Ni in effluents of several industries in Nairobi Industrial area but only Zn (0.58-95.5 mg/L), Pb (1.2-75.3 mg/L) and Cd (0.88-52.7 mg/L) were above the limits for discharge into the environment set by NEMA (0.01 mg/L for Pb and Cd, 0.5 mg/L for Zn). The discharge of heavy metal bearing waste by industries has resulted in heavy metal poisoning in the country such as the lead poisoning case in Owino Uhuru slam in

Mombasa, Kenya near a former lead smelting industry, that led to the death of three people and endangering the lives of other 3,000 people (Githinji *et al.,* 2019).

Studies by Miruka (2016) and Sewe (2010) reported the presence of Cd, Pb, Mn and Zn in the final treated effluents of Kariobangi and Dandora wastewater treatment plants in Nairobi County. The effluents from the Kariobangi wastewater treatment plant had 0.85-1.447 mg/L of Cd and 1.0-1.9 mg/L of Zn. Similarly, effluents from the Dandora wastewater treatment plant had 0.025-0.033 mg/L of Cd, 0.083-0.332 mg/L of Pb and 0.085-0.748 mg/L of Mn. The concentrations of these heavy metals were beyond the limits (0.01 mg/L for Pb and Cd, 0.2 mg/L for Mn) setup by NEMA, thereby, polluting the receiving water bodies such as Nairobi River and Athi River (Musyoki, 2012). Sayo *et al.* (2020) reported the presence of Cu (0.484-1.834 mg/L), Zn (1.432-4.612 mg/L), Cd (0.015-0.358 mg/L) and Pb (0.011-2.125 mg/L) in the final effluents of Embu sewage treatment plant in Embu County. The concentrations levels of these heavy metals were above the WHO permissible levels for discharge into the environment therefore, polluting the receiving river Rupingazi. Chege *et al.* (2018) reported high levels of Cr (0.023-2.089 mg/L), Zn (0.7434 mg/L) and Pb (0.1621 mg/L) in the treated effluents of Njoro sewerage works in Nakuru county thereby polluting Njoro river which drains into Lake Nakuru and in turn exposing the wildlife in Lake Nakuru national park to risk of heavy metal pollution.

Due to their non-biodegradable nature, these heavy metals accumulate in the environment and are eventually incorporated into human food chain (Sun *et al.,* 2019). Enyogoi *et al.* (2020) reported the presence of Pb and Cd in vegetables irrigated with wastewaters in Nakuru and Nairobi Counties while Nyingi *et al.* (2016) and Omwenga *et al.* (2014) reported the presence of Cd and Pb in fish from Lake Baringo and farmed fish in Machakos and Kiambu Counties respectively. The concentration of these heavy metals exceeded the maximum permissible limits stipulated by WHO. Such vegetables and fish pose great health risks when consumed either raw or after processing. From the above studies, it is evident that industries and wastewater treatment plants in Kenya need to treat their effluents laden with heavy metals before discharge into the environment.

2.4 Classification of Heavy Metals and their Toxicity

According to Hossain (2013), heavy metals can be classified into three groups of concern: toxic metals (such as Hg, Cr, Pb, Cd, As, etc.), precious metals (such as Pd, Pt, Ag, Au, Ru etc.) and radionuclides such as U, Th, Ra, Am, Pu etc. Heavy metals may also be classified as essential or non-essential elements regarding to their role in biological systems (Shamim, 2018; Khalef *et al.,* 2022). Essential heavy metals such as Fe, Ni, Co, Cu, Mo, Zn, Cr and Mn serve as micronutrients (Majumder *et al.,* 2014) and are usually required by living organisms in trace amounts for vital physiological and biochemical functions, but they are highly toxic at higher concentrations (Kumar *et al.,* 2016). Pb, Hg, Cd and As are usually regarded as non-essential and are highly toxic to living organisms even at low concentration (Khalef *et al.,* 2022).

Heavy metals are hazardous pollutants of great environmental concern especially at high concentrations. Cd, Cr, Cu, Ni, Zn, Pb, As and Hg are considered priority pollutants (He *et al.,* 2013) due to their toxicity, prevalent existence and persistence in the environment (Tripathy and Ranjan, 2015; El Sayed, 2018). These heavy metals are known to cause immune system dysfunction, birth defects, cancer, damage to vital organs such as kidneys, liver, lungs, heart, reproductive system, central nervous system (CNS) and gastrointestinal track even at lower level of exposure (Vidu *et al.,* 2020; Balali-Mood *et al.,* 2021).

The International Agency for Research in Cancer (IARC) has classified hexavalent Cr, Cd, As and Ni and their compounds as group 1 human carcinogens (Kamunda *et al.,* 2016) while organic mercury and Pb have been regarded as human mutagens and probable carcinogens (Suvarapu and Baek, 2017). Exposure to heavy metals mays occur through ingestion of contaminated water, food and soil, inhalation of contaminated dust particles and occupational exposure (Kinuthia *et al.,* 2020). In plants, heavy metals impact negatively on plant growth causing chlorosis, reduced water and nutrient uptake, alteration of roots growth and reduced photosynthesis. This in turn leads to stunted growth, reduced yield or death of the plant (Khalef *et al.,* 2022).

2.4.1 Lead

Lead is one of the most toxic heavy metals mainly found in water as Pb (II) or Pb (IV) ions with Pb (II) being the most stable ion (Amer, 2015). The USEPA and the IARC have classified lead as a probable human carcinogen with a maximum contaminant level (MCL) of 0.01 mg/L in drinking water as set by the WHO (Kinuthia *et al.,* 2020). The main sources of lead are manufacture of lead-acid accumulators, solder wire, pigments, ammunition in the form of bullets and shotgun shells and as an additive in gasoline especially for aircrafts (Ungureanu and Mustatea, 2022).

Chronic exposure to lead can cause several unwanted health effects such as damage to the kidneys, cardiovascular system, increased blood pressure, anemia, declined fertility in men through sperm damage, miscarriage and stillbirths in pregnant women, stunted growth and diminished learning abilities in children (Wani *et al.,* 2015). According to Ungureanu and Mustatea, (2022), exposure to high concentrations of lead greatly affects the nervous system in children and adults leading to learning disabilities, speech impairment, diminished intelligence and impaired neurobehavioral development.

2.4.2 Cadmium

Cadmium is a heavy metal with an oxidation state of +2 that is highly toxic even at low concentrations due to its low excretion rate (Ungureanu and Mustatea, 2022). Cd is a major environmental pollutant due to its extensive use in industrial processes such as fabrication of nickel-cadmium batteries, electroplating of steel, rubber curing, as a stabilizer in PVC products, paint pigments, as a neutron absorber in nuclear power plants (Francis, 2015) and the production and use of phosphate fertilizers (Gautam *et al*., 2014), insecticides and fungicides (Sebastian and Prasad, 2014). According to the NEMA and the WHO, the MCL for cadmium in drinking water is 0.01 mg/l and 0.003 mg/l respectively. The NEMA MCL for discharge of Cd (II) ions into the environment is 0.01 mg/L (Kinuthia *et al.,* 2020).

Cadmium and its compounds have been classified by the IARC as group 1 human carcinogens mainly causing lung cancer, renal cancer and prostate cancer. Chronic cadmium ingestion can cause irreversible damage to several vital organs, among which kidneys, liver, respiratory tract and the bones are the most sensitive (Ungureanu and

Mustatea, 2022). Cadmium bio accumulates in the human body particularly the kidneys, liver and the bones causing renal dysfunction, kidney damage and bone defects such as osteomalacia and osteoporosis (Idrees *et al*., 2018; Francis, 2015). Other health effects of cadmium accumulation in the body are anaemia, hypertension, cardiac failure and cerebrovascular infarction (Sebastian and Prasad, 2014).

2.5 Remediation of Heavy Metals from Wastewater

Removal of heavy metals from wastewater is essential in order to improve the quality of the wastewater and also meet the disposal regulations. Several technologies have been put in place to remove heavy metal ions from wastewaters namely chemical precipitation, coagulation and flocculation, ion exchange, membrane filtration techniques, biological treatment methods and adsorption. These methods can be used separately or inclusively based on the need (Gunatilake, 2015).

2.5 1. Chemical Precipitation

Chemical precipitation mainly involves converting heavy metal ions in wastewater into insoluble forms by using precipitating agents such as hydroxides, carbonates or sulphides followed by solid separation methods such as coagulation, sedimentation and filtration (Lupa and Cocheci, 2023). Hydroxide precipitation involves adding alkalis such as calcium hydroxide (lime) or sodium hydroxide to the wastewater and stirring in reaction tanks to form insoluble metal-hydroxide precipitates (Mahajan-Tatpate *et al.*, 2021). Carbonates such as sodium carbonate or calcium carbonate and soluble sulphides like sodium sulphide or sodium hydrogen sulphide can also be used as alternatives to hydroxides (Lupa and Cocheci, 2023). Chemical precipitation requires a large amount of chemicals to reduce metals to an acceptable level for discharge and also generates huge amounts of sludge which requires further treatment before disposal hence increasing the operational cost (Hutchenson, 2016; Amer, 2015).

2.5.2 Coagulation and Flocculation

Coagulation-flocculation is a physico-chemical method that mainly involves the addition of coagulants such as aluminum sulfate (alum), ferrous sulfate, ferric chloride and ferric sulphate, aluminium chloride and poly aluminium chloride salts to wastewater to effect destabilization of colloids and flocculation process (Lupa and

Cocheci, 2023). According to Lakherwal (2014), the coagulant encourages the colloidal particles join together and form agglomerates that can then be removed by filtration. The main demerits of coagulation in heavy metal removal are the production of heavy metal bearing sludge that requires extra treatment before disposal and the effectiveness of the process greatly depends on the coagulant used (Mahajan-Tatpate *et al.,* 2021).

2.5.3 Biological Treatment Methods

Biological treatment of water laden with heavy metals can be categorized mainly as bioaccumulation or biosorption. Bioaccumulation involves the use of living organisms such as plants or microorganism (algae, fungi and yeast) to take up and sequester heavy metals intracellularly through use of proteins and peptide ligands (Diep *et al.,* 2018). Certain plant species have an enormous ability to uptake and accumulate very high concentrations of metals in their tissues without-showing toxicity and are referred to as hyperaccumulator plants (Kumar *et al.,* 2016). Such plants can be used successfully to clean up heavy metal polluted soils and water and the process is referred to as phytoremediation process. However, since phytoremediation is plant based, slow growth of plants and the requirement of sufficient light limits its large-scale application (Yan *et al.,* 2020).

In contrast, biosorption of heavy metals involves the use non-living biological materials such as agricultural wastes and food processing wastes like corn cobs, fruit peels, soya bean hulls, cotton seeds hulls etc. to remove heavy metals from waste water (Shamim, 2018). Biosorption employs the use of functional groups such as carboxyl, hydroxyl, sulphate, amino and phosphate groups present in the cells of the biosorbents to sequester heavy metal ions from wastewater (Sharma, *et al.,* 2017).

2.5.4 Ion Exchange

Ion exchange is an effective wastewater treatment technique particularly for treating wastewater with low heavy metal concentration (Gunatilake, 2015). Ion exchange involves a reversible exchange of ions between a liquid phase and a porous solid resin (Hossain, 2013). The resins are water-insoluble solid substances that can adsorb the heavy metals ions from a solution and in turn release an equivalent amount of similarly charged ions such as H^+, Na^+, or OH^- into the solution without undergoing structural

changes in the resin. The ion-exchange resins can either be synthetic or natural solids such as zeolites and clinoptilolite (Lupa and Cocheci, 2023).

The most common cation exchangers are strongly acidic resins with sulfonic acid groups (-SO_3H) and weakly acid resins with carboxylic acid groups (-COOH) that exchange the hydrogen ions in the sulfonic group or carboxylic group of the resin with metal cations in the wastewater (Krishna *et al.,* 2017; Mahajan-Tatpate *et al.,* 2021). Ion-exchange processes have a high heavy metal removal efficiency and does not produce sludge (Pokhrel, 2017). Despite these advantages, the ion exchange resins are expensive and are easily fouled by suspended colloids and some organic compounds. In addition, backwashing of exhausted resin during regeneration results secondary pollution due to production of large quantities of effluents that require treatment. This increases the operational cost (Mahajan-Tatpate *et al.,* 2021).

2.5.5 Membrane Filtration Technologies

Membrane filtration has gained considerable attention in wastewater treatment because it is capable of purifying water of suspended solids, dissolved salts and organic compounds (Mahajan-Tatpate *et al.,* 2021). Depending on the pore size of the membranes, pressure driven membrane filtration processes can be categorised as microfiltration (MF), ultrafiltration (UF), nanofiltration (NF) and reverse osmosis (RO) while electrically driven membrane process comprises of electrodialysis (Lupa and Cocheci, 2023). In pressure driven membrane filtration processes, heavy metal bearing wastewater is forced under pressure through a porous membrane that only allow molecules to pass through on the basis of size and blocks molecules and ions larger than the pore size (Hossain, 2013).

To obtain high efficiency in heavy metal removal, UF requires the addition of water-soluble polymeric ligands that bind to the metal ions to form macromolecular complexes since the pore sizes of UF membranes are larger than the dissolved metal ions (Gunatilake, 2015). NF membranes have pore size of about 1nm wide that are able to remove bacteria, viruses and heavy metals and organic molecules (Mahajan-Tatpate *et al.,* 2021). RO and electro-dialysis use semi-permeable membranes to recovery metal ions from dilute wastewater. In RO, a solvent is forced from a region of high solute

concentration through a semi-permeable membrane in to a region of low solute concentration by applying a pressure in excess of the osmotic pressure (Lakherwal, 2014). Electro-dialysis uses selective membranes comprising of alternate cation and anion membranes fitted between the electrodes of an electrolytic cell. Under continuous electrical current, the associated ion migrates allowing the recovery of metals (Vidu *et al.*, 2020). Membrane separation techniques have high degree of separation selectivity but the membranes are easily fouled by suspended colloids (Hutchenson, 2016).

2.6 Adsorption

Adsorption is basically a mass transfer process by which a substance is transferred from the liquid phase to the surface of a solid and becomes bound by physical or chemical interactions or both (Tripathi and Ranjan, 2015). The substance that is removed from the bulk solution is referred to as the adsorbate and the solid substance that collects the adsorbate is referred to as the adsorbent. According to Halnor (2015), adsorption process may be classified as physical or chemical adsorption depending on the intermolecular attractive forces involved between the adsorbent surface and the adsorbed group. Physical adsorption is primarily due to Van der Waals forces of attraction originating from the interaction between induced, permanent and transient electric dipoles (Tripathi and Ranjan, 2015), while chemical adsorption involves a chemical reaction between the adsorbate and adsorbent (Hutchenson, 2016).

Adsorbents with high surface area and large pore volume are highly effective in the removal of pollutants from wastewater since these factors determine the number of active sites available for cation adsorption (Saptiama *et al.*, 2017). Adsorption has been found to be superior in wastewater treatment compared to other techniques due to its low cost, simplicity of design, lack of production of sludge, ease of operation and insensitivity to toxic substances (Halnor, 2015). The adsorbent may be of mineral, organic or biological origin. They may be obtained commercially or be low-cost adsorbents derived from agricultural and industrial wastes, Low-cost adsorbents may also be in the form of natural minerals such as zeolites (Tripathy and Ranjan, 2015).

2.6.1 Commercial Adsorbents

2.6.1.1 Activated Carbon

Activated carbon is one of the most widely used and effective adsorbent material for the removal of heavy metals from wastewater because of its large surface area, micro porous character and its high degree of surface reactivity (Hussain *et al.*, 2021) but its high cost limits its use (Al-Malack and Basaleh, 2016; Alalwan *et al.*, 2020;) even in the developed countries. Due to its high cost, various researchers have shifted attention to the synthesis of activated carbon from cheaper materials like macadamia husk (Wattanasiriwech *et al.*, 2023), olive stones (Yakout and El-Deen, 2016), oil palm and coconut shells (Rahman *et al.*, 2014), maize cobs (Abdelfattah *et al.*, 2016), maize stalks (Zhao *et al.*, 2020), rice husk (Babatunde and Ibrahim, 2020) etc with significant heavy metal removal capacities. The synthesis of activated carbons from these carbonaceous materials generally involves pyrolysis of the raw material followed by physical or chemical activation of the resulting carbonized substances. The characteristics and efficiency of the prepared activated carbon in pollutant remediation depends on the raw material and the activating conditions used (Hussain *et al.*, 2021).

2.6.1.2 Activated Alumina

Activated form of alumina is a commonly used heavy metal adsorbent that mainly comprises of aluminium oxide (Al_2O_3) with high porosity, large specific surface area and acid-base properties (Miloševića *et al.*, 2019). Alumina is reported to exist in several crystalline phases but the gamma phase has been highly desirable for adsorption because of its superior micro-structural properties and enhanced thermodynamic stability (Banerjee, *et al.*, 2017). Studies have shown that activated alumina is an effective adsorbent for removal of Cu^{2+}, Pb^{2+} and Cd^{2+} (Szatyłowicz and Skoczko, 2018), Pb^{2+} and Ni^{2+} (Ghomi, 2021) and As (V) (Camacho *et al.*, 2015). Despite the fact that activated alumina has a large specific surface area, high porosity, exists in several structures and has amphoteric properties, its high cost limits its wide application (Crini *et al.*, 2019).

2.6.1.3 Silica Gel

Silica gel is a non-toxic and efficient support characterised by a highly porous structure with a large surface area, excellent thermal and mechanical stability (He *et al.*, 2016).

Silica gel is regarded as a polymer of silicic acid consisting of interlinked SiO_4 tetrahedral with various functional groups such as siloxane group (-Si–O–Si-), hydroxyl groups (-OH) and silanol groups (-Si–OH) which can either be free silanols (isolated groups), vicinal (bridged silanols) or geminal silanols (Shahata, 2016). The presence of reactive hydroxyl groups on the surface of silica gel has enabled the chemical functionalization of the silica gel surface through the addition of functional groups, polymers and ligands (He *et al.,* 2016).

The functionalized silica gel composites have been found to possess very strong chelating adsorption ability for heavy-metal ions. Li *et al.* (2019) reported that silica gel functionalized with nitrilotriacetic acid (NTA-silica gel) exhibited high efficiency for the removal of Cu^{2+}, Cd^{2+}, and Pb^{2+} metal ions from water. Similarly, He *et al.* (2016) synthesized silica gel functionalized with multidentate ligands for heavy metals removal. They observed that the functionalized silica gel had a high affinity toward Pb (II) and Hg (II) removal. The main advantages of silica gel include high surface area, high adsorption capability, high mechanical and thermal stability and easy surface modification through its surface silanol groups (Radi *et al.,* 2014).

2.6.2 Low-Cost Adsorbents

2.6.2.1 Agricultural Waste

In the recent years, the use of agricultural wastes as low-cost adsorbents for heavy metal removal from wastewater has significantly increased (Tripathi and Ranjan, 2015). Agricultural materials are usually composed of lignin and cellulose as major constituents but they may also include other polar functional groups of lignin, such as phenolic, alcohols, ketones, carboxylic, aldehydes, hydroxyl, ether and carbonyl groups (Ibisi and Asoluka, 2018). These groups have the ability to bind heavy metals by donating an electron pair to form complexes with the metal ions in solution (Hossain,2013). Agricultural by-products such as rice husk, neem bark (Hegazi, 2013), rice husk and orange peels (Naik *et al.,* 2023), peanut shells and banana peels (Jaishankar *et al.,* 2014), banana stalks, Maize cob and sunflower achene (Mahmood-ul-Hassan *et al.,* 2015), tea leaves (Shrestha and Ghimire, 2016), egg shells and wheat bran (Renu *et al.,* 2017), and egg shells (Tariq *et al.,* 2018) have been used successfully to remove heavy metals from wastewater.

Agricultural wastes are cheap and readily available but require chemical modification to improve metal adsorption capacity (Ibisi and Asoluka, 2018). Furthermore, the use of untreated agricultural wastes as adsorbents may lead to elevated chemical oxygen demand (COD), biological oxygen demand (BOD) and total organic carbon (TOC) due to discharge of soluble organic compounds contained in the plant material (Tripathi and Ranjan, 2015). This may result in depletion of oxygen content in the water hence posing a threat to aquatic life.

2.6.2.2 Industrial By-Products and Waste

Industrial waste products and by-products from several industrial processes are inexpensive and abundantly available materials that can be employed as low-cost adsorbents for heavy metal removal. Various industrial by-products such as fly-ash, red mud, blast furnace sludge, iron (III) hydroxide, waste slurry etc. have been employed in the removal of heavy metals from waste solutions. These industrial by-products have good heavy metal adsorptive capabilities but their efficiencies may be improved upon slight processing or modification (Tripathi and Ranjun, 2015). Studies conducted on the utilization of industrial by-products in heavy metals removal indicate that blast furnace slag, a by-product of steel and iron making process was effective in the remediation of Cu, Zn and Cd (Wang *et al*., 2016); Co (II) and Pb (II) (Abdelbasir and Khalek, 2022).

Es-Said *et al.* (2020) evaluated the use of phosphogypsum, a waste material of the wet process of phosphoric acid production, in the removal of Cd, Cu and Zn from aqueous solutions. In their study, they reported that heavy metal adsorption onto phosphogypsum was greatly affect by the solution pH and the heavy metal selectivity by the phosphogypsum was in the order Cd>Cu>Zn. Tsamo *et al.* (2018) employed red mud, a residue of alumina production from bauxite, in the removal of Cr (VI), Cu (II) and Pb (II) while He *et al.* (2016) employed zeolite synthesized from coal fly ash for the removal of Pb (II), Cd (II), Cu (II), Ni (II) and Mn (II). In their studies they concluded that these industrial by-products had good adsorption capacities for heavy metals, therefore, they could be used as alternative low-cost adsorbents for heavy metal remediation.

2.6.2.3 Natural Minerals

Natural porous minerals with a large specific surface area, high CEC, chemical and mechanical stability such as clay, limestone, natural zeolites etc can be used effectively as adsorbents for heavy metal removal (Li *et al.,* 2014). These minerals are cheap and widely abundant on the earth's crust. Their heavy metal adsorption capacity is lower than that of commercial adsorbents such as activated carbon but their easy availability, low-cost and the potential to be improved by modification compensates for their less efficiency (Tripathi and Ranjan, 2015). Various researches have investigated the heavy metal adsorption capability of clay minerals (Uddin, 2017), limestone (Shin *et al.,* 2014) and natural zeolites (Rahimi and Mahmoudi, 2020; Azizi *et al.,* 2021). They concluded that these minerals hold great potential to remove of toxic heavy metals from wastewaters.

2.6.2.4 Diatomaceous Earth

Diatomaceous earth or diatomite ($SiO_2.nH_2O$) is a pale, soft, lightweight sedimentary rock composed principally of silica microfossils of aquatic unicellular algae called diatoms (Hanna *et al.,* 2014). The main component of diatomite is silica (SiO_2) with small percentage of other oxides such as alumina (Al_2O_3), iron oxide (Fe_2O_3), magnesium oxide (MgO) (Kipsanai, 2017), calcium oxide (CaO) potassium oxide (K_2O), sodium oxide (Na_2O) among others but the total content varies depending on the source (Bello *et al.,* 2014). Diatomite has unique physical and chemical properties such as high porosity, low density, fine particle size, high permeability, large surface area and low thermal conductivity (El Sayed, 2018). This makes diatomite suitable for a wide range of industrial applications use such as the manufacture of, fillers, pesticides, chromatography supports, water purification, clarification of liquors and juices, separation of various oils and chemicals and wastewater filtration (Nenadović *et al.,* 2015).

In aqueous solutions, the surface of diatomite particles has a negative charge due to the dissociation of surface silanols (Si–OH) into $Si{-}O^-$ and H^+, therefore, diatomite possesses a strong attractive force for cations (Du *et al.,* 2015). Studies by Du *et al.* (2014), El Sayed, (2018) and Muntean *et al.* (2023) have shown that diatomite has good adsorption capability for heavy metals and the sorption capacity can further be

enhanced through modification of diatomite surface using metal oxides and organic compounds such as surfactants (Zhao *et al.,* 2019). These studies focused on the removal of single heavy metal ions from wastewater using diatomite. Therefore, there is little literature available on the removal of binary heavy metal mixture from wastewater using diatomite. Furthermore, Kenya has huge deposits of diatomite yet there is no available literature on its use in heavy metal removal in the country. Therefore, the present work is directed to the use of Kenyan diatomite as an adsorbent in heavy metal removal and also as a raw material for the synthesis of MnO_2-diatomite composite.

2.6.2.5 MnO_2 modified Diatomite

MnO_2 adsorbents have been synthesized by various researchers for use in the removal of pollutants like dyes, radionuclides and heavy metals from wastewater. Furthermore, MnO_2 has also been used as a modifier of other adsorbents such as activated carbon, clay and diatomite to improve their adsorption properties. This is mainly due to the mixed valence of manganese, small particle size, structural defects and thus negative charges on the surface of manganese oxide compared to other metal oxides (Li *et al.,* 2015; Wu *et al.,* 2019). In addition, manganese oxides have great oxidation properties that make them suitable for the removal of dyes. According to Mounika *et al.* (2023), manganese oxide nanomaterials and their composites can be prepared by various methods such as hydrothermal method, co-precipitation, sol-gel process, redox method, laser ablation techniques and quick precipitation method.

In addition, MnO_2 can be synthesized by oxidation of Mn (II) ions in basic solution (Chaudhry *et al.,* 2016), oxidation of Mn (II) ions by H_2O_2, $K_2S_2O_8$/ $NH_4S_2O_8$, MnO_4^- and oxygen or through acid reduction of MnO_4^- using concentrated HCl among other different routes (Dang *et al.,* 2016). Pookmanee *et al.* (2012) and Du *et al.* (2015) have synthesized manganese oxide diatomite composites by low temperature hydrothermal route using manganese chloride and manganese sulphate/potassium permanganate mixture respectively as the manganese oxide precursors. In their research, the manganese oxide coated diatomite showed enhance removal of heavy metals ions compared to the unmodified diatomite.

Dang *et al.* (2016) synthesized MnO_2 coated diatomite composite by acid reduction of $KMnO_4$ with concentrated HCl acid for the degradation of methylene blue and methyl orange dyes. They reported that the dye degradation over the MnO_2 coated diatomite was highly efficient and rapid. Jiang *et al.* (2018) synthesized bentonite-Fe_3O_4-MnO_2 composite by combining bentonite with Fe_3O_4 and MnO_2 through co-precipitation. The obtained bentonite-Fe_3O_4-MnO_2 consisted of Fe_3O_4 nanoparticles orderly assembled on the bentonite surface with MnO_2 sheets coating the outer layer. The bentonite-Fe_3O_4-MnO_2 composite showed good recovery and reusability in removing Cd (II) ions from solution. These studies show that diatomite and other adsorbents can be modified by coating their surface with MnO_2 nanoparticles.

Among all the methods for synthesizing MnO_2 coated diatomite, MnO_2 coated diatomite synthesized by acid reduction of $KMnO_4$ has not been extensively used and there is little information about the method. To the best of our knowledge, there exists no information about use of Kenyan diatomite in synthesizing MnO_2-diatomite composite for use in waste water remediation. In addition, MnO_2 coated diatomite synthesized by acid reduction of $KMnO_4$ has mostly been used in the degradation of dyes. For instance, Khataee *et al.* (2015), Dang *et al.* (2016) and Jiang *et al.* (2016) synthesized MnO_2/diatomite by acid reduction of $KMnO_4$ for the degradation of Azo dyes, methylene blue and methyl orange dyes and aniline respectively. In this study, MnO_2-diatomite composite was synthesized using Kenyan diatomite from Kariandusi, Gilgil in Nakuru County. The MnO_2-diatomite composite was synthesized by acid reduction of $KMnO_4$/diatomite mixture using concentrated hydrochloric acid at room temperature. The raw Kenyan diatomite and the synthesized MnO_2-diatomite composite were used in the adsorption of Pb (II) and Cd (II) ions from wastewater.

2.7 Adsorption Isotherms

2.7.1 Langmuir Isotherm

The Langmuir isotherm assumes a monolayer adsorption (the adsorbed layer is one molecule in thickness) onto a solid surface containing a finite number of equivalent adsorption sites and the neighbouring adsorbate molecules do not interact with each other (Li *eta al.,* 2014). Once a site is filled, no further sorption can take place at that site. This indicates that the surface reaches a saturation point where the maximum

adsorption of the surface will be achieved (Ajenifuja *et al.*, 2017). The linear form of Langmuir isotherm is represented as follows.

$$\frac{C_e}{Q_e} = \frac{1}{bQ_o} + \frac{C_e}{Q_o} \quad (2.1)$$

Where C_e refers to the equilibrium concentration of adsorbate (in mg/L), Q_e refers to the amount of metal adsorbed per gram of the adsorbent at equilibrium (in mg/g), Q_o is the maximum monolayer coverage capacity (in mg/g), and b is the Langmuir isotherm constant (in L/mg).

The constants Q_o and b relate to the maximum adsorption capacity and the energy of adsorption, and their values are calculated from the slope and interception of the plot of C_e / Q_e against C_e. The essential characteristics of the Langmuir equation can also be expressed in terms of a dimensionless separation factor, R_L whose value indicates the nature of the adsorption process.

$$RL = \frac{1}{1 + bC_o} \quad (2.2)$$

Where C_o is the initial concentration (in mg/L). The magnitude of the factor indicates the nature of the interaction and the isotherm type; unfavourable ($R_L > 1$), linear ($R_L = 1$), favourable ($0 < R_L < 1$), or irreversible ($R_L = 0$). The R_L values between 0 and 1 indicate favourable adsorption. Langmuir adsorption isotherms were plotted and their agreement with the experimental data was determined using correlation co-efficient.

2.7.2 Freundlich Isotherm

The Freundlich isotherm accounts for intermolecular interactions between adsorbate molecules. The isotherm model assumes that adsorption occurs on a heterogeneous surface at binding sites with different energy of adsorption and non-identical adsorption sites that are not always available (Ayawei *et al.*, 2017). Freundlich isotherm also assumes that adsorption occurs in the decreasing order of energy where the stronger binding sites are occupied first and the binding strength decreases with the increasing degree of site occupation (Li *et al.*, 2014). The linearized form of Freundlich isotherm model can be illustrated as follows;

$$\log Q_e = \log Kf + \frac{1}{n}\log C_e \quad (2.3)$$

Where Q_e refers to the amount adsorbed (in mg/g), *Kf* refers to the Freundlich constant related to the adsorption capacity, *n* refers to the Freundlich constant related to the adsorption intensity, *Ce* refers to the liquid phase metal concentration at equilibrium (in mg/l).

The values of *n* and *Kf* are obtained from the slope and intercept respectively of the plot log Q_e against log *Ce*. The *n* value indicates the degree of nonlinearity between solution concentration and adsorption as follows: if $n = 1$, then adsorption is linear; if $n < 1$, then adsorption is a chemical process; if $n > 1$, then adsorption is a physical process. The coefficient of determination (R^2) will be employed to analyse the fitting degree of isotherm with experimental data.

2.7.3 Temkin Adsorption Isotherm

The Temkin adsorption isotherm contains a factor that takes into account the interaction between adsorbates (Edet and Ifelebuegu, 2020). By ignoring the extremely low and large value of concentrations, the Temkin isotherm model assumes that heat of adsorption (function of temperature) of all molecules in the layer will decrease linearly rather than logarithmically with coverage at average concentrations (Chaudhry *et al.*, 2016). The heat of adsorption is characterized by a uniform distribution of binding energies up to some maximum binding energy. The model is expressed as:

$$Q_e = \frac{RT}{b} In(A_t C_e) \quad (2.4)$$

The Linearized form of Temkin isotherm equation is illustrated as follows:

$$Q_e = \frac{RT}{b_t}\ln A_t + \left(\frac{RT}{b_t}\right)\ln C_e \quad (2.5)$$

If $B = RT/(b_t)$, then equation 2.5 becomes;

$$Q_e = B \ln A_t + B \ln C_e \quad (2.6)$$

Where Q_e is the adsorption capacity ((mg/g), C_e is the equilibrium concentration of adsorbate (mg/L), A_t refers to Temkin isotherm equilibrium binding constant (L/g), b_t is the Temkin isotherm constant, *B* is a parameter related to the heat of adsorption (J/mol), *R* is the universal gas constant (8.314 J/molK), and *T* is temperature at 298K.

The values for constants A_t and b_t are determined from the intercept and slope, respectively, of the plot of Q_e against ln C_e.

2.8 Adsorption Kinetics

Adsorption kinetics are significant in wastewater treatment since they provide valuable insight into the sorption rate and also the sorption mechanism involving diffusion, mass transfer and reactions on the adsorbent surface during the adsorption process (Krstić, 2021). The most common kinetic models used to investigate the kinetics of the adsorption process are Lagergren's pseudo-first-order model and Ho's pseudo-second-order kinetic models.

2.8.1 Pseudo-First Order Model

The pseudo-first-order model determines the relationship between change in time and the adsorption capacity with order of one. This kinetic model considers that the rate of occupation of the adsorption sites is proportional to the number of unoccupied sites (Miyah *et al.,* 2017). According to Ndung'u (2021), pseudo-first-order assumes physisorption as the rate limit step and is dependent on the number of unoccupied sites. The pseudo-first-order equation is expressed by equation 2.7.

$$\frac{dq_t}{dt} = k_1(q_e - q_t) \tag{2.7}$$

The linearized form of pseudo-first-order model is represented as follows;

$$In(q_e - q_t) = Inq_e - k_1 t \tag{2.8}$$

Where q_e and $q_t$are the adsorption capacities at equilibrium time and at time t (mg/g) respectively, k_1 is the pseudo-first-order rate constant (min $^{-1}$) and t is the time (min). The values of k_1 and qe are determined from the slope and intercept of the linear plot of $In(q_e - q_t)$ verses t.

2.8.2 Pseudo-Second Order Model

The pseudo-second-order model is based on the assumption that the rate -limiting step is chemisorption (Ngugi, 2015), where the adsorbate removal from solution is due to physicochemical interactions involving valance force by sharing or exchange of electrons between adsorbent and adsorbate (Robati, 2013). This kinetic model considers

that the rate of occupation of the adsorption sites is proportional to the square of the number of unoccupied sites. It is expressed as;

$$\frac{dq_t}{dt} = k_2(q_e - q_t)^2 \quad (2.9)$$

The linear form of the model is represented by equation 2.10.

$$\frac{t}{q_t} = \frac{1}{k_2 {q_e}^2} + \frac{t}{q_e} \quad (2.10)$$

Where q_e and $q_t$are the adsorption capacities at equilibrium time and at time t (mg/g) respectively, k_2 is the pseudo-second-order rate constant (g/mg.min) and t is the time (min). the plot of t/q_t verses t should give a straight line and the values of the values of k_2 and q_e can be determined from the intercept and slope respectively. According to Zhang (2014), the experimental estimation of q_e is not necessary in the application of this model and the model can predict the behaviour over the whole range of time studied.

2.9 Thermodynamic Studies

Thermodynamic parameters such as change in Gibbs free energy (ΔG°), enthalpy change (ΔH°) and entropy change (ΔS°) provide in-depth information on the nature of the adsorption (spontaneity, randomness, exothermicity, or endothermicity) through the characteristic energy changes associated with the adsorption process. These parameters were determined using equations 2.11-12.14.

$$\Delta G° = -RT \ln K_C \quad (2.11)$$

$$K_C = \frac{C_{ads}}{C_e} \quad (2.12)$$

$$\Delta G° = \Delta H° - T\Delta S° \quad (2.13)$$

$$\ln K_C = \frac{\Delta S°}{R} - \frac{\Delta H°}{RT} \quad (2.14)$$

Where K_C is the equilibrium constant; C_{ads} is the adsorbent phase concentration at equilibrium (mg/L); Ce is the equilibrium concentration in the solution (mg/L); R is the universal gas constant (8.314 J/mol/K); T is the absolute solution temperature (K). The magnitude of ΔH° (kJ/mol) and ΔS° (J/mol/K) were determined from the slope and

intercept of the Van 't Hoff plots of ln K_C against 1/T respectively. The values of ΔG° (kJ/mol) were determined using equation 2.11.

In general, the ΔG° values indicate the favourability and spontaneity of the adsorption process (Ndung'u, 2021). A negative ΔG° value indicates that the adsorption process is feasible and spontaneous at a known temperature. The ΔH° indicates whether adsorption process is exothermic or endothermic in nature. Positive ΔH° values suggest an endothermic nature of the adsorption of pollutant by the adsorbents while a negative ΔH° value correspond to exothermic process (Raji *et al.*, 2023). The ΔS° provides information about the disorderliness (randomness) of an adsorbent surface during adsorbent-adsorbate interactions. Positive ΔS° illustrates an increase in the randomness of the adsorption process at the solid/liquid interface while a negative ΔS° indicates decreased randomness (increased order) at the solid/liquid interface (Ndung'u, 2021).

According to Raji *et al.* (2023), thermodynamic properties associated with the adsorption of metal ions vary depending on the adsorbents structure, composition and surface characteristics. Additionally, distinct metal ions species possess varying thermodynamic affinities due to their unique charge densities and electronic configurations. This leads to different removal affinities of the pollutants by the adsorbents. Therefore, thermodynamic parameters should be accurately evaluated in order to gain adequate knowledge to understand the adsorptive behavior of heavy metal ions towards the adsorbents.

2.10 Adsorbent Characterization Techniques

Various techniques were used to characterize the adsorbents for morphology, structural properties, chemical composition, surface area and porosity properties. These characterization techniques include: XRD, FT-IR, BET/BJH and XRF.

2.10.1 X-Ray Powder Diffraction (XRD)

X-ray powder diffraction (XRD) is a non-destructive analytical technique primarily used for qualitative identification of the crystalline phases of a material and can also provide information on structures, preferred crystal orientation, and other structural parameters, such as average grain size and strain distribution (Bunaciu *et al.*, 2015).

Samples to be analyzed using XRD must be crystalline since the technique is not particularly sensitive for non-crystalline materials, such as amorphous silicates (Civan, 2015), however the technique can provide the degree of crystallinity in polymers (Nasrazadani and Hassani, 2016). The analysed material is finely ground, homogenized, and the average bulk composition is determined by passing X-rays of known wavelength through the sample.

2.10.1.1 Working Principles of XRD

X-ray diffraction is based on the constructive interference of in-phase monochromatic X-rays and a crystalline sample. When X-rays photons propagate through a substance, they can be scattered or absorbed and the analysis of the coherently scattered X-rays is utilized in diffraction techniques (Forbes, 2018). These X-rays are generated by an X-ray tube, they are filtered to produce monochromatic radiation, collimated to concentrate, and are then directed toward the sample where they are diffracted by the lattice of the crystal to give a unique pattern of peaks of 'reflections' of different intensity at differing angles (Hossain, 2013). The diffracted X-rays are then detected, processed and counted.

Depending on the phase shift of the waves, constructive or destructive interference can arise between two X-ray waves scattered by the parallel atomic planes. Therefore, interaction of sample with the incident rays only produces constructive interference of the diffracted rays when the conditions satisfy Bragg's law shown in equation 2.15.

$$n\lambda = 2dsin\theta \qquad (2.15)$$

Where n is an integer; λ is the wavelength of the X-rays; d is the interplanar spacing generating the diffraction; θ is the diffraction angle. Bragg's law relates the wavelength of electromagnetic radiation to the diffraction angle and the lattice spacing in a crystalline sample. All possible diffraction directions of lattice structures due to the random orientation of the powdered material are obtained by scanning the sample through a range of 2θ angles (Bunaciu *et al.*, 2015).

The X-ray diffraction pattern obtained for a material is specific to the atom's arrangement in the material; therefore, it is considered to be a chemical fingerprint of

the material. As a result, chemical identification of the substance is performed by comparing this diffraction pattern to a database of known patterns (Unruh and Forbes, 2019; Bunaciu *et al.,* 2015). The powder diffraction method is thus ideally suited for characterization and identification of polycrystalline phases. Furthermore, the areas under the peak are related to the amount of each phase present in the sample.

2.10.1.2 Instrumentation of XRD

A typical X-ray diffractometer used in a materials analysis consists of the following essential components: an X-ray tube, X-ray filters and monochromators, sample holder, goniometer and the X-ray detector.

2.10.1.2.1 An X-ray Tube

The most common source of X-rays for analytical work is the X-ray tube in which X-rays are produced by bombardment of a metal target with a beam of high-energy electrons. The X-ray tube consists of a highly evacuated tube containing a tungsten filament as the cathode and heavy block of copper metal with a target plate embedded on its surface as the anode. The target materials are usually metals such as tungsten, molybdenum, copper, chromium, rhodium, cobalt, silver and scandium (Skoog *et al.*, 2017). Application of a current through the filament in the cathode produces electrons by thermionic emission and they are accelerated toward the target by the high potential difference of the order 100kV between the anode and cathode. When the beam of electrons has sufficient energy to dislodge inner shell electrons of the target material, characteristic X-ray spectra is produced when the high-energy electrons are decelerated by the target material.

The X-ray spectra consist of several components, the most common being Kα and Kβ. The Kα consists, in part, of $K\alpha_1$ and $K\alpha_2$ which have sufficiently close wavelengths such that a weighted average of the two is used. $K\alpha_1$ has a slightly shorter wavelength but twice the intensity of $K\alpha_2$ and the specific wavelengths are characteristic of the target material used (Falsafi *et al.,* 2020; Bunaciu *et al.,* 2015). Cu, Mo, and Co are the most commonly used target metals in cathode ray tubes producing Kα radiations having a wavelength of 1.5418, 0.70932 and 1.7902 A˚, respectively (Forbes, 2018).

2.10.1.2.2 X-ray Filters and Monochromators

Filtering, by crystal monochromators or foils, is required to produce monochromatic X-rays needed for diffraction. Both filters and monochromators are used to produce X-ray beam with a narrow wavelength range by removing the Kβ line and most of the continuum emitted from the target leaving pure Kα line available for analytical purposes. The X-ray monochromator consists of a pair of beam collimators, which are a series of closely spaced metal plates or tubes that absorb all but the parallel beams of radiation (Skoog *et al.,* 2017). The collimated X-rays are then directed onto the sample for XRD analysis. Monochromator are also be installed in the diffracted beam at the position of the detector in order to improve the signal-to-background ratio of the diffraction pattern by decreasing the background radiation originating within the specimen (Fultz and Howe, 2012).

2.10.1.2.3 Sample holder

During XRD analysis, samples are stabilized at the center of the X-ray beam using sample holders (Falsafi *et al.,* 2020). The sample holder is usually located between the X-ray source and the detector. A typical sample holder consists of a silica plate with a small cavity in the center to accommodate the powdered sample.

2.10.1.2.4 Goniometer

A goniometer is a rotatable table that permits variation and precise determination of the angle θ between the crystal face and the collimated incident X-ray beam. In order to fulfill the geometry of diffraction and produce a spectrum, the scattered x-rays must leave the specimen at angle θ, therefore, the detector must be rotated precisely by the angle 2θ. These mechanical movements of the detector and specimen with respect to the source of monochromatic X-rays are performed by the goniometer (Fultz and Howe, 2012; Falsafi *et al.*, 2020).

2.10.1.2.5 X-ray detector

An X-ray detector convert the individual X-ray photons into pulses of current that can be transformed into information regarding the intensity and position of the diffracted beam (Unruh and Forbes, 2019). Three types of X-ray detectors are generally used: gas-filled detectors, scintillation counters and semiconductor detectors. Gas-filled detectors

operate on the principle that X-ray photons can ionize inert gas atoms such as argon, xenon or krypton into positive gaseous ions and electrons (Skoog *et al.,* 2017). Under the influence of an applied voltage, the electrons migrate toward the central wire anode causing further ionization by gas amplification phenomenon, hence, an enhanced signal is produced. The burst of electrons on the wire is converted into a voltage pulse which is then shaped and counted by the electronics.

On the other hand, scintillation detectors operate on the principle of luminescence produced when radiation strikes a phosphor. X-ray photons collide with phosphor coating on a thallium doped sodium iodide crystal thereby producing photons in the blue region of the visible spectrum. These are subsequently converted to voltage pulses by means of a photomultiplier tube attached directly behind the scintillator (Skoog *et al.,* 2017). The number of electrons ejected by the photocathode is proportional to the number of visible photons which strike it, which in turn is proportional to the energy of the original X-ray photon.

Most of the current detectors are solid-state detectors that are made from silicon or germanium diodes, operated with reverse bias. Electrical contacts to the semiconductor surfaces are typically provided by thin layers of gold (Fultz and Howe, 2012). The most important of these devices are the lithium-drifted silicon detector, Si(Li), lithium-drifted germanium detector, Ge(Li), silicon drift detector and the silicon pin photodiode. Absorption of an X-ray photon results in formation of a highly energetic photoelectron, which then loses its kinetic energy by elevating several thousand electrons in the silicon to the conduction band leading to an increase in conductivity. When a voltage is applied across the crystal, a current pulse proportional to the energy of the absorbed photon accompanies the absorption of each photon (Skoog *et al*., 2017).

2.10.2 Fourier-Transform Infrared Spectroscopy (FT-IR)

Fourier transform infra-red (FT-IR) spectroscopy is a non-destructive technique mainly used in the identification of functional groups present in a given sample and also the identification of both organic and inorganic compounds. FT-IR is based on the excitation of molecular vibrations in the sample by absorption of infrared light followed by the measurement of the wavelength and intensity of the absorption of infrared light

by a sample. The wavelengths of infrared radiation absorbed by the sample are characteristic of its molecular structures (Mbonyiryivuze *et al.,* 2015).

In FT-IR spectroscopy, polychromatic infrared radiation is passed through the interferometer where 'spectral encoding' takes place. The resulting interferogram signal then exits the interferometer and it is passed through the sample. Some of the infrared radiation is absorbed by the sample while some is transmitted through the sample. The beam finally passes through to the detector for final measurement. The resulting spectrum represents the molecular absorption and transmission of the sample with absorption peaks which correspond to the frequencies of vibrations between the bonds of the atoms making up the material (Hossain, 2013; Mbonyiryivuze *et al.,* 2015).

In addition, the intensity of the peaks in the spectrum indicates the amount of the material present. This creates a unique molecular fingerprint of the sample where no two unique molecular structures can produce the same infrared spectrum. Due to this, FT-IR spectroscopy is useful in identification of an unknown material, quality control of samples and the determination of amounts of components in a mixture (Hossain, 2013). The main components of FT-IR spectrometer are: the infrared source, interferometer, the sample holder, detector and the computer system.

2.10.2.1 Infrared Source

IR sources consist of an inert solid that is electrically heated to produce continuum radiation approximating that of a blackbody. Most FT-IR spectrometers are used for measurements in the mid and near infrared (IR) regions. Mid IR (4,000–200 cm^{-1}) energy is usually emitted from a heated silicon carbide element (Skoog *et al.,* 2017).

2.10.2.2 Interferometer

Most FTIR spectrometers use a Michelson interferometer which comprises of a configuration of mirrors, one of which is moved by a motor. As the polychromatic IR beam enters the interferometer, "spectral encoding" takes place. This is accomplished by use of a beam splitter which splits the IR beam into two beams whose path lengths can be varied periodically to give interference patterns called interferogram (Skoog *et*

al., 2017; Cozzolino, 2018). The resulting interferogram signal then exits the interferometer and is focused on to the sample.

2.10.2.3 Sample Compartment

This is where the sample absorbs specific frequencies of IR radiation, which are uniquely characteristic of the sample. The IR beam is energetic enough; therefore, it excites molecular vibrations to higher energy states. Since the wavelength of many IR absorption bands is characteristic of specific types of chemical bonds, a spectral fingerprint of the sample is therefore created (Mbonyiryivuze *et al.*, 2015).

2.10.2.4 Detector

After leaving the sample, the beam finally passes to the detector for final measurement. The FT-IR detectors used are specially designed to measure the special interferogram signal. Pyroelectric detectors using deuterated triglycine sulphate or lithium tantalate as the sensitive element are commonly used in mid-IR spectrometers and they respond to changes in temperature as the intensity of the IR radiation falling on them varies (Cozzolino, 2018; Karthika *et al.*, 2022).

2.10.2.5 Computer System

The measured signal is digitized and then sent to a computer for processing. The raw data is converted into the actual spectrum by the computer through use of Fourier transformation. The final infrared spectrum is then presented to the user for interpretation (Cozzolino, 2018).

2.10.3 BET and BJH

Brunauer–Emmett–Teller (BET) and Barrett–Joyner–Halenda (BJH) methods are non-destructive techniques used to obtain the specific surface area, pore volume and pore size distribution of nanoparticles. These techniques are based on the physical adsorption and desorption of nitrogen gas by the nanoparticle materials at 77K. Prior to analysis, the sample materials are first degassed in vacuum and heated to completely remove contaminants that may be present on the active sites of the sample (Bardestani *et al.*, 2019).

In BET analysis, the sample is placed in an analysis tube under partial vacuum and cooled to a temperature of 77K using liquid nitrogen. Cooling the samples enables detectable amounts of adsorption to be obtained since interaction between the solid and gaseous phases is weak (Joudeh and Linke, 2022). Nitrogen gas is then introduced to the solid sample in controlled increments starting from low pressures until a saturation pressure is reached and adsorption ceases. The sample is then removed from the nitrogen atmosphere and heated to make the adsorbed nitrogen to be desorbed from the sample material and quantified (Bardestani *et al.*, 2019).

The data obtained is displayed inform of isotherms showing volume of nitrogen adsorbed as a function of relative pressure (ratio of actual to saturation pressures) at constant temperature and the information used to determine the surface area of the sample (Joudeh and Linke, 2022). According to Shimizu and Matubayasi (2022), the low-pressure region of the isotherm corresponds to monolayer adsorption while the higher-pressure region of the isotherm showing a steep rise in uptake represents multilayer adsorption. The monolayer segment of the isotherm is used to determine the surface area of the sample by the BET method.

Similar to the BET method, the BJH method also involves the physical adsorption and desorption of nitrogen gas by the sample materials at 77K. Therefore, data on pore volume, pore distribution and surface area are usually obtained from the same experiment. According to Joudeh and Linke (2022), the adsorption process in BJH analysis is extended so that the gas condenses in the sample pores as pressure increases. This continues until a saturation point is achieved, at which all the sample pores are filled with liquid. Afterwards, the process is reversed by reducing the relative pressure thus the condensate is allowed to evaporate and the desorption data is obtained. The pore size distribution is then calculated from the desorption data using a modified Kelvin equation (Kelvin model of pore filling).

2.10.4 X-Ray Fluorescence Spectroscopy

X-ray fluorescence spectroscopy (XRF) is a non-destructive analytical technique used to determine the elemental composition of a material. The sample materials may be metals, alloys, geological materials, ceramics, liquids etc. XRF spectroscopy provides

both qualitative and quantitative information about the material composition. XRF analysis employs measuring the characteristic fluorescent X-rays (secondary X-rays) produced by a material as a result of irradiating the material with a high-energy primary X-ray source. When the sample material is irradiated with high energy X-rays (primary radiation), the X-ray photons excite the atoms in the sample material causing them to fluorescence as they return to the ground state thereby emitting secondary X-rays of various wavelengths (Oyedotun, 2019; Feng *et al.*, 2022).

The fluorescent X-rays emitted possess energies that are characteristic to the elements present in the sample, therefore, they are recorded and analyzed in order to identify the elements present in the sample. According to Igwebike-Ossi (2017) and Feng *et al.* (2022), each element in the sample material emits a set of characteristic fluorescent X-rays that are unique for that specific element and their intensity is related to the concentration of the element in the sample. As a result, both qualitative and quantitative information is obtained about the sample material. XRF spectrometry is divided into wavelength dispersive (WDXRF) spectrometry and energy dispersive (EDXRF) spectrometry depending dispersion and detection method used. Wavelength dispersive XRF spectrometer disperses the emitted fluorescent X-rays from the sample using an analyzing crystal and goniometer thereby physically separating the fluorescent X-rays according to their wavelengths. The energy dispersive XRF spectrometer on the other hand directly measures the energies of the fluorescent X-rays and generates the XRF spectrum by counting and plotting the relative numbers of X-rays at each energy (Brouwer, 2018; Marguí *et al.*, 2022). The key components of a typical XRF are: X-ray source, sample holder and the detector system.

2.10.4.1 X-ray source

X-rays are produced in an X-ray tube when a beam of high energy electrons produced by a cathode tungsten filament are accelerated and bombarded onto a metal target (anode). The metal target may be tungsten, copper, chromium or molybdenum depending on the sample to be analyzed. The X-ray tube is highly evacuated to prevent obstruction of the electron beam by air molecules (Igwebike-Ossi, 2017; Skoog *et al.*, 2017; Brouwer, 2018).

2.10.4.2 Sample holder

The sample holder is situated in between the detector and the X-ray source. The sample chamber, the X-ray source and the detectors are mounted in a vacuum chamber to avoid absorption of low energy X-rays by air. However, XRF analysis of liquid and wet powder samples is carried out in helium-filled spectrometers. This is because the liquids would instantly boil and evaporate under vacuum conditions. In addition, the helium gas absorbs the radiation of light elements up to fluorine, therefore, if present in the liquid sample, these elements cannot be measured (Brouwer, 2018).

XRF samples are prepared depending on the nature of the sample, solid or liquid. Metallic samples are prepared by cleaning and polishing to remove rust and oxide layers be for XRF analysis. Solid earth materials are prepared by crushing and grinding into fine powder. The powdered samples are usually pressed into a pellet/tablet which is then analyzed. A binder such as wax, boric acid, starch or cellulose may be added to the pellet to avoid pellet breakage (Marguí *et al.*, 2022). Liquid samples are usually poured into special cups with supporting films and then placed in helium-filled sample chamber followed by XRF analysis (Brouwer, 2018).

2.10.4.3 Detector

XRF spectrometers used different types of detectors depending on whether they are WDXRF or EDXRF. WDXRF spectrometers used scintillation and gas filled detectors while EDXRF spectrometers use solid state silicon or germanium detectors (Brouwer, 2018). According to Igwebike-Ossi (2017), gas filled detectors are employed in measuring longer wavelengths produced by light elements in WDXRF while scintillation detectors are used in measuring short wavelengths from heavy elements. XRF detectors work on the principal production of an electrical pulses when X-rays enters the detectors. The electrical pulses are then amplified and counted by a multi-channel analyzer. Solid state detectors comprise of a germanium or silicon semiconductor materials which produces electrical pulses through creation of electron-hole pairs when X-rays enter the detector. The depth of the electrical pulse produced depends on the number of electrons produced which is proportional to the energy of the incoming X-ray photons (Skoog *et al.*, 2017; Brouwer, 2018).

Gas filled detectors comprise of a metal cylinder (cathode) filled with an inert gas such as argon and a co-axial tungsten wire (anode) that is raised to high potential difference. When X-rays enter the detector, it ionizes the gas, therefore, creating small burst of electrons which are attracted by the anode tungsten wire. This leads to production of an electrical pulse which is counted by the muti channel analyzer. Scintillation detectors comprise of sodium iodide crystal and photomultiplier tube fitted. Incoming X-rays collide with the scintillator crystal producing a flash of a blue light photons which in turn produces a bust of electrons with the help of photomultiplier. This is registered as electrical pulses in the amplifier whose height are proportional to the number of electrons produced, hence the energy of the incoming X-rays (Skoog *et al.*, 2017; Brouwer, 2018).

2.10.5 Atomic Absorption Spectrometry

Atomic Absorption Spectrometry (AAS) is an analytical technique utilized for quantitative analysis of trace metals in a sample by measuring the absorbed radiation by the chemical element of interest. The technique is applicable directly to a wide range of metals and some metalloids (Kimathi, 2013). AAS works on the principle of absorption of radiation energy of a particular wavelength by free atoms. In AAS analysis, the sample is atomized then a beam of light energy is passed through the vaporized sample. The atoms of the element of interest in the sample in their ground state, absorb the electromagnetic radiation of a specific wavelength are and elevated to an excited state. The wavelength at which absorption occurs is characteristic of the element and the degree of absorption is a function of concentration of atoms in the vapour, therefore, the greater the number of atoms in the sample, the more radiation is absorbed (Owiti, 2015; Cosmas, 2016).

The concentration of a certain element in the sample is therefore determined by application of Beer-Lambert law. If an incident radiation of power $\mathbf{P_0}$, passes through a solution of an absorbing species at concentration **c** and path length **b**, is attenuated and emerges with radiant power **P**, then absorbance is given by equation 2.16 (Skoog *et al.*, 2017);

$$A = \log(\frac{P_o}{P}) = abc \qquad (2.16)$$

Where A is absorbance; a is a proportionality constant called the absorptivity in $Lg^{-1}cm^{-1}$; b is the path length in centimeters; c is the concentration of the absorbing species in grams per liter. The relationship between absorbance (A) and concentration (c) is linear over a wide range of concentrations (Beer's law), therefore, the concentration of analyte is usually determined from a calibration curve, obtained using standards of known concentration (García and Báez, 2012). The main components of an atomic absorption spectrometer include: radiation source, atomizer, monochromator, detector and the readout system.

2.10.5.1 Radiation Source

The most common radiation source for atomic absorption measurements is the hollow-cathode lamp. The lamp consists of a tungsten anode and a cylindrical cathode in a sealed glass tube filled with neon or argon at a pressure of 1 to 5 torr (Francis, 2015**)**. The cathode is constructed of the metal of interest whose spectrum is desired. By application of a high voltage applied across the anode and cathode, the fill gas ionizes, the gas ions are accelerated towards the cathode and dislodge some metal atoms from the cathode surface through sputtering. A portion of the sputtered metal atoms are in excited states and thus emit their characteristic radiation as they return to the ground state (Skoog *et al.,* 2017).

2.10.5.2 Atomizer

The main function of the atomizer (sample cell) is to produce ground state atoms of the analyte necessary for atomic absorption to occur. This involves application of thermal energy to break the bonds that hold atoms together as molecules. Two types of atomizers are commonly used namely: flame and electrothermal atomizers. In flame atomizer, the sample solution is nebulized by the flow of gaseous fuel-oxidant mixture and evaporated to produce a solid molecular aerosol. The aerosol is then volatilized to form gaseous molecules which dissociate and forms an atomic gas. Some of the atoms ionize to form cations and electrons (Mathenge, 2014; Skoog *et al.,* 2017). In electrothermal atomizers, the analyte solution is first evaporated at low temperature and ashed at a slightly higher temperature in electrically heated graphite tube. After ashing, the temperature is increased to 2000-3000 ^{o}C to atomize the sample (Skoog *et al.,* 2017).

2.10.5.3 Monochromator

The monochromator is an essential part of the AAS spectrometer since it is used to select the specific wavelength of light (spectral line) that is absorbed by element of interest in the sample and exclude other wavelengths. This allows for the specific identification of the element of interest even when it occurs in the presence of other elements in the sample (García and Báez, 2012). Monochromator use lenses, mirrors, prisms and diffraction gratings to disperse and isolate the appropriate wavelength band to be transmitted to a detector (Francis, 2015).

2.10.5.4 Detector

The specific wavelength of light selected by the monochromator is directed onto a detector which converts the light signal into an electrical signal proportional to the light intensity (García and Báez, 2012). Common detectors used in AAS include photomultipliers tubes, phototubes or photodiode array detectors (Skoog *et al.,* 2017).

2.10.5.5 Readout system

A readout system is an electronic device coupled with microprocessors that programs and performs mathematical operations on the electrical signal from the transducer which appear on the readout system as peaks of energy absorption at discrete wavelengths (García and Báez, 2012). Modern AAS instruments use computer systems as readout systems that are used to control parameters of the AAS instrument and also manipulate data (Skoog *et al.,* 2017).

CHAPTER THREE
METHODOLOGY

3.1 Materials

3.1.1 Apparatus

All masses were weighed using analytical balance. All volume measurements were done using volumetric flasks (100mL, 250mL and 1000mL), pipette (10mL, 25mL and 50mL) and burette (50mL). Titration experiments for the standardization of solutions were done in 250mL Erlenmeyer flasks. 100mL stoppered plastic bottles were used for the adsorption process while 250ml glass beakers were used only during the adsorption process when investigating the of effect of temperature. Mercury thermometer was used to measure the temperature changes during the adsorption process. pH measurements in the study were done using a pH meter (Model HANNA HI 2211). During the study, samples were stirred using an orbital shaker (BioBase SK-0180-Pro) and gravity filtration of the samples was done using Whatman filter paper No.40. Atomic Absorption Spectrometer (Model PG 990) was used to analyse the quantity of heavy metals in the samples. Sample characterization was done using FT-IR (Shimadzu IRAffinity-1S FT-IR spectrophotometer), XRF (Empyrean PANalytical XRF spectrometer), XRD (Rigaku Miniflex II desktop X-ray Diffractometer) and BET/BJH (Micromerics ASAP 2000).

3.1.2 Reagents

All the reagents were analytical grade purchased from Sigma-Aldrich and were used without further purification. They include: lead (II) nitrate [$Pb(NO_3)_2$; 99%], cadmium nitrate tetrahydrate [$Cd(NO_3)_2.4H_2O$; 99%], potassium permanganate ($KMnO_4$; 99.0%), hydrochloric acid (HCl; 37%), nitric acid (HNO_3; 70%), sodium hydroxide pellets (NaOH, 98%), potassium hydrogen phthalate ($KHC_8H_4O_4$; 99.5%), phenolphthalein indicator ($C_{20}H_{14}O_4$; 0.1% in ethanol 90%, denatured). Distilled water used was obtained from Chuka University Chemistry Laboratory. The raw diatomite sample was obtained from the African Diatomite Industries Limited (ADIL) in Kariandusi, Gilgil, Nakuru County, Kenya.

3.2 Preparation of Solutions

0.1M NaOH solution was prepared by dissolving 1.000 g of NaOH in 250 mL of distilled water. 0.1M HNO_3 solution was prepared by dissolving 1.6 mL of concentrated HNO_3 acid (70%, density=1.42 g/cm^3) in 50 mL of water in a 250 mL volumetric flask and the solution was topped up to the mark. A dilute 0.1M potassium permanganate solution, $KMnO_4$, was prepared by dissolving 15.8 g of $KMnO_4$ in 500 mL of distilled water. The solution was then transferred to a one-liter volumetric flask and toped up to the mark. The 6M HCl acid was prepared by diluting 50 mL of 12M HCl with distilled water in a 100 ml volumetric flask and topped up to the mark. Similarly, 4M HCl acid also was prepared through dilution of the 12M HCl acid by adding 333 mL of the concentrated acid was into a 1000mL volumetric flask containing 200 ml of distilled water. The mixture was then swirled and topped with distilled water up to the mark. The preparation and dilution of these solutions was done at the Chemistry Laboratory, Chuka university.

3.2.1 Standardization of solutions

The NaOH, HCl and HNO_3 solutions were standardized employing the procedure followed by Haque and Ahmad (2019). The NaOH solution was standardized with a primary standard solution of potassium hydrogen phthalate (KHP). The burette was rinsed with 10 mL of the NaOH solution and then it was filled with the NaOH solution. 0.500 g of KHP was then accurately weighed and transferred into a clean 250 mL Erlenmeyer flask. 25mL of distilled water was then added into the flask to dissolve the solid. Three drops of phenolphthalein indicator (0.1%) were added into the Erlenmeyer flask and the KHP solution was slowly titrated with the NaOH solution until the first appearance of a permanent pink colour. The final burette reading was then recorded. Replicate analysis was conducted two more times and the average volume of NaOH used was utilized to calculate the exact molar concentration of the NaOH solution.

The standardized NaOH solution was used then to standardize the HCl and HNO_3 acids. The 6M and 4M HCl acid solutions prepared were diluted by adding 10mL and 15mL of the acids respectively into 250 mL volumetric flasks containing 50 mL of distilled water. The mixtures were swirled and then topped with distilled water up to the mark. The burette was then filled with the standard NaOH solution. 25 mL of the dilute acid

was then transferred into a clean 250 mL Erlenmeyer flask and three drops of phenolphthalein indicator (0.1%) were added. The acid solution was slowly titrated with the standard NaOH solution until the first appearance of a permanent pink colour. The final burette reading was recorded and then two replicate analyses were conducted. The average volume of NaOH used was utilized to calculate the exact molar concentration of the acid solution.

3.2.2 Preparation of Synthetic Wastewater

Stock solution of Pb (II) ions of concentration 1000mg/L was prepared by dissolving 1.615 g of $Pb(NO_3)_2$ in 200 mL of distilled water in a beaker. The solution was then carefully transferred to a 1000ml volumetric flask. The beaker was rinsed several times with distilled water and the rinsing water added to the volumetric flask. The solution was then topped up to the mark. Similarly, stock solution of Cd (II) ions was prepared by dissolving 2.772 g of $Cd(NO_3)_2.4H_2O$ in about 200 mL of distilled water in a beaker and the solution was transferred to a 1000 ml volumetric flask. After rinsing the beaker with distilled water and the rinsing water added to the volumetric flask, the solution was topped up to the mark to form 1000 mg/L solution of Cd (II) ions.

Working solutions of different concentrations of Pb (II) and Cd (II) ions were prepared through serial dilution of the stock solutions. Concentrations of 10, 20, 30, 40, 50, 60 and 70 mg/L were prepared for both Pb (II) and Cd (II) single ions by adding 10, 20, 30, 40, 50, 60 and 70 mL respectively of the stock solution in a 1000 mL volumetric flask and diluting it to the mark using distilled water. The binary metal ion working solutions of different concentrations were prepared by mixing equal volumes of Pb (II) and Cd (II) stock solutions and then diluting with distilled water to give equal concentration (in mg/L) of the metal ions in the mixture. The preparation and dilution of synthetic wastewater were done at the Chemistry Laboratory, Chuka University.

3.3 Synthesis of Adsorbents

3.3.1 Preparation of Raw Diatomite

The powdered diatomite sample was obtained from the African Diatomite Industries Limited (ADIL) in Kariandusi, Gilgil, Nakuru County, Kenya. 250 g of the diatomite sample was washed with distilled water to remove any adhered impurities and dried at

100 ^{o}C in an oven for 6 hours. After cooling, the diatomite sample was acid treated employing the procedure followed by (Zhang *et al.,* 2013) with modification. During the acid treatment, the diatomite sample was reacted with 500mL of 4M HNO_3 acid in a 1000 mL glass beaker for 30 minutes to remove impurities such as calcite that maybe present. The diatomite sample was then filtered through Whatman filter paper No. 40 and washed with plenty of distilled water until the pH of rinsing water was 7.

The sample was then oven dried at 100 ^{o}C for 6 hours. The diatomite sample was then ground into powder using mortar and pestle and then divided into two portions. The portions were then stored in zip lock polyethene bags for future use. One portion of the sample was labelled raw diatomite while the second portion was used to prepare MnO_2-diatomite composite. The washing and preparation of raw diatomite was done at the Chemistry Laboratory, Chuka university.

3.3.2 Synthesis of MnO_2-diatomite Composite

The MnO_2-diatomite composite was prepared by acidic reduction of $KMnO_4$ at Chuka University chemistry laboratory. The procedure followed by Dang *et al*. (2016) was employed with modification. Two MnO_2-diatomite composite samples were prepared by varying the concentration of $KMnO_4$ used as shown in table 3.1. In general, 30 g of raw diatomite was suspended in 300 mL of 0.1M $KMnO_4$ solution at room temperature and the mixture was stirred at 240 rpm (Model BioBase SK-0180-Pro) for 2 hours. 60mL of 6M HCl acid was then added into the mixture and then stirred further for 6 hours at room temperature. The resulting wet solid was filtered through Whatman filter paper No. 40 and washed with distilled water until a pH of 7 was reached. The sample was then air dried at room temperature for 48 hours, to obtain MnO_2-diatomite composite 1.

MnO_2-diatomite composite 2 was prepared using the same procedure but the concentration of $KMnO_4$ solution used was 0.05M. Upon drying, the samples were then ground into powder and stored in a zip lock polyethene bags for future use. The modified diatomite samples were labelled MnO_2-diatomite composite 1 and 2. The synthesis of MnO_2-diatomite composites was done at the Chemistry Laboratory, Chuka university.

Table 3.1: Parameters used in preparing different samples of MnO_2-diatomite composites.

Sample	Diatomite Amount (g)	Concentration of $KMnO_4$ (mols/L)	Concentration of HNO_3 (mols/L)	Temperature used (^OC)
1	30	0.1	6	Room temperature
2	30	0.05	6	Room temperature

3.4 Characterization of the Prepared Adsorbents

The adsorbents (Raw diatomite and MnO_2-diatomite composite) were characterized using a number of techniques including: X-ray diffraction (XRD) analysis, Fourier transform infrared spectroscopy (FT-IR), X-Ray fluorescence (XRF), Brunauer-Emmet-Teller (BET) for surface area analysis and Barrett-Joyner-Halenda (BJH) pore size and volume analysis.

3.4 1 Brunauer-Emmet-Teller (BET) and Barrett-Joyner-Halenda (BJH)

The Brunauer–Emmett–Teller (BET) and Barret–Joyner–Halenda (BJH) methods were used to determine the surface area and pore size distribution of nanocomposites in nitrogen adsorption–desorption experiments at 77 K. The specific surface area of prepared adsorbents was determined by the Brunauer-Emmett-Teller (BET) method using Micromeritics (ASAP 2000) analyzer (University of KwaZulu-Natal, South Africa). The procedure used by Muntean *et al.* (2023) was employed. Prior to analysis, the samples were degassed at 200 ^oC for 6 hours and then analyzed by physical adsorption and desorption of nitrogen gas at 77 K. The surface area was then calculated using the BET method. The porosity of the adsorbents was determined by Barrett-Joyner-Halenda (BJH) method using Micromeritics (ASAP 2000) porosity analyzer (University of KwaZulu-Natal, South Africa).

3.4.2 X-Ray Diffraction (XRD)

The structural characterization and phase identification analysis of both raw diatomite and MnO_2-Diatomite composite was done by powder X-ray diffraction (XRD) using Rigaku Miniflex II desktop X-ray Diffractometer at the Geothermal Development Company (GDC) at Menengai Crater in Nakuru County, Kenya. Prior to XRD analysis, the samples were crushed into fine powder with agate mortar and pestle and then mounted on a glass plate sample holder for XRD analysis. The diffraction patterns were collected using Cu-Kα 1 (1.540598A) radiation, an accelerating voltage of 30 kV and

a current of 15mA while scanning the samples in the 2θ range of 3° to 90° at the rate of 2°/minute. The diffraction patterns were then analysed by Crystal impact match software (version 3.15 Build 270) with open reference database (COD-Inorganic 2023-06-06) for the mineral phase identification.

3.4.3 X-Ray Fluorescence (XRF)

XRF technique was used to determine the chemical composition of the adsorbents. Prior to XRF analysis, the samples were ground into a powder then pressed firmly into the sampler holder. The samples were irradiated with an X-ray beam and the fluorescent X-Rays produced were recorded and analyzed. The XRF analysis was conducted using Empyrean, PANalytical XRF spectrometer with 60 kV energy of the X-ray tube. The XRF analysis were done at the ministry of mining, department of Mines and Geology in Nairobi County.

3.4.4 Fourier Transform Infrared Spectroscopy (FT-IR)

The functional groups present on the surface of Raw diatomite and MnO_2-diatomite composite were determined using FT-IR spectroscopy using Shimadzu IRAffinity-1S FT-IR spectrophotometer, Chuka University. 0.001 g of the samples was mixed homogeneously with KBr at a ratio of 1:100. The mixture was crushed into fine powder with agate mortar and pestle and then pressed into a transparent pellet using Shimadzu MHP-1 mini handpress. The transparent pellet was then scanned with an IR beam and the IR spectra, in the wave number range from 400 cm^{-1} to 4000 cm^{-1} was obtained. The FT-IR analysis was done at Chuka University Chemistry Laboratory.

3.5 Batch Adsorption Studies

Batch adsorption studies of both single and binary heavy metal ions were carried out at the Chemistry Laboratory in Chuka university.

3.5.1 Single Ion Studies

The adsorption of Pb (II) and Cd (II) single ions on each adsorbent (Raw diatomite and MnO_2-diatomite composite) was studied by batch technique in 150 mL polypropylene bottles. In all sets of experiments, fixed volumes (50 mL) of single metal ion solutions of various concentrations (10, 20, 30, 40, 50, 60 and 70) mg/L and pH (2-6) was

thoroughly mixed at temperatures (25^{o}C - 65^{o}C) with a known mass of each adsorbent (0.02 -05) g dose at a stirring speed of 240 rpm for a known period of time (20-140) minutes. Experimental parameters i.e., adsorbent dosage, contact time, pH, temperature and initial metal ion concentration were investigated by changing one parameter at a time while keeping the other parameters constant. After equilibrium, the mixture was gravity filtered through Whatman filter paper No.40 and the concentration of heavy metal ions remaining in the solution was determined by AAS using PG 990 atomic absorption spectrophotometer.

The percentage heavy metal removal by both adsorbents (Raw diatomite and MnO_2-diatomite composite) was calculated using the following equation;

$$\% \, Removal = \frac{(Co - Ce)}{Co} \times 100 \tag{3.4}$$

Where *C*o and *C*e are the initial and equilibrium concentrations (mg/L) of the metal ions in the test solution. The adsorption Capacity Q_e (in mg/g) at equilibrium of both adsorbents was calculated using the equation below;

$$Qe = \frac{(Co - Ce)V}{W} \tag{3.5}$$

Where *C*o and *C*e are the initial and equilibrium concentrations (mg/L) of metal ions in the test solution respectively. *W* is the mass of the adsorbent mass (g) while *V* is the volume of the test solution used (L).

3.5.2 Binary Ion Studies

Batch adsorption experiments on binary metal ion solution were carried out using the raw diatomite because it had the highest adsorption capacity for Pb (II) and Cd (II) single ions. The experiments were carried out at a stirring speed of 240 rpm to establish the optimal working parameters: pH, contact time, initial concentration, temperature and adsorbent dose. Experiments were carried out at pH values ranging from 2 to 6, adsorbent dose (0.02-0.5) g, contact time (20-120) minutes and initial heavy metal concentration of (10-70) mg/L at a stirring speed of 240 rpm. The mixtures were filtered after a predetermined period of time through Whatman filter paper No. 40 and the filtrate was analyzed for residual heavy metal ions using AAS (PG 990, Chuka

University). The percentage heavy metal removal by raw diatomite composite was calculated using equation 3.4;

$$\% \, Removal = \frac{(Co - Ce)}{Co} \times 100 \tag{3.4}$$

Where *C*o and *C*e are the initial and equilibrium concentrations (mg/L) of the metal ions in the test solution. The adsorption Capacity Q_e (in mg/g) at equilibrium of MnO_2-diatomite composite was calculated using the equation 3.5;

$$Qe = \frac{(Co - Ce)V}{W} \tag{3.5}$$

Where *C*o and *C*e are the initial and equilibrium concentrations (mg/L) of metal ions in the test solution respectively. *W* is the mass of the adsorbent mass (g) while *V* is the volume of the test solution used (L).

3.5.3 Effect of Initial Metal Ion Concentration

Effect of initial concentration was investigated by varying the initial concentration of heavy metal ions from 10 to 70 mg/L while keeping the other parameters constant. 0.1g of adsorbent material in several polypropylene bottles was mixed with 50 mL metal ion solutions of concentrations 10, 20, 30, 40, 50, 60 and 70 mg/L at a pH of 4.0±0.2 for Pb (II), pH of 6.0±0.2 for Cd (II) and a temperature of 25±2 ℃. The mixtures were stirred at 240 rpm for one hour, then filtered and the filtrate analysed by FAAS for residual metal ions. From the data, a graph of percentage heavy metal removal against initial metal ion concentration was plotted. The data was also fitted to the linear forms of Langmuir, Freundlich and Temkin isotherms in order to describe the adsorption process. The applicability of these equations to the adsorption data was determined by judging their correlation coefficients (R^2).

3.5.4 Effect of pH

The effect of solution pH on the adsorption capacity of the adsorbents was studied by varying the pH from 2 to 6 while keeping the other parameters constant. The pH adjustments were done by adding 0.1M HNO_3 or 0.1M NaOH solution. Fixed amounts of adsorbent (0.1 g) were placed in contact with 50 mL of 10 mg/L working solutions at different pH of 2, 3, 4, 5 and 6. The mixtures were then placed in an orbital shaker

(BioBase SK-0180-Pro) and shaken continuously at 240 rpm for one hour at a temperature 25± 2 ℃. The mixtures were then successively withdrawn and filtered through Whatman filter paper No. 40. The concentration of residual metal ions was then determined by FAAS (PG 990, Chuka University). From the data, the percentage heavy metal removal against pH was plotted.

3.5.5 Effect of Contact Time

The effect of contact time on adsorption was studied by varying the contact time from 20 to 140 minutes while keeping other parameters constant. 0.1 g of adsorbent dose was agitated in 50 mL of 10 mg/L metal ion solution over time periods of 20, 40, 60, 80, 100, 120 and 140 minutes at a constant agitation speed of 240 rpm. The pH was held constant at 4.0±0.2 for Pb (II), 6.0±0.2 for Cd (II) while the temperature was maintained at 25±2 ℃. At the predetermined time, the samples were withdrawn, filtered and the residual metal ions of interest were then determined by FAAS (PG 990, Chuka University). The data obtained was fitted to pseudo-first and second order kinetic models in order to describe the adsorption behaviour of raw diatomite and MnO_2-diatomite composite. A plot of percentage heavy metal removal against contact time was also plotted using the data.

3.5.6 Effect of Adsorbent Dose

Effect of adsorbent dose on adsorption of Pb (II) and Cd (II) ions was investigated by varying the adsorbent dose from 0.02 to 0.5 g. For this, 0.02, 0.05, 0.1, 0.2, 03, 0.4 and 0.5 g of adsorbents were suspended in 50 mL solutions of metal ion of interest at an initial concentration of 10 mg/L, pH of 4.0±0.2 for Pb (II), pH of 6.0±0.2 for Cd (II) and a temperature of 25±2 ℃. The samples were then stirred at 240 rpm for a predetermined time and subsequently withdrawn, filtered and analysed for residual metal ions by FAAS (PG 990, Chuka University). From the data obtained, a plot of percentage removal verses adsorbent dose (in g/L) was then plotted.

3.5.7 Effect of Temperature

Effect of temperature on the adsorption capacity was investigated by adding 0.1 g of adsorbent material into 50 mL metal ion solutions in 250 mL glass beakers. The pH of the solutions was held constant at pH of 4.0±0.2 for Pb (II) and pH of 6.0±0.2 for Cd

(II) while the initial concentration of both Pb (II) and Cd (II) ions was held constant at 10 mg/L. The beakers were then placed on thermostatic hotplate and stirred at 240 rpm at varying temperature of 25±2, 35±2, 45±2, 55±2 and 65±2 ℃ for one hour. The samples were then withdrawn from the heater, filtered and analysed for residual heavy metal ions by FAAS (PG 990, Chuka University). Form the data obtained, a pot of percentage removal verses temperature was plotted to analyze the effect of temperature on the percentage removal of Pb (II) and Cd (II) ions. The data obtained was also used to determine thermodynamic parameters namely change in Gibbs free energy (ΔG°), enthalpy (ΔH°) and entropy (ΔS°) that were used to describe the adsorption process.

3.6 Analysis of Heavy Metal ions

The residual concentration of Pb (II) and Cd (II) ions in the filtrate samples were analysed by AAS (PG 990, Chuka University). Before the heavy metal analysis, the AAS was calibrated using blanks and standards prepared through serial dilution of Pb (II) and Cd (II) stock solutions. The corresponding linear calibration curves obtained were used to determine the unknown concentration of the metal ions in the samples. During the metal analysis, the Pb (II) and Cd (II) ions were analysed one metal at a time. The sample solutions were aspirated into the atomic absorption spectrophotometer and their respective concentrations recorded.

Depending on the concentration of the metal ions in the samples, some samples were diluted to a certain dilution factor in order to make sure their concentrations were within the concentration scope of the standards. The AAS operating parameters during the analysis are presented in table 3.2.

Table 3.2: The operating conditions for AAS (PG 990, Chuka University) instrument

Metal	Operating Parameters				
	Lamp Current (mA)	Wavelength (nm)	Slit Width (nm)	Flame	Oxidant Flow Rate (L/min)
Pb	5	283.7	1.0	Air-Acetylene	1.5 or 2.0
Cd	4	228.8	0.5	Air-Acetylene	1.5 or 1.8

Source: Operating manual of AAS (PG 990)

3.7 Data Analysis

The adsorption data was analyzed using Microsoft excel 2019 version 2409 (Build 18025.20104) and Origin pro 2019b (Build 9.6.5.169) data analysis and graphing software for plotting graphs. Freundlich, Langmuir and Temkin isotherms were used to determine adsorption capacities of raw diatomite and MnO_2-diatomite composite. Pseudo-first-order and pseudo-second-order kinetic models were also used to describe the adsorption behaviour of raw diatomite and MnO_2-diatomite composite. Thermodynamic parameters such as change in Gibbs free energy ($\Delta G°$), enthalpy ($\Delta H°$) and entropy ($\Delta S°$) were also determined in order to describe the adsorption process.

3.8 Ethical Consideration

Attribution and credit have been given to all contributing to the research. The research permit was acquired from the National Committee of Science, Technology and Innovation (NACOSTI) before the start of the research (Appendix XXXVII). The study also ensured that the laid down policies were followed and should there be need for use of the study results for policy matters, the information will be released to requesting institution in consultation with Chuka University.

CHAPTER FOUR

RESULTS AND DISCUSSION

4.1 Synthesis of Adsorbents and Characterization

4.1.1 Synthesis of Adsorbents

The raw diatomite obtained from ADIL in Kariandusi, Gilgil, Nakuru County, Kenya was uncalcined natural diatomite (KENSIL SSF grade) that is mainly used for filtration purposes. Washing the raw diatomite and treating it with 4M HNO_3 acid removed any impurities that might have been present; producing raw diatomite that was pure as supported by the XRD analysis data. The raw diatomite was a white powder in appearance with a particle size of <150 µm.

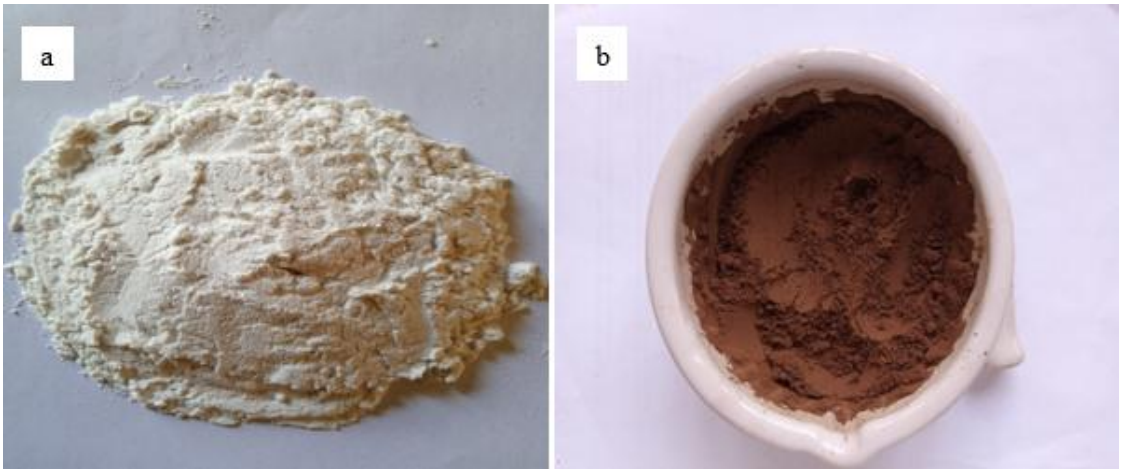

Figure 4.1: Showing as-received raw diatomite (a) and as-synthesized MnO_2-diatomite composite 2 (b).

MnO_2-diatomite composite was prepared by room temperature reduction of $KMnO_4$ under acidic conditions using concentrated HCl acid. Two MnO_2-diatomite composites were prepared by varying the concentration of $KMnO_4$ used while holding the HCl acid concentration and diatomite mass constant. MnO_2-diatomite composite 1 was prepared using 0.1M $KMnO_4$ while MnO_2-diatomite composite 2 was prepared using 0.05M $KMnO_4$ solution. Studies by Dang *et al*. (2013) and Barai *et al*. (2016) indicated that the acidic reduction of $KMnO_4$ led to the following chemical reactions.

$$2KMnO_{4\,(aq)} + 16HCl_{\,(aq)} \longrightarrow 2KCl_{(aq)} + 2MnCl_{2(aq)} + 8H_2O_{(l)} + 5Cl_{2(g)} \quad (4.1)$$

$$2KMnO_{4\,(aq)} + 3\,MnCl_{2\,(aq)} + 2H_2O_{(l)} \longrightarrow 5MnO_{2(s)} + 2KCl_{(aq)} + 4HCl_{2(aq)} \quad (4.2)$$

The formation of MnO_2-diatomite composites involved the acidic reduction of $KMnO_4$ solution to form $MnCl_2$ salt (Eq 4.1). The $MnCl_2$ salt formed was further oxidized to MnO_2 by the excess $KMnO_4$ solution (Eq 4.2). The MnO_2 nanoparticles produced were deposited on the raw diatomite to form MnO2-diatomite composite. Upon addition of concentrated HCl acid into the $KMnO_4$-diatomite mixture, the solution became dark brown in colour and chlorine vapours were produced. The time to reaction completion was based on the cessation of emission of chlorine gas. After filtering from the acid, washing thoroughly with distilled water, drying and crushing, a dark brown powder of MnO_2-diatomite composite was obtained.

4.1.2 Characterization of the Adsorbents

4.1.2.1 Fourier Transform Infrared Spectroscopy (FT-IR)

FT-IR spectral analysis was carried out in order to identify the functional groups present in the adsorbents that might be involved in the adsorption process. The spectrum was obtained in the wave number range from 400 cm^{-1} to 4000 cm^{-1}. The FT-IR spectrum of raw diatomite is presented in Figure 4.2. Raw diatomite had absorption bands which are characteristic of diatomite at around 3995.71 cm^{-1}, 3463.34 cm^{-1}, 3406.44 cm^{-1}, 2926.14 cm^{-1}, 2859.59 cm^{-1}, 1650 cm^{-1}, 1088.86 cm^{-1}, 791.81 cm^{-1}, 618.21 cm^{-1} and 476.44 cm^{-1}. The broad absorption band observed at 3700 cm^{-1}-3300 cm^{-1} was due to overlap of the -OH stretching vibration modes of hydrogen-bonded water molecules and also SiO-H stretching of surface silanols hydrogen-bonded to water molecules (Gómez *et al*., 2015; Chaudhry *et al.,* 2016).

The broad band observed at 3463.34 cm^{-1} was attributed to the asymmetrical and symmetrical stretching vibration modes of -OH group while the peak at 1650 cm^{-1} corresponds to bending vibrations of -OH group from the physically adsorbed water in diatomite (Wang *et al.,* 2014; Du *et al.,* 2015; Chaudhry *et al.,* 2016). The simultaneous presence of both of these absorption bands clearly indicates the existence of adsorbed water molecules in the raw diatomite matrix. The weak peak at 2380.26 cm^{-1} corresponded to stretching vibration of Si-H bonds (Rezig and Hadjel, 2015). The absorption band at 3995.71 was ascribed to stretching vibration modes of free surface silanol groups (Chaudhry *et al.,* 2016; Hernández-Ávila *et al.,* 2017). The presence of silica (SiO_2) in the raw diatomite was verified by absorption bands at 1088.86 cm^{-1} and

476.44 cm^{-1} in the spectrum which are attributed to the siloxane (Si-O-Si) asymmetric stretching and bending vibration modes respectively. In addition, the absorption bands at 618.21 cm^{-1} and 719.81 cm^{-1} correspond to stretching vibrational modes of Al-O-Si bond in diatomite (Wang *et al.,* 2014; Du *et al.,* 2015; Akafu *et al.,* 2019).

The weak absorption bands at 2926.14 cm^{-1} and 2859.59 cm^{-1} were ascribed to asymmetric and symmetric stretching of the alkyl (C–H) group respectively while the peak at 2013.77 cm^{-1} was ascribed to stretching of the C≡C group. These peaks were as a result of the presence of organic matter impurities in the raw diatomite (Zhang *et al.,* 2019; Aroke *et al.,* 2013). The FT-IR spectrum confirmed that the raw diatomite was mainly composed of silica which is in agreement with studies done by Wang *et al.* (2014). The presence of siloxane (-Si-O-Si-) groups bridged with oxygen atoms and also -OH groups from both hydrogen-bonded water molecules and isolated or hydrogen-bounded silanol (-SiOH) groups act as the main adsorption sites on the diatomite surface (Zhao *et al.,* 2019). The FT-IR data for raw diatomite is in agreement with studies by Muntean *et al*. (2023) and Akafu *et al*. (2019) for diatomite from Ghidirim village, republic of Moldova and Bedele brewery in Oromia Regional State in Ethiopia respectively.

After the MnO_2 modification processes, the characteristic bands of diatomite displayed changes in their intensities and positions which was assigned to the interaction effect of the loaded MnO_2 nanoparticles with diatomite. Figure 4.3 shows the FT-IR spectrum for MnO_2-diatomite composite. The spectrum for MnO_2-diatomite composite had six main absorption peaks at 3419.94 cm^{-1}, 1636.67 cm^{-1}, 1094.65 cm^{-1}, 800.49 cm^{-1}, 466.79 cm^{-1} and 456.79 cm^{-1}. For MnO_2-diatomite composite, there was an increase in the intensity and a shift of peaks corresponding to -OH group to lower frequencies of 3419.94 cm^{-1} and 3409.33 cm^{-1} for -OH stretching and 1636.67 cm^{-1} for -OH bending vibration modes of hydrogen-bonded water compared to those of raw diatomite. The bands at 1094.65 cm^{-1}, 466.76 cm^{-1} and 456.79 cm^{-1} were attributed to the asymmetric stretching and bending vibration modes of siloxane (Si-O-Si) group respectively (Akafu *et al.,* 2019).

The peak at 800.49 cm^{-1} was ascribed to the symmetric stretching of Si-O-Al group. This bands indicate the presence of silica and alumina in the MnO_2-diatomite

composite. There was a disappearance of peaks at 2926.14 cm^{-1} and 2859.59 cm^{-1} related to C-H stretching due removal of organic impurities after HCl acid treatment of diatomite during diatomite modification by acid reduction of $KMnO_4$. The peak at 2373.51 cm^{-1} corresponded to stretching vibration of Si-H bonds (Rezig and Hadjel, 2015). A new weak peak was observed at 2284.78 cm^{-1} in MnO_2-diatomite composite. This peak together with peak at 2150.72 cm^{-1} might be due to O-H stretching and bending vibrations of water bound to the manganese oxide structure (Chaudhry *et al.,* 2016) in the MnO_2-diatomite composite. The formation of a new peak inform of a shoulder at 550 cm^{-1} was attributed to stretching modes of Mn-O (Du *et al.,* 2015; Chaudhry *et al.,* 2016) indicating the presence of MnO_2 in the composite. The FT-IR spectrum for MnO_2-diatomite composite was similar to the spectrum reported by Khataee *et al*. (2015) and Du *et al*. (2015).

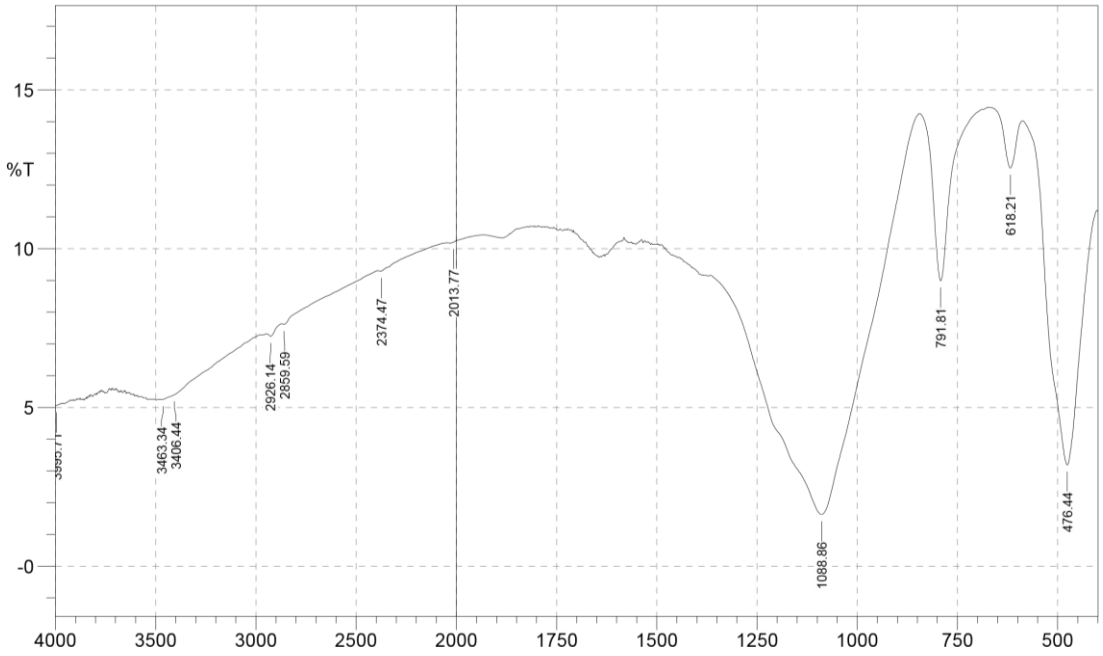

Figure 4.2: FT-IR spectrum of raw diatomite.

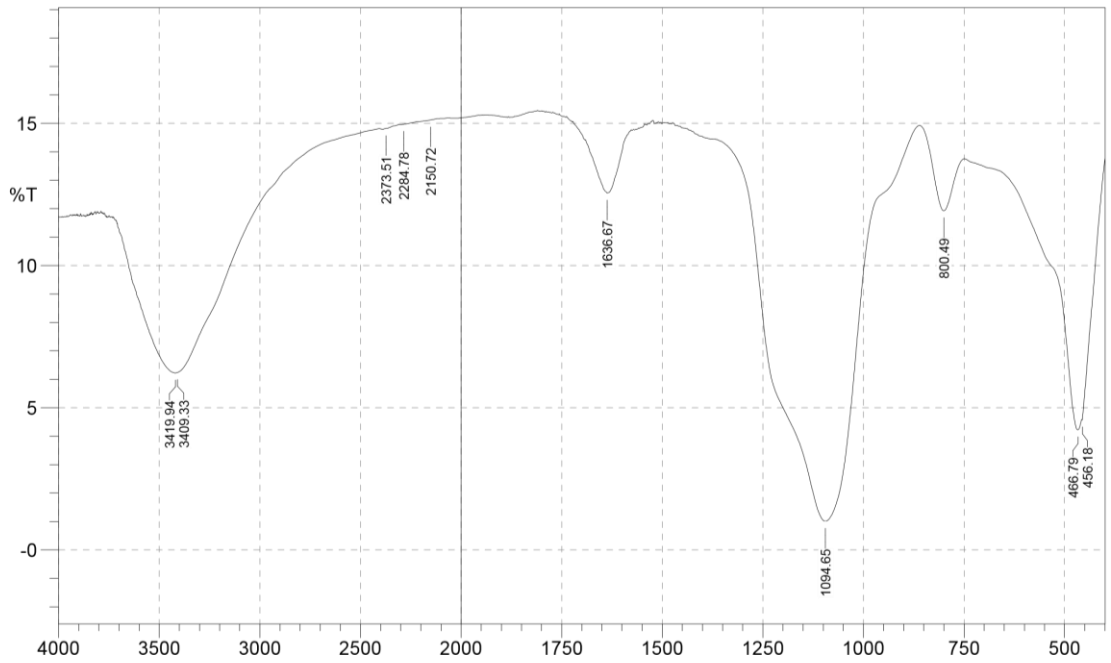

Figure 4.3: FT-IR spectrum of MnO_2-diatomite composite 2

4.1.2.2 XRF

The chemical composition of the raw diatomite and MnO_2-diatomite composites 1 and 2 were obtained by X-ray Fluorescence Spectrometer. The XRF analysis indicated that raw diatomite was mainly composed of silica (SiO_2), 90.73 %; alumina (Al_2O_3), 4.51%; iron oxide (Fe_2O_3), 1.53%; magnesium oxide (MgO), 1.33%; calcium oxide (CaO), 0.80%; potassium oxide, (K_2O), 0.69%, among other traces such as titanium (Ti), 0.14%, chlorine (Cl), 0.057% and manganese (Mn), 0.039%. The XRF studies proof that diatomite is mainly composed of silica and the results are in agreement with studies by Kipsanai (2017) and Flores-Cano *et al.* (2013) on diatomite from Kenya and Jalisco in Mexico respectively. Table 4.1 shows the chemical composition the adsorbents. The XRF data for raw diatomite mirrors those reported by Marczyk *et al.* (2020) and Wang *et al.* (2015) for diatomite from Carpathian Foothills in Poland and Tianjin Fengchuan Chemical technology in China respectively. Marczyk *et al.* (2020) observed that diatomite from Carpathian Foothills in Poland mainly composed of SiO_2 (81.57%), Al_2O_3 (11.01%), Fe_2O_3 (3.57%), K_2O (1.906%), MgO (1.045) among other minor metal oxides.

A slight change was observed in the chemical composition of diatomite upon the surface modification with MnO_2 particles. The chemical composition of MnO_2-

diatomite composites showed a higher content of manganese (5.56% for MnO_2-diatomite composites 1 and 4.73% for MnO_2-diatomite composites 2) than in raw diatomite. The high manganese content in MnO_2-diatomite composites compared to that of raw diatomite indicates that MnO_2 particles were incorporated into the diatomite structure during the modification process.

Table 4.1: Chemical composition (wt %) of raw diatomite and MnO_2/diatomite composites

	SiO_2	Al_2O_3	Fe_2O_3	MgO	CaO	K_2O	P_2O_5	Ti	Cl	Mn
Raw Diatomite	90.73	4.51	1.53	1.33	0.80	0.69	0.04	0.14	0.06	0.04
MnO_2-diatomite Composite 1	83.26	3.49	1.43	0.00	0.43	1.38	0.25	0.11	1.68	5.56
MnO_2-diatomite Composite 2	86.03	4.07	1.39	0.00	0.23	1.13	0.07	0.12	1.15	4.73

wt % - weight in percentage

Silica does not react with acids, therefore, the predominant constituent of MnO_2-diatomite composites 1 and 2 was silica occurring at 83.26% and 86.03% respectively. In addition, the MnO_2-diatomite composites also had a lower content of other oxides and elements present compared to raw diatomite as shown in table 4.1. This was mainly due to the dissolution of the oxides and elements in the HCl acid during the adsorbent modification process. The occurrence of alumina, iron oxide, magnesium oxide and calcium oxide in small amounts in both raw diatomite and MnO_2-diatomite composites indicate a low content of impurities that are usually in diatomite such as Kaolinite, feldspar and dolomite. Higher content of these impurities may lower the adsorption capacity of raw diatomite and MnO_2-diatomite composites (Marín-Alzate *et al.*, 2021).

Due to the use of $KMnO_4$ and HCl acid in the modification process, the amount of potassium and chlorine in the composites also increased. MnO_2-diatomite composites 1 had 1.38% K_2O, 1.68% chlorine while MnO_2-diatomite composites 2 had 1.13% K_2O and 1.15% chlorine compared to 0.69% K_2O and 0.06% chlorine for raw diatomite. Conversely, the decrease in the amount of silica and alumina in the MnO_2-diatomite composites 1 and 2 compared to raw diatomite may be due to their involvement in bonding with MnO_2. The XRF data for MnO_2-diatomite composites 1 and 2 were in agreement with findings reported by Pookmanee *et al*. (2012) and Vassileva *et al*. (2013). Pookmanee *et al*. (2012) observed that the chemical composition of manganese

oxide modified diatomite had higher content of MnO (11.86%) and a lower content of other oxides (46.1% SiO_2, 9.1% Fe_2O_3, 7.3% Al_2O_3) compared to natural diatomite (62.8% SiO_2, 11.4% Fe_2O_3, 9.7% Al_2O_3).

4.1.2.3 XRD

Powder X-ray diffraction (XRD) analysis was carried to identify the crystalline phase present in both raw diatomite and MnO_2-diatomite composites. The diffraction data were obtained by Rigaku Miniflex II desktop X-ray Diffractometer at the Geothermal Development Company (GDC) at Menengai Crater in Nakuru County. The XRD patterns were acquired by exposing the powder samples to Cu-Kα radiation (λ=1.540598 Å) at 30 kV and 15 mA between 3° to 90° (2θ range). Crystal impact match software with open reference database (COD-Inorganic 2023-06-06) was used for the mineral phase identification. Figures 4.4, 4.5 and 4.6 shows the XRD patterns for Raw diatomite and MnO_2-diatomite composites.

The diffraction patterns indicated that both raw diatomite and MnO_2-diatomite composites 1 and 2 mainly consists of amorphous silica (SiO_2) with a very small traces of crystalline phase of silica. This was due to lack of major peaks which showed that the samples were mainly amorphous in nature and poorly crystallized. The lack of other obvious diffraction peaks due to impurities also suggested that the raw diatomite was highly pure. In all the samples, the presence of an amorphous band in the range between 15° and 32° 2θ was associated with the glass formation of silica (Flores-Cano *et al.*, 2013). In raw diatomite, the small peaks at 21.68° and 22.76° 2θ were due to the presence of tridymite crystalline phase which is one of the polymorphs of SiO_2.

After the modification of diatomite with MnO_2 particles, no new characteristic peaks related to manganese oxide were observed in the pattern of both the as prepared MnO_2-diatomite composites. This indicates that the MnO_2 formed is amorphous or had low crystallinity due to the lack of distinct intense peaks. A very small quantity of tridymite crystalline phase was still present in the MnO_2-diatomite composites with tiny peaks at 21.50°, 22.88° for MnO_2-diatomite composite1 and 22.0°, 23.06° for MnO_2-diatomite composite 2. The XRD pattern of raw diatomite was very similar to that reported by Li *et al.* (2018) for diatomite from Jilin Province in China. In their study, they reported

that the raw diatomite from Jilin Province in China only had a broad band at around 22.5° due to the presence of amorphous silica and the lack of other peaks was due to high purity of their diatomite sample. The XRD patterns for MnO_2-diatomite composites 1 and 2 were also similar to that reported by Li *et al.* (2014). In their study, Li and his co-workers observed that no obvious peak related to Mn was found after coating diatomite with MnO_2 particles, therefore, they concluded that the MnO_2 particles deposited on the diatomite surface were amorphous.

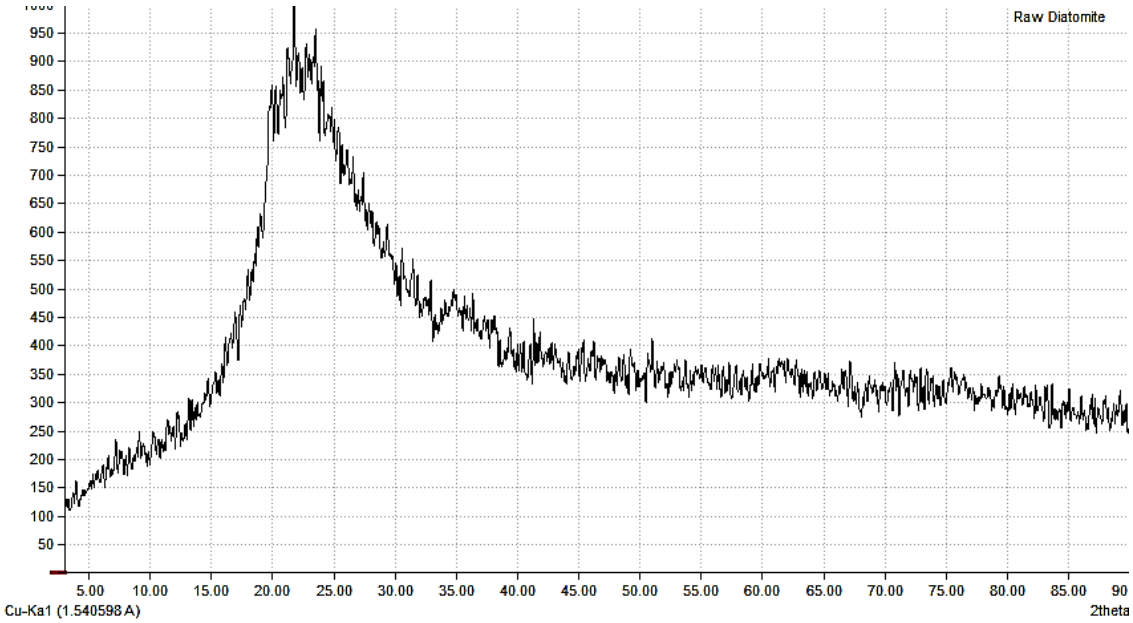

Figure 4.4: XRD pattern of Raw diatomite.

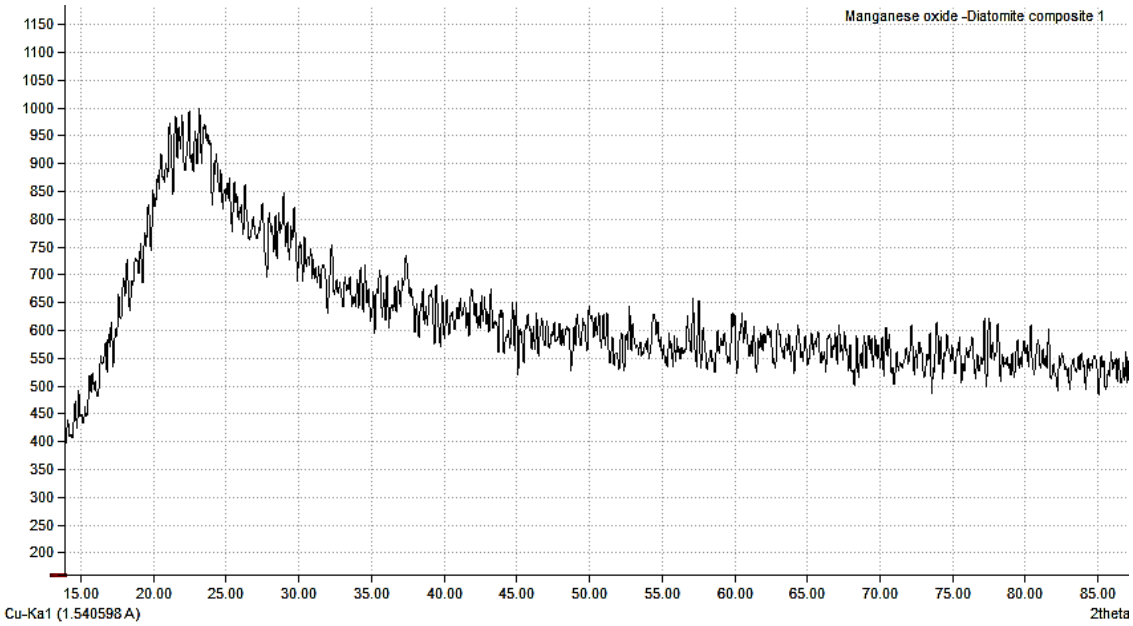

Figure 4.5:XRD pattern of MnO_2-diatomite composite 1.

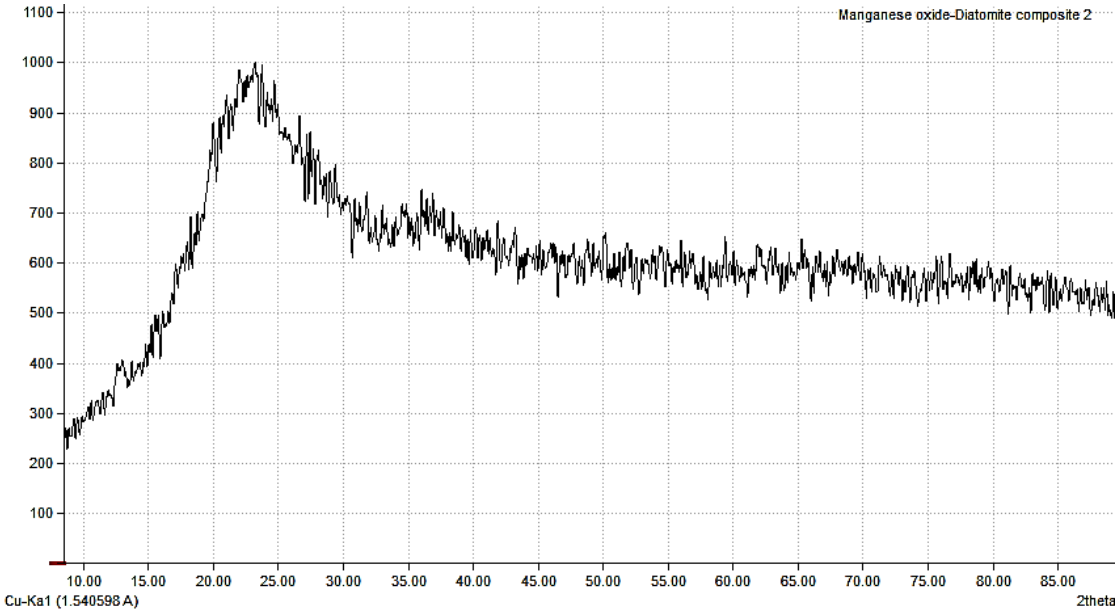

Figure 4.6: XRD pattern of MnO_2-diatomite composite 2.

4.1.2.4 BET and BJH

The surface area and porosity of any adsorbent greatly influences their adsorption capacity, therefore, the specific surface area, pore volume and pore diameter of the adsorbents were determined in this study. The surface area of the adsorbents was determined by BET method while the pore volume and diameter were determined by BJH method. The BJH pore size distributions were calculated from the desorption branches of the nitrogen sorption isotherms. Figures 4.7 and 4.8 show the N_2 adsorption-desorption isotherms and the corresponding pore-size distributions of raw diatomite and MnO_2-diatomite composite 2.

According to the International Union of Pure and Applied Chemistry (IUPAC) classification (Sing *et al.*, 1985), the N_2 adsorption-desorption isotherms of both raw diatomite and MnO_2-diatomite composite 2 were of type IV with a H3 type hysteresis loop (at about 0.50-0.99 relative pressure, P/Po) due to capillary condensation, indicating the presence of mesopores with a nonuniform size. This was confirmed by their broad BJH pore size distribution plots calculated from the desorption branches of the nitrogen sorption isotherms as shown in figure 4.8. This indicated that both raw diatomite and MnO_2-diatomite composite 2 had mesoporous structure with pore diameters of 16.38nm and 11.54nm respectively.

The BET surface area (S_{BET}) for raw diatomite was 32.29 m^2/g while that for MnO_2-diatomite composite 2 was 30.48 m^2/g. The average BJH pore volume and pore size for raw diatomite were 0.1105 cm^3/g and 16.38 nm respectively compared to 0.0792 cm^3/g and 11.54 nm for MnO_2-diatomite composite 2. Similar observations were observed by Muntean *et al.* (2023) and Du *et al.* (2014) for raw diatomite and MnO_2 nanowires-diatomite composite respectively. Muntean *et al.* (2023) reported that diatomite from Ghidirim village in Republic of Moldova had mesoporous structure with a pore volume and pore diameter of 0.080 cm^3 and 5.7 nm. The diatomite also had a specific surface area of 36 m^2/g.

Both the mesopores of the raw diatomite reduced after manganese oxide deposition onto the diatomite surface during the modification process. This suggests that the porous structure of diatomite changed upon manganese oxides deposition onto its surface (Zhang *et al.,* 2020). This was confirmed by the decrease in the pore volume and pore size of MnO_2-diatomite composite 2 (0.0792 m^3/g; 11.54nm) compared to raw diatomite (0.1105 m^3/g; 16.38 nm) respectively. Table 4.2 shows the textural parameters of both raw diatomite and MnO_2-diatomite composite 2.

Table 4.2: Textural parameters of raw diatomite and MnO_2-diatomite composite

Adsorbent	Surface area (S_{BET})(m^2/g)	Pore Area (m^2/g)		Pore Volume (m^3/g)		Pore Size (nm)
		Micropore (t-plot)	Mesopore (BJH)	Micropore (t-plot)	Mesopore (BJH)	(BJH)
Raw diatomite	32.29	11.14	27.15	0.00212	0.1105	16.38
MnO_2-diatomite composite 2	30.48	9.53	27.57	0.00134	0.0792	11.54

From the BET and BJH analysis, it is evident that the surface area and porosity of raw diatomite was higher than that of MnO_2-diatomite composite 2. This was due to the filling and blockage of pores on the diatomite surface by MnO_2 particles during the modification process. Similar observations were reported by Rao *et al.* (2019) during the synthesis of doped MnO_2-diatomite composite for catalysis ozone decomposition. In their study, the surface area of diatomite reduced after MnO_2 loading and attributed this reduction in surface area to the filling of cavities or channels on the diatomite

surface with MnO_2 particles. This shows that the surface area of diatomite can reduce during the surface modification with MnO_2.

Zhang *et al.* (2020) reported similar observations during the synthesis of manganese dioxide-loaded biochar. In their study, the BET surface area, total pore volume and pore diameter decreased from 181 m^2/g, 0.25 cm^3/g and 3.7 nm to 12.5 m^2/g, 0.03 cm^3/g and 2.0 nm respectively when the MnO_2 loading was increased from 18.4% to 30.2%. They attributed the decrease in surface area, pore volume and pore diameter to excessive deposition of MnO_2 nanoparticles leading to pore blockage and destruction of some micropore structure. Wang *et al.* (2015) synthesized MnO_2 biochar (BC MnO_2) by room temperature reaction of potassium manganate (VII) with manganese chloride. In their study, they attributed the decreased surface area of MnO_2 biochar in comparison to their other adsorbent ($BCMnSO_4$) to the scattering of manganese oxide particles in the micropores blocking part of the pores resulting in reduced surface area and pore volume.

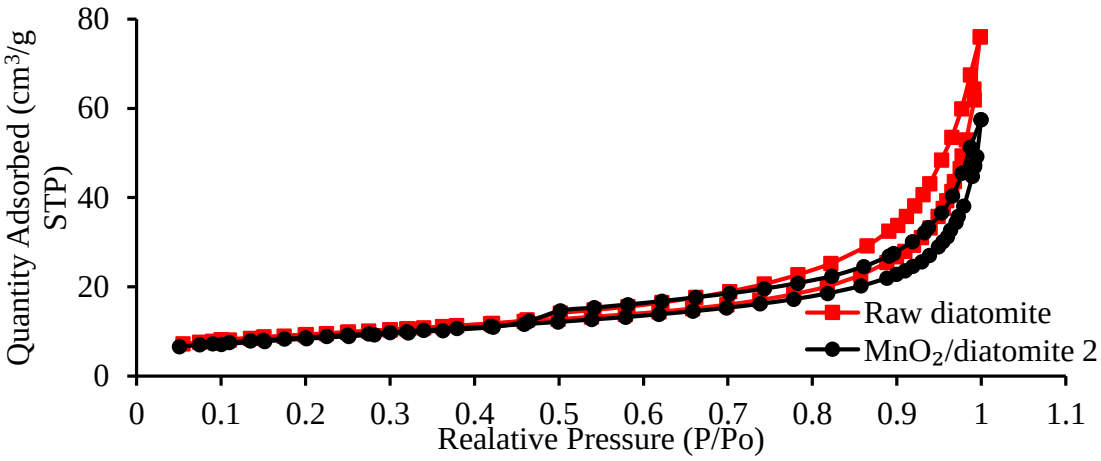

Figure 4.7: N_2 adsorption-desorption isotherms for raw diatomite and MnO_2-diatomite composite 2.

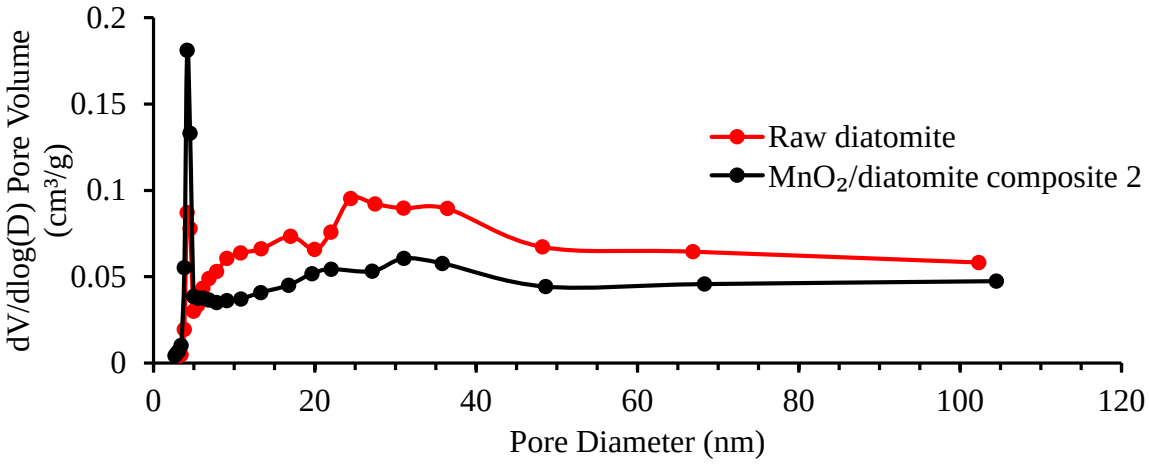

Figure 4.8: Pore size distribution plots for raw diatomite and MnO_2-diatomite composite calculated from the desorption branches of the nitrogen sorption isotherms.

4.2 Single Ion Adsorption Studies

4.2.1 Effect of $KMnO_4$ Concentration on MnO_2 Loading onto Diatomite.

In order to investigate the effect of $KMnO_4$ concentration on the MnO_2 loading onto diatomite, different concentrations of $KMnO_4$ were used while the concentration of HCl was held constant at 6M. During the synthesis, 0.1M $KMnO_4$ was used to prepare MnO_2-diatomite composite 1 and 0.05M $KMnO_4$ was used to prepare MnO_2-diatomite composite 2. Both preparations were done at room temperature. It was observed that a high concentration of $KMnO_4$ lead to more MnO_2 loading onto the diatomite surface as supported by the XRF analysis of the MnO_2-diatomite composites. From the XRF studies, MnO_2-diatomite composite 1 had a higher manganese content than MnO_2-diatomite composite 2. Since both the MnO_2-diatomite composites had amorphous MnO_2 as supported by the XRD analysis, then the solution temperature had no effect on the crystalline phase of the MnO_2 composited synthesized.

The MnO_2-diatomite composite samples were compared for their effectiveness in the removal of both of Pb (II) and Cd (II) ions in order to select the MnO_2-diatomite composite with the highest efficiency removal. During the analysis, 0.1 g of each adsorbent was placed in contact with 50 mg/L of Pb (II) and Cd (II) ions at 25±2 ^oC for 1 hour. The pH of the solutions was varied between 4 and 6. Low pH values were not considered due to high competition for adsorption sites between the metal ions and hydrogen ions. In addition, pH values higher than 6 were not used since Pb (II) ions

would precipitate out inform of $Pb(OH)_2$. Figure 4.9 shows the percentage removal of Pb (II) and Cd (II) ions by MnO_2-diatomite composites 1 and 2 verses pH. As shown in figure 4.9, MnO_2-diatomite composite 2 had a higher percentage removal of both Pb (II) and Cd (II) ions at all the pH values than MnO_2-diatomite composite 1.

This was attributed to a high number of adsorption sites on the MnO_2-diatomite composite 2 surface compared to MnO_2-diatomite composite 1. This was mainly due to the filling and blocking of the pores and channels on the diatomite surface by MnO_2 particles and this blocking effect was more at higher concentration of $KMnO_4$ used (Rao *et al.,* 2019). This led to decreased surface area and porosity of MnO_2-diatomite composites as supported by the BET/BJH data. According to the BET/BJH data, MnO_2-diatomite composite 2 had a lower surface area of 30.48 m^2/g compared to raw diatomite with a surface area of 32.29 m^2/g.

Similar results were obtained by Rao *et al.* (2019). In their study, the surface area of diatomite reduced after MnO_2 loading and attributed this reduction in surface area to the filling of cavities or channels on the diatomite surface with MnO_2 particles. This shows that the surface area of diatomite may be reduce upon surface modification. Han *et al*. (2012) investigated the effect of $KMnO_4$ concentration on the structure and electrochemical behaviour of MnO_2 and reported that increase in $KMnO_4$ concentration led to formation of more MnO_2 particles especially MnO_2 particles that had high crystalline structure. At low $KMnO_4$ concentration, MnO_2 particles with weakly crystallized structure were formed. This shows that the concentration of $KMnO_4$ greatly influences the amount of MnO_2 formed. Due to the high removal efficiency of Pb (II) and Cd (II) by MnO_2-diatomite composite 2, it was selected for use in the batch adsorption studies and referred to as MnO_2-diatomite composite.

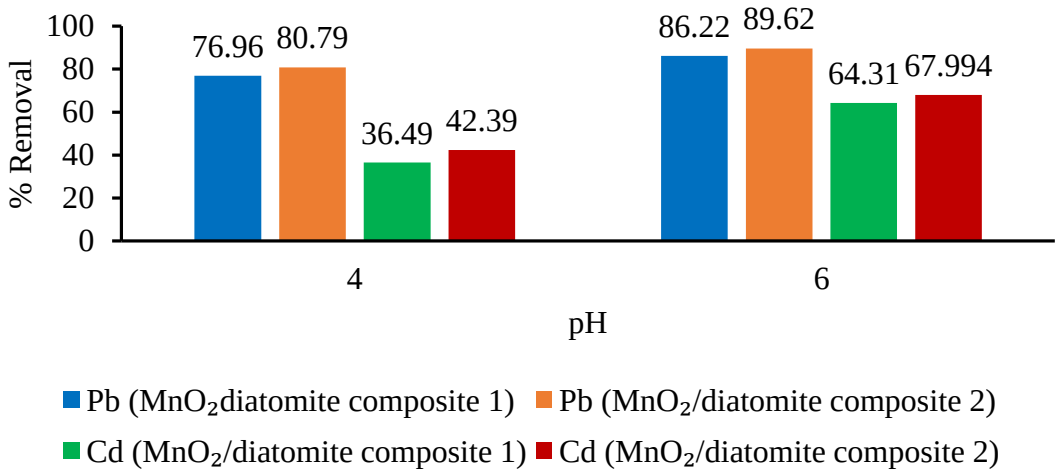

Figure 4.9: Percentage removal of Pb (II) and Cd (II) ions by MnO_2-diatomite composites 1 and 2 at different pH values.

4.2.2 Effect of Initial Metal Ion Concentration on the Adsorption of Pb (II) and Cd (II) Ions

The adsorption of heavy metal ions greatly depends on the initial concentration of the metal ions. To investigate the effect of initial metal ion concentration, the concentrations were varied from 10 mg/L to 70 mg/L for both Pb (II) and Cd (II). In the experiments, 50ml solutions of different metal ion concentrations (10, 20, 30, 40, 50, 60 and 70 mg/L) were brought into contact with 2 g/L of adsorbent for 60 minutes. Other parameters were held constant (pH of 4 for Pb (II) and pH of 6 for Cd (II); shaking speed of 240 rpm; temperature of 25±2 ^{o}C). Figures 4.10 and 4.11 show the effect of initial metal ion concentration on the removal of Pb (II) and Cd (II) ions respectively.

It is evident from figure 4.10 that increase in initial concentration of Pb (II) from 10 mg/L to 70 mg/L resulted in the decrease in the percentage removal of Pb (II) from 99.21% to 97.89% for raw diatomite and from 93.20% to 49.16% for MnO_2-diatomite composite. These were mainly due to the presence of sufficient adsorption sites available for adsorption at lower initial concentrations thus leading to higher efficiency (Ushakumary, 2013). At higher initial concentrations, most of active binding sites on the adsorbents surface were saturated leading lower efficiencies. However, the adsorption capacity of Pb (II) increased from 4.961 mg/g to 34.264 mg/g for raw diatomite and form 4.66 mg/g to 17.21 mg/g for MnO_2-diatomite composite when the initial concentration of Pb (II) was increased from 10 mg/L to 70 mg/L. This was attributed to the increased rate of mass transfer due to the increased diffusivity of the

driving force (Gebretsadik *et al.*, 2020). These results mirror those obtained by Sun *et al*. (2019) and Chaudhry *et al.* (2016) on the adsorption of lead using raw diatomite and manganese oxide coated sand respectively.

The trend for Cd (II) using both adsorbents was similar to that of Pb (II). From figure 4.11 it was observed that, increasing the initial concentration of Cd (II) from 10 mg/L to 70 mg/L resulted in a decrease in the percentage removal of Cd^{2+} from 90.82% to 57.35% for raw diatomite and 83.45% to 35.38% for MnO_2-diatomite composite. This was attributed to availability of binding sites on the adsorbents at low metal ion concentrations while at higher concentrations, the amount of heavy metal ions is relatively higher compared to available adsorption sites (Thakur and Parmar, 2013).

The adsorption capacity of Cd (II) ions however, increased from 4.541 mg/g to 20.074 mg/g for raw diatomite and 4.173 mg/g to 12.383 mg/g for MnO_2-diatomite composite when concentrations were increased from 10mg/L to 70mg/L. According to Ouyang *et al.* (2019), the increased adsorption capacity at higher concentrations was due to enhanced driving force at the solid-liquid interface until the adsorption sites were saturated. Similar trends were observed by Thakur and Parmar (2013) for adsorption of Cu^{2+}, Ni^{2+} and Zn^{2+} from synthetic waste water by tea waste adsorbent and Dargahi *et al.* (2016) for removal of lead and chromium from aqueous solutions using magnesium oxide nanoparticles.

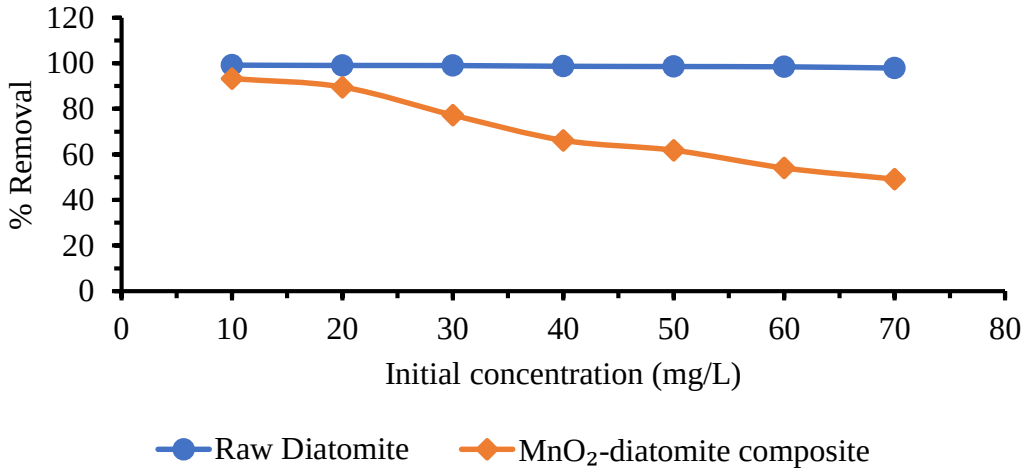

Figure 4.10: Effect of initial metal ion concentration on the adsorption of lead ions using raw diatomite and MnO_2-diatomite composite. (Contact time 60 minutes; pH of 4; adsorbent dosage 2 g/L; temperature 25±2 ^oC; shaking speed 240 rpm)

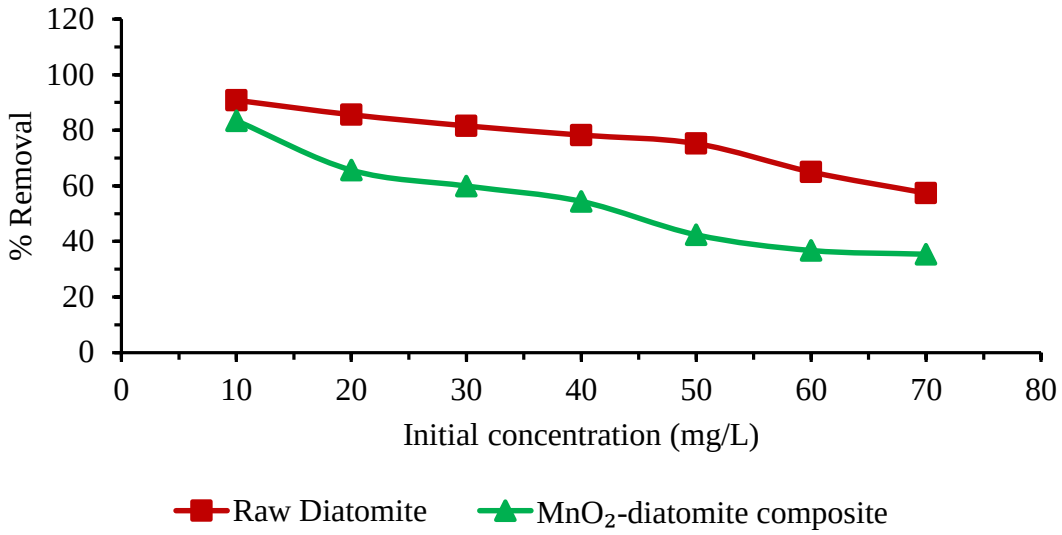

Figure 4.11: Effect of initial metal ion concentration on the adsorption of cadmium ions using raw diatomite and MnO_2-diatomite composite. (Contact time 60 minutes; pH of 6; adsorbent dosage 2 g/L; temperature 25±2 ^oC; shaking speed 240 rpm)

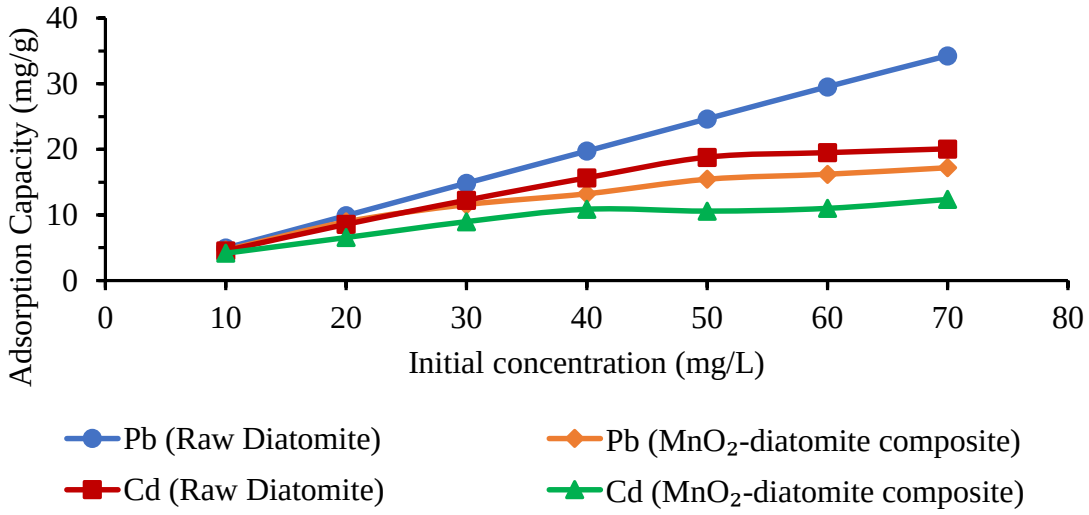

Figure 4.12: Effect of initial metal ion concentration on the adsorption capacity of Pb (II) and Cd (II) ions using raw diatomite and MnO_2-diatomite composite. (Contact time 60 minutes; adsorbent dosage 2 g/L; temperature 25±2 ^oC; shaking speed 240 rpm; pH of 4 for lead and pH of 6 for cadmium)

4.2.3 Effect of pH on the Adsorption of Pb (II) and Cd (II) Ions

The pH of the solution is one of the most important parameters affecting the adsorption process. As it is known, the pH value of a solution greatly influences the chemical speciation of the metal ions in sorbate and also the ionization of functional groups on the adsorbent surface (Abbar *et al.*, 2017). Therefore, a change in the pH value could

cause a change in the adsorption capacity. According to Bilgin and Tulun (2015), the hydroxyl groups on the diatomite surface may gain or lose a proton by changing the solution pH. The diatomite surface therefore acquires a net positive charge when the surface gains a proton at low pH.

$$\text{-Si-OH} + H^+ \longrightarrow \text{-Si-OH}_2^+ \quad (4.2)$$

The hydroxides on the surface lose a proton at higher pH values and the surface is charged negatively.

$$\text{-Si-OH} + OH^- \longrightarrow \text{-Si-O}^- + H_2O \quad (4.3)$$

At low pH values, the hydrogen ions could strongly compete with the heavy metal ions and saturate the active binding sites on the adsorbent surface thereby reducing the adsorption of the metal ions (Ouyang *et al.,* 2019: Abbar *et al.,* 2017: Ngugi, 2015). The effect of pH on the removal efficiency of Pb (II) and Cd (II) using raw diatomite and MnO_2-diatomite composite were studied by varying the pH from 2 to 6. The adsorbent dosage, contact time, shaking speed and temperature were held constant at 2 g/L, 60 minutes, 240 rpm and 25±2^oC respectively. Optimal initial concentration of metal ions was used as 10mg/L for both Pb (II) and Cd (II).

4.2.3.1 Effect of pH on Adsorption of Pb (II) Ions

Figure 4.13 represents a plot of percentage removal of Pb (II) ions against pH values. It was observed that a gradual increase in the removal of Pb (II) ions from 77.22% to 99.21% occurred when the pH of the solution was increased from 2 to 4 using raw diatomite composite. This was attributed to the saturation of active binding sites with hydrogen ions at low pH and also due to the competition for the active binding sites between hydrogen ions and Pb (II) ions at low pH values leading to low adsorption of Pb (II)ions. Optimum adsorption of Pb (II) ions was observed at pH 4 with a percentage removal of 99.21% and a maximum adsorption capacity of 4.961 mg/g for raw diatomite. Further increase in pH from 4 to 6 led to a slight decrease in Pb (II) ions removal from 99.21% to 98.93% when using raw diatomite as adsorbent because hydrolysis and precipitation begin to play an important role in the adsorption of lead (Salman *et al.,* 2015). Similar trends were observed by El Sayed (2018) and Salman *et al.,* (2015) on using diatomite as an effective adsorbent for heavy metals.

When MnO_2-diatomite composite was used, increase in pH showed a gradual increase in the percentage removal of Pb (II) ions from 65.65% at pH 2 to 89.19, 93.20%, 97.00% and 98.42% at pH of 3,4,5 and 6 respectively. The increased uptake of Pb (II) ions mainly originated from the enhanced deprotonation of MnO_2-diatomite composite surface with increasing pH values of the solution. The maximum adsorption of Pb (II) ions was observed at pH 6 with a percentage removal of 98.37% for MnO_2-diatomite composite. Similar results were obtained by Huo and Xiao (2014) who used manganese oxides for adsorption of lead. They attributed the increased removal of lead at higher pH values to the less competition for adsorptive sites between metal ions and protons.

The maximum adsorption capacity of Pb (II) ions was 4.961 mg/g and 4.921 mg/g for raw diatomite and MnO_2-diatomite composite at pH of 4 and 6 respectively. Based on these results, both raw diatomite and MnO_2-diatomite composite exhibited good capacity for removal of Pb (II) ions from solution at optimum pH values of 4 and 6 respectively. pH values between 2 and 6 were only considered in this study because at higher pH values, the precipitation of Pb (II) ions inform of metal hydroxide would have been the dominant mechanism in the metal removal process. This condition is often not desirable since the metal precipitation could lead to a misunderstanding of the adsorption capacity (Francis, 2015). In addition, diatomite is unstable at higher pH values because the silica present in diatomite dissolves in alkaline solution (El Sayed, 2018).

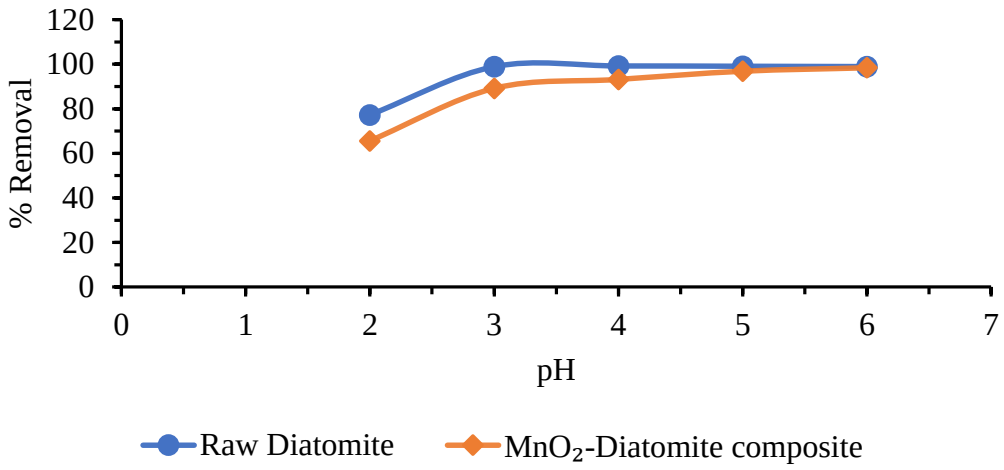

Figure 4.13: The effect of pH on the adsorption of Pb (II) ions using raw diatomite and MnO_2-diatomite composite. (Adsorbent dose: 2 g/L; contact time 60 minutes; temperature 25±2 ^oC; shaking speed 240 rpm; initial concentration 10 mg/L)

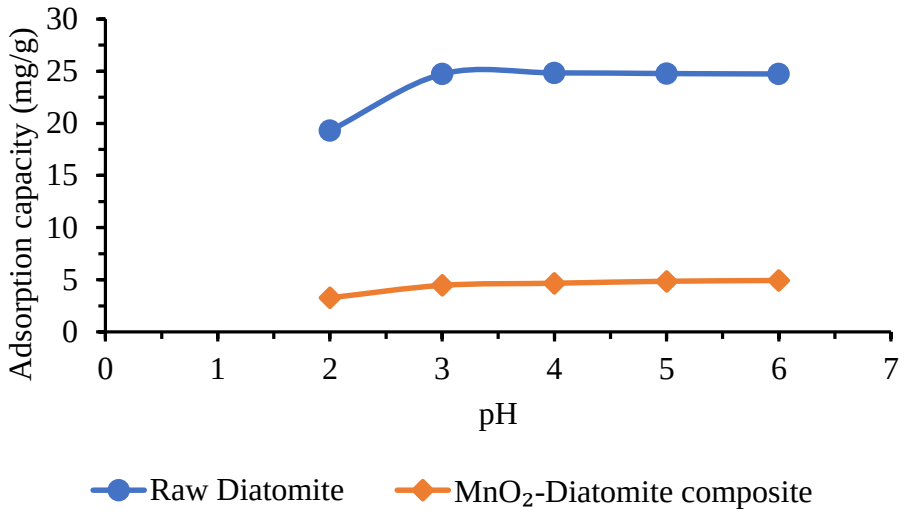

Figure 4.14: The effect of pH on the adsorption capacity of Pb (II) ions using raw diatomite and MnO_2-diatomite composite. (Adsorbent dose: 2 g/L; contact time 60 minutes; temperature 25±2 ^oC; shaking speed 240 rpm; initial concentration 10 mg/L).

4.2.3.2 Effect of pH on Adsorption of Cd (II) Ions

The solution pH greatly influenced the percentage removal of Cd (II) ions using raw diatomite and MnO_2-diatomite composite as adsorbents. A general increase in adsorption of Cd (II) ions with increasing pH of solution was observed for both raw diatomite and MnO_2-diatomite composite. The percentage removal of Cd (II) ions using raw diatomite increased from 57.07% at pH of 2 to 69.74%, 77.93%, 84.53% and 90.80% at pH 3,4,5 and 6 respectively. Similarly, the percentage removal of Cd (II) ions increased from 38.43% at pH 2 to 83.45% at pH 6 for MnO_2-diatomite composite.

The adsorption capacity of Cd (II) ions increased from 2.854 mg/g at pH of 2 to 4.54 mg/g at pH of 6 for raw diatomite while for MnO_2-diatomite composite it increased from 1.922 mg/g at pH 2 to 4.172 mg/g at pH 6. Figure 4.15 shows a plot of percentage removal of Cd (II) ions against pH values for raw diatomite and MnO_2-diatomite composite. A similar behaviour was reported by Flores-Cano *et al.* (2013) and Safa *et al.* (2012) for the uptake of Cd (II) and other metal ions using diatomite. Sun *et al.* (2019) reported as similar trend of Pb (II)and Cd (II) removal using nanostructured silicates on diatomite.

According to ElSayed (2018) and Sun *et al*. (2019), the active binding sites protonated at low pH values leading to electrostatic repulsion between the adsorbent surface and positively charged metal ions. This hinders the access of the metal ions to the surface functional groups. High concentration of hydrogen ions in the solution at low pH values may also have triggered competition for adsorption sites between the heavy metal ions and hydrogen ions, leading to low metal ion adsorption (Zhang *et al.,* 2020). However, this competition decreased with increasing pH values leading to enhanced metal ion adsorption on the adsorbents. Only pH values below 6 were considered in this study due to precipitation of metal ions inform of metal hydroxides at higher pH values above 6 and also due to deterioration of the diatomite structure through dissolving of silica in alkaline solutions (ElSayed, 2018).

Similar observations were reported by Flores-Cano *et al*. (2013) and Sun *et al*. (2019) for the adsorption of Cd (II) ions using diatomite and nanostructured silicates on diatomite respectively. Flores-Cano *et al*. (2013) observed that the adsorption capacity for Cd (II) ions onto diatomite augmented 6.3 times when the pH was raised from 4 to 7 and ascribed it to decrease in repulsion of Cd (II) ions by the diatomite surface as the surface charges on diatomite reduced with increasing pH.

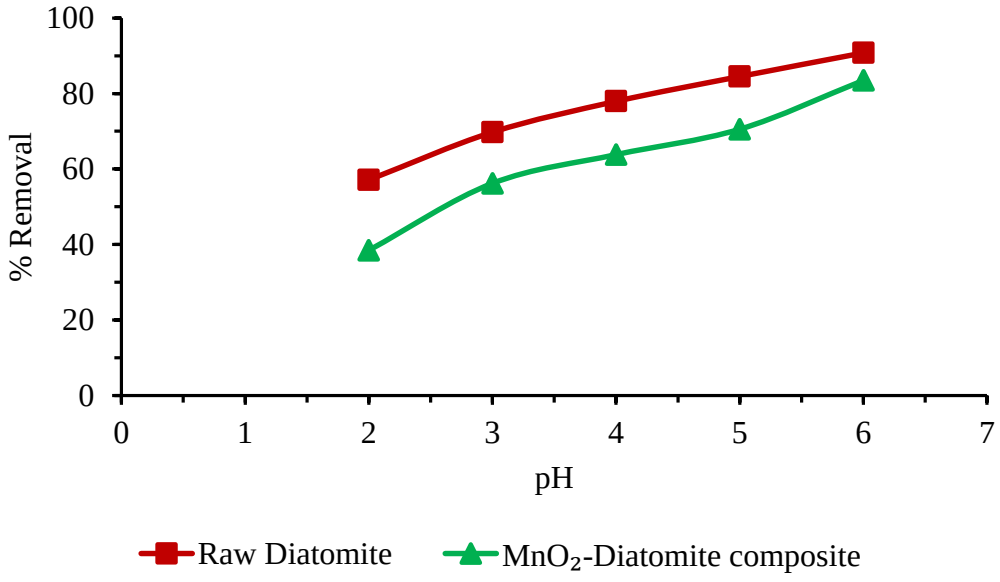

Figure 4.15: The effect of pH on the adsorption of cadmium ions using raw diatomite and MnO_2-diatomite composite. (Adsorbent dose: 2g/L; initial metal ion concentration 10 mg/L; contact time 60 minutes; shaking speed 240 rpm; temperature 25±2 ^{o}C).

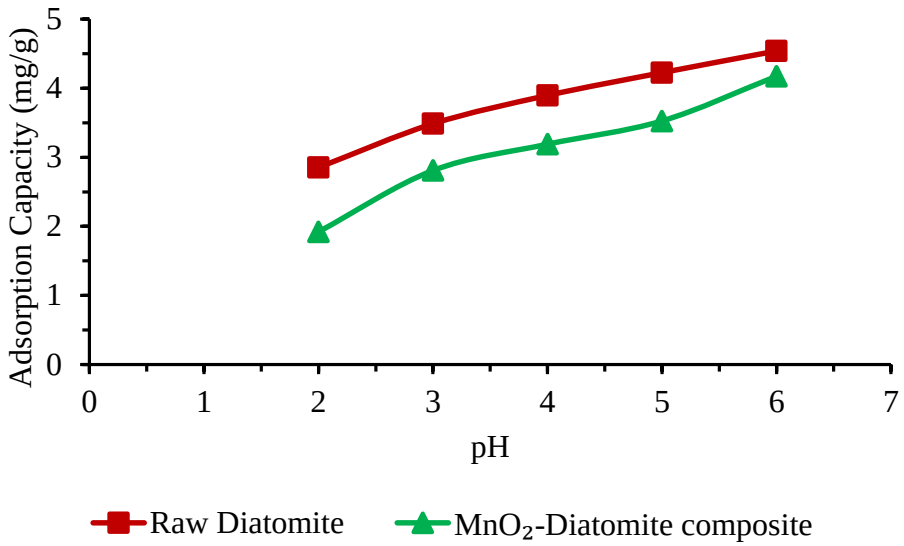

Figure 4.16: The effect of pH on the adsorption capacity of cadmium ions using raw diatomite and MnO_2-diatomite composite. (Adsorbent dose: 2 g/L; initial metal ion concentration 10 mg/L; temperature 25±2 ^oC; contact time 60 minutes; shaking speed 240 rpm)

4.2.4 Effect of Contact Time on the Adsorption of Pb (II) and Cd (II) Ions

Contact time is an important parameter that greatly influences the adsorption process. Hence, monitoring the effect of contact time and the determination of the equilibrium time helps in modelling the adsorption experiments. The effect of contact time on the adsorption of Pb (II) and Cd (II) ions was studied at different contact times in the range of 20 min to 140 min at optimal initial concentrations (10 mg/L) and pH (pH of 4 and 6 for Pb (II) using raw diatomite MnO_2-diatomite composite; pH of 4 for Cd (II)). The adsorbent dosage, temperature and shaking speed were held constant at 2 g/L, 25±2 ^oC and 240rpm respectively for all the experiments. Figures 4.17 and 4.18 shows the effect of contact time on the percentage removal of Pb (II) and Cd (II) respectively.

It was observed that in all the cases, the percentage removal of Pb (II) was rapid for the first 20 minutes, then the it slowly increased and equilibrium was finally reached after 60 minutes. Further increase in contact time led to no change in the percentage removal of Pb (II) ions for both raw diatomite and MnO_2-diatomite composite. The rapid increase in percentage removal of Pb (II) at the beginning can be expounded by the high number of active binding sites on the adsorbent surface. As contact time is increased, these sites reduced in number leading to slow uptake of metal ions. The maximum

percentage removals of Pb (II) were 99.21% and 98.42% at 60 minutes for raw diatomite and MnO_2-diatomite composite respectively.

A similar trend was also observed for the removal of Cd (II) ions for both raw diatomite and MnO_2-diatomite composite. The percentage removal of Cd (II) increased rapidly for the first 40 minutes then it slowly increased and equilibrium was finally reached after 80 minutes. Further increase in contact time had no effect in the percentage removal since equilibrium had already been attained. According to Mbuvi and Mwihaki, (2017), the percentage removal of the metal ions remains stable after equilibrium time because no more adsorption could take place due to equal rates of adsorption and desorption of the metal ions. The maximum percentage removal of Cd (II) ions at equilibrium was 90.93% for raw diatomite and 84.50% for MnO_2-diatomite composite respectively. The same adsorption behaviour of Pb (II) and Cd (II) were reported by Bilgin and Tulun (2015), Taman *et al.* (2015), Mbuvi and Mwihaki (2017) and El Sayed (2018).

Raw diatomite had the highest percentage removal of both Pb (II) and Cd (II) ions at equilibrium compared to MnO_2-diatomited composite due to its larger surface area and porosity. The percentage removal of Pb (II) and Cd (II) for raw diatomite at equilibrium time (60 minutes for Pb (II) and 80 minutes for Cd (II)) were 99.21% and 90.93% while those for MnO_2-diatomite composite were 98.42% and 84.50% for Pb (II) and Cd (II) respectively at constant adsorbent dose, temperature and shaking speed. According to Iwuozor *et al.* (2021), the surface area of an adsorbent is directly proportional to the adsorptive performance of the material since a large surface area leads to a high number of the active sites present for the adsorption process. Therefore, the high surface area and porosity of raw diatomite was responsible for the high percentage removal of Pb (II) and Cd (II) ions compared to raw diatomite.

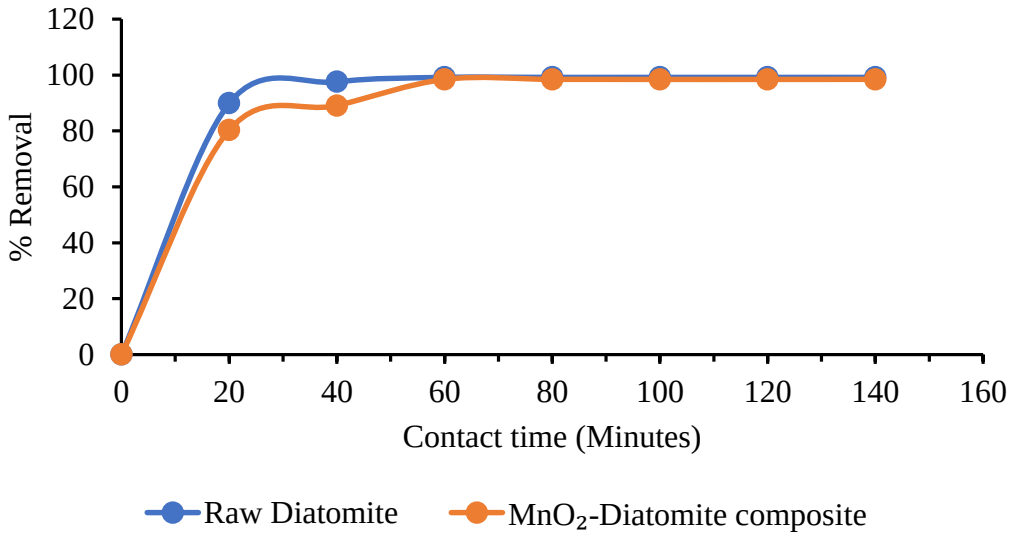

Figure 4.17: Effect of contact time on the adsorption of Pb (II) ions using raw diatomite and MnO_2-diatomite composite. (Adsorbent dosage 2 g/L; temperature 25±2 ^oC; shaking speed 240 rpm; Initial concentration 10mg/L; pH of 4 for raw diatomite and pH of 6 for MnO_2- diatomite composite)

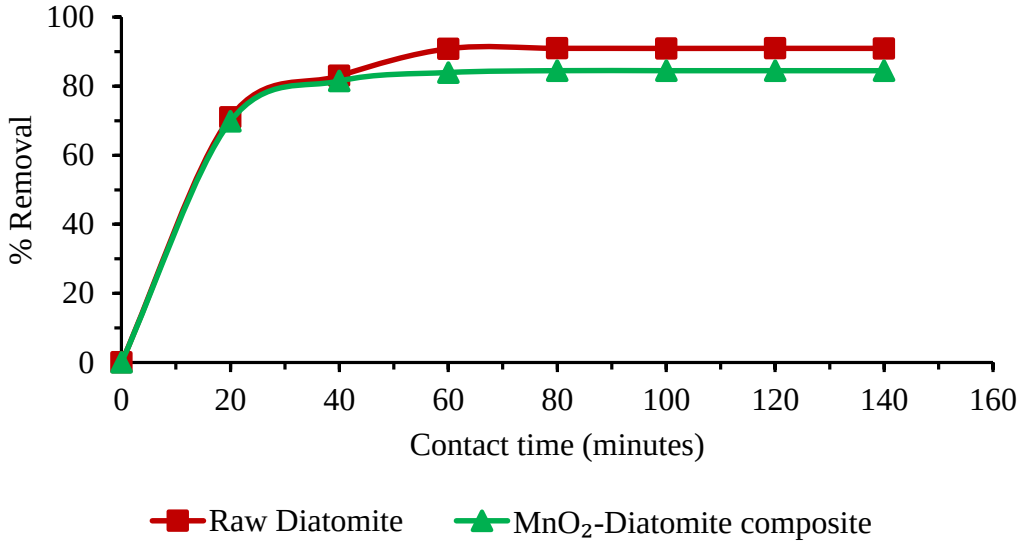

Figure 4.18: Effect of contact time on the adsorption of Cd (II) ions using raw diatomite and MnO_2-diatomite composite. (Initial concentration 10 mg/L; pH of 6; adsorbent dosage 2 g/L; temperature 25±2 ^oC; shaking speed 240 rpm)

4.2.5 Effect of Adsorbent Dosage on the Adsorption of Pb (II) and Cd (II) Ions

The effect of adsorbent dosage was investigated by varying the dosage from 0.4 g/L to 10 g/L while holding the other parameters constant.

4.2.5.1 Effect of Adsorbent Dosage on the Adsorption of Pb (II) Ions

The effect of adsorbent dosage on the adsorption of Pb (II) ions using both raw diatomite and MnO_2-diatomite composite was investigated by increasing the dosage from 0.4 g/L to 10 g/L at optimal conditions (Initial concentration 10 mg/L; pH of 4 and 6 for raw diatomite MnO_2-diatomite composite; contact time of 60 minutes). The solution temperature was held constant at 25±2 ^oC while the shaking speed at 240 rpm. Figure 4.19 shows the percentage removal of Pb (II) ions as a function of adsorbent dosage. It was observed that percentage removal of Pb (II) increased with increase in the adsorbent dosage for both adsorbents.

The percentage removal of lead was 95.45% at 0.4 g/L, 99.21% at 2 g/L for raw diatomite and 89.55% at 0.4 g/L, 99.88% at 4 g/L for MnO_2-diatomite composite. The percentage removal of lead was enhanced 1.0394 times for raw diatomite and 1.115 times for MnO_2-diatomite composite when the adsorbents dosage was increased from 0.4 g/L to 2 g/L and 4 g/L respectively. When the adsorbent dosage was further increased, it led to 100% removal of Pb (II) ions. The increase in heavy metal ion removal with increasing adsorbent dosage was attributed to increase in adsorbent surface area, the availability of more binding sites for adsorption of metal ions and increased probability of collision between adsorbent particles and metal ions in the solution as the adsorbent dosage increased (Dargahi *et al.*, 2016). Similar trends were observed in the removal of various heavy metal ions such as Cu (II), Ni (II) and Zn (II) from waste water using tea waste adsorbent (Thakur and Parmar, 2013); Pb (II) using diatomite (Bilgin and Tulun, 2015); Cr(VI) and As(V) using MnO_2 nanowires-deposited diatomite.

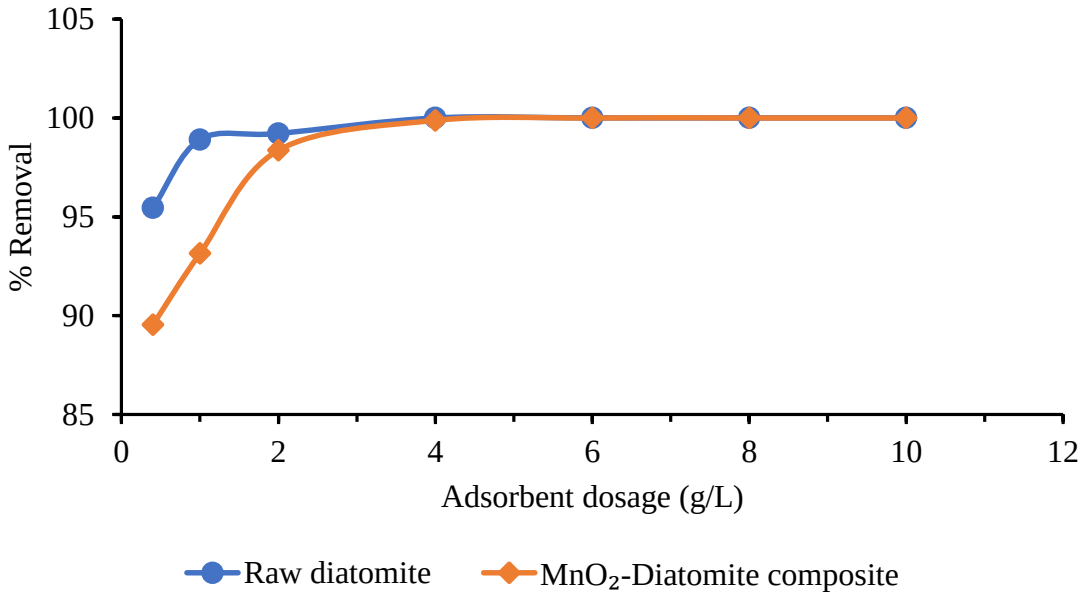

Figure 4.19: Effect of adsorbent dosage on the adsorption of Pb (II) ions using raw diatomite and MnO_2-diatomite composite. (Contact time 60 minutes; temperature 25±2 ^oC; shaking speed 240 rpm; Initial concentration 10 mg/L; pH of 4 for raw diatomite and pH of 6 for MnO_2-diatomite composite)

4.2.5.2 Effect of Adsorbent Dosage on the Adsorption of Cd (II) Ions

The effect of adsorbent dosage had a great effect on the adsorption of Cd (II) ions using both raw diatomite and MnO_2-diatomite composite. In this study, the effect of adsorbent dose was studied by varying the adsorbents dosage from 0.4 g/L to 10 g/Lg at constant pH of 6, initial metal ion concentration of 10 mg/L, temperature of 25±2 ^oC, shaking speed of 240 rpm and a contact time of 80 minutes. Figure 4.20 shows the effect of adsorbent dose of raw diatomite and MnO_2-diatomite composite on the percentage removal of Cd (II) ions.

It was observed that the percentage removal of Cd (II) ions increased from 76.17% to 100% when the adsorbent dose of raw diatomite was increased from 0.4 g/L to 6 g/L. For MnO_2-diatomite composite, the percentage removal increased from 70.69% to 100% when the dosage of MnO_2-diatomite composite was increased from 0.4 g/L to 8 g/L. As a result, the percentage removal of Cd (II) increased 1.313 times and 1.415 times when dosage of raw diatomite and of MnO_2-diatomite composite were increased form 0.4 g/L to 6 g/L and 8 g/L respectively. This was due to increase in the overall

surface area of the adsorbent and also increase in the number of active binding sites on the adsorbents available for adsorption whenever the adsorbent dose was increased.

Taman *et al*. (2015) and El Sayed (2018) obtained a similar trend when studying the removal of Cd (II) and other heavy metal ions using metal oxide nano-particles and natural diatomite as adsorbents respectively. Arowojobe *et al.* (2020) reported an increase in the percentage removal of Cd (II) and Pb (II) ions with increase in mass of *Persea americana* seed coat biosorbent. They attributed the increase in percentage removal to the increase in surface area and the number of adsorption sites available for adsorption when higher biosorbent doses were used.

It was also observed that raw diatomite had a higher percentage removal for Cd (II) compared to MnO_2-diatomite composite for all the adsorbent dosage used. This was attributed to the large surface area and more binding sites on the raw diatomite surface compared to MnO_2-diatomite composite 2. This was mainly due to blockage of pores on the diatomite surface by MnO_2 particles during the diatomite surface modification leading to reduced surface area and pore volume. This was evident in the BET/BJH results which showed that raw diatomite had a larger surface area than MnO_2-diatomite composite 2.

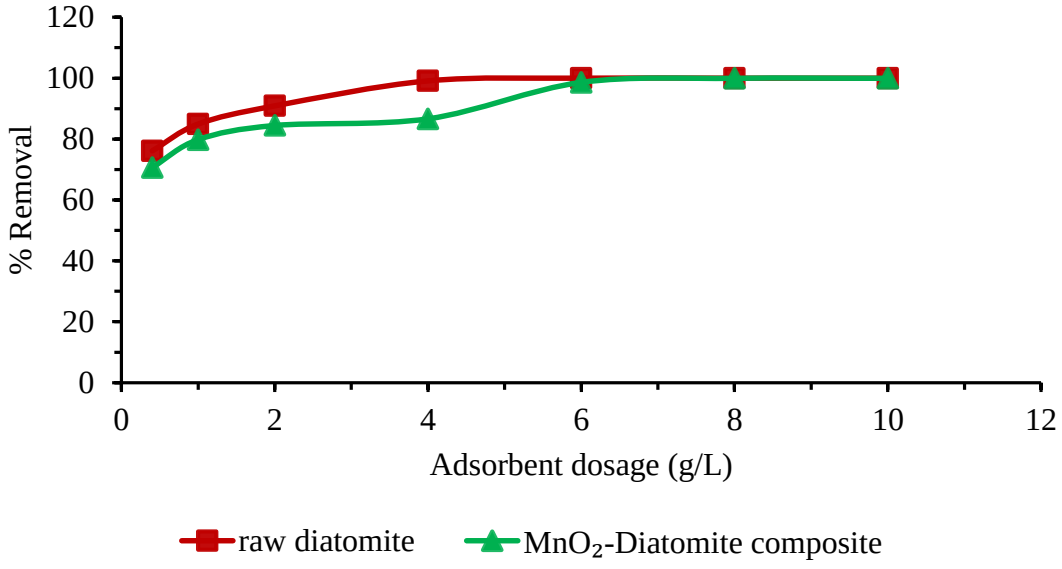

Figure 4.20: Effect of adsorbent dosage on the adsorption of Cd (II) using raw diatomite and MnO_2-diatomite composite. (Contact time 80 minutes; pH of 6; initial metal ion concentration 10 mg/L; temperature 25±2 ^oC; shaking speed 240 rpm).

4.2.6 Effect of Temperature on the Adsorption of Pb (II) and Cd (II) Ions

The effect of temperature on the adsorption of Pb (II) and Cd (II) ions was investigated in the temperature range of 298-338 K while keeping the other optimal parameters constant. Figure 4.21 shows variations of percentage removal of Pb (II) ions with increasing temperature. From the figure, it is clear that the percentage removal of Pb (II) ions decreased with increasing temperature of the solution for both raw diatomite and MnO_2-diatomite composite adsorbents. The maximum percentage removal of Pb (II)ions were obtained at low temperatures. Raw diatomite had the highest percentage removal of 99.21% at 298 K which decreased to 98.76% at 338 K. Similarly, 98.36% of Pb (II) ions were removed at 298 K using MnO_2-diatomite composite which reduced to 86.15% at 338 K.

The decrease in percentage removal of Pb (II) ions with increasing temperature suggest a weak interaction between the adsorbents and the adsorbate which represents physisorption process. As a result, rate of desorption was more significant than the rate of adsorption at higher temperatures implying that the adsorption process was an exothermic reaction (Francis, 2015). According to Budnyak (2020), increase in temperature may weaken the adsorptive forces between the metal ion and the active sites on the adsorbent surface thereby reducing the percentage removal at higher temperatures. Similar observations were reported by Hamadi *et al.* (2014) and Francis, (2015). Studies by Liu *et al*. (2013) showed contrary behaviour in the adsorption of Pb (II) ions on modified diatomite.

According to Hamadi *et al.* (2014), temperature may affect the adsorption process in the following ways. Firstly, increase in temperature affects the adsorption capacity of the adsorbent depending on whether the adsorption process is exothermic or endothermic. Lastly, increase in temperature increases the rate of adsorbate diffusion in the internal pores of the adsorbent particles and also across the external boundary layer due to decreased liquid viscosity as temperature increases. Due to these, if the adsorption process is exothermic, an increase in temperature results in decrease in the percentage removal.

An opposite trend was observed for adsorption of Cd (II) ions using both raw diatomite and MnO_2-diatomite composite as shown in figure 4.22. Increase in temperature resulted in an increase in the percentage removal of Cd (II) ions. An increase in temperature from 298K to 338 K lead to the increase in percentage removal of Cd (II) ions from 90.93% to 99.83% for raw diatomite and 84.50% to 96.61% for MnO_2-diatomite composite. The increase in percentage removal with increase in temperature implies that the adsorption of Cd (II) ions on to the adsorbents was an endothermic reaction. Similar trends have been reported in the adsorption of Cd (II) ions on diatomite by Flores-Cano *et al.* (2013) and Liu *et al.* (2013).

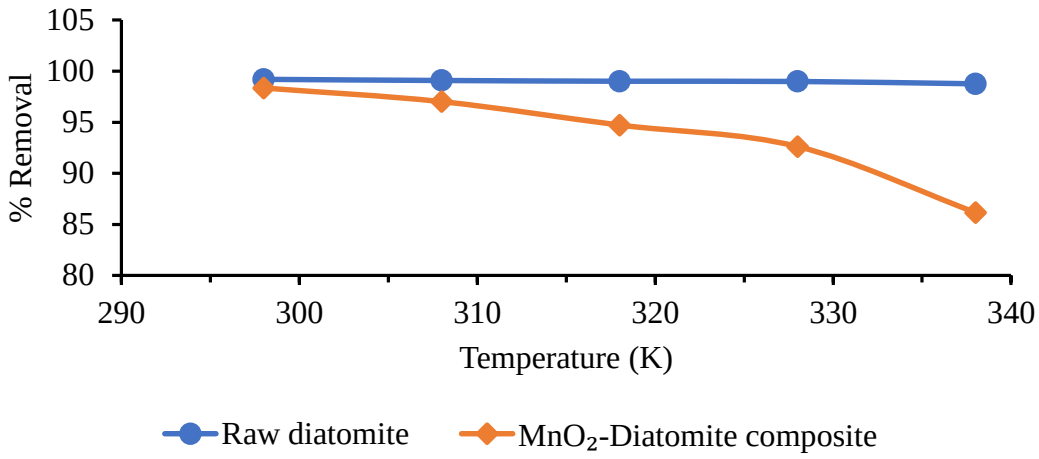

Figure 4.21: Effect of temperature on the adsorption of Pb (II) ions using raw diatomite and MnO_2-diatomite composite. (Contact time 60 minutes; adsorbent dose 2 g/L; shaking speed 240 rpm; Initial concentration 10 mg/L; pH of 4 for raw diatomite and pH of 6 for MnO_2- diatomite composite).

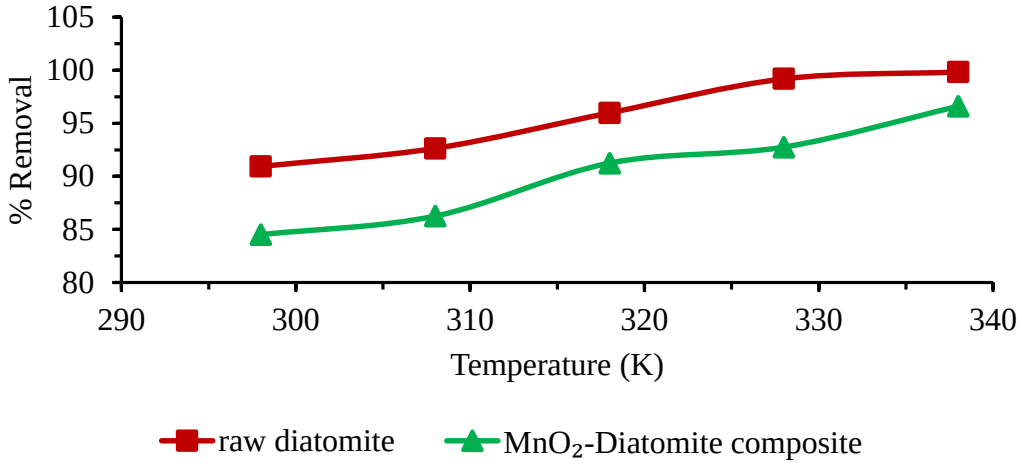

Figure 4.22: Effect of temperature on the adsorption of Cd (II) ions using raw diatomite and MnO_2-diatomite composite. (Initial concentration 10 mg/L; contact time 80 minutes; pH of 6; adsorbent dosage 2 g/L; shaking speed 240 rpm).

4.3 Adsorption Isotherms, Kinetics and Thermodynamics

4.3.1 Adsorption Isotherms

In order to determine the maximum adsorption capacity and the nature of interaction between the heavy metal ions and the adsorbents, the adsorption data was applied to various adsorption isotherms such as Langmuir, Freundlich and Temkin isotherm models. The fitting of the adsorption data to the models is also significant in obtaining useful information such as favorability of the adsorption process and adsorbate affinity for a particular adsorbent.

4.3.1.1 Adsorption Isotherms for Pb (II) ions

Figures 4.23, 4.24 and 4.25 represent the Langmuir, Freundlich and Temkin isotherms isotherm for Pb (II) ions adsorption using raw diatomite. The isotherm parameters obtained for the adsorption of Pb (II) ions onto raw diatomite and MnO_2-diatomite composite are shown in table 4.3. The equilibrium data for the adsorption of Pb (II) onto raw diatomite was found to correlate well with the Langmuir isotherm model (R^2=0.9906) compared to the Freundlich (R^2= 0.9846) and Temkin (R^2= 0.9703) isotherm models. This indicates monolayer adsorption onto the raw diatomite surface containing a finite number of adsorption sites.

The maximum adsorption capacity for the adsorption of Pb (II) onto raw diatomite was 52.632 mg/g. From the Langmuir isotherm, the value of separation factor R_L= 0.07272 which is between 0 and 1 indicating that adsorption of Pb (II) ions onto raw diatomite is favourable. From the Freundlich isotherm model, n>1 indicating that the adsorption of Pb (II) ions onto raw diatomite was a physical process.

Langmuir, Freundlich and Temkin isotherms models were also applied to the equilibrium uptake data obtained for sorption of Pb (II) ions from their solutions using MnO_2-diatomite composite as shown in figures 14.26, 14.27 and 14.28 respectively. The correlation coefficient (R^2) values obtained from the three models indicate that the adsorption data of Pb (II) on to MnO_2-diatomite composite best fits the Langmuir isotherm model (R^2= 0.9924) followed by Temkin isotherm (R^2= 0.9885) and lastly Freundlich isotherm (R^2= 0.956). Therefore, from the Langmuir isotherm model, the

adsorption of Pb (II) onto MnO_2-diatomite composite was found to be favourable since the separation factor, RL is between 0 and 1 (R_L= 0.2372).

Table 4.3: Langmuir, Freundlich and Temkin isotherm parameters for the adsorption of Pb (II) ions onto raw diatomite and MnO_2-diatomite composite.

	Parameters	Raw diatomite	MnO_2-diatomite composite
Langmuir	Qmax (mg/g)	52.632	18.182
	K_L (L/mg)	1.275	0.3216
	R_L	0.01108 – 0.0727	0.04253 - 0.2372
	R^2	0.9906	0.9924
Freundlich	K_f (L/mg)	29.985	6.0353
	n	1.493	3.237
	R^2	0.9846	0.956
Temkin	B (J/mol)	10.319	3.0597
	A_t (L/g)	1.432	7.1904
	b_t	240.098	809.743
	R^2	0.9703	0.9885

Where, Qmax is the maximum monolayer coverage capacity (in mg/g), K_L is the Langmuir isotherm constant (in L/mg), R_L is dimensionless factor named separation factor, R^2 is the correlation coefficient, K_f refers to the Freundlich constant related to the adsorption capacity, *n* refers to the Freundlich constant related to the adsorption intensity, A_t refers to Temkin isotherm equilibrium binding constant (L/g), b_t is the Temkin isotherm constant, *B* is a parameter related to the heat of adsorption (J/mol).

The maximum monolayer adsorption capacity (Qmax) for adsorption of Pb (II) onto MnO_2-diatomite composite was 18.182 mg/g. This was less than the 52.632 mg/g obtained as the maximum adsorption capacity for Pb (II) onto raw diatomite. This shows that Pb (II) ions have a higher affinity for the binding sites present on raw diatomite surface than for the binding sites on the MnO_2-diatomite composite.

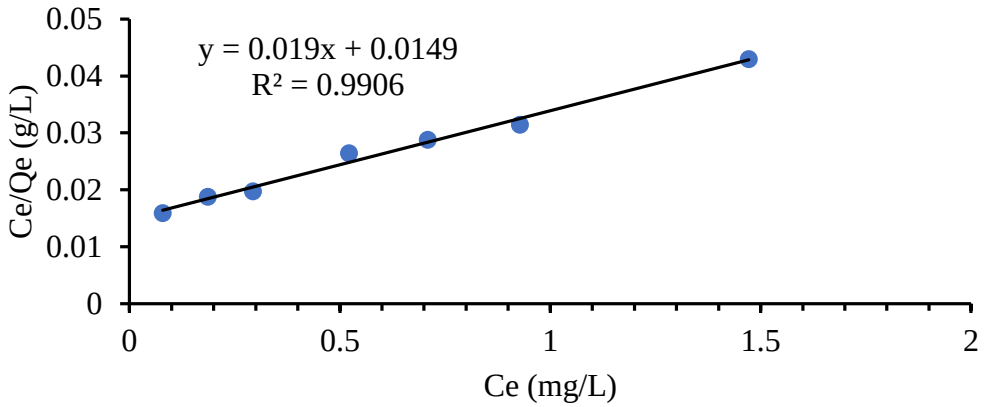

Figure 4.23: Linearized Langmuir plot for the adsorption of Pb (II) ions onto raw diatomite.

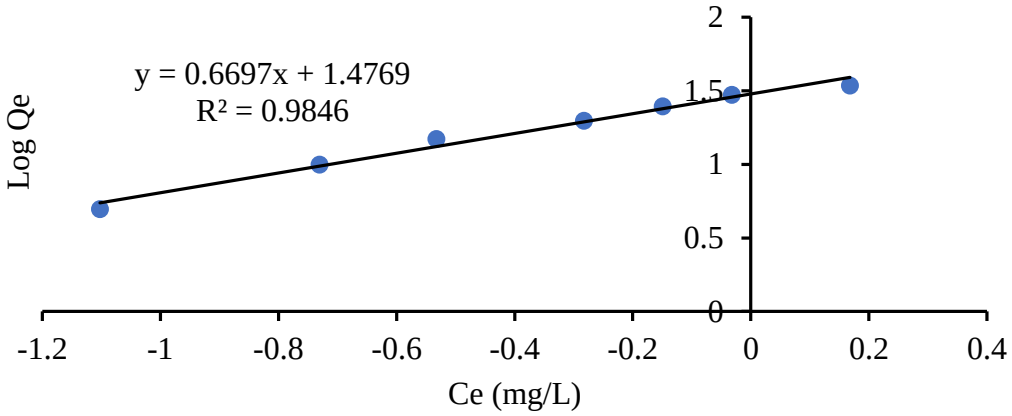

Figure 4.24: Linearized Freundlich plot for the adsorption of Pb (II) ions onto raw diatomite

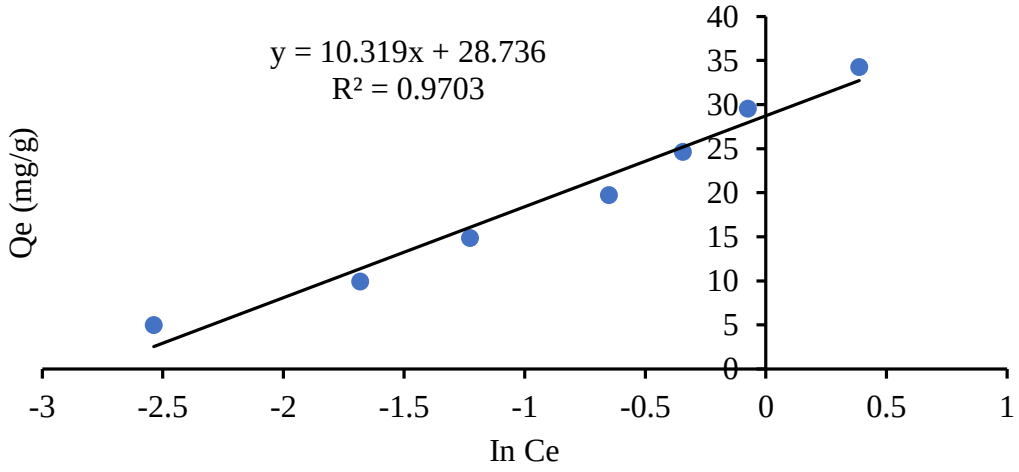

Figure 4.25: Linearized Temkin plot for the adsorption of Pb (II) ions onto raw diatomite

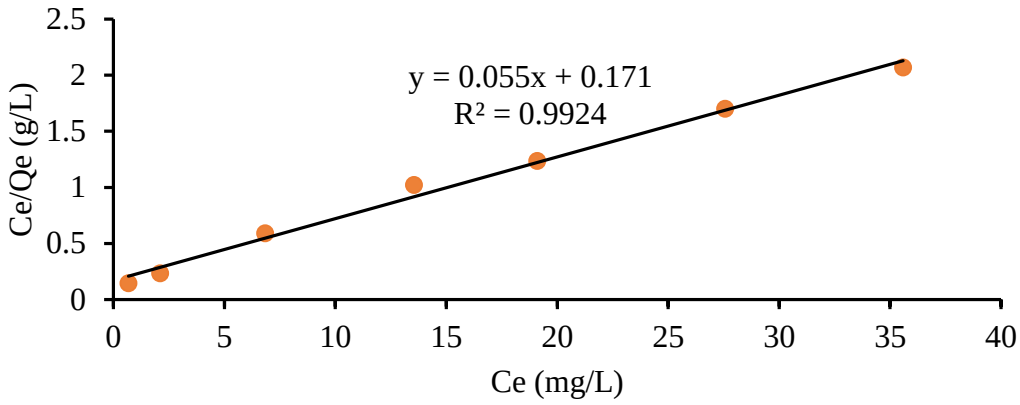

Figure 4.26: Linearized Langmuir plot for the adsorption of Pb (II) ions onto MnO_2-diatomite composite.

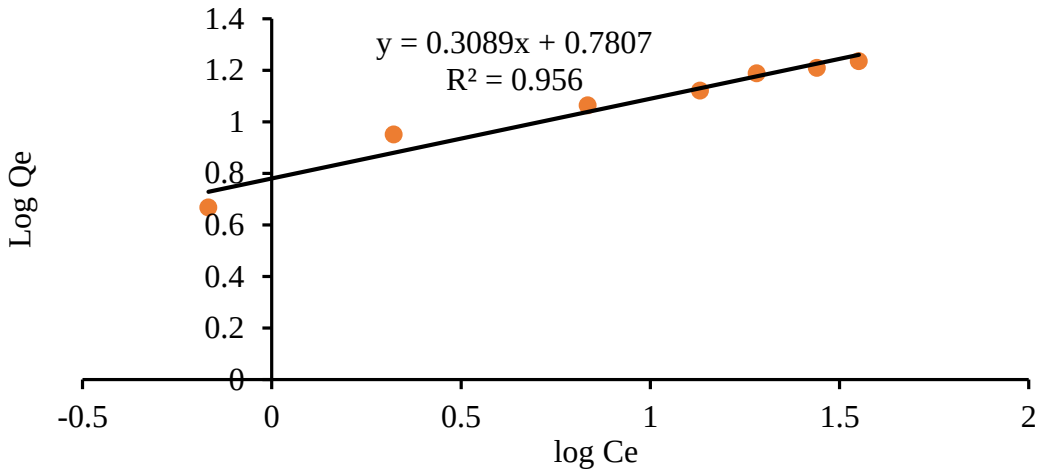

Figure 4.27: Linearized Freundlich plot for the adsorption of Pb (II) ions onto MnO_2-diatomite composite.

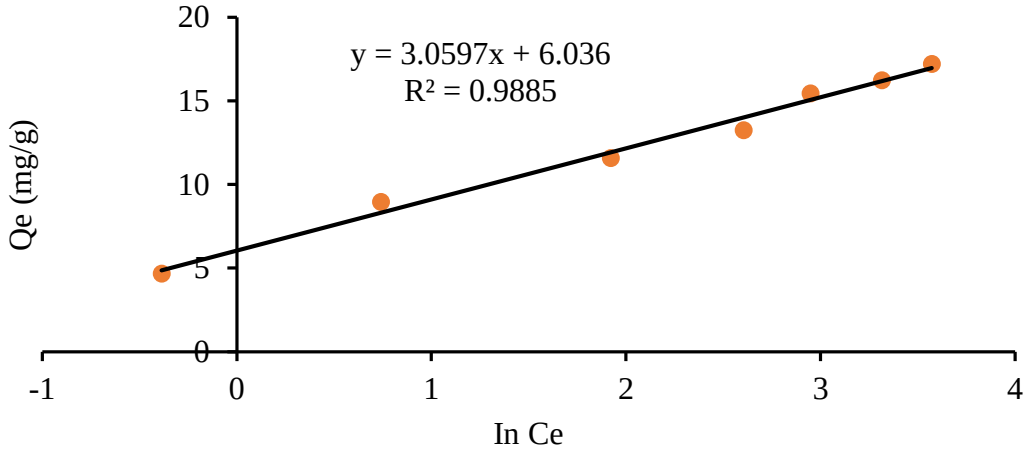

Figure 4.28: Linearized Temkin plot for the adsorption of Pb (II) ions onto MnO_2-diatomite composite.

4.3.1.2 Adsorption isotherms for Cd (II) ions

The experimental data obtained for sorption of Cd (II) ions from their solutions using raw diatomite and MnO_2-diatomite composite was applied to Langmuir, Freundlich and Temkin isotherm models. Figures 4.29, 4.30 and 4.31 represent plots of the linearized forms of Langmuir, Freundlich and Temkin isotherm models for adsorption of Cd (II) ions onto Raw diatomite while figures 4.32,4.33 and 4.34 for adsorption of Cd (II) ions onto MnO_2-diatomite composite. Table 4.4 shows the isotherm parameters obtained for the adsorption of Cd (II) ions onto raw diatomite and MnO_2-diatomite composite.

Table 4.4: Langmuir, Freundlich and Temkin isotherm parameters for the adsorption of Cd (II) ions onto raw diatomite and MnO_2-diatomite composite.

	Parameters	Raw diatomite	MnO_2-diatomite composite
Langmuir	Qmax (mg/g)	23.256	13.158
	K_L (L/mg)	0.237	0.1897
	R_L	0.05693 - 0.2970	0.07003 - 0.3452
	R^2	0.9952	0.987
Freundlich	K_f (L/mg)	5.3000	3.6788
	n	2.246	3.0779
	R^2	0.9499	0.9552
Temkin	B (J/mol)	4.899	2.4403
	A_t (L/g)	2.524	3.069
	b_t	505.771	1015.27
	R^2	0.9665	0.9495

Where, Qmax is the maximum monolayer coverage capacity (in mg/g), K_L is the Langmuir isotherm constant (in L/mg), R_L is dimensionless factor, R^2 is the correlation coefficient, K_f refers to the Freundlich constant related to the adsorption capacity, n refers to the Freundlich constant related to the adsorption intensity, A_t refers to Temkin isotherm equilibrium binding constant (L/g), b_t is the Temkin isotherm constant, B is a parameter related to the heat of adsorption (J/mol).

In view of the values of the linear regression coefficients, Langmuir model fits very well to the sorption data of Cd (II) ions using both raw diatomite and MnO_2-diatomite composite in the concentration range studied. Langmuir model had a regression coefficient, R^2= 0.9952 for raw diatomite and R^2= 0.9871for MnO_2-diatomite composite compared to Freundlich (R^2= 0.9499 for raw diatomite, R^2= 0.9552 for

MnO_2-diatomite composite) and Temkin (R^2= 0.9882 for raw diatomite, R^2= 0.9495 for MnO_2-diatomite composite) isotherm models.

This shows implies that adsorption of Cd (II) ions onto using raw diatomite and MnO_2-diatomite composite was monolayer adsorption and there was no interaction between the neighbouring adsorbate molecules. The minimum and maximum separation factor (R_L) values range obtained were 0.05693 to 0.2970 and 0.07003 to 0.3452 for raw diatomite and MnO_2-diatomite composite respectively. These R_L values lie between 0 and 1 which signifies that the adsorption of Cd (II) ions onto using raw diatomite and MnO_2-diatomite composite was favourable.

The monolayer saturation capacities (Qmax) were found to be 23.256 and 13.158 mg/g for the adsorption of Cd (II) onto raw diatomite and MnO_2-diatomite composite respectively, which were close to the experimental data (20.074 and 12.383 mg/g for raw diatomite and MnO_2-diatomite composite respectively). These confirms that Langmuir isotherm model properly explained the equilibrium adsorption of Cd (II) onto both raw diatomite and MnO_2-diatomite composite.

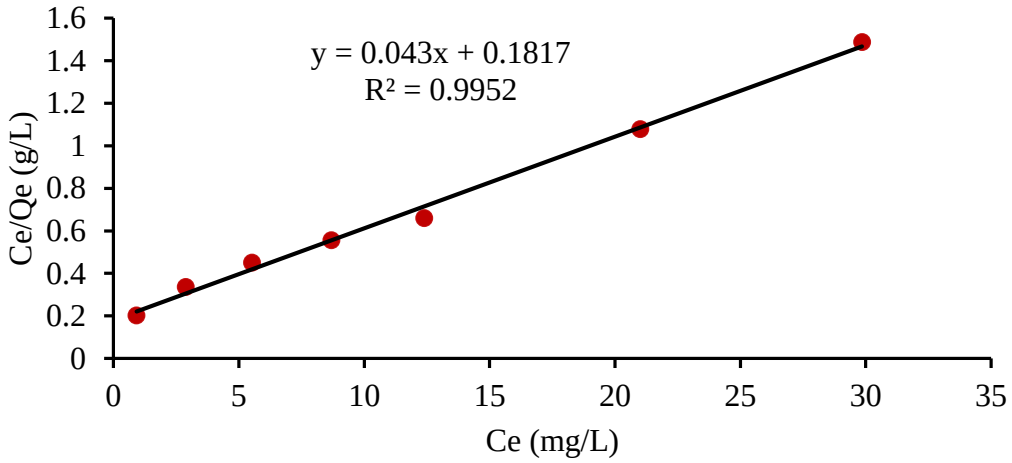

Figure 4.29: Linearized Langmuir plot for the adsorption of Cd (II) ions onto raw diatomite.

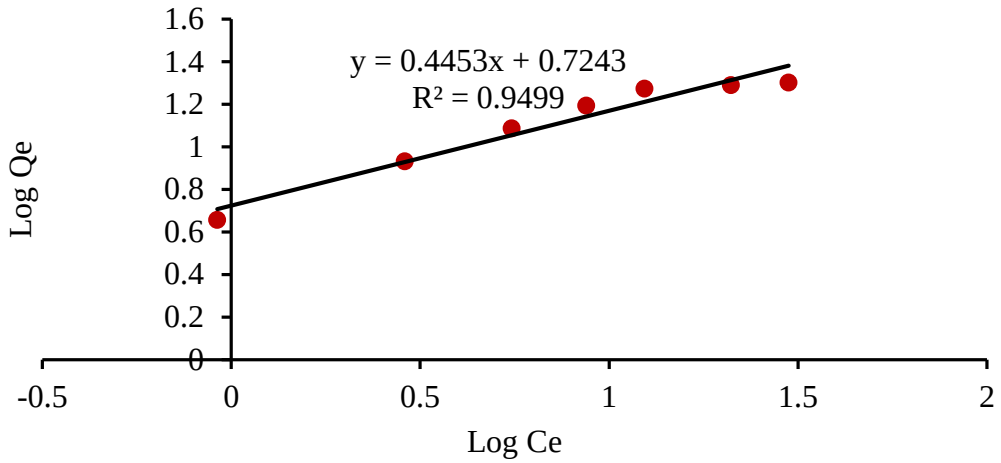

Figure 4.30: Linearized Freundlich plot for the adsorption of Cd (II) ions onto raw diatomite.

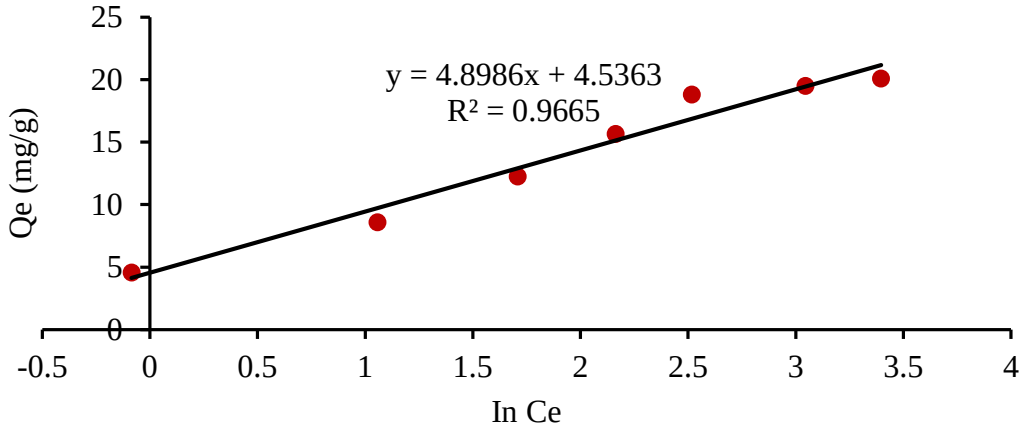

Figure 4.31: Linearized Temkin plot for the adsorption of Cd (II) ions onto raw diatomite.

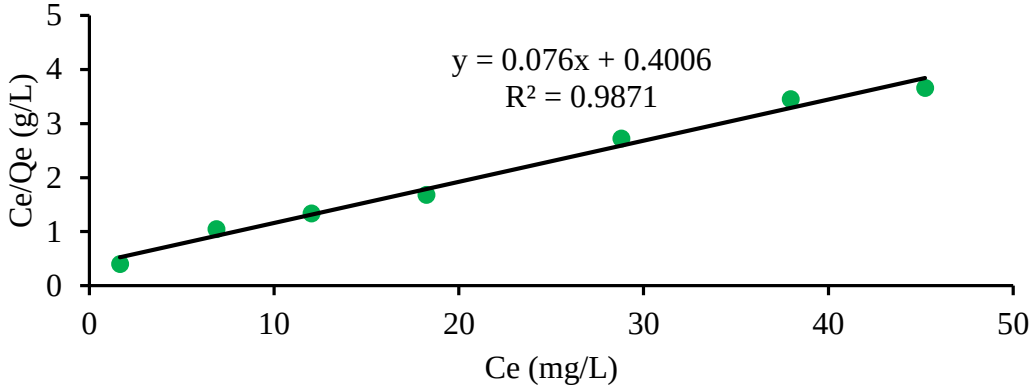

Figure 4.32: Linearized Langmuir plot for the adsorption of Cd (II) ions onto MnO_2-diatomite composite.

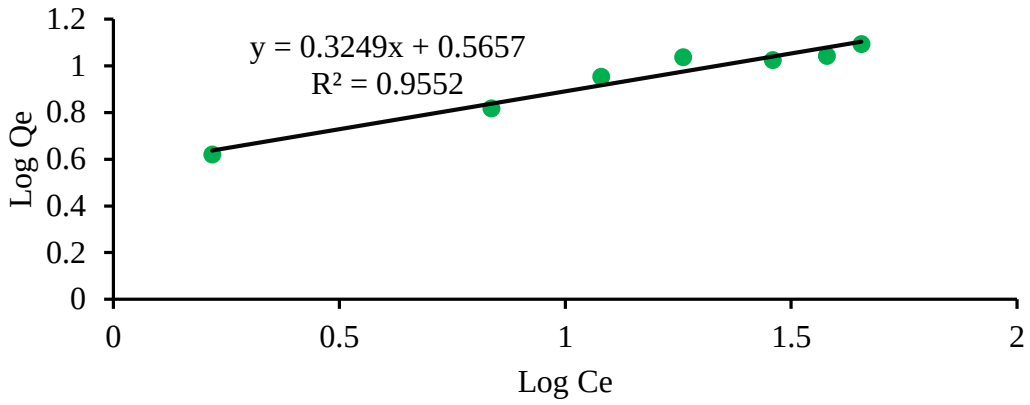

Figure 4. 33: Linearized Freundlich plot for the adsorption of Cd (II) ions onto MnO_2-diatomite composite.

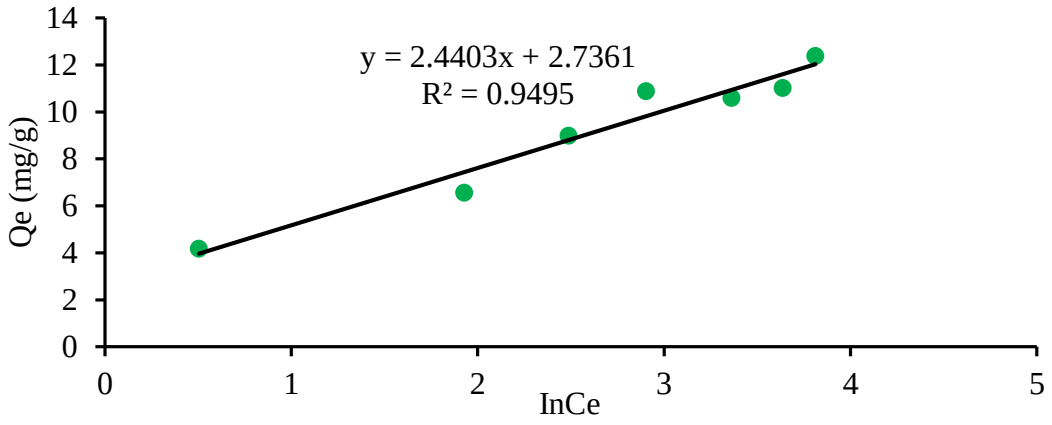

Figure 4.34: Linearized Temkin plot for the adsorption of Cd (II) ions onto MnO_2-diatomite composite.

4.3.2 Adsorption Kinetics

The study of adsorption kinetics is important as it predicts the adsorption mechanisms, which is important for efficiency of the process. Kinetics is considered as rate of the reaction, which is defined as the change in concentration/movement of reactant or product with time. Therefore, the dynamics of adsorption kinetics describes the rate at which the adsorbate is adsorbed onto the adsorbent. This in turn controls the time at the particle-metal interface. In order to fully determine the adsorption kinetics of Pb (II) and Cd (II) ions, kinetic parameters of adsorption process were studied for the range of contact time 0 to 140 minutes. Pseudo-first order and pseudo-second order kinetic adsorption models were then applied to the experimental data in order to elucidate the mechanism of Pb (II) and Cd (II) ions adsorption onto raw diatomite and MnO_2-

diatomite composite. Table 4.5 shows the linear forms of pseudo-first order and pseudo-second order kinetic adsorption models.

Table 4.5: Linear forms of pseudo-first order and pseudo-second order kinetic adsorption models.

Pseudo-first order	Pseudo-second
$In(q_e - q_t) = Inq_e - k_1 t$	$t/q_t = 1/(k_2 {q_e}^2) + (1/q_e)t$

Where, k_1 is the pseudo-first-order rate constant (min^{-1}) of adsorption, q_e and q_t are the adsorption capacities at equilibrium and at time t (min), k_2 is the rate constant of pseudo-second-order adsorption (g/mg min).

The kinetic parameters for pseudo-first and pseudo-second order kinetic models were determined by the linear plots of $In(q_e-q_t)$ vs t and (t/q_t) vs t; respectively to determine the predicted q_e in order to compare them with experimental q_e. The experimental and model predicted parameters are tabulated in Table 4.6.

Table 4.6: Parameters of pseudo-first order and pseudo-second order kinetic models for adsorption of Pb (II) and Cd (II) onto raw diatomite and MnO_2-diatomite composite

Metals	Kinetic Model	Parameters	Raw diatomite	MnO_2-diatomite composite
Experimental		q_e (mg/g)	4.9605	4.9212
Pb (II)	PFO	q_e (mg/g)	3.6277	12.2411
		k_1	0.1241	0.1153
		R^2	0.9513	0.9226
	PSO	q_e (g/mg.min)	4.99	5.123
		k_2	0.2944	0.04274
		R^2	1	0.999
Experimental		q_e (mg/g)	4.5464	4.2249
Cd (II)	PFO	q_e (mg/g)	2.1652	8.1743
		k_1	0.0693	0.1054
		R^2	0.8851	0.9632
	PSO	q_e (g/mg.min)	4.7551	4.3478
		k_2	0.0413	0.0714
		R^2	0.9989	0.9995

Where, PFO is pseudo-first-order and PSO is pseudo-second order.

From the data, it was observed that pseudo-second order model fit well with $R^2 > 0.99$ to describe the kinetics of adsorption of Pb (II) and Cd (II) ions onto both raw diatomite and MnO_2-diatomite composite compared to pseudo-first order. This indicated that chemisorption was the rate limiting step in the sorption of Pb (II) and Cd (II) ions onto both raw diatomite and MnO_2-diatomite composite. In addition, the model predicted equilibrium adsorption capacities (q_e) had better consistencies with the experimental equilibrium adsorption capacities for pseudo-second order model than the pseudo-first order model. This confirmed that pseudo-second order model was the better model to describe the adsorption of Pb (II) and Cd (II) ions onto raw diatomite and MnO_2-diatomite composite.

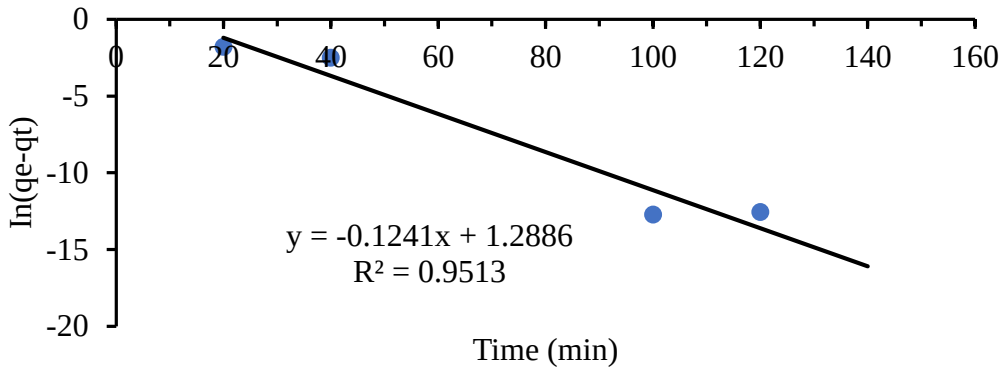

Figure 4.35: Pseudo-first order plot for the adsorption of Pb (II) ions onto raw diatomite.

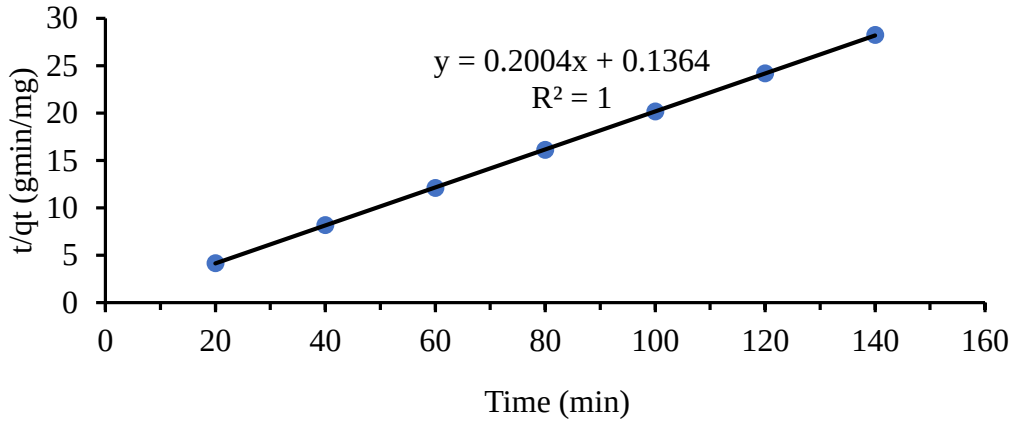

Figure 4.36: Pseudo-second order kinetic plot for the adsorption of Pb (II) ions onto raw diatomite.

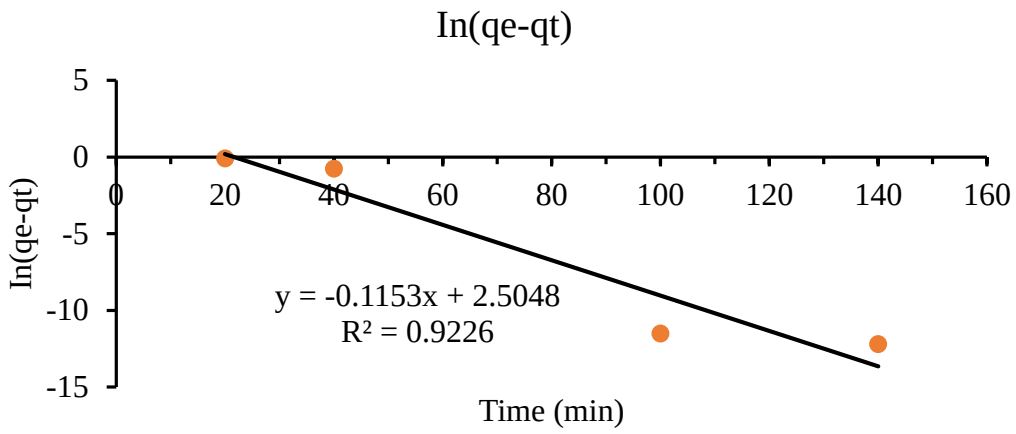

Figure 4.37: Pseudo-first order kinetic plot for the adsorption of Pb (II) ions onto MnO_2-diatomite composite.

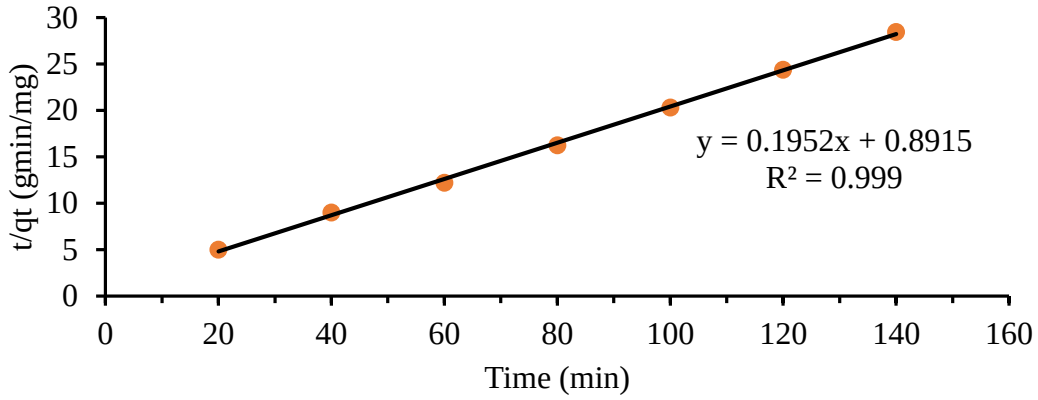

Figure 4.38: Pseudo-second order kinetic plot for the adsorption of Pb (II) ions onto MnO_2-diatomite composite.

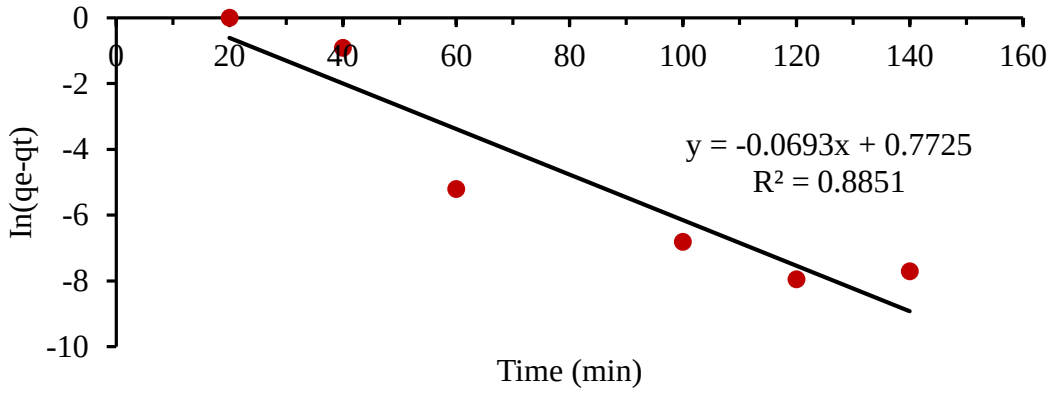

Figure 4.39: Pseudo-first order plot for the adsorption of Cd (II) ions onto raw diatomite.

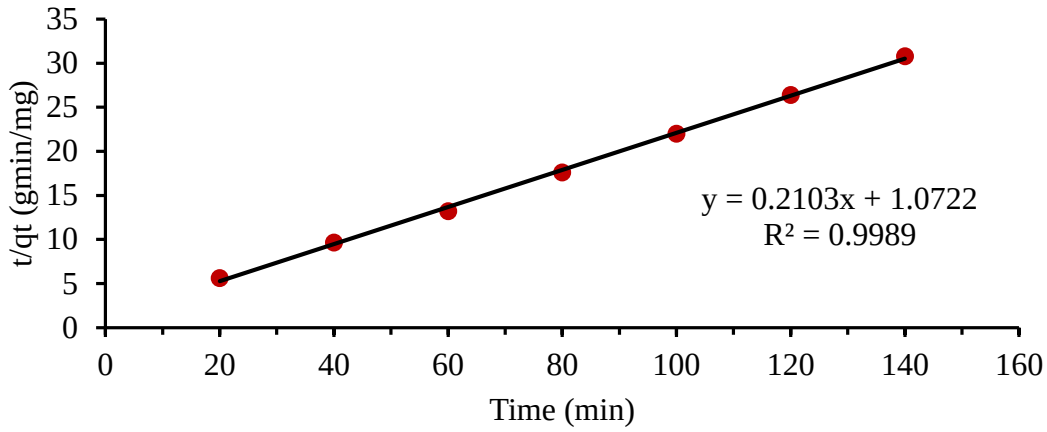

Figure 4.40: Pseudo-second order plot for the adsorption of Cd (II) ions onto raw diatomite.

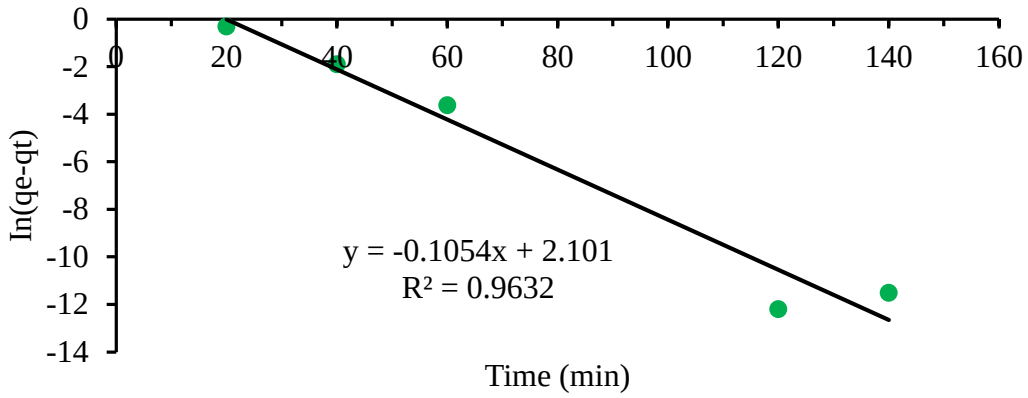

Figure 4.41: Pseudo-first order plot for the adsorption of Cd (II) ions onto MnO_2-diatomite composite.

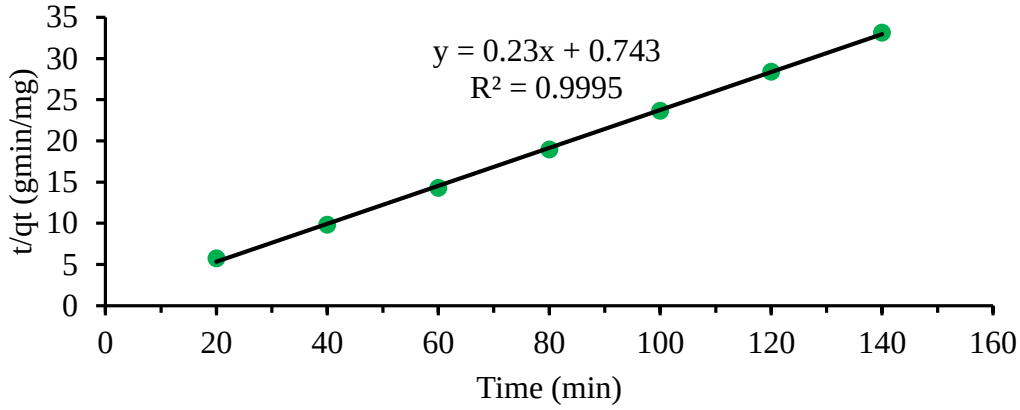

Figure 4.42: Pseudo-second order plot for the adsorption of Cd (II) ions onto MnO_2-diatomite composite.

4.3.3 Adsorption Thermodynamics

Thermodynamic studies were conducted to evaluate the effect of temperature on the adsorption of Pb (II) and Cd (II) ions onto raw diatomite and MnO_2-diatomite composite at different temperatures (298, 308, 318, 328 and 338 K) while keeping the other optimal parameters constant. Thermodynamic parameters such as change in Gibbs free energy (ΔG°), enthalpy change (ΔH°) and entropy change (ΔS°) which are essential in determining the nature of the adsorption process were determined. The magnitude of ΔH° (kJ/mol) and ΔS° ($Jmol^{-1}K^{-1}$) were determined from the slope and intercept, respectively of Van't Hoff plot of $\ln K_C$ against 1/T. The calculated thermodynamic parameters are shown in table 4.7.

The values of Gibbs free energy (ΔG°) determined were all negative indicating that the adsorption processes of Pb (II) and Cd (II) ions onto raw diatomite and MnO_2-diatomite composite were feasible and spontaneous. The ΔG° values for adsorption of Pb (II) onto MnO_2-diatomite composite became less negative with increasing temperature suggesting that the adsorption of Pb (II) ions became less spontaneous at higher temperatures. This was also observed for adsorption of Pb (II) onto raw diatomite when solution temperature was increased from 328 K to 338 K. This may be due to deterioration of the adsorbent structure at higher temperatures resulting in loss of adsorptive surfaces (Abunah, *et al.,* 2019) leading to reduction in the removal efficiency of Pb (II) ions at higher temperatures. In contrast, the negative ΔG° values of Cd (II) ions became more negative with increasing temperature, implying that the adsorption was more efficient and spontaneous at higher temperatures.

Table 4. 7: Thermodynamic parameters for the adsorption of Pb (II) and Cd (II) ions onto raw diatomite and MnO_2-diatomite composite.

Metal ions	Adsorbent	ΔG° (kJ/mol)					ΔH° (kJ/mol)	ΔS° (J/mol/K)
		298K	308K	318K	328K	338K		
Pb (II)	Raw diatomite	-11.974	-12.024	-12.204	-12.526	-12.309	-8.407	11.951
	MnO_2-diatomite composite	-10.146	-8.921	-7.637	-6.899	-5.137	-45.940	-120.096
Cd (II)	Raw diatomite	-5.710	-6.484	-8.389	-13.094	-17.966	86.432	304.259
	MnO_2-diatomite composite	-4.201	-4.702	-6.198	-6.954	-9.412	33.372	124.752

The enthalpy changes (ΔH°) values for the adsorption of Pb (II) were all negative indicating that the adsorption of Pb (II) onto raw diatomite and MnO_2-diatomite composite was exothermic and that increase in temperature led to decrease in adsorption and removal efficiency. In addition, the entropy change (ΔS°) value for adsorption of Pb (II) onto raw diatomite was positive corresponding to increase in randomness at the solid-solution interphase. However, for MnO_2-diatomite composite, the ΔS° value was negative corresponding to a decrease in the degree of freedom of adsorbed Pb (II) ions with increasing temperature. This indicates that there is reduced randomness (increased order) at the solid/liquid interphase of Pb (II) ions onto MnO_2-diatomite composite.

In contrast, the ΔH° for Cd (II) adsorption were all positive indicating that the adsorption process of Cd (II) onto both raw diatomite and MnO_2-diatomite composite were endothermic processes. Furthermore, the ΔS° values for adsorption of Cd (II) onto both raw diatomite and MnO_2-diatomite composite were all positive implying an increase in randomness at the solid-solution interphase. These results show that increase in temperature is beneficial to the adsorption of Cd (II) ions onto both raw diatomite and MnO_2-diatomite composite, but not conducive to the adsorption of Pb (II) ions.

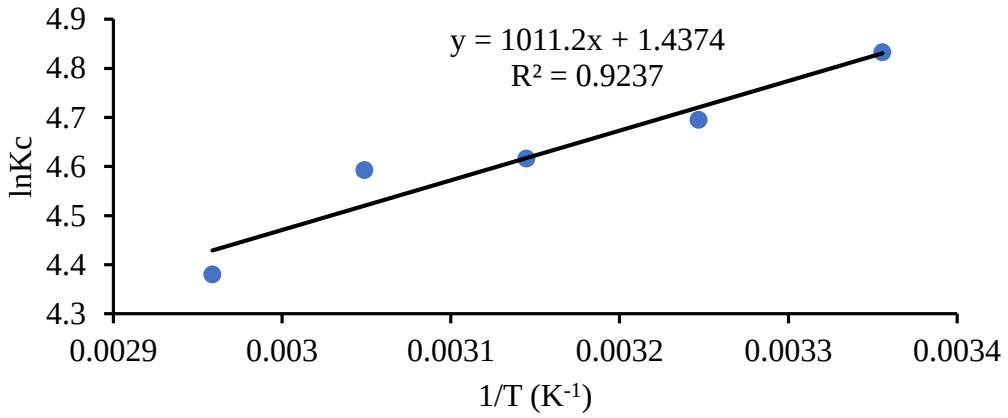

Figure 4.43: Van't Hoff plot for adsorption of Pb (II) onto raw diatomite.

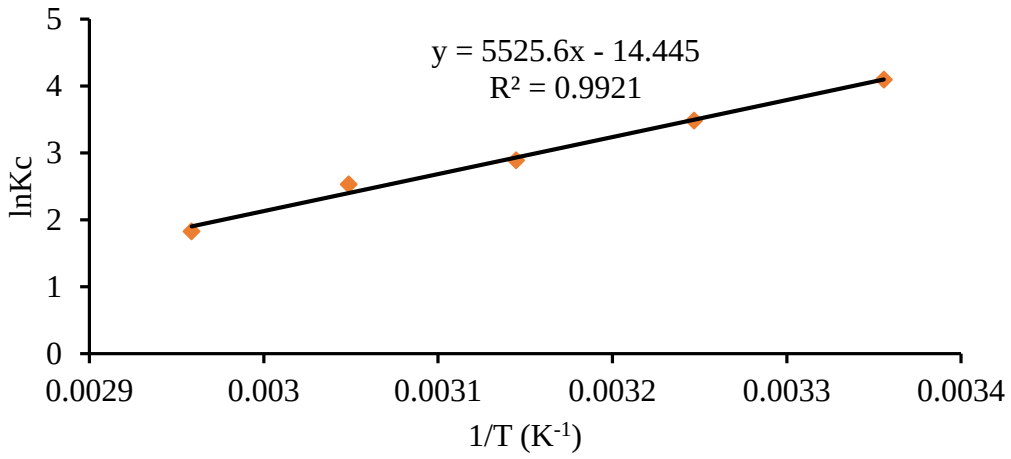

Figure 4.44: Van't Hoff plot for adsorption of Pb (II) onto MnO_2-diatomite composite

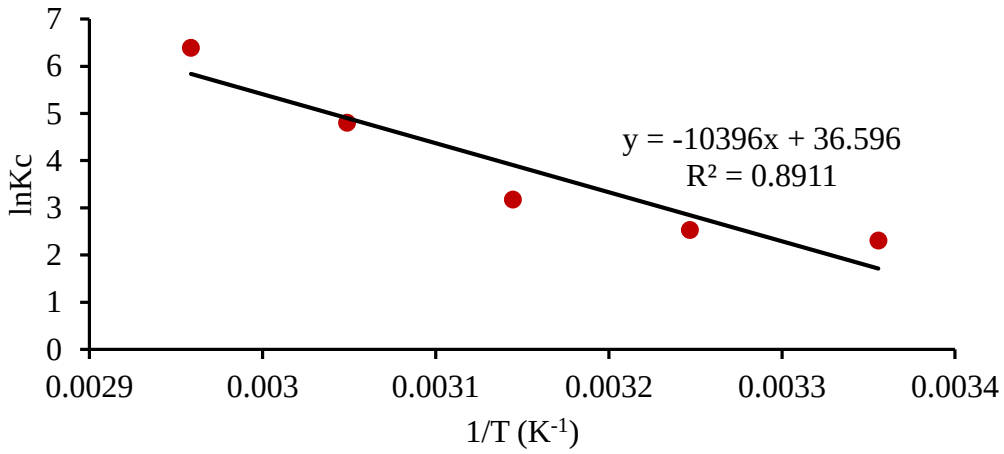

Figure 4.45: Van't Hoff plot for adsorption of Cd (II) onto raw diatomite.

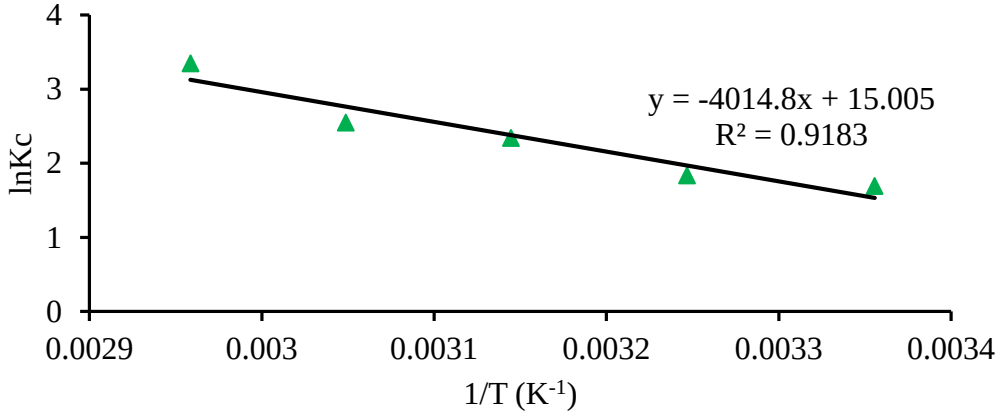

Figure 4.46: Van't Hoff plot for adsorption of Cd (II) onto MnO_2-diatomite composite

4.4 Binary Ion Studies

Industrial effluents and wastewater from treatment plants usually contain several metal ion contaminants, therefore, there is need to remove more than one metal ion contaminant during adsorption process. This is of outmost importance because the presence of other metal ions may hinder the adsorption process in multi-component systems due to competition for adsorption sites (Yemisi *et al.*, 2021; Elkhatib *et al.*, 2022). As a result, this study investigated the competition for active binding sites between Pb (II) and Cd (II) ions in order to determine whether their interactions were synergistic or antagonistic. Raw diatomite was chosen as the preferred adsorbent because it had better adsorption for both Pb (II) and Cd (II) ions from single ion solutions. Adsorption parameters such as pH, adsorbent dosage, contact time, initial metal ion concentration and temperature were investigated to check their effect on the percentage removal of Pb (II) and Cd (II) ions from binary ion solution.

4.4.1 Effect of pH on the Competitive Adsorption of Pb (II) and Cd (II) ions form Binary Ion Solution.

In single ion studies, the optimum pH for the adsorption of Pb (II) and Cd (II) ions onto raw diatomite were 4 and 6 respectively. Since the two metal ions had different optimum pH, the effect of pH on the competitive adsorption of these metal ions from binary ion solution was investigated by varying the pH in the range 2, 3, 4, 5 and 6. pH above 6 were not considered in this study due to the precipitation of Pb (II) ions inform of $Pb(OH)_2$ at higher pH. The adsorbent dosage, contact time, shaking speed and temperature were held constant at 2 g/L, 80 minutes, 240 rpm and 25±2^{o}C respectively. Optimal initial metal ion concentration was held constant at 10 mg/L for each metal. Figure 4.47 shows the effect of pH on the competitive removal of Pb (II) and Cd (II) ions.

From figure 4.47, it was observed that the solution pH greatly affected the competitive removal of Pb (II) and Cd (II) ions. The percentage removal of Pb (II) and Cd (II) ions increased with increase in the solution pH. The removal efficiency of Pb (II) increased from 67.77% to 98.99% when the pH was raised from 2 to 4. Further increase in pH did not result in increase in the removal of Pb (II) ions. Similarly, the percentage removal of Cd (II) ions increased from 41.96% to 88.52% when the pH was increased

from 2 to 6. The low percentage removal of Pb (II) and Cd (II) ions at low pH values was attributed to the high concentration of hydrogen ions leading to increased competition for binding sites between the metal ions and hydrogen ions. This results in reduced adsorption of the metal ions by the raw diatomite.

Moreover, the overall surface charge of the raw diatomite become positive at low pH values due to protonation of the hydroxyl and silanol groups on the diatomite surface. This resulted in increased electrostatic repulsion between the positively charge adsorbent surface and the metal ions therefore, hindering the adsorption process (Bilgin and Tulun, 2015). As the solution pH increased, the concentration of hydrogen ions in the solution reduces gradually leading to decreased competition for the sorption sites between the hydrogen ions and the metal ions. At higher pH values, the diatomite surface becomes negatively charged (ElSayed, 2018). which favours the adsorption of Pb (II) and Cd (II) at higher pH values.

In comparison with single ions, the percentage removal of Pb (II) and Cd (II) ions from binary ion solution were lower compared to those of single ions. The highest percentage removal of Pb (II) was 99.21% at pH of 4 in single ion studies which reduced slightly to 98.99% at pH of 4 in binary ion studies. Similarly, the percentage removal of Cd (II) ions reduced from 90.8% to 88.52% at pH of 6 for single and binary ion studies respectively. These shows that the presence of another metal ion has antagonistic effect in the adsorption of both Pb (II) and Cd (II) ions due to competition for the active binding sites between the metal ions.

Similar observations were reported by Lavado-Meza *et al.* (2023) in removal of Pb (II) and Cd (II) ions from single and binary solutions using *Opuntia ficus* biosorbent. Since increasing the pH from 4 to 6 had a slight decrease in the percentage removal of Pb (II) ions from 98.99% to 98.69% while at pH of 6, the percentage removal of Cd (II) ions was maximum (88.52%), pH of 6 was chosen as the optimum pH for the subsequent competitive adsorption experiments.

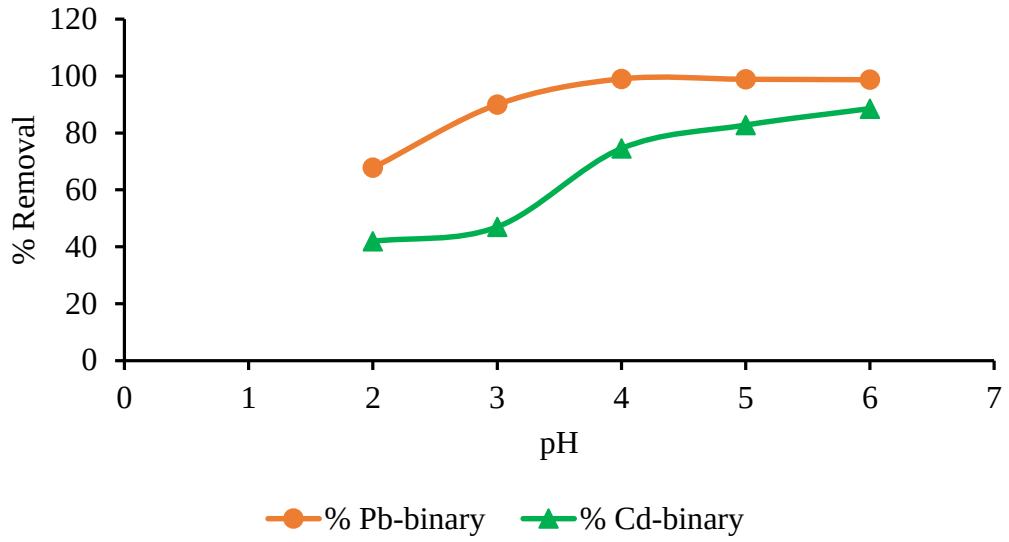

Figure 4.47: Effect of pH on the percentage removal of Pb (II) and Cd (II) ions from Pb-Cd binary ion solution using raw diatomite. (Initial concentration 10 mg/L; contact time 80 minutes; adsorbent dosage 2 g/L; temperature 25±2 ^{o}C; shaking speed 240 rpm)

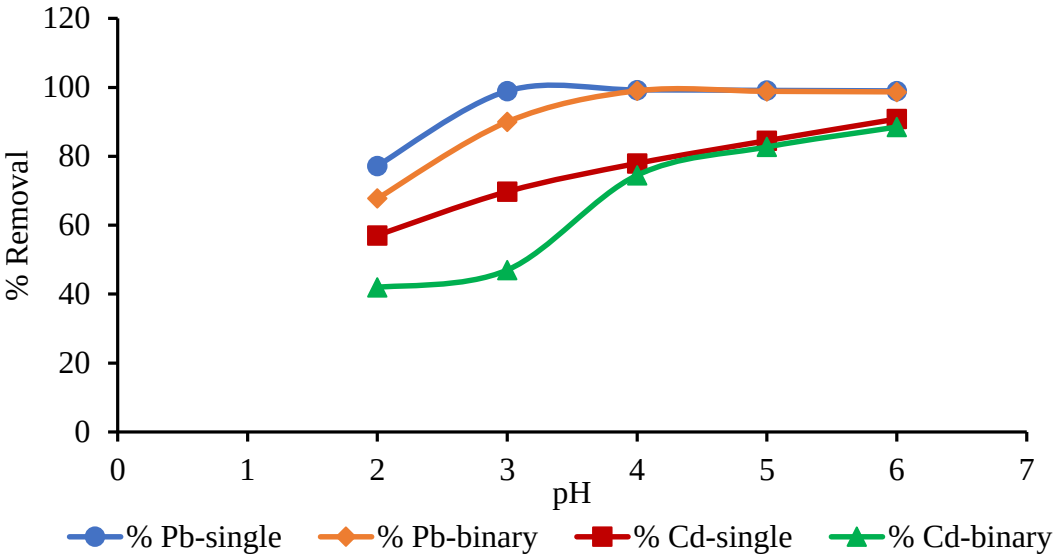

Figure 4.48: Comparison on the effect of pH on the percentage removal of Pb (II) and Cd (II) ions from single and binary ion solutions using raw diatomite.

4.4.2 Effect of Initial Metal Ion Concentration on the Competitive Adsorption of Pb (II) and Cd (II) ions in Binary Ion Solutions.

The study of multi-component adsorption is essential since most industrial effluents contain several pollutants. Multi-component adsorption is important as it illustrates the interference of one pollutant to the adsorption of the other (Yemisi *et al.*, 2021). In order to investigate the effect of concentration of the competing metal ion species on

the removal of Pb (II) and Cd (II), batch experiments were carried out at optimal pH of 6 while adsorbent dosage, contact time, shaking speed and temperature were held constant at 2 g/L, 80 minutes, 240 rpm and 25±2^{o}C respectively. During the batch experiments, the concentration of one metal ion species was varied from 10 mg/L to 70 mg/L while holding the concentration of the other metal ion constant at 10 mg/L and 30 mg/L.

In binary metal ion solution, there was a general decrease in the percentage removal of both Pb (II) and Cd (II) ions compared to that of single metal ions solutions. The percentage removal of Pb (II) ions was slightly reduced by the presence of Cd (II) ions in the binary metal ion solution compared to that of single ion solutions. The maximum percentage removal of Pb (II) ions was 98.944% for single ions which reduced to 98.69% and 96.49% when the concentration of interfering Cd (II) ions was 10 mg/L and 30 mg/L respectively. Similarly, the presence of Pb (II) ions had an inhibitory effect on the percentage removal of Cd (II) ions onto raw diatomite. The removal efficiency of Cd (II) ions decreased substantially from 90.82% in single ion solution to 88.52% and 82.15% when in the presence of Pb (II) ions at an initial concentration of 10 mg/L and 30 mg/L respectively.

This shows that each metal ion had an antagonistic effect on the percentage removal of the other metal ion in binary ion solutions. This was attributed to the competition for the active adsorption sites on the raw diatomite surface between the metal ions. According to Elkhatib *et al.* (2022), the decrease in competitive adsorption of the heavy metal ions can also be attributed to increase in ionic strength of the solution since the cations are charged species. Similar observations have been reported by Wang *et al*. (2011), Wu *et al.* (2019) and Elkhatib *et al.* (2022).

To better understand the binary ion adsorption on raw diatomite, the competitive effect of the metal ions on the adsorption capacity of Pb (II) and Cd (II) ions was evaluated by computing the ratio of equilibrium sorption capacities as shown in equation 4.4.

$$r = \frac{Q_{mix}}{Q_{\mathrm{e}}} \tag{4.4}$$

Where Q_{mix} and Q_{e} are the equilibrium adsorption capacities of the metal ion in the binary and single ion solutions respectively under similar conditions. According to

Shikuku *et al*. (2018) and Cholico-Gonzalez *et al.* (2020), when r>1, the presence of competing ions in binary ion solution (multicomponent system) enhances the adsorption of pollutant, therefore, synergistic effect and if r =1, there is no interaction between the two metal ions. In contrast, if r <1, then the adsorption of pollutant is diminished by the presence of the other metal ion, therefore, antagonistic effect. The calculated r values are shown in table 4.8.

Table 4.8: Relationship between the adsorption capacities from single and binary ion solutions for both Pb (II) and Cd (II) ions.

Metal ion	Equilibrium adsorption capacities (mg/g)			Ratio $r = \frac{Q_{mix}}{Q_e}$	
	Single ion solution	Binary ion solution			
		10 mg/L of competing ion	30 mg/L of competing ion	For 10 mg/L of competing ion	For 30 mg/L of competing ion
Pb (II)	4.961	4.935	4.824	0.995	0.972
Cd (II)	4.541	4.426	4.108	0.975	0.905

Initial concentration of target metal ion 10mg/L, adsorbent dosage 2g/L, contact time 60 minutes, pH=6, shaking speed 240rpm, temperature 25±2^{o}C.

According to table 4.8, the presence of Pb (II) ions as the interfering ions induced an antagonistic effect on the adsorption of Cd (II) ions obtaining r values of 0.975 and 0.905 when the concentration of Pb (II) was10 mg/L and 30 mg/L respectively. However, at low concentrations of Cd (II) as the interfering ions, the presence of Cd (II) ions did not result in significant competition for the active sites over Pb (II) since the r value was very close to unity. At higher concentrations of Cd (II) as the interfering ions, there was a slight increase in the competition for the active sites on raw diatomite as r values reduced to 0.972. This led to the reduction in the percentage removal of Pb (II) ions by 2.2% when the concentration of Cd (II) as the interfering ions was increased from 10 mg/L to 30 mg/L. This shows that the antagonistic effect increases with increase in the concentration of the interfering ion due to increased competition for active sites at higher concentrations.

In addition, the inhibitory effect of Pb (II) on Cd (II) removal was more than that of Cd (II) on Pb (II) ions removal at all concentrations. According to Sati *et al.* (2014), Alexander *et al*. (2017) and Chukwuemeka-Okorie *et al.* (2018), the difference in the adsorption trend of Pb (II) and Cd (II) may be attributed to differences in the

physicochemical properties of the metal ions such as electronegativity, atomic weight and hydration radius. Pb (II) ion has a smaller hydration radius (0.401 nm) than Cd (II) (0.426 nm) thus it is able to pass through the pores and channels of the raw diatomite structure with ease compared to Cd (II) leading to high adsorption of Pb (II) ions.

Additionally, Pb (II) ion is more electronegative than that of Cd (II) ions. Pb (II) ions have Pauling electronegativity of 1.87 compared to electronegativity of 1.69 for Cd (II) ions (Fan *et al.,* 2021), therefore, Pb (II) ion was able to form bonds more easily with the functional groups on the diatomite surface more easily than Cd (II) ions. In the same context, the hydration energy of the metal ions plays an important role in the preferential adsorption of Pb (II) and Cd (II) ions. According to Arowojobe *et al*. (2020), the lower the hydration energy, the higher the adsorption affinity of the metal ions. Pb (II) has a lower hydration energy of -1481 kJ/mol compared to -1807 kJ/mole for Cd (II) ions (Fertu *et al.,* 2022). The percentage removal and adsorption capacity of the metals species in binary ion solutions was in the order of Pb (II) > Cd (II), and was in agreement with decreasing electronegativity and also the increasing hydrated ionic radii of metals ions.

A similar trend was observed by López-Sotelo *et al*. (2017) in the competitive adsorption of Pb (II) and Cd (II) on to poultry hatchery waste biosorbent. They credited the high adsorption of Pb (II) ions to the high electronegativity and atomic weight of Pb (II) ions as compared to Cd (II) ions. Similarly, Alexander *et al*. (2017) observed that the adsorption of metal ions onto natural bentonite clay was in the order Pb (II) > Cd (II) > Mn (II) ions and attributed the high adsorption of Pb (II) ions to its high electronegativity along with the smaller hydrated radii of Pb (II) (0.401nm) compared to that of Cd (II) (0.426 nm) and Mn (II) ions (0.438 nm).

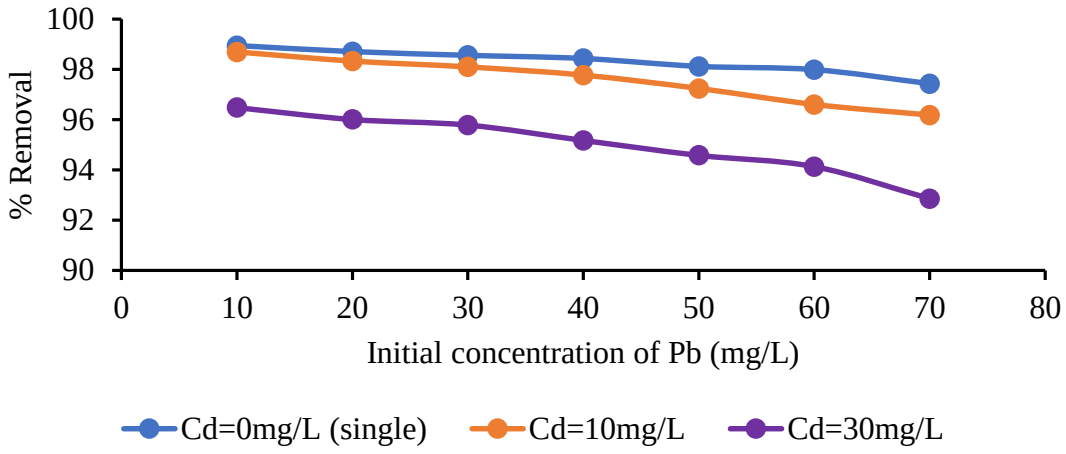

Figure 4.49: Effect of initial concentration on the removal of Pb (II) ions from Pb-Cd binary ion solution using raw diatomite at different concentrations of Cd (II) as the competing ions. (pH of 6; contact time 80 minutes; adsorbent dosage 2 g/L; temperature 25±2 ^{o}C; shaking speed 240 rpm)

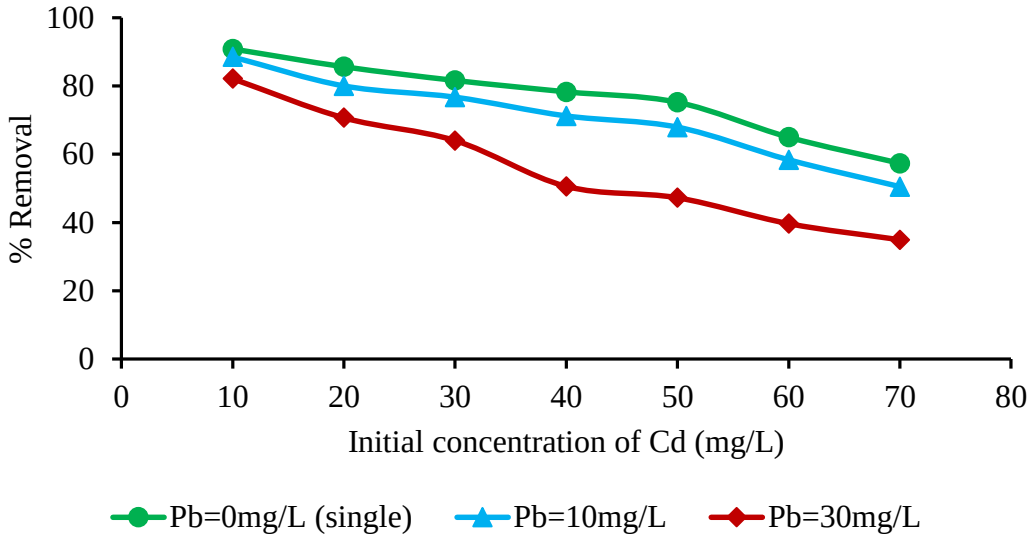

Figure 4.50: Effect of initial concentration on the removal of Cd (II) ions from Pb-Cd binary ion solution using raw diatomite different concentrations of Pb (II) as the competing ions. (pH of 6; contact time 80 minutes; adsorbent dosage 2 g/L; temperature 25±2 ^{o}C; shaking speed 240 rpm)

4.4.3 Effect of Adsorbent Dosage on Competitive Adsorption of Pb (II) and Cd (II) ions form Binary Ion Solution.

The effect of adsorbent dosage on the percentage removal of Pb (II) and Cd (II) ions from Pb-Cd binary ion solution was investigated by varying the adsorbent dose from 0.4 g/L to 10 g/L at optimal pH of 6 and contact time of 80 minutes. Equimolar solution of Pb-Cd mixture (10 mg/L of each ion) was placed in contact with a certain dosage of raw diatomite for 80 minutes at constant temperature of 25±2°C and shaking speed of

240 rpm. It was observed that percentage removal of both Pb (II) and Cd (II) increased with increase in the adsorbent dosage. Efficiency removal of Pb (II) ions increased from 93.88% at 0.4 g/L to 100% at 8 g/L. Removal of Cd (II) ions increased from 17.69% to 100% at 10 g/L.

Increasing the adsorbent dosage increased the number of active binding sites available for adsorption process (Yemisi *et al*., 2021; Ndung'u, 2021). The increase in percentage removal of Pb (II) and Cd (II) ions was rapid at lower dosage but after dosage of 2 g/L for Pb (II) ions and 4 g/L for Cd (II), the increase was small. The almost steady state after these adsorbent doses was due to overlapping and screening effect of the active adsorption sites on the adsorbent surface due to overcrowding of the adsorbent particles (Ndung'u, 2021). The percentage removal efficiency of Pb (II) and Cd (II) ions as a function of adsorbent dose is displayed in figure 4.57.

The efficacy of raw diatomite in binary ion solution was however lower compared to that of single ion studies. Higher adsorbent dosage was required in binary studies to achieve the same percentage removal observed in single ion studies. In binary ion solution, the maximum percentage removal of both Pb (II) and Cd (II) ions were 100% at 8 g/L and 10 g/L respectively. These adsorbent doses were however higher compared to those of single ion studies (4 g/L for Pb (II) and 6 g/L for Cd (II)) for the same percentage removal of 100%. This was attributed to the competition between Pb (II) and Cd (II) ions for the active binding sites on the raw diatomite surface. Since a specific amount of raw diatomite had a determinate number of active binding sites, competition for these sites automatically lead to mutual interference and inhibition in the adsorption of each metal ion. In addition, the raw diatomite also had a high affinity for Pb (II) than for Cd (II) mainly due to the high electronegativity of Pb (II) compared to Cd (II) ions. This led to the higher percentage removal of Pb (II) ions compared to Cd (II) ions. These findings are in agreement with those reported by Yemisi *et al.* (2021).

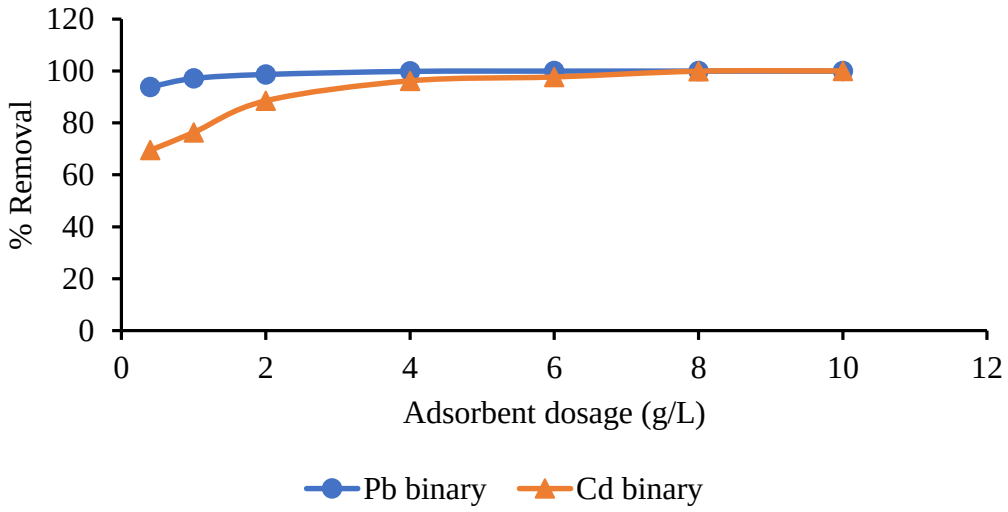

Figure 4.51: Effect of adsorbent dosage on the percentage removal of Pb (II) and Cd (II) ions from Pb-Cd binary ion solution. (Initial concentration 10 mg/L; contact time 80 minutes; pH of 6; temperature 25±2 ºC; shaking speed 240 rpm).

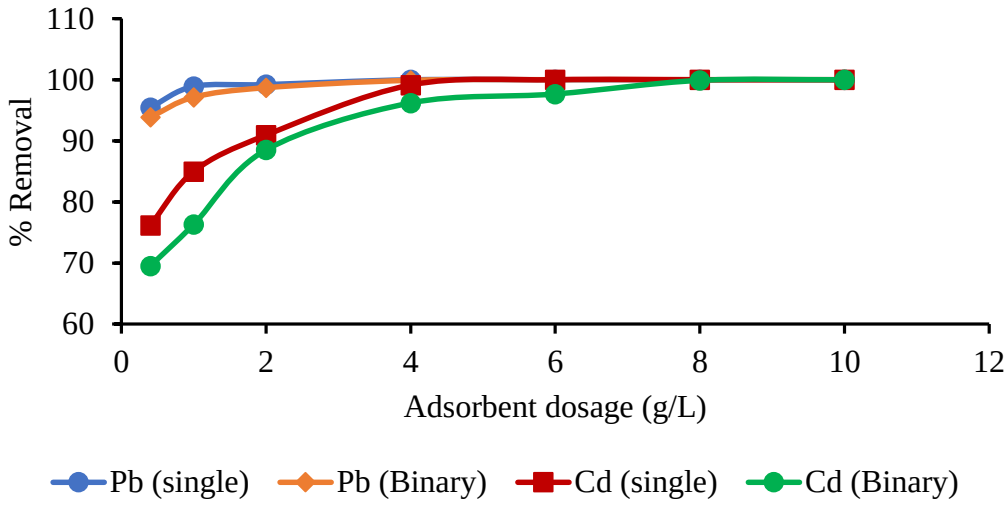

Figure 4.52: Comparison of the effect of adsorbent dosage on the percentage removal of Pb (II) and Cd (II) ions from single and binary ion solutions.

4.4.4 Effect of Contact Time on the Competitive Adsorption of Pb (II) and Cd (II) ions from Binary Ion Solution.

The effect of contact time on the simultaneous removal of Pb (II) and Cd (II) ions from binary ion solution was investigated by varying the contact time from 20 minutes to 120 minutes at optimal pH of 6. Equimolar solution of Pb-Cd mixture (10 mg/L of each ion) was placed in contact with 2 g/L of raw diatomite for a predetermined contact time at constant temperature of 25±2°C and shaking speed of 240 rpm. It was observed that

the percentage removal of both Pb (II) and Cd (II) increased rapidly for the first 40 minutes due to the high number of active sites responsible for adsorption on the raw diatomite surface. As the contact time progressed, these active binding sites were occupied with heavy metal ions and their number therefore reduced with time leading to the slow uptake. Equilibrium was finally reached at 60 minutes and 80 minutes for Pb (II) and Cd (II) ions respectively.

The maximum percentage removal of both Pb (II) and Cd (II) ions were 98.69% and 88.52% at contact times 60 and 80 minutes respectively. These was however lower than that of single ion studies (99.21% for Pb (II) at 60 minutes and 90.93% for Cd (II) at 80 minutes). This was attributed to the antagonistic effect that each metal ion had on the adsorption of each other due to competition for the active binding sites on the raw diatomite surface. For Pb (II) ions, the percentage removal in binary ion solution reduced by a very small margin of 0.52% compared to single ion solution while for Cd (II) ions, it reduced by 2.41%. This was mainly because the presence of Cd had a slight antagonistic effect on the removal of Pb (II) ions from binary solutions.

In contrast, the presence of Pb (II) ions had a great interference and inhibition in the adsorption of Cd (II) ions from binary solutions. This was mainly due to the high electronegativity and high atomic weight of Pb (II) ions compared to Cd (II) ions (Zhang *et al.,* 2020; Fan *et al.,* 2021) leading to the raw diatomite having a high affinity for Pb (II) ions adsorption than that of Cd (II) ions. Similar observations were reported by Wang *et al.* (2011) for the competitive adsorption of Pb (II), Cu (II) and Cd (II) ions using wheat residue derived carbon as the adsorbent. Since the adsorption of Pb (II) ions attained equilibrium at contact time of 60 minutes while Cd (II) ions at 80 minutes, a contact time of 80 minutes was selected as the optimal contact time for the adsorption of both Pb (II) and Cd (II) ions from Pb-Cd binary ion solution.

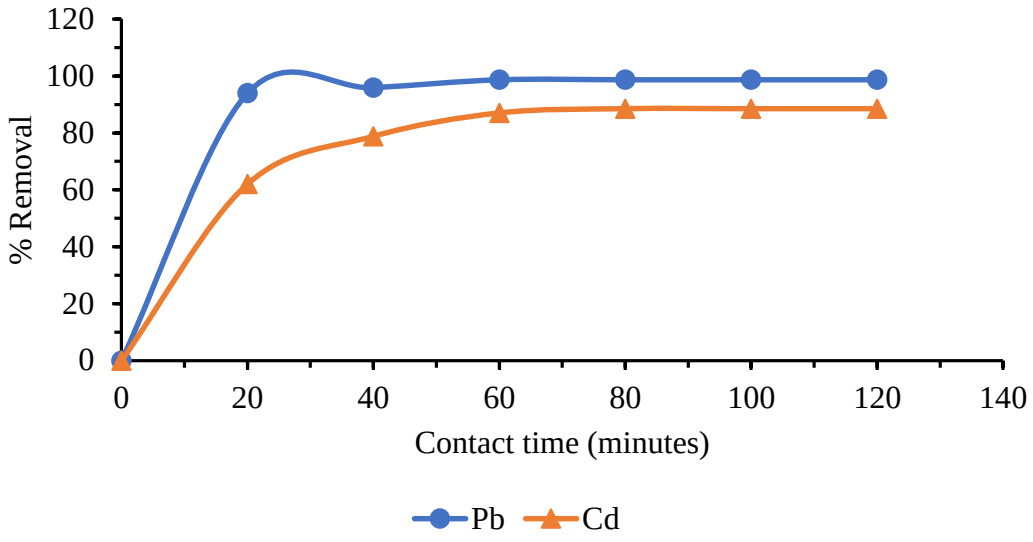

Figure 4.53: Effect of contact time on the percentage removal of Pb (II) and Cd (II) ions from Pb-Cd binary ion solutions. (Initial concentration 10 mg/L; pH of 6; adsorbent dosage 2 g/L; temperature 25±2 ^{o}C; shaking speed 240 rpm).

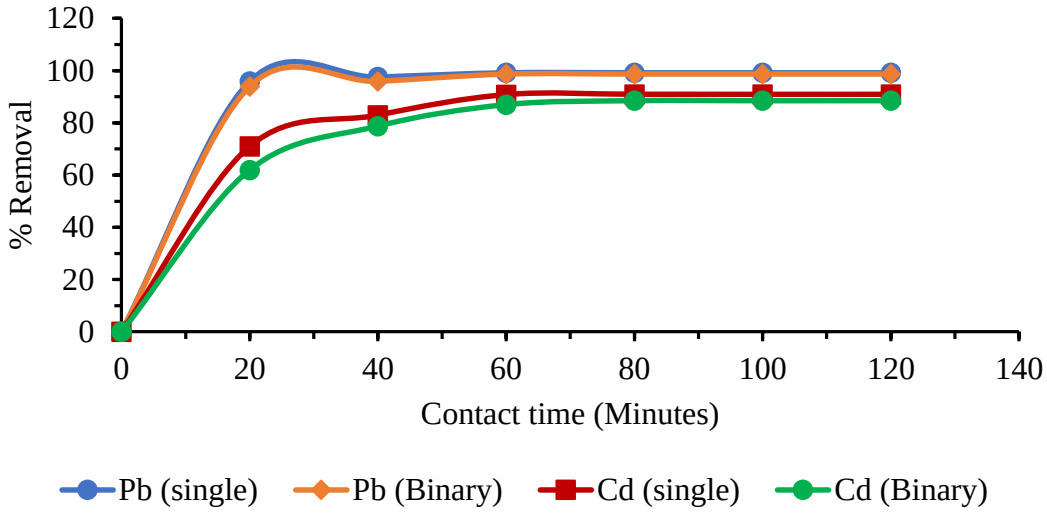

Figure 4.54: Comparison of the effect of contact time on the percentage removal of Pb (II) and Cd (II) ions from single and binary ion solutions.

4.4.4.1 Kinetic Parameters for Binary Ion Studies

In order to understand the adsorption kinetics in binary ion solution and in turn the adsorption mechanism, the adsorption data on effect of contact time was applied to pseudo-first order and pseudo-second order kinetic models. Kinetic parameters were obtained from the linear plots of $In(q_e-q_t)$ vs t and (t/q_t) vs t; for pseudo-first-order and pseudo-second order kinetic models respectively. The predicted and experimental equilibrium sorption capacities (q_e) were tabulated in table 4.9. From the data, it was

observed that pseudo-second order model fit well to describe the competitive adsorption kinetics of Pb (II) and Cd (II) ions from binary ion solutions ($R^2 > 0.99$). This was also confirmed by the fact that the predicted and experimental equilibrium sorption capacities (q_e) were almost equal for pseudo-first order model. The experimental equilibrium adsorption capacities for Pb (II) and Cd (II) in binary ion solution were 4.934 mg/g and 4.426 mg/g respectively which were consistent with the predicted sorption capacities of 4.935 mg/g for Pb (II) and 4.831 mg/g for Cd (II) ions. This indicated that chemisorption was the rate limiting step in the competitive adsorption of Pb (II) and Cd (II) ions onto raw diatomite.

Table 4. 9: Parameters of pseudo-first order and pseudo-second order kinetic models for the competitive adsorption of Pb (II) and Cd (II) ions from binary ion solution using raw diatomite.

Kinetic Model	Parameters	Metal Ions	
		Pb (II)	Cd (II)
Experimental	q_e (mg/g)	4.935	4.426
PFO	q_e (mg/g)	11.551	52.374
	k_1	0.1483	0.1308
	R^2	0.9621	0.9414
PSO	q_e (mg/g)	4.995	4.831
	k_2	0.1633	0.0229
	R^2	0.9999	0.9976

PFO is pseudo-first-order and PSO is pseudo-second order.

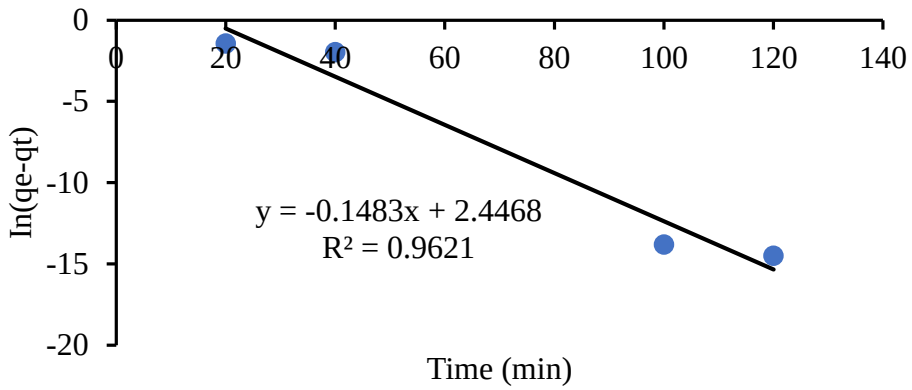

Figure 4.55: Pseudo-first order plot for the competitive adsorption of Pb (II) ions onto raw diatomite from binary ion solution.

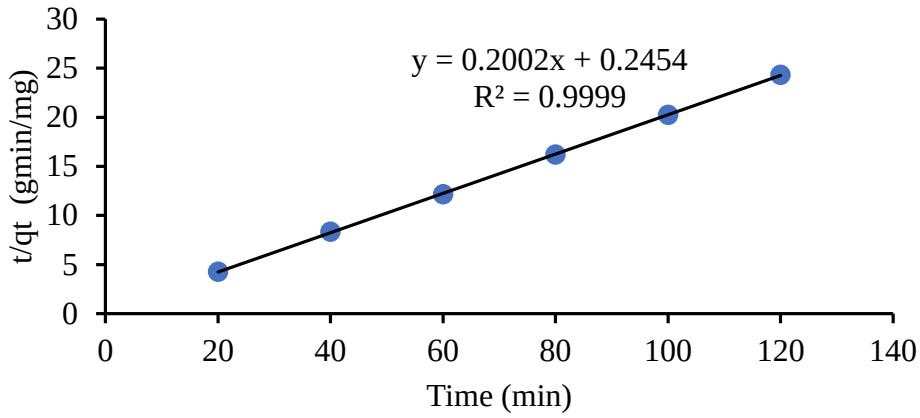

Figure 4.56: Pseudo-second order plot for the competitive adsorption of Pb (II) ions onto raw diatomite from binary ion solution.

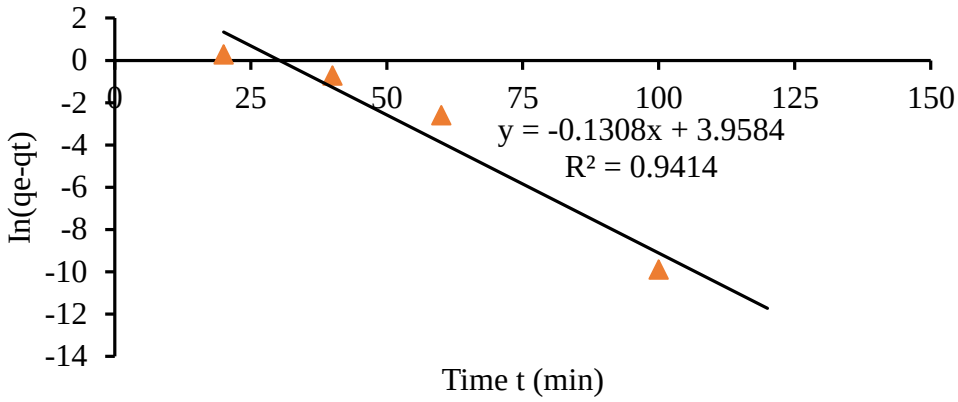

Figure 4.57: Pseudo-first order plot for the competitive adsorption of Cd (II) ions onto raw diatomite from binary ion solution.

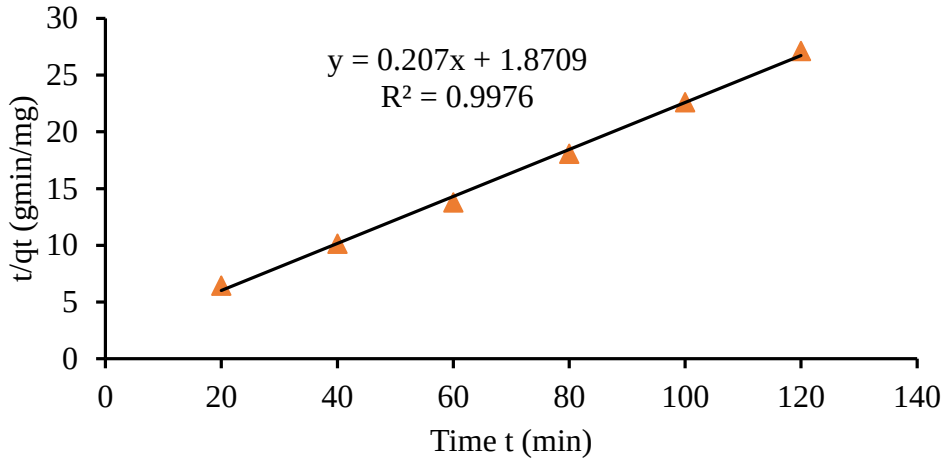

Figure 4.58: Pseudo-second order plot for the competitive adsorption of Cd (II) ions onto raw diatomite from binary ion solution.

4.4.5 Effect of Temperature on Competitive Adsorption of Pb (II) and Cd (II) ions from Binary Ion Solution.

The effect of temperature on the competitive adsorption of Pb (II) and Cd (II) ions was evaluated by varying the solution temperature from 298 K to 338 K while keeping the other parameters constant: Contact time of 80 minutes, pH of 6, initial concentration of each metal ion 10 mg/L, adsorbent dosage 2 g/L and shaking speed at 240 rpm. It was observed that increase in temperature from 298 K to 338 K resulted in the decrease in the removal of Pb (II) ions from 98.96% to 97.58%. This was due to the exothermic nature of the adsorption of Pb (II) ions onto the raw diatomite surface. In contrast, increase in temperature from 298 K to 338 K resulted in increased removal of Cd (II) ions owing to the endothermic nature of the adsorption process. These trends were similar to those obtained in single ion systems. Figure 4.59 shows the percentage removal of Pb (II) and Cd (II) ions from binary ion solution as a function of temperature.

The presence of both metal ions in binary ion solution had antagonistic effect on the adsorption of the target pollutant. This was evident by the decrease in the percentage removal of both Pb (II) and Cd (II) ions in binary ion solutions compared to single ion solutions. For instance, the presence of Cd (II) ions in binary ion solution had a slight inhibitory effect on the adsorption of Pb (II) as the target pollutant. In the presence of Cd (II) ions, the removal of Pb (II) reduced by 1.11% (from 98.69% to 97.58%) in binary ion solution compared to 0.45% (from 99.21% to 98.76%) in single ion solution when the temperature was increased in the range of 298 K to 338 K.

In addition, the presence of Pb (II) ions as interfering ions had a major inhibitory effect on the removal of Cd (II) ions. Under the same conditions, the removal of Cd (II) ions increased by 8.9% from 90.93% to 99.83% in single ion solution as the temperature increased from 298 K to 338 K while in binary ion solution, it increased only by 2.18% when the temperature was increased from 298 K (88.52%) to 338 K (90.70%). This great inhibitory effect of Pb (II) on adsorption of Cd (II) ions was due to the high electronegativity of Pb (II) ions leading to raw diatomite having a higher affinity for Pb (II) ions than Cd (II) ions (Chukwuemeka-Okorie *et al.*, 2018). According to Arowojobe *et al*. (2020) and Fertu *et al.* (2022), Pb (II) has lower hydrated radii (0.401 nm) as well as hydration energy (-1481 kJ/mol) than Cd (II) (0.426 nm and -1807

kJ/mol) respectively, therefore, Pb (II) has a higher affinity for adsorption compared to Cd (II) ions. These observations mirror those reported by Taha *et al.* (2016).

Since increase in temperature from 298 K to 338 K only led to a slight decrease in the percentage removal of Pb (II) ions by 1.11% (i.e. from 98.69% to 97.58%) in the binary ion studies while for Cd (II)ions it led to a maximum percentage removal at 338 K, the temperature of 338 K was therefore considered as the optimum temperature for the removal of Pb (II) and Cd (II) ions from Pb-Cd binary ion solution.

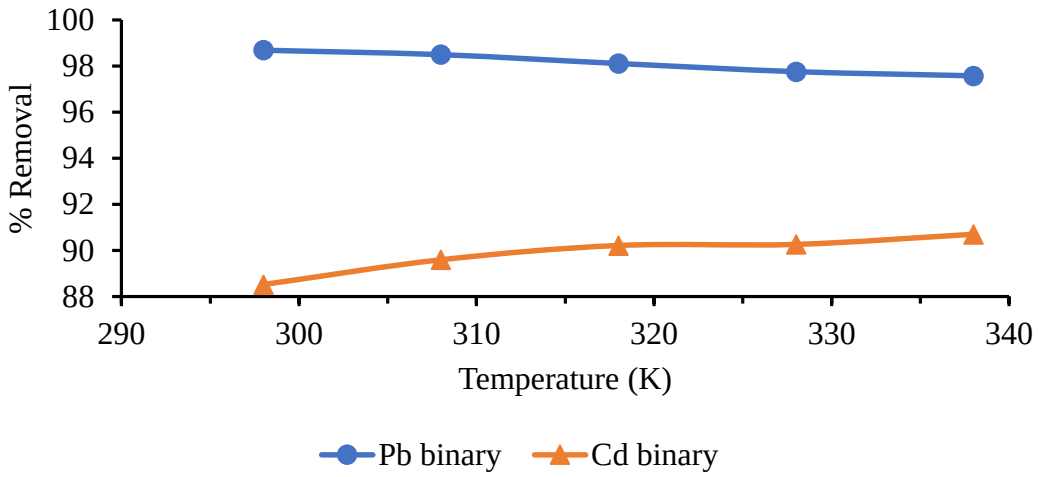

Figure 4.59: Effect of temperature on the percentage removal of Pb (II) and Cd (II) ions from Pb-Cd binary ion solution. (Initial concentration 10 mg/L; contact time 80 minutes; adsorbent dosage 2 g/L; pH of 6; shaking speed 240 rpm).

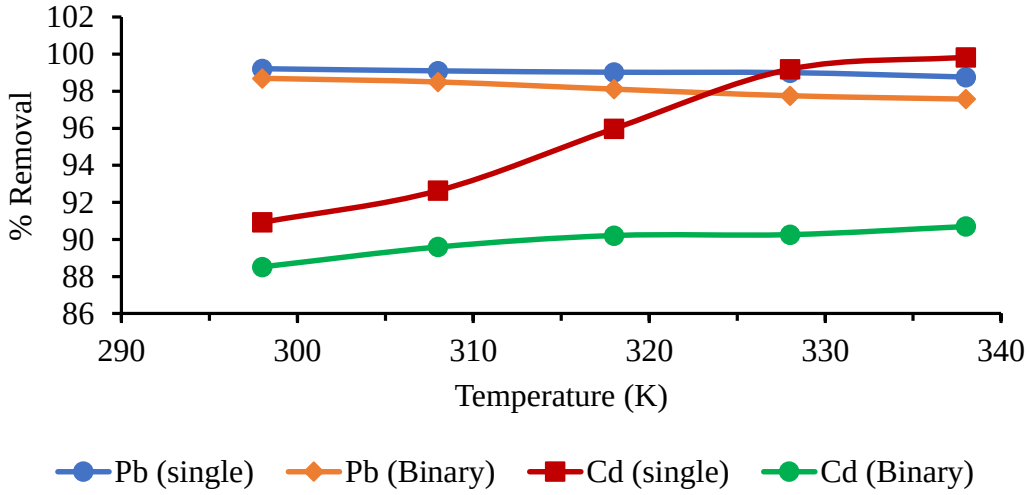

Figure 4.60: Comparison of the effect of temperature on the percentage removal of Pb (II) and Cd (II) ions from single and binary ion solutions.

4.4.5.1 Thermodynamics parameters for Binary Ion Studies

In order to determine the nature, feasibility and favorability of the adsorption process in binary system, thermodynamic parameters (change in Gibbs free energy (ΔG°), enthalpy change (ΔH°) and entropy change (ΔS°) were determined for the competitive adsorption of Pb (II) and CD (II) ions. Van't Hoff plot was applied to determine the magnitude of ΔH° (kJ/mol) and ΔS° ($kJmol^{-1}K^{-1}$) from the slope and intercept, respectively as shown in figures 4.61 and 4.62. Table 4.10 shows the calculated thermodynamic parameters.

Table 4. 10: Thermodynamic parameters for the competitive adsorption of Pb (II) and Cd (II) ions from binary ion solution using raw diatomite.

Metal ions	Adsorbent	ΔG° (kJ/mol)					ΔH° (kJ/mol)	ΔS° (J/mol/K)
		298K	308K	318K	328K	338K		
Pb (II)	Raw diatomite	-10.715	-10.714	-10.446	-10.295	-10.385	-13.993	-10.952
Cd (II)	Raw diatomite	-5.061	-5.513	-5.873	-6.072	-6.401	4.599	33.652

The calculated Gibbs free energy change (ΔG°) values were all negative indicating that the competitive adsorption of Pb (II) and Cd (II) ions onto raw diatomite from binary ion solution was feasible and spontaneous. The magnitude of ΔG° values for Pb (II) ions became less negative with increasing temperature indicating that the competitive adsorption of Pb (II) ions in binary ions solution became less spontaneous as the temperature increased from 298 K to 338 K. This resulted in reduction in the removal efficiency of Pb (II) ions at higher temperatures in binary ion solution. According to Abunah, *et al.* (2019), this may be due to deterioration of the raw diatomite structure at higher temperatures resulting in the loss of active adsorptive surfaces with high affinity for Pb (II) ions. Contrarily, the magnitude of ΔG° values for Cd (II) ions became more negative with increasing temperature, implying that the adsorption was more efficient and spontaneous at higher temperatures. This was evident in the increased removal efficiency of Cd (II) ions from 88.52% at 298 K to 90.70% at 338 K.

The enthalpy changes (ΔH°) values for the competitive adsorption of Pb (II) was negative indicating that the competitive adsorption of Pb (II) onto raw diatomite was exothermic. This was evident in the decreased removal efficiency of Pb (II) ions from 98.69% to 97.58% as temperatures increased from 298 K to 338 K. In contrast, the ΔH°

for competitive adsorption of Cd (II) ions was positive indicating that the adsorption process of Cd (II) onto raw diatomite in binary ion solution was an endothermic process.

Furthermore, the entropy change (ΔS°) value for competitive adsorption of Pb (II) ions was negative corresponding to a decrease in the degree of freedom of adsorbed Pb (II) ions with increasing temperature leading to reduced randomness (increased order) at the solid-liquid interface. However, the ΔS° values for competitive adsorption of Cd (II) ions in binary ion solution was positive corresponding to an increase in randomness at the solid-solution interface. This implies that an increase in temperature is beneficial to the competitive adsorption of Cd (II) ions onto both raw diatomite in binary ion solution as evident in the increase in the removal efficiency 88.52% at 298 K to 90.70% at 338 K.

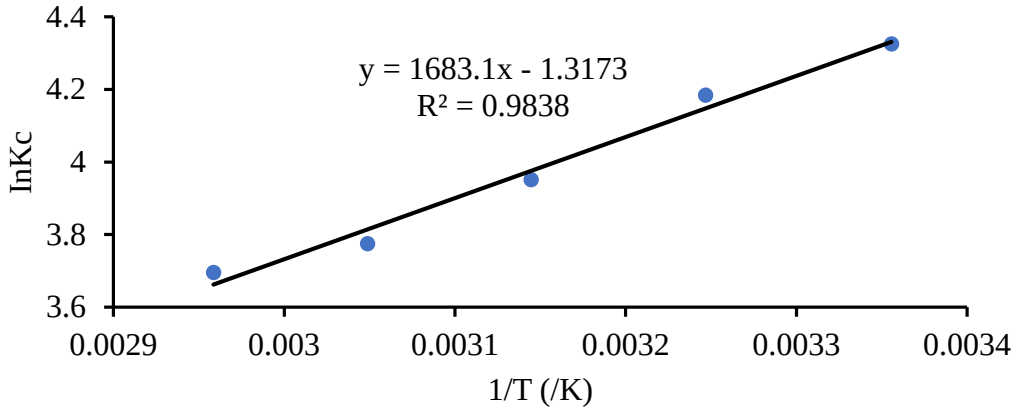

Figure 4.61: Van't Hoff plot for adsorption of Pb (II) onto raw diatomite from Pb-Cd binary ion solution.

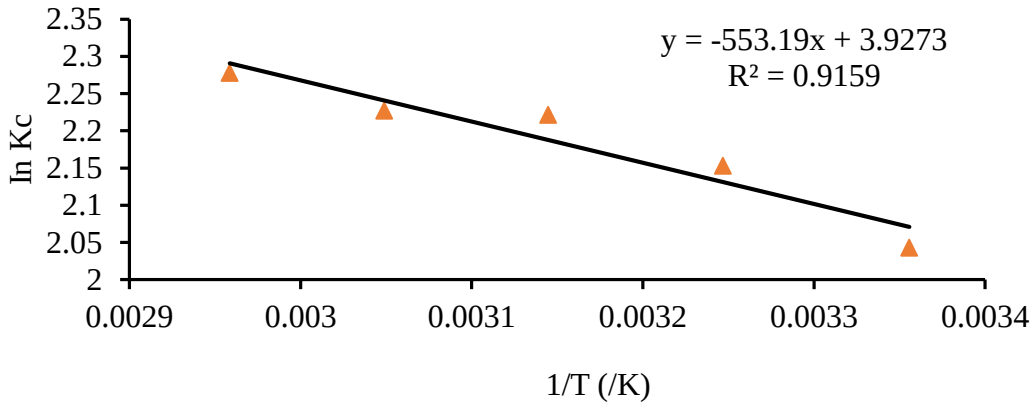

Figure 4.62: Van't Hoff plot for adsorption of Cd (II) onto raw diatomite from Pb-Cd binary ion solution.

CHAPTER FIVE

SUMMARY, CONCLUSION AND RECOMMENDATIONS

5.1 Summary

The overall objective of this study was to synthesize MnO_2-diatomite composite using Kenyan diatomite and use both the raw diatomite and MnO_2-diatomite composites for the removal of Pb (II) and Cd (II) ions from aqueous solutions. MnO_2-diatomite composite was successfully synthesized by acid reduction of $KMnO_4$/diatomite mixture using 6M HCl acid at room temperature. The concentration of $KMnO_4$ influenced the amount of MnO_2 formed in MnO_2 -diatomite composite. Higher $KMnO_4$ concentrations resulted in more MnO_2 particles formed which in turn reduced the surface area of the MnO_2-diatomite composite compared to diatomite. The MnO_2-diatomite composites prepared were dark brown powders compared to the white powder of raw diatomite. XRD, FTIR and XRF characterization techniques illustrated that both raw diatomite and MnO_2-diatomite composites were mainly composed of silica. The XRD spectrum also indicated that these adsorbents were amorphous in nature. BET/BJH analysis revealed that raw diatomite and MnO_2-diatomite composite 2 nanoparticles were mesoporous with a surface area, pore volume and pore size of 32.29 m^2/g, 0.1105 m^3/g, 16.38 nm and 30.48 m^2/g, 0.0792 m^3/g, 11.54 nm respectively.

The batch adsorption studies revealed that raw diatomite and MnO_2-diatomite composite can effectively be employed as adsorbents for the removal of Pb (II) and Cd (II) ions from aqueous solution. In single ion and binary ion studies, the adsorption process was influenced by factors such as pH, adsorbent dosage, contact time, temperature and initial metal ion concentration. The removal of metal ions increased with increase in contact time, adsorbent dosage and pH in both single ions and binary ions solutions. The optimum contact time varied with the metal ion, therefore, Pb (II) ions had an optimum contact time of 60 minutes while Cd (II) ions had 80 minutes for both adsorbents. The efficiency removal of the metal ions increased with increase in adsorbent dosage due to increase in the number of active sites available for adsorption. The efficiency removal of the metal ions also increased with increase in pH. At low pH values, protonation of the active sites on the adsorbent surface occurred which prevented the adsorption of the metal ions.

The removal of Pb (II) and Cd (II) ions was found to be highly dependent on initial concentration of metal ions. The efficiency removal of metal ions decreased with increase in initial metal ion concentration. The variation of efficacy removal of the metal ions with respect to temperature was dependent on the metal ion. The percentage removal of Pb (II) ions decreased with increase in temperature indicating that the adsorption of Pb (II) ions by the adsorbents was an exothermic process. In contrast, the percentage removal of Cd (II) ions increased with increase in temperature representing an endothermic process. In single ion studies, the optimum conditions for removal of Pb (II) ions by raw diatomite and MnO_2-diatomite composite were initial concentration of 10 mg/L, contact time of 60 minutes and temperature of 25ºC. Optimum pH was pH of 4 and 6 while adsorbent dosage was 4 g/L and 6 g/L for raw diatomite and MnO_2-diatomite composite respectively. The optimum conditions for Cd (II) ions removal were pH of 6, contact time 80 minutes, initial metal ion concentration 10 mg/L, temperature 65 ºC and adsorbent dosage of 6 g/L (raw diatomite) and 8 g/L (MnO_2-diatomite composite).

The experimental data for single ion studies was evaluated by Langmuir, Freundlich and Temkin isotherms to assess the adsorption behaviour of the adsorbents. The adsorption data fit well with Langmuir isotherm implying that monolayer adsorption of Pb (II) and Cd (II) ions occurred at the adsorbent surface without interaction of neighbouring adsorbate molecules. The maximum adsorption capacities (Qmax) as per Langmuir isotherm for Pb (II) was 52.63 mg/g for raw diatomite and 18.18 mg/g for MnO_2-diatomite composite. Qmax for Cd (II) was 23.26 mg/g and 13.16 mg/g for raw diatomite and MnO_2-diatomite composite respectively. Kinetic modelling of the adsorption data was used to predict the adsorption mechanism in single ion and binary ion studies. Kinetic modelling showed that the adsorption of Pb (II) and Cd (II) ions from single and binary ion solutions was well described by pseudo second order kinetic model ($R^2 > 0.99$) indicating that chemisorption was the rate limiting step in the adsorption process.

Thermodynamic studies indicated that the Pb (II) and Cd (II) adsorption onto raw diatomite and MnO_2-diatomite composite for both single ion and binary ion solutions was spontaneous and feasible (all with negative $\Delta G°$ values). The adsorption of Pb (II)

ions by the adsorbents from single ion and binary ion solutions was exothermic (ΔH°= -8.41 kJ/mol, -45.94 kJ/mol and -13.99 kJ/mol when using raw diatomite, MnO_2-diatomite composite and for binary ion studies respectively). In contrast, the adsorption of Cd (II) ions was an endothermic process (ΔH°= 86.43 kJ/mol, 33.37 kJ/mol and 32.65 kJ/mol when using raw diatomite, MnO_2-diatomite composite and for binary ion studies respectively). The ΔS° for Cd (II) ions in single and binary ion solutions were positive indicating there was increased randomness at the solid-solution interphase. The ΔS° for adsorption of Pb (II) onto raw diatomite from single ion solution was also positive (ΔS°= 11.95 J/mol/K). However, the ΔS° for Pb (II) adsorption onto MnO_2-diatomite composite and from binary ion solutions was negative (ΔS°= -120 J/mol/K and -10.95 J/mol/K respectively) indicating that there was a decrease in the degree of freedom of the adsorbed Pb (II) ions with increasing temperature.

Raw diatomite was found to be the most effective adsorbent in the removal of metal ions compared to MnO_2-diatomite composite due to blocking of pores and channels by MnO_2 particles on the MnO_2-diatomite composite surface during modification process. This in turn led to decreased surface area and porosity of MnO_2-diatomite composite compared to raw diatomite. Due to this, raw diatomite was selected as the preferred adsorbent in binary studies. Binary studies showed that the coexistence of Pb (II) and Cd (II) ions in the same solution had antagonistic effect on the adsorption each ion. The percentage removal of metal ions from binary ion solutions greatly reduced compared to single ion solutions for the same operating conditions. This was due to competition between the coexisting Pb (II) and Cd (II) ions for the free active adsorption sites on the raw diatomite surface. In both single ion and binary ion studies, it was found that Pb (II) ions were the most preferred metal ions to be adsorbed onto both raw diatomite and MnO_2-diatomite composite adsorbents than Cd (II) ions. The order of removal efficiency was Pb (II) > Cd (II) due to the physiochemical characteristics of Pb (II) ions such as high electronegativity.

5.2 Conclusion

This study clearly shows that Kenyan raw diatomite and MnO_2-diatomite composite have great adsorption capabilities, therefore, they can effectively be used in sequestering heavy metal ions from aqueous solutions. Adsorption of Pb (II) and Cd

(II) ions from single ion and binary ion solutions using raw diatomite and MnO_2-diatomite composite as adsorbents was greatly influenced by pH, contact time, initial metal ion concentration, adsorbent dosage and temperature. The removal efficiency of the metal ions by raw diatomite and MnO_2-diatomite composite was in the order Pb (II) > Cd (II) ions. This was due to Pb (II) ions being more electronegative than Cd (II) ions and also Pb (II) ions having a smaller hydration radius enabling them to pass through the pores and channels. Raw diatomite had the highest surface area and porosity which enabled it to have the highest efficiency removal of Pb (II) and Cd (II) ions compared to MnO_2-diatomite composite. This shows that Kenyan raw diatomite can efficiency be used in treatment of waste water ladened with heavy metal ions without the need of modification. Raw diatomite is cheap and available in Kenya in huge deposits in Nakuru and Baringo counties, therefore, it can effectively be used as a low-cost adsorbent for heavy metal removal.

5.3 Recommendations

The following recommendations are therefore made.

i. Since both raw diatomite and MnO_2-diatomite composite have proved to be successful in removing heavy metal ions from wastewater, a pilot study should be set-up to evaluate the applicability of both raw diatomite and MnO_2-diatomite composite in the treatment of industrial wastewater effluents.
ii. The effect of concentration of $KMnO_4$ on the synthesis of MnO_2-diatomite composite using Kenyan raw diatomite should be studied further to determine the optimum $KMnO_4$ concentration that results in MnO_2-diatomite composite with a high surface area and removal efficiency towards heavy metal ions compared to the original raw diatomite.
iii. Regeneration studies should be carried out on metal-laden adsorbents to assess whether the adsorbents can be re-used for heavy metal uptake.
iv. More studies be conducted on the modification of Kenyan raw diatomite with other metal oxides such as ferric oxides, zinc oxides, aluminium oxides to evaluate their effect on metal oxide-diatomite composite with respect to the adsorption of heavy metals.

REFERENCES

Abbar, B., Alem, A., Marcotte, S., Pantet, A., Ahfir, N. D., Bizet, L., & Duriatti, D. (2017). Experimental investigation on removal of heavy metals (Cu^{2+}, Pb^{2+}, and Zn^{2+}) from aqueous solution by flax fibres. *Process Safety and Environmental Protection, 109*: 639-647.

Abdelbasir, S. M., & Khalek, M. A. A. (2022). From waste to waste: iron blast furnace slag for heavy metal ions removal from aqueous system. *Environmental Science and Pollution Research*, *29*(38): 57964-57979.

Abdelfattah, I., El Sayed, F., & Almedolab, A. (2016). Removal of heavy metals from wastewater using corn cob. *Research Journal of Pharmaceutical, Biological and Chemical Sciences, 7*(2): 239-248.

Abunah, D., Onindo, C., Andala, D., & Ochoti, E. (2019). Physico-chemical removal of heavy metals from contaminated water using recyclable montmorillonite cellulose nanocomposite. *Journal of Materials and Environmental Science*, *10*(12): 1349-1361.

Ahenda, S. O., Wangeci, A. N., & Nyang'au, J. O. (2020). Physico-chemical and heavy metal assessment of paint industry effluents in Nairobi County, Kenya. *Global Scientific Journal, 8*(3): 2573-2580.

Ahogle, A. M. A., Letema, S., Schaab, G., Ngure, V., Mwesigye, A. R., & Korir, N. K. (2023). Heavy metals and trace elements contamination risks in peri-urban agricultural soils in Nairobi city catchment, Kenya. *Frontiers in Soil Science*, *2*: 1-17.

Ajenifuja, E., Ajao, J. A., & Ajayi, E. O. B. (2017). Adsorption isotherm studies of Cu (II) and Co (II) in high concentration aqueous solutions on photocatalytically modified diatomaceous ceramic adsorbents. *Applied Water Science, 7*(7): 3793-3801.

Akafu, T., Chimdi, A., & Gomoro, K. (2019). Removal of fluoride from drinking water by sorption using diatomite modified with aluminum hydroxide. *Journal of Analytical Methods in Chemistry, 2019*: 1-11

Akpor, O. B., Ohiobor, G. O., & Olaolu, T. D. (2014). Heavy metal pollutants in wastewater effluents: sources, effects and remediation. *Advances in Bioscience and Bioengineering*, *2*(4): 37-43.

Alalwan, H. A., Kadhom, M. A., & Alminshid, A. H. (2020). Removal of heavy metals from wastewater using agricultural byproducts. *Journal of Water Supply: Research and Technology—AQUA, 69*(2): 99-112.

Alexander, J. A., Surajudeen, A., Aliyu, E. N. U., Omeiza, A. U., & Zaini, M. A. A. (2017). Multi-metals column adsorption of lead (II), cadmium (II) and manganese (II) onto natural bentonite clay. *Water Science and Technology*, *76*(8): 2232-2241.

Amer, H. A. T. (2015) *Removal of lead from industrial wastewater using a low-cost waste material* (Masters' Thesis). The American University in Cairo, Egypt.

Aroke, U. O., Abdulkarim, A., & Ogubunka, R. O. (2013). Fourier-transform infrared characterization of kaolin, granite, bentonite and barite. *ATBU journal of environmental technology*, *6*(1): 42-53.

Arowojobe, Y., Aiyesanmi, A. F., & Adebayo, M. A. (2020). Removal of aqueous lead and cadmium using persea americana seed coat: single and binary studies. *Advanced Journal of Chemistry-Section B*, *3*(1): 16-24.

Ayawei, N., Ebelegi, A. N., & Wankasi, D. (2017). Modelling and interpretation of adsorption isotherms. *Journal of Chemistry*, *2017*: 1-11.

Azizi, B., Vaezihir, A., Siahcheshm, K., Sheydaei, M., & Aber, S. (2021). Remediation of heavy metals from contaminated river water using natural zeolite and limestone. *Arabian Journal of Geosciences*, *14*: 1-13.

Babatunde, R. I., & Ibrahim, A. A. (2020). Removal of heavy metal from waste water using activated carbon from rice husk. *International Journal of Advances in Scientific Research and Engineering*, *6*(2): 104-112.

Balali-Mood, M., Naseri, K., Tahergorabi, Z., Khazdair, M. R., & Sadeghi, M. (2021). Toxic mechanisms of five heavy metals: mercury, lead, chromium, cadmium, and arsenic. *Frontiers in pharmacology*, *12*: 1-19.

Banerjee, S., Dubey, S., Gautam, R. K., Chattopadhyaya, M. C., Sharma, Y. C. (2017). Adsorption characteristics of alumina nanoparticles for the removal of hazardous dye, Orange G from aqueous solutions. *Arabian Journal of Chemistry 10*(1): 1878-1894.

Barai, H. R., Banerjee, A. N., Hamnabard, N., & Joo, S. W. (2016). Synthesis of amorphous manganese oxide nanoparticles–to–crystalline nanorods through a simple wet-chemical technique using K^+ ions as a 'growth director'and their morphology-controlled high performance supercapacitor applications. *Royal Society of Chemistry Advances*, *6*(82): 78887-78908.

Bardestani, R., Patience, G. S., & Kaliaguine, S. (2019). Experimental methods in chemical engineering: specific surface area and pore size distribution measurements-BET, BJH, and DFT. *The Canadian Journal of Chemical Engineering*, *97*(11), 2781-2791.

Bello, O. S., Adegoke, K. A., & Oyewole, R. O. (2014). Insights into the adsorption of heavy metals from wastewater using diatomaceous earth. *Separation Science and Technology*, *49*(12): 1787-1806.

Bilgin, M., & Tulun, S. (2015). Use of diatomite for the removal of lead ions from water: thermodynamics and kinetics. *Biotechnology & Biotechnological Equipment*, *29*(4): 696-704.

Brouwer, P. (2018). *Theory of XRF. Getting Acquainted with the Principles* (5th ed.). Malvern Panalytical, Almelo. Netherlands. pp. 39-41.

Budnyak, T. M., Błachnio, M., Slabon, A., Jaworski, A., Tertykh, V. A., Deryło-Marczewska, A., & Marczewski, A. W. (2020). Chitosan deposited onto fumed silica surface as sustainable hybrid biosorbent for Acid Orange 8 dye capture: Effect of temperature in adsorption equilibrium and kinetics. *The Journal of Physical Chemistry C*, *124*(28): 15312-15323.

Bunaciu, A. A., UdriŞTioiu, E. G., & Aboul-Enein, H. Y. (2015). X-ray diffraction: instrumentation and applications. *Critical Reviews in Analytical Chemistry, 45*(4): 289-299.

Burakov, A. E., Galunin, E. V., Burakova, I. V., Kucherova, A. E., Agarwal, S., Tkachev, A. G., & Gupta, V. K. (2018). Adsorption of heavy metals on conventional and nanostructured materials for wastewater treatment purposes: A review. *Ecotoxicology and Environmental Safety*, *148*: 702-712.

Camacho, L. M., Ponnusamy, S., Campos, I., Davis, T. A., & Deng, S. (2015). Evaluation of novel modified activated alumina as adsorbent for arsenic removal. *In:* S. J. S. Flora (Ed.). *Handbook of Arsenic Toxicology*. Academic Press, Cambridge, Massachusetts, USA. pp. 121-136.

Chaudhary, K., Jan, S., & Khan, S. (2016). Heavy Metal ATPase (HMA2, HMA3, and HMA4) Genes in Hyperaccumulation Mechanism of Heavy Metals. *In:* P. Ahmad (Ed.). *Plant Metal Interaction*. Elsevier, Netherlands. pp. 545-556.

Chaudhry, S. A., Khan, T. A., & Ali, I. (2016). Adsorptive removal of Pb (II) and Zn (II) from water onto manganese oxide-coated sand: isotherm, thermodynamic and kinetic studies. *Egyptian Journal of Basic and Applied Sciences, 3*(3): 287-300.

Chege, B. G., Moturi, W. N., & Makindi, S. M. (2018). Physical Chemical Parameters of Waste water. A case Study of Njoro Sewage Works, Nakuru, Kenya. *Journal of Environment and Earth Science, 8*(12): 80-88.

Cholico-Gonzalez, D., Ortiz Lara, N., Fernandez Macedo, A. M., & Chavez Salas, J. (2020). Adsorption behavior of Pb (II), Cd (II), and Zn (II) onto agave bagasse, characterization, and mechanism. *American Chemical Society Omega*, *5*(7): 3302-3314.

Chowdhury, R., A., Datta, R., & Sarkar, D. (2018). Heavy metal pollution and remediation. *In:* B. Torok, & T. Dransfield (Eds.). *Green Chemistry: an inclusive approach.* Elsevier, Netherlands. pp. 359-373.

Chukwuemeka-Okorie, H. O., Ekemezie, P. N., Akpomie, K. G., & Olikagu, C. S. (2018). Calcined corncob-kaolinite Combo as new sorbent for sequestration of toxic metal ions from polluted aqua media and desorption. *Frontiers in chemistry*, *6* (273): 1-13.

Civan, F. (2015). *Reservoir formation damage*. Gulf Professional Publishing, Burlington, USA. pp. 154-173.

Cosmas, K. K. (2016). *Determination of levels of selected heavy metals in soil and vegetables grown at the Market Dumpsite in Eldoret, Kenya* (Doctoral dissertation). Moi University, Kenya.

Cozzolino, D. (2018). Fourier transform spectroscopy. *In:* S.A. Franca, & M. L. Nollet (Eds.). *Spectroscopic methods in food analysis.* CRC press, Florida, USA. pp. 103-110.

Dang, T. D., Banerjee, A. N., Joo, S. W., & Min, B. K. (2013). Effect of potassium ions on the formation of crystalline manganese oxide nanorods via acidic reduction of potassium permanganate. *Industrial & Engineering Chemistry Research, 52*(39): 14154-14159.

Dang, T. D., Banerjee, A. N., Tran, Q. T., & Roy, S. (2016). Fast degradation of dyes in water using manganese-oxide-coated diatomite for environmental remediation. *Journal of Physics and Chemistry of Solids*, *98*: 50-58.

Dargahi, A., Golestanifar, H., Darvishi, P., Karami, A., Hasan, S. H., Poormohammadi, A., & Behzadnia, A. (2016). An investigation and comparison of removing heavy metals (lead and chromium) from aqueous solutions using magnesium oxide nanoparticles. *Polish Journal of Environmental Studies, 25*(2): 557-562.

Diep, P., Mahadevan, R., & Yakunin, A. F. (2018). Heavy metal removal by bioaccumulation using genetically engineered microorganisms. *Frontiers in bioengineering and biotechnology*, *6*(157): 1-20.

Du, Y., Wang, L., Wang, J., Zheng, G., Wu, J., & Dai, H. (2015). Flower-, wire-, and sheet-like MnO_2-deposited diatomites: Highly efficient absorbents for the removal of Cr (VI). *Journal of Environmental Sciences, 29*: 71-81.

Du, Y., Zheng, G., Wang, J., Wang, L., Wu, J., & Dai, H. (2014). MnO_2 nanowires in situ grown on diatomite: highly efficient absorbents for the removal of Cr (VI) and As (V). *Microporous and Mesoporous Materials, 200*: 27-34.

Edet, U. A., & Ifelebuegu, A. O. (2020). Kinetics, Isotherms, and Thermodynamic Modeling of the Adsorption of Phosphates from Model Wastewater Using Recycled Brick Waste. *Processes, 8*(6): 665-679.

El Sayed, E. E. (2018). Natural diatomite as an effective adsorbent for heavy metals in water and wastewater treatment (a batch study). *Water Science*, *32*(1): 32-43.

Elkhatib, E. A., Moharem, M. L., Saad, A. F., & Attia, F. A. (2022). Using nano-magnesium oxide/bentonite composite for cadmium removal from industrial wastewater. *Environmental Engineering Research, 28*(2): 210545-210556.

Enyogoi, F., Kibet, J. K., Kiplangat, K., & Kaya, J. (2020). Analysis of Heavy Metals (Pb, Cd, Zn, and Ni) in Selected Vegetables from Nakuru and Nairobi Counties-

Kenya. *International Journals of Applied Sciences and Engineering Development, 1*(5): 1-6.

Es-Said, A., Nafai, H., Hamdaoui, L. E., Bouhaouss, A., & Bchitou, R. (2020). Adsorptivity and selectivity of heavy metals Cd (II), Cu (II), and Zn (II) toward phosphogypsum. *Desalination Water Treat, 197*: 291-299.

Falsafi, S. R., Rostamabadi, H., & Jafari, S. M. (2020). X-ray diffraction (XRD) of nanoencapsulated food ingredients. *In*: S. M. Jafari (Ed.). *Characterization of Nanoencapsulated Food Ingredients* (Vol. 4), Academic Press, Cambridge, Massachusetts, USA. pp. 271-293.

Fan, X., Liu, H., Anang, E., & Ren, D. (2021). Effects of electronegativity and hydration energy on the selective adsorption of heavy metal ions by synthetic NaX zeolite. *Materials, 14*(15): 4066-4082.

Feng, X., Zhang, H., & Yu, P. (2021). X-ray fluorescence application in food, feed, and agricultural science: a critical review. *Critical Reviews in Food Science and Nutrition*, *61*(14): 2340-2350.

Fertu, D. I., Dragoi, E. N., Bulgariu, L., Curteanu, S., & Gavrilescu, M. (2022). Modeling the biosorption process of heavy metal ions on soybean-based low-cost biosorbents using artificial neural networks. *Processes*, *10*(3): 603-628.

Flores-Cano, J. V., Leyva-Ramos, R., Padilla-Ortega, E., & Mendoza-Barron, J. (2013). Adsorption of heavy metals on diatomite: mechanism and effect of operating variables. *Adsorption Science & Technology*, *31*(2-3): 275-291.

Forbes, T.Z. (2018). X-ray diffraction. *In*: W. White (Ed.). *Earth Science Series. Encyclopedia of Geochemistry*. Springer Publishing, New York, USA. pp. 1-4.

Francis, M. M. (2015). *Aluminophosphates derived from tea leaves and pumpkin seeds ashes for removal of sellected heavy metals from contaminated water* (Master's Thesis). Kenyatta University, Kenya.

Fultz, B., & Howe, J. M. (2012). *Transmission electron microscopy and diffractometry of materials* (4th ed.). Springer Science, Heidelberg, Germany. pp. 22-35.

García, R., & Báez, A. P. (2012). Atomic absorption spectrometry (AAS). *In*: A. M. Farrukh (Ed.). *Atomic absorption spectroscopy*. Intechopen Ltd, Rijeka, Croatia. pp. 1-13.

Gautam, R. K., Sharma, S. K., & Chattopadhyaya, M. C. (2014). Functionalized Magnetic Nanoparticles for Heavy Metals Removal from Aqueous Solutions. *In:* S. K. Sharma (Ed.), *Heavy metals in water: presence, removal and safety.* The Royal Society of Chemistry, Cambridge, UK. pp 57-85.

Gebretsadik, H., Gebrekidan, A., & Demlie, L. (2020). Removal of heavy metals from aqueous solutions using Eucalyptus Camaldulensis: An alternate lowcost adsorbent. *Cogent Chemistry*, *6*(1): 1720892.

Ghomi Avili, F. (2021). Removal of heavy metals (lead and nickel) from water sources by adsorption of activated alumina. *Anthropogenic pollution, 5*(2): 1-7.

Githinji, M. W., Mwaura, F., & Wamalwa, J. (2019). Land Use and Water Pollution along the Altitudinal Gradient of the Likii River, Laikipia County, Kenya. *Journal of Environment Pollution and Human Health, 7*(1): 39-52.

Gómez, J., Gil, M. L. A., De La Rosa-Fox, N., & Alguacil, M. (2015). Formation of siliceous sediments in brandy after diatomite filtration. *Food Chemistry*, *170*: 84-89.

Gunatilake, S. K. (2015). Methods of removing heavy metals from industrial wastewater. *Methods*, *1*(1): 12-18.

Guterres, A. (2023). *The Sustainable Development Goals Report 2023: Special Edition*. United Nations Department of Economic and Social Affairs: New York, USA. pp. 24-25.

Halnor, S. (2015). Removal of heavy metals from wastewater: A review. *International Journal of Application or Innovation in Engineering and Management, 4*(1): 19-22.

Hamadi, N. J., Abd Mohammed, A., & Ali, A. H. (2014). Removal of Pb^{2+}, Cu^{2+} and Cd^{2+} metals from simulated wastewater in single and competitive system using locally porcelanite. *International Journal of Engineering Sciences and Research Technology*, *3*(7): 245-257.

Han, R., Xing, S., Ma, Z., Wu, Y., & Gao, Y. (2012). Effect of the $KMnO_4$ concentration on the structure and electrochemical behavior of MnO_2. *Journal of Materials Science*, *47*: 3822-3827.

Hanna, A. A., Sherief, M. A., & Aboelenin, R. M. M. (2014). Removal of some heavy metals from wastewater by using diatomaceous earth. *Research Journal of Pharmaceutical, Biological and Chemical Sciences*, *5*(3): 198-205.

Haque, S. M., & Ahmad, A. (2019). Development and validation of analytical method for quantification of acetic acid content in amlodipine besylate. *International Journal of Pharmacy and Pharmaceutical Sciences*, *11*(4): 8-11.

He, B., Yun, Z., Shi, J., & Jiang, G. (2013). Research progress of heavy metal pollution in China: sources, analytical methods, status, and toxicity. *Chinese Science Bulletin*, *58*(2): 134-140.

He, K., Chen, Y., Tang, Z., & Hu, Y. (2016). Removal of heavy metal ions from aqueous solution by zeolite synthesized from fly ash. *Environmental Science and Pollution Research*, *23*: 2778-2788.

He, S., Zhao, C., Yao, P., & Yang, S. (2016). Chemical modification of silica gel with multidentate ligands for heavy metals removal. *Desalination and Water Treatment*, *57*(4): 1722-1732.

Hegazi, H. A. (2013). Removal of heavy metals from wastewater using agricultural and industrial wastes as adsorbents. *Housing and Building National Research Center Journal, 9*(3): 276-282.

Hernández-Ávila, J., Salinas-Rodríguez, E., Cerecedo-Sáenz, E., Reyes-Valderrama, M. I., Arenas-Flores, A., Román-Gutiérrez, A. D., & Rodríguez-Lugo, V. (2017). Diatoms and their capability for heavy metal removal by cationic exchange. *Metals, 7*(5): 169-179.

Hossain, M. A. (2013). *Development of novel biosorbents in removing heavy metals from aqueous solution* (Doctoral dissertation). University of Technology, Sydney, Australia.

Huo, Q., & Xiao, H. (2014). Synthesis of MnO_2 nanowires and its adsorption property to lead ion in water. *Journal of Chemical and Pharmaceutical Research, 6*(4): 270-275.

Hussain, A., Madan, S., & Madan, R. (2021). Removal of heavy metals from wastewater by adsorption. *In:* M. Nazal, & H. Zhao (Eds.). *Heavy metals: Their environmental impacts and mitigation*. Intechopen Ltd, Rijeka, Croatia. pp.1-25.

Hutchenson, S. (2016). Characterization of heavy metal removal from aqueous solutions using natural fiber impregnated with metallic nanoparticles (Master's Thesis). University of Montana, USA.

Ibisi, N. E., & Asoluka, C. A. (2018). Use of agro-waste (Musa paradisiaca peels) as a sustainable biosorbent for toxic metal ions removal from contaminated water. *Chemistry International, 4*(1): 52-59.

Idrees, N., Tabassum, B., Abd_Allah, E. F., Hashem, A., Sarah, R., & Hashim, M. (2018). Groundwater contamination with cadmium concentrations in some West UP Regions, India. *Saudi Journal of Biological Sciences, 25*(7): 1365-1368.

Igwebike-Ossi, C. D. (2017). X-ray techniques. *In*: A. Ali (Ed.). *Failure Analysis and Prevention*. Intechopen Ltd, Rijeka, Croatia. pp. 153-171.

Iwuozor, K. O., Ighalo, J. O., Emenike, E. C., Igwegbe, C. A., & Adeniyi, A. G. (2021). Do adsorbent pore size and specific surface area affect the kinetics of methyl orange aqueous phase adsorption? *Journal of Chemistry Letters, 2*(4): 188-198.

Jaishankar, M., Mathew, B. B., Shah, M. S., & Gowda, K. R. S. (2014). Biosorption of few heavy metal ions using agricultural wastes. *Journal of Environment Pollution and Human Health, 2*(1): 1-6.

Jiang, L., Liu, L., Xiao, S., & Chen, J. (2016). Preparation of a novel manganese oxide-modified diatomite and its aniline removal mechanism from solution. *Chemical Engineering Journal, 284*: 609-619.

Jiang, L., Ye, Q., Chen, J., Chen, Z., & Gu, Y. (2018). Preparation of magnetically recoverable bentonite–Fe3O4–MnO_2 composite particles for Cd (II) removal from aqueous solutions. *Journal of colloid and interface science*, *513*: 748-759.

Joudeh, N., & Linke, D. (2022). Nanoparticle classification, physicochemical properties, characterization, and applications: a comprehensive review for biologists. *Journal of Nanobiotechnology, 20*(1): 262-291.

Kamunda, C., Mathuthu, M., & Madhuku, M. (2016). Health risk assessment of heavy metals in soils from Witwatersrand gold mining basin, South Africa. *International Journal of Environmental Research and Public Health*, *13*(7): 663-644.

Karthika, B. R., Nishad, V.M., & Prasobh, G.R. (2022). An overview on infrared spectroscopy. *International Journal of Research Publication and Reviews*, 3(4): 526-552.

Kaur, V., & Mahajan, R. (2016). Water Crisis: Towards a Way to Improve the Situation. *Ritu Mahajan International Journal of Engineering Technology Science and Research*, *3*(6): 51-56.

Khalef, R. N., Hassan, A. I., & Saleh, H. M. (2022). Heavy metal's environmental impact. *In:* M. H. Saleh, & I. A. Hassan (Eds.). *Environmental impact and remediation of heavy metals*. Intechopen Ltd, Rijeka, Croatia. pp. 1-17.

Khataee, A., Bozorg, S., Vahid, B., Dang, T. D., Hanifehpour, Y., & Woo Joo, S. (2015). Synthesis and Immobilization of MnO_2 Nanoparticles on Bio-silica for the Efficient Degradation of an Azo Dye in the Aqueous Solution. *Current Nanoscience*, *11*(1): 129-134.

Kimathi, E. T. (2013). *The Potential of Arrowroots (Colocasia esculanta) in Phytoremediation of Heavy Metals in the Meru Region* (Doctoral dissertation). Jomo Kenyatta University of Agriculture and Technology, Kenya.

Kinuthia, G. K., Ngure, V., Beti, D., Lugalia, R., Wangila, A., & Kamau, L. (2020). Levels of heavy metals in wastewater and soil samples from open drainage channels in Nairobi, Kenya: community health implication. *Scientific reports*, *10*(1): 8434-8447.

Kipsanai, J. J. (2017). Exploring the use of Kenyan diatomite as a source of refractory materials. *International Journal of Scientific and Research Publications, 7*(10): 351-361.

Kithiia, S. M. (2012). Water quality degradation trends in Kenya over the last decade. *In:* K. Voudouris & D. Vousta (Eds.). *Water Quality Monitoring and Assessment.* Intechopen Ltd, Rijeka, Croatia. pp. 509-526.

Krishna, I. M., Manickam, V., Shah, A., & Davergave, N. (2017). *Environmental management: science and engineering for industry*. Butterworth-Heinemann, Oxford, UK.

Krstić, V. (2021). Role of zeolite adsorbent in water treatment. *In*: B. A. Bhanvase, S. Sonawane, V. B. Pawade & A. B. Pandit (Eds.). *Handbook of Nanomaterials for Wastewater Treatment: Fundamentals and scale up issues*. Elsevier, Netherlands. pp. 417-481.

Kumar, R., Mishra, R. K., Mishra, V., Qidwai, A., Pandey, A., Shukla, S. K., ... & Dikshit, A. (2016). Detoxification and tolerance of heavy metals in plants. *In:* P. Ahmad (Ed.). *Plant Metal Interaction*. Elsevier Ltd, Amsterdam, Netherlands. pp. 336-359.

Lakherwal, D. (2014). Adsorption of heavy metals: a review. *International Journal of Environmental Research and Development*, *4*(1): 41-48.

Langat, N. K. (2018). *Isolation and Molecular Characterization of Chromium Reducing Bacterial Strains from Selected Chrome Contaminated Tannery Waste Sites in Nairobi, Kenya* (Doctoral dissertation). Jomo Kenyatta University of Agriculture and Technology, Kenya.

Lavado-Meza, C., Fernandez-Pezua, M. C., Gamarra-Gómez, F., Sacari-Sacari, E., Angeles-Suazo, J., & Dávalos-Prado, J. Z. (2023). Single and Binary Removals of Pb (II) and Cd (II) with Chemically Modified Opuntia ficus indica Cladodes. *Molecules*, *28*(11): 4451-4468.

Li, H., Liu, F., Zhu, M., Feng, X., Zhang, J., & Yin, H. (2015). Structure and properties of Co-doped cryptomelane and its enhanced removal of Pb^{2+} and Cr^{3+} from wastewater. *Journal of Environmental Sciences*, *34*: 77-85.

Li, S., Li, D., Su, F., Ren, Y., & Qin, G. (2014). Uniform surface modification of diatomaceous earth with amorphous manganese oxide and its adsorption characteristics for lead ions. *Applied Surface Science*, *317*: 724-729.

Li, Y., He, J., Zhang, K., Liu, T., Hu, Y., Chen, X., ... & Liu, J. (2019). Super rapid removal of copper, cadmium and lead ions from water by NTA-silica gel. *The Royal Society of Chemistry*, *9*(1): 397-407.

Li, Z., Tang, X., Liu, K., Huang, J., Xu, Y., Peng, Q., & Ao, M. (2018). Synthesis of a MnO2/Fe3O4/diatomite nanocomposite as an efficient heterogeneous Fenton-like catalyst for methylene blue degradation. *Beilstein Journal of Nanotechnology*, *9*(1): 1940-1950.

Liu, J., Wang, H. L., Lü, C. X., Liu, H. F., Guo, Z. X., & Kang, C. L. (2013). Remove of heavy metals (Cu^{2+}, Pb^{2+}, Zn^{2+} and Cd^{2+}) in water through modified diatomite. *Chemical Research in Chinese Universities*, *29*(3): 445-448.

Liu, P. (2015). *Adsorption behavior of heavy metal ions from aqueous medium on nanocellulose* (Doctoral dissertation). Luleå university of Technology, Sweden.

López-Sotelo, J. B., Quina, M. J., Gando-Ferreira, L., Sánchez-Báscones, M., & Navas-Gracia, L. M. (2017). Compost from poultry hatchery waste as a biosorbent for removal of Cd (II) and Pb (II) from aqueous solutions. *The Canadian Journal of Chemical Engineering*, *95*(5): 839-848.

Lupa, L., & Cocheci, L. (2023). Heavy Metals Removal from Water and Wastewater. *In:* A. A. Basim (Ed.). (2023). *Heavy Metals: Recent Advances*. Intechopen Ltd, Rijeka, Croatia. pp.1-29.

Mahajan-Tatpate, P., Dhume, S., & Chendake, Y. (2021). Removal of heavy metals from water: Technological advances and today's lookout through membrane applications. *International Journal of Membrane Science and Technology*, *8*(1): 1-21

Mahmood-ul-Hassan, M., Suthor, V., Rafique, E., & Yasin, M. (2015). Removal of Cd, Cr, and Pb from aqueous solution by unmodified and modified agricultural wastes. *Environmental monitoring and assessment*, *187*: 1-8.

Majumder, S., Gupta, S., & Raghuvanshi, S. (2014). Removal of dissolved metals by bioremediation. *In:* S. K. Sharma (Ed.). *Heavy metals in water: presence, removal and safety.* The Royal Society of Chemistry, Cambridge, UK. pp 44-56

Marczyk, J., Pławecka, K., Hebdowska-Krupa, M., Nykiel, M., & Łach, M. (2022). Research on diatomite from Polish deposits and the possibilities of its use. *Journal of Achievements in Materials and Manufacturing Engineering*, *115*(1): 5-15.

Marguí, E., Queralt, I., & de Almeida, E. (2022). X-ray fluorescence spectrometry for environmental analysis: Basic principles, instrumentation, applications and recent trends. *Chemosphere*, *303*(1): 1-18.

Marín-Alzate, N., Tobón, J. I., Bertolotti, B., Quintana Cáceda, M. E., & Flores, E. (2021). Evaluation of the properties of diatomaceous earth in relation to their performance in the removal of heavy metals from contaminated effluents. *Water, Air, & Soil Pollution*, *232*: 1-14.

Mathenge, S. G. (2014). *Assessment of metals in untreated wastewater, vegetables and soils in eastern Nairobi, Kenya* (Doctorate dissertation). Kenyatta University, Kenya.

Mbonyiryivuze, A., Mwakikunga, B. W., Dhlamini, S. M., & Maaza, M. (2015). Fourier transform infrared spectroscopy for sepia melanin. *Physics and Materials Chemistry, 3*(2): 25-29

Mbuvi, H., & Mwihaki Ng'ang'a, M. (2017). Removal of Pb^{2+} and Cd^{2+} ions, colour and turbidity from water using carbon and ash derived from maize cobs. *International Organization of Scientific Research Journal of Applied Chemistry*, *10*(6): 58-68.

Miloševića, D., Tomićb, N., Đokićb, V., Vidovića, M., Veličkovićc, Z., Jančić-Heinemannd, R., & Marinkovićd, A. D. (2019). Structural and surface modification of highly ordered alumina for enhanced removal of Pb^{2+}, Cd^{2+} and Ni^{2+} from aqueous solution. *Desalination and Water Treatment*, *178*: 220-239.

Miruka, A. (2016). *The Efficiency of Nairobi's Kariobangi Wastewater Treatment Plant* (Master's Thesis). University of Nairobi, Nairobi, Kenya.

Miyah, Y., Lahrichi, A., Idrissi, M., Boujraf, S., Taouda, H., & Zerrouq, F. (2017). Assessment of adsorption kinetics for removal potential of Crystal Violet dye from aqueous solutions using Moroccan pyrophyllite. *Journal of the Association of Arab Universities for Basic and Applied Sciences, 23*: 20-28.

Mounika, T., Belagali, S., & Vadiraj, K. (2023). Manganese oxide nanoparticles synthesis route, characterization and optical properties. *Materials Today: Proceedings, 75*: 72-76.

Munene, M. J. (2019). *Sequestering of selected heavy metal ions in wastewater from industrial area in Nairobi using water hyacinth as a low-cost adsorbent* (Doctoral dissertation). University of Nairobi, Kenya.

Muntean, S. G., Nistor, M. A., Nastas, R., & Petuhov, O. (2023). Dyes and Heavy Metals Removal from Aqueous Solutions Using Raw and Modified Diatomite. *Processes, 11*(8): 2245-2262.

Musyoki A. Moki. (2012). *The bacteriologic quality of Dandora sewage treatment plant and the receiving waters of Nairobi and Athi Rivers* (Master's thesis). Kenyatta University, Kenya.

Naik, R. L., Kumar, M. R., & Narsaiah, T. B. (2023). Removal of heavy metals (Cu & Ni) from wastewater using rice husk and orange peel as adsorbents. *Materials Today: Proceedings, 72*: 92-98.

Nasrazadani, S., & Hassani, S. (2016). Modern analytical techniques in failure analysis of aerospace, chemical, and oil and gas industries. *In*: A. S.H. Makhlouf & M, Aliofkhazraei (Eds.). *Handbook of Materials Failure Analysis with Case Studies from the Oil and Gas Industry*. Butterworth-Heinemann, United Kingdom. pp. 39-54

Ndung'u, S. N. (2021). *Kinetic, equilibrium and thermodynamic adsorption studies of selected heavy metal ions by raw and modified jackfruit seeds from aqueous media* (Masters' Thesis). Kenyatta University, Kenya.

Nenadović, S., Kljajević, L., Marković, S., Omerašević, M., Jovanović, U., Andrić, V., & Vukanac, I. (2015). Natural diatomite (Rudovci, Serbia) as adsorbent for removal Cs from radioactive waste liquids. *Science of Sintering, 47*(3): 299-309.

Ngugi, F. (2015). *Adsorption of heavy metals from aqueous solutions usingmangroves from Kenyan coast* (Masters' Thesis). University of Nairobi, Kenya.

Nyabaro, O. M., Mosoti, D., Muthoka, T. M., & Onyancha, E. (2013). Determination of Pollution Levels of Waste Water from Nakuru Tanners, Kenya. *African Journal of Education, Science and Technology, 1*(3): 200-210.

Nyingi, B., Gitahi, K. J., Kiptoo, M., & Jackson, K. (2016). Heavy metal concentrations in water and selected fish species (tilapia, cat fish and lung fish) from lake Baringo, Kenya. *International Journal of Science, Environment and Technology, 5*(6): 4288-4295.

Nzeve, J. K., Njuguna, S. G., & Kitur, E. C. (2015). Assessment of heavy metal contamination in surface water of Masinga Reservoir, Kenya. *Journal of Natural Sciences Research, 5*(2): 101-108.

Omwenga, I., Kanja, L., Nguta, J., Mbaria, J., & Irungu, P. (2014). Assessment of lead and cadmium residues in farmed fish in Machakos and Kiambu counties, Kenya. *Toxicological & Environmental Chemistry, 96*(1): 58-67.

Ouyang, D., Zhuo, Y., Hu, L., Zeng, Q., Hu, Y., & He, Z. (2019). Research on the adsorption behavior of heavy metal ions by porous material prepared with silicate tailings. *Minerals, 9*(5): 291-307.

Owiti, O. T. (2015). *Assessment of selected plants growing along Nairobi River for uptake of copper, zinc and cadmium, Nairobi County, Kenya* (Doctoral dissertation). Jomo Kenyatta University of Agriculture and Technology, Kenya.

Oyedotun, T. D. T. (2018). X-ray fluorescence (XRF) in the investigation of the composition of earth materials: a review and an overview. *Geology, Ecology, and Landscapes*, *2*(2): 148-154.

Plessis, A. (2017). *Freshwater Challenges of South Africa and Its Upper Vaal River*. Springer, New York. pp. 3-111.

Pokhrel, N. (2017), *Removal of heavy metals from wastewater using electrocoagulation* (Master's Thesis). Metropolia University of Applied Sciences, Finland.

Pookmanee, P., Thippraphan, P., Jansanthea, P., & Phanichphant, S. (2012). Characterization and adsorption efficiency of the natural and the modified diatomite via the low temperature hydrothermal route. *Advanced Materials Research*, *506*: 425-428.

Radi, S., Tighadouini, S., Bacquet, M., Degoutin, S., Cazier, F., Zaghrioui, M., & Mabkhot, Y. N. (2014). Organically modified silica with pyrazole-3-carbaldehyde as a new sorbent for solid-liquid extraction of heavy metals. *Molecules*, *19*(1): 247-262.

Rahimi, M., & Mahmoudi, J. (2020). Heavy metals removal from aqueous solution by modified natural zeolites using central composite design. *Periodica polytechnica chemical engineering*, *64*(1): 106-115.

Rahman, M. M., Adil, M., Yusof, A. M., Kamaruzzaman, Y. B., & Ansary, R. H. (2014). Removal of heavy metal ions with acid activated carbons derived from oil palm and coconut shells. *Materials, 7*(5): 3634-3650.

Raji, Z., Karim, A., Karam, A., & Khalloufi, S. (2023, September). Adsorption of Heavy Metals: Mechanisms, Kinetics, and Applications of Various Adsorbents in Wastewater Remediation-A Review. *Waste, 1*(3): 775-805.

Rao, Y., Zeng, D., Cao, X., Qin, G., & Li, S. (2019). Synthesis of doped MnOx/diatomite composites for catalyzing ozone decomposition. *Ceramics International*, *45*(6): 6966-6971.

Renu, M. A., Singh, K., Upadhyaya, S., & Dohare, R. K. (2017). Removal of heavy metals from wastewater using modified agricultural adsorbents. *Materials Today: Proceedings*, *4*(9): 10534-10538.

Rezig, W., & Hadjel, M. (2015). Preparation and characterization of iron oxide modified diatomite system. *Der Pharma Chemica*, *7*(2): 5-11.

Rezig, W., & Hadjel, M. (2015). Visible light assisted heterogeneous photodecolourisation of Vat Orange O_2 textile dye in aqueous solution using calcined ferrihydrite modified diatomite. *International Journal of Chemtech Research*, *8*(7): 111-115.

Robati, D. (2013). Pseudo-second-order kinetic equations for modeling adsorption systems for removal of lead ions using multi-walled carbon nanotube. *Journal of Nanostructure in Chemistry*, *3*: 1-6.

Safa, M., Larouci, M., Meddah, B., & Valemens, P. (2012). The sorption of lead, cadmium, copper and zinc ions from aqueous solutions on a raw diatomite from Algeria. *Water Science and Technology*, *65*(10): 1729-1737.

Salman, T., Temel, F. A., Turan, N. G., & Ardali, Y. (2015). Adsorption of lead (II) ions onto diatomite from aqueous solutions: Mechanism, isotherm and kinetic studies. *Global Nest Journal*, *18*(1): 1-10.

Saptiama, I., Kaneti, Y. V., Suzuki, Y., Suzuki, Y., Tsuchiya, K., Sakae, T., ... & Ariga, K. (2017). Mesoporous alumina as an effective adsorbent for molybdenum (Mo) toward instant production of radioisotope for medical use. *Bulletin of the Chemical Society of Japan*, *90*(10): 1174-1179.

Sati, M., Verma, M., & Rai, J. P. N. (2014). Biosorption of heavy metals from single and multimetal solutions by free and immobilized cells of Bacillus megaterium. *International Journal of Advanced Research*, *2*: 923-934.

Sayo, S., Kiratu, J. M., & Nyamato, G. S. (2020). Heavy metal concentrations in soil and vegetables irrigated with sewage effluent: A case study of Embu sewage treatment plant, Kenya. *Scientific African, 8*(2): 1-8

Sebastian, A., & Prasad, M. N. V. (2014). Cadmium minimization in rice. A review. *Agronomy for Sustainable Development*, *34*(1): 155-173.

Sewe, H.A. (2010). *A study on the Efficiency of Dandora Domestic and Industrial Wastewater Treatment Plant in Nairobi.* (Master's Thesis). Jomo Kenyatta University of Agriculture and Technology, Juja, Kenya.

Shahata, M. M. (2016). Adsorption of some heavy metal ions by used different immobilized substances on silica gel. *Arabian journal of chemistry*, *9*(6): 755-763.

Shamim, S. (2018). Biosorption of Heavy Metals. *In:* J. Derco (Ed.). *Biosorption.* Intechopen Ltd, London, UK. pp. 21-49.

Sharma, R. K., Yadav, M., & Gupta, R. (2017). Water Quality and Sustainability in India: Challenges and Opportunities. *In:* S. Ahuja (Ed.). *Chemistry and Water.* Elsevier, Amsterdam, Netherlands. pp. 183-205.

Shikuku, V. O., Zanella, R., Kowenje, C. O., Donato, F. F., Bandeira, N. M., & Prestes, O. D. (2018). Single and binary adsorption of sulfonamide antibiotics onto iron-modified clay: linear and nonlinear isotherms, kinetics, thermodynamics, and mechanistic studies. *Applied Water Science*, *8*: 1-12

Shimizu, S., & Matubayasi, N. (2022). Surface Area Estimation: Replacing the Brunauer–Emmett–Teller Model with the Statistical Thermodynamic Fluctuation Theory. *Langmuir*, *38*(26): 7989-8002.

Shin, W. S., Kang, K., & Kim, Y. K. (2014). Adsorption characteristics of multi-metal ions by red mud, zeolite, limestone, and oyster shell. *Environmental Engineering Research*, *19*(1): 15-22.

Shrestha, B., Kour, J., & Ghimire, K. N. (2016). Adsorptive removal of heavy metals from aqueous solution with environmentally friendly material—exhausted tea leaves. *Advances in Chemical Engineering and Science*, *6*(4): 525-540.

Sing, K. S. (1985). Reporting physisorption data for gas/solid systems with special reference to the determination of surface area and porosity (Recommendations 1984). *Pure and applied chemistry*, *57*(4), 603-619.

Singh, N., & Gupta, K. S. (2016). Adsorption of heavy metals: A review. *International Journal of Innovative Research in Science, Engineering and Technology*, *5*(2): 2267-2280.

Skoog, D. A., Holler, F. J., & Crouch, S. R. (2017). *Principles of instrumental analysis*. Cengage learning, Boston, Massachusetts, USA. pp. 210-298.

Spasovski, O., Sijakova-Ivanova, T., Doneva, B., & Spasovski, D. (2016). New findings for diatomite (Diatomaceous earth) between the villages of manastir and Bešište (Mariovo). *Geologica Macedonica*, *30*(2): 161-171.

Sun, L., Wang, J., Wu, J., Wang, T., Du, Y., Li, Y., & Li, H. (2019). Constructing nanostructured silicates on diatomite for Pb (II) and Cd (II) removal. *Journal of Materials Science*, *54*(9): 6882-6894.

Suvarapu, L. N., & Baek, S. O. (2017). Determination of heavy metals in the ambient atmosphere: A review. *Toxicology and Industrial Health*, *33*(1): 79-96.

Szatyłowicz, E., & Skoczko, I. (2018). The use of activated alumina and magnetic field for the removal heavy metals from water. *Journal of Ecological Engineering*, *19*(3): 61-67.

Taha, A. A., Shreadah, M. A., Ahmed, A. M., & Heiba, H. F. (2016). Multi-component adsorption of Pb (II), Cd (II), and Ni (II) onto Egyptian Na-activated bentonite; equilibrium, kinetics, thermodynamics, and application for seawater desalination. *Journal of environmental chemical engineering*, *4*(1): 1166-1180.

Taman, R., Ossman, M. E., Mansour, M. S., & Farag, H. A. (2015). Metal oxide nano-particles as an adsorbent for removal of heavy metals. *Journal of Advanced Chemical Engineering*, *5*(3): 1-8.

Tariq, W., Saifullah, M., Anjum, T., Javed, M., Tayyab, N., & Shoukat, I. (2018). Removal of Heavy Metals from Chemical Industrial Wastewater Using Agro Based Bio-Sorbents. *Acta Chemica Malaysia*, *2*(2): 9-14.

Thakur, L. S., & Parmar, M. (2013). Adsorption of heavy metal (Cu^{2+}, Ni^{2+} and Zn^{2+}) from synthetic waste water by tea waste adsorbent. *International Journal of Chemical and Physical Sciences*, *2*(6): 6-19.

Tomno, R. M., Nzeve, J. K., Mailu, S. N., Shitanda, D., & Waswa, F. (2020). Heavy metal contamination of water, soil and vegetables in urban streams in Machakos municipality, Kenya. *Scientific African*, *9*: 1-9.

Tripathi, A., & Ranjan, M. R. (2015). Heavy metal removal from wastewater using low-cost adsorbents. *Journal of Bioremediation & Biodegradation*, *6*(6): 1-5.

Tsamo, C., Djomou Djonga, P. N., Dangwang Dikdim, J. M., & Kamga, R. (2018). Kinetic and equilibrium studies of Cr (VI), Cu (II) and Pb (II) removal from aqueous solution using red mud, a low-cost adsorbent. *Arabian Journal for Science and Engineering*, *43*: 2353-2368.

Tutic, A., Novakovic, S., Lutovac, M., Biocanin, R., Ketin, S., & Omerovic, N. (2015). The heavy metals in agrosystems and impact on health and quality of life. *Open Access Macedonian Journal of Medical Sciences*, *3*(2): 345-355.

Uddin, M. K. (2017). A review on the adsorption of heavy metals by clay minerals, with special focus on the past decade. *Chemical Engineering Journal*, *308*: 438-462.

Ungureanu, E. L., & Mustatea, G. (2022). Toxicity of heavy metals. *In:* M. H. Saleh, & I. A. Hassan (Eds.). *Environmental Impact and Remediation of Heavy Metals*. Intechopen Ltd, Rijeka, Croatia. pp. 18-39.

Unruh, D., & Forbes, T. (2019). X-ray Diffraction Techniques. *In*: J. Kenney, H. Veeramani, & D. Alessi (Eds.). *Analytical Geomicrobiology: A Handbook of Instrumental Techniques*. Cambridge University Press, Cambridge, England. pp. 215-237.

Ushakumary, E. R. (2013). *Waste water treatment using low-cost natural adsorbents* (Doctoral dissertation). Cochin University of Science and Technology, India.

Vassileva, P. S., Apostolova, M. S., Detcheva, A. K., & Ivanova, E. H. (2013). Bulgarian natural diatomites: modification and characterization. *Chemical Papers*, *67*(3): 342-349.

Vidu, R., Matei, E., Predescu, A. M., Alhalaili, B., Pantilimon, C., Tarcea, C., & Predescu, C. (2020). Removal of heavy metals from wastewaters: A challenge from current treatment methods to nanotechnology applications. *Toxics*, *8*(4): 101-138.

Visa, M., Luminita, I., & Duta, A. (2014). Remediation of wastewater containing heavy metals using modified diatomite. *Journal of Membrane and Separation Technology*, *3*(3): 154-161.

Wafula, G., Tole, M., Dharani, N., & Nadir, S. (2020). Effectiveness of a wastewater treatment plant located at EPZ in reducing pollutants discharged into River Athi, Kenya. *Journal of Environmental Science and Engineering*, *9*: 261-276.

Wang, S., Gao, B., Li, Y., Mosa, A., Zimmerman, A. R., Ma, L. Q., ... & Migliaccio, K. W. (2015). Manganese oxide-modified biochars: preparation, characterization, and sorption of arsenate and lead. *Bioresource Technology*, *181*: 13-17.

Wang, Y., Lu, Y. F., Jiang, Y., Ma, L., Ma, L. J., & Wang, M. Y. (2015). Sorption of Pb (II) on iron hydroxide modified diatomite. *Advanced Materials Research*, *1095*: 367-370.

Wang, Y., Lu, Y., Chen, R., Ma, L., Jiang, Y., & Wang, H. (2014). Lead ions sorption from waste solution using aluminum hydroxide modified diatomite. *Journal of Environmental Protection*, *5*(6): 509-516.

Wang, Z., Huang, G., An, C., Chen, L., & Liu, J. (2016). Removal of copper, zinc and cadmium ions through adsorption on water-quenched blast furnace slag. *Desalination and Water Treatment*, *57*(47): 22493-22506.

Wani, A. L., Ara, A., & Usmani, J. A. (2015). Lead toxicity: a review. *Interdisciplinary toxicology*, *8*(2): 55-64.

Wattanasiriwech, S., Naradisorn, M., & Wattanasiriwech, D. (2023). Adsorption performance of macadamia husk-activated carbon from a household pyrolysis kiln. *Green Materials*, *11*(3): 137-144.

World Health Organization (WHO). (2014). UN-water global analysis and assessment of sanitation and drinking-water (GLAAS) 2014 report: investing in water and sanitation: increasing access, reducing inequalities. WHO Press, Geneva.

Wu, S., Xie, F., Chen, S., & Fu, B. (2019). The removal of Pb (II) and Cd (II) with hydrous manganese dioxide: mechanism on zeta potential and adsorption behavior. *Environmental Technology*, *41*(24): 3219-3232.

Yakout, S. M., & El-Deen, G. S. (2016). Characterization of activated carbon prepared by phosphoric acid activation of olive stones. *Arabian Journal of Chemistry*, *9*: S1155-S1162.

Yan, A., Wang, Y., Tan, S. N., Mohd Yusof, M. L., Ghosh, S., & Chen, Z. (2020). Phytoremediation: a promising approach for revegetation of heavy metal-polluted land. *Frontiers in plant science*, *11*(359): 1-15.

Yemisi, A., Aiyesanmi, A. F., & Adebayo, M. A. (2021). Removal of Aqueous Lead and Cadmium using Persea americana Seed Coat: Single and Binary Studies. *Advanced Journal of Chemistry-Section B: Natural Products and Medical Chemistry*, *3*(1): 16-24.

Zhang, G., Cai, D., Wang, M., Zhang, C., Zhang, J., & Wu, Z. (2013). Microstructural modification of diatomite by acid treatment, high-speed shear, and ultrasound. *Microporous and Mesoporous Materials*, *165*: 106-112.

Zhang, H. (2014). *Biosorption of heavy metals from aqueous solutions using keratin biomaterials* (Doctoral Dissertation). Autonomous University of Barcelona, Spain.

Zhang, H., Xu, F., Xue, J., Chen, S., Wang, J., & Yang, Y. (2020). Enhanced removal of heavy metal ions from aqueous solution using manganese dioxide-loaded biochar: Behavior and mechanism. *Scientific Reports*, *10*(1): 1-13.

Zhang, M., Yin, Q., Ji, X., Wang, F., Gao, X., & Zhao, M. (2020). High and fast adsorption of Cd (II) and Pb (II) ions from aqueous solutions by a waste biomassbased hydrogel. *Scientific reports*, *10*(1), 3285-3298.

Zhang, P., Guo, Q., Tao, J., Ma, D., & Wang, Y. (2019). Aging mechanism of a diatomite-modified asphalt binder using Fourier-Transform Infrared (FTIR) Spectroscopy analysis. *Materials*, *12*(6): 988-999.

Zhang, Y. X., Hao, X. D., Li, F., Diao, Z. P., Guo, Z. Y., & Li, J. (2014). pH-dependent degradation of methylene blue via rational-designed MnO_2 nanosheet-decorated diatomites. *Industrial & Engineering Chemistry Research*, *53*(17): 6966-6977.

Zhao, J., Yu, L., Ma, H., Zhou, F., Yang, K., & Wu, G. (2020). Corn stalk-based activated carbon synthesized by a novel activation method for high-performance adsorption of hexavalent chromium in aqueous solutions. *Journal of colloid and interface science*, *578*: 650-659.

Zhao, Y., Tian, G., Duan, X., Liang, X., Meng, J., & Liang, J. (2019). Environmental applications of diatomite minerals in removing heavy metals from water. *Industrial & Engineering Chemistry Research*, *58*(27): 11638-11652.

APPENDICES

Appendix I: Calibration curve for Lead

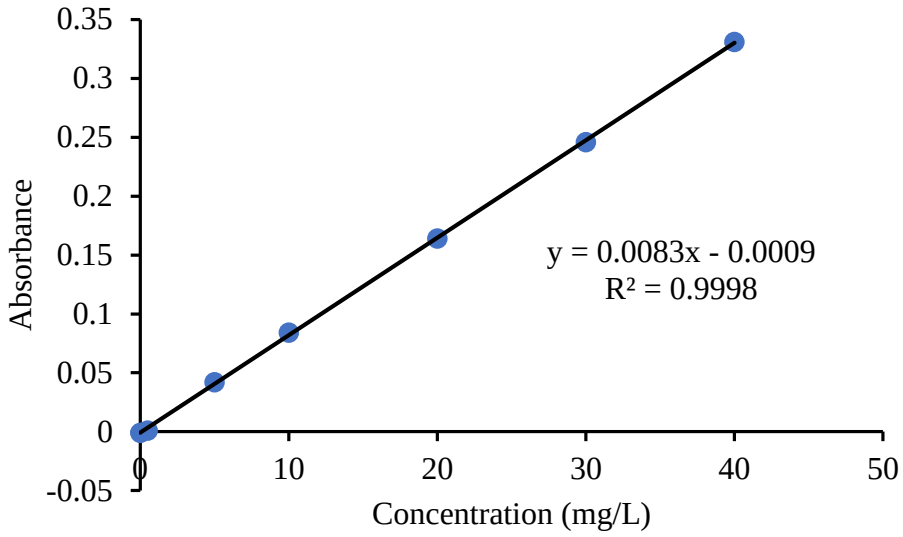

Appendix II: Calibration curve for Cadmium

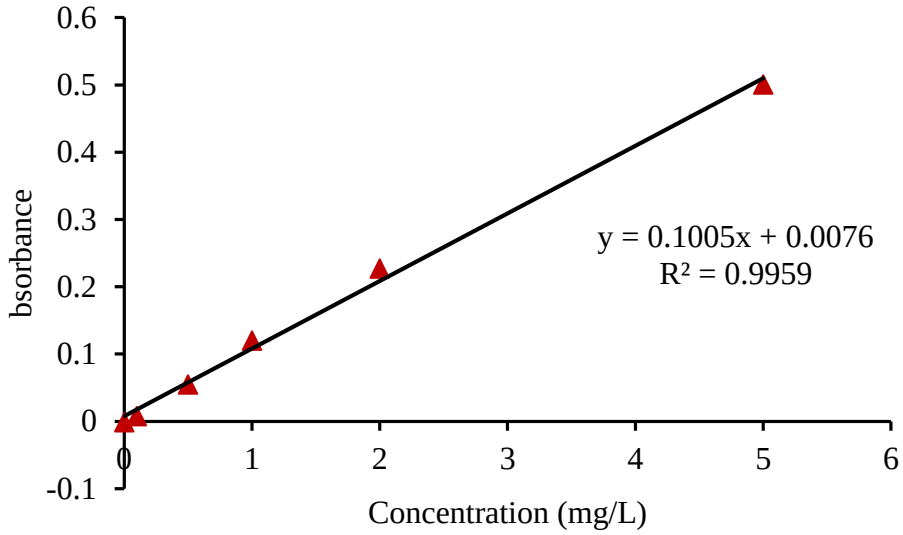

Appendix III: Removal of Pb (II) and Cd (II) ions by MnO_2-diatomite composites 1 and 2 at different pH values.

	MnO_2-diatomite composite 1		MnO_2-diatomite composite 2	
pH	% Pb Removal	% Cd Removal	% Pb Removal	% Cd Removal
4	76.96	36.49	80.79	42.39
6	86.22	64.31	89.62	67.994

Appendix IV: Effect of initial concentration on removal of Pb (II) ions using raw diatomite and MnO_2-diatomite composite.

Initial concentration (mg/L)	% Removal of Pb (II)	
	Raw Diatomite	MnO_2-diatomite composite
10	99.21	93.201
20	99.0694	91.5065
30	99.0219	89.21
40	98.69583	83.9048
50	98.5822	80.7966
60	98.4533	78.3862
70	97.897	73.3077

Appendix V: Effect of initial concentration on removal of Cd (II) ions using raw diatomite and MnO_2-diatomite composite.

Initial concentration (mg/L)	% removal Cd (II)	
	Raw Diatomite	MnO_2-diatomite composite
10	90.816	83.453
20	85.606	65.66
30	81.597	59.9467
40	78.261	54.41
50	75.212	42.39
60	64.984	36.7333
70	57.354	35.3786

Appendix VI: Effect of initial metal ion concentration on the adsorption capacity of Pb (II) and Cd (II) ions using raw diatomite and MnO_2-diatomite composite.

Initial concentration (mg/L)	Adsorption capacity (mg/g)			
	Pb (Raw diatomite)	Pb (MnO_2-diatomite composite)	Cd (Raw diatomite)	Cd (MnO_2-diatomite composite)
10	4.9605	4.66005	4.5408	4.17265
20	9.90694	9.15065	8.5606	6.566
30	14.853285	13.3815	12.23955	8.992
40	19.739166	16.781	15.6522	10.882
50	24.64555	20.1992	18.803	10.5975
60	29.53599	23.5159	19.4952	11.02
70	34.26395	25.6577	20.0739	12.3825

Appendix VII: Effect of pH on the removal of Pb (II) ions using raw diatomite and MnO_2-diatomite composite.

pH	% Removal	
	Raw diatomite	MnO_2-diatomite composite
2	77.222	65.65
3	98.8974	89.187
4	99.2102	93.201
5	99.0814	96.88
6	98.944	98.422

Appendix VIII: Effect of pH on the removal of (II) ions using raw diatomite and MnO_2-diatomite composite.

pH	% Removal	
	Raw Diatomite	MnO_2-Diatomite composite
2	57.074	38.432
3	69.738	56.17
4	77.933	63.79
5	84.526	70.52
6	90.804	83.447

Appendix IX: Effect of contact time on the adsorption of Pb (II) ions using raw diatomite and MnO_2-diatomite composite

Contact Time (min)	% Removal	
	Raw diatomite	MnO_2-diatomite composite
0	0	0
20	95.924	80.278
40	97.588	89.053
60	99.2101	98.424
80	99.21	98.423
100	99.21	98.397
120	99.209	98.397
140	99.208	98.421

Appendix X: Effect of contact time on the adsorption of Cd (II) ions using raw diatomite and MnO_2-diatomite composite

Contact Time (min)	% Removal	
	Raw diatomite	MnO_2-diatomite composite
0	0	0
20	70.982	69.833
40	82.9533	81.5
60	90.818	83.967
80	90.927	84.498
100	90.905	84.4893
120	90.92	84.489
140	90.918	84.488

Appendix XI: Effect of adsorbent dosage on the adsorption of Pb (II) ions using raw diatomite and MnO_2-diatomite composite

Dosage (g/L)	% Removal	
	Raw diatomite	MnO_2-diatomite composite
0.4	95.448	89.549
1	98.8974	93.151
2	99.209	98.368
4	100	99.879
6	100	100
8	100	100
10	100	100

Appendix XII: Effect of adsorbent dosage on the adsorption of Cd (II) ions using raw diatomite and MnO_2-diatomite composite

Dosage (g/L)	% Removal	
	Raw diatomite	MnO_2-diatomite composite
0.4	76.173	70.691
1	84.974	79.851
2	90.926	84.496
4	99.13	86.687
6	100	98.672
8	100	100
10	100	100

Appendix XIII: Effect of temperature on the adsorption of Pb (II) ions using raw diatomite and MnO_2-diatomite composite.

Temperature (K)	% Removal	
	Raw diatomite	MnO_2-diatomite composite
298	99.21	98.362
308	99.0946	97.0226
318	99.0206	94.727
328	98.9981	92.6214
338	98.7634	86.154

Appendix XIV: Effect of temperature on the adsorption of Cd (II) ions using raw diatomite and MnO_2-diatomite composite.

Temperature (K)	% Removal	
	Raw diatomite	MnO_2-diatomite composite
298	90.927	84.498
308	92.636	86.25
318	95.98	91.247
328	99.185	92.758
338	99.833	96.608

Appendix XV: Effect of pH on the competitive removal of Pb (II) and Cd (II) ions from Pb-Cd binary ion solution using raw diatomite.

pH	% Removal	
	Pb (II)	Cd (II)
2	67.7733	41.955
3	89.988	47.002
4	98.99411	74.513
5	98.8515	82.737
6	98.6934	88.52

Appendix XVI: Effect of initial metal ion concentration on the removal of Pb (II) ions from Pb-Cd binary ion solution using raw diatomite at different concentrations of Cd (II) as the competing ions.

Initial concentration of Pb (II) (mg/L)	% Removal of Pb (II) at varying concentrations of Cd (II) as competing ions		
	Cd=0mg/L (single)	Cd=10mg/L	Cd=30mg/L
10	98.94401	98.6934	96.485
20	98.70379	98.3294	96.0113
30	98.55560667	98.0974	95.79
40	98.42983025	97.771	95.179
50	98.11628	97.241	94.5831
60	97.9873	96.6032	94.1358
70	97.431	96.1824	92.8624

Appendix XVII: Effect of initial metal ion concentration on the removal of Cd (II) ions from Pb-Cd binary ion solution using raw diatomite at different concentrations of Pb (II) as the competing ions.

Initial concentration of Cd (II) (mg/L)	% Removal of Cd (II) at varying concentrations of Pb (II) as competing ions		
	Pb=0mg/L (single)	Pb=10mg/L	Pb=30mg/L
10	90.816	88.52	82.151
20	85.606	80.031	70.692
30	81.597	76.729	64.018
40	78.261	71.2316	50.597
50	75.212	67.942	47.25
60	64.984	58.378	39.67
70	57.354	50.5017	34.94

Appendix XVIII: Effect of contact time on the competitive removal of Pb (II) and Cd (II) ions from Pb-Cd binary ion solutions using raw diatomite.

Contact Time (min)	% Removal	
	Pb (II)	Cd (II)
0	0	0
20	93.9632	62.007
40	95.9192	78.7933
60	98.6934	87.0225
80	98.6934	88.52
100	98.6934	88.519
120	98.6934	88.52

Appendix XIX: Effect of adsorbent dosage on the competitive removal of Pb (II) and Cd (II) ions from Pb-Cd binary ion solution using raw diatomite.

Adsorbent dosage (g/L)	% Removal	
	Pb (II)	Cd (II)
0.4	93.88	69.52
1	97.133333	76.3264
2	98.6934	88.5201
4	99.8997	96.2022
6	99.998	97.66667
8	100	99.8969
10	100	100

Appendix XX: Effect of temperature on the competitive removal of Pb (II) and Cd (II) ions from Pb-Cd binary ion solution using raw diatomite.

Temperature (K)	% Removal	
	Pb (II)	Cd (II)
298	98.6934	88.52
308	98.499	89.595
318	98.113	90.2146
328	97.758	90.2627
338	97.5767	90.70101

Appendix XXI: Equilibrium data for Pb (II) ions adsorption using raw diatomite and MnO2-diatomite composite.

Raw diatomite								
			Langmuir		Freundlich		Temkin	
Co	Ce	Qe	Ce	Ce/Qe	Log Ce	Log Qe	InCe	Qe
10	0.079	4.9605	0.079	0.015925814	-1.102372909	0.695525454	-2.5383074	4.9605
20	0.18612	9.90694	0.18612	0.01878683	-0.730206956	0.995939533	-1.6813637	9.90694
30	0.29343	14.8533	0.29343	0.019755226	-0.532495486	1.171822514	-1.2261162	14.853285
40	0.52167	19.7392	0.52167	0.026428067	-0.282605803	1.295328799	-0.6507239	19.739166
50	0.7089	24.6456	0.7089	0.028763813	-0.149415024	1.391738514	-0.3440408	24.64555
60	0.92802	29.536	0.92802	0.031419973	-0.032442664	1.470351532	-0.074702	29.53599
70	1.4721	34.264	1.4721	0.042963523	0.167937313	1.534837428	0.38668995	34.26395
MnO_2-diatomite composite								
			Langmuir		Freundlich		Temkin	
Co	Ce	Qe	Ce	Ce/Qe	log Ce	Log Qe	InCe	Qe
10	0.6799	4.66005	0.6799	0.145899722	-0.167554959	0.668390576	-0.3858096	4.66005
20	1.6987	9.15065	1.6987	0.185637086	0.230116687	0.961451944	0.52986325	9.15065
30	3.237	13.3815	3.237	0.241901132	0.510142699	1.126504798	1.17464697	13.3815
40	6.4381	16.781	6.4381	0.383655276	0.808757718	1.224816543	1.86223347	16.78095
50	9.6017	20.1992	9.6017	0.475351686	0.982348133	1.305333094	2.26194017	20.19915
60	12.9683	23.5159	12.9683	0.551470604	1.112883049	1.371360681	2.56250792	23.51585
70	18.6846	25.6577	18.6846	0.728225835	1.271483805	1.409217723	2.92769966	25.6577

Appendix XXII: Equilibrium data for Cd (II) ions adsorption using raw diatomite and MnO_2-diatomite composite.

Raw diatomite								
			Langmuir		Freundlich		Temkin	
Co	Ce	Qe	ce	Ce/Qe	logCe	logQe	InCe	Qe
10	0.9184	4.5408	0.9184	0.202255109	-0.036968125	0.657132374	-0.0851223	4.5408
20	2.8788	8.5606	2.8788	0.33628484	0.459211494	0.932504205	1.05737354	8.5606
30	5.5209	12.23955	5.5209	0.451070505	0.742009881	1.087765451	1.70854089	12.23955
40	8.6956	15.6522	8.6956	0.555551296	0.939299554	1.194575389	2.16281715	15.6522
50	12.394	18.803	12.394	0.659150136	1.093211492	1.274227146	2.51721248	18.803
60	21.0096	19.4952	21.0096	1.07768066	1.322417784	1.289927695	3.04497948	19.4952
70	29.8522	20.0739	29.8522	1.48711511	1.474976343	1.302631756	3.39625854	20.0739
MnO_2-diatomite composite								
			Langmuir		Freundlich		Temkin	
Co	Ce	Qe	Ce	Ce/Qe	logCe	logQe	InCe	Qe
10	1.6547	4.17265	1.6547	0.396558542	0.218719267	0.620411958	0.50361972	4.17265
20	6.868	6.566	6.868	1.045994517	0.836830286	0.817300878	1.92687294	6.566
30	12.016	8.992	12.016	1.336298932	1.07975992	0.953856298	2.4862391	8.992
40	18.236	10.882	18.236	1.675794891	1.260929584	1.036708722	2.90339766	10.882
50	28.805	10.5975	28.805	2.71809389	1.45946788	1.025203425	3.36054898	10.5975
60	37.96	11.02	37.96	3.444646098	1.579326204	1.042181595	3.63653297	11.02
70	45.235	12.3825	45.235	3.653139511	1.655474595	1.092808337	3.81187112	12.3825

Appendix XXIII: Adsorption isotherms for Pb (II) ions adsorption using raw diatomite and MnO_2-diatomite composite

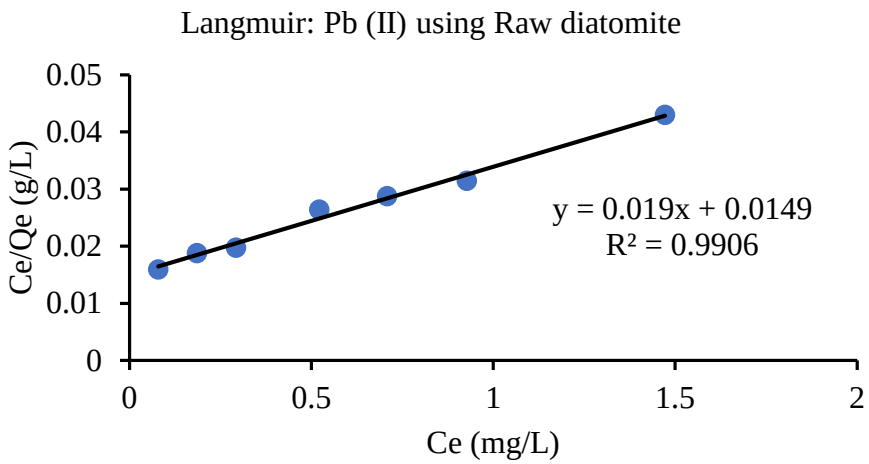

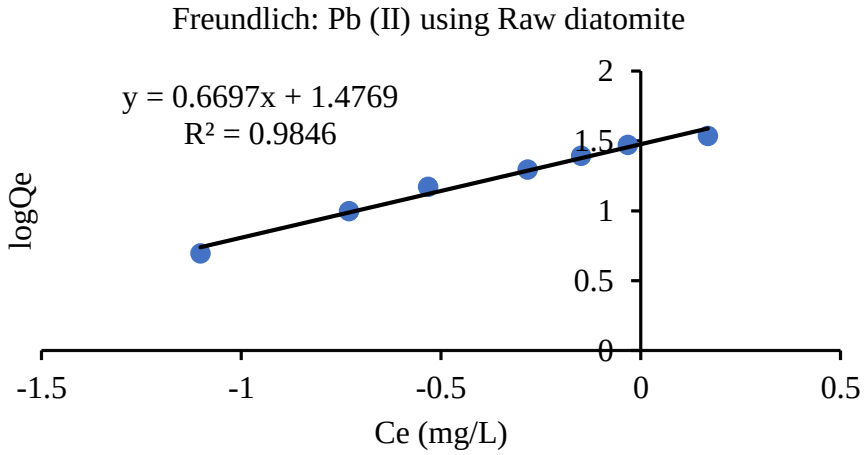

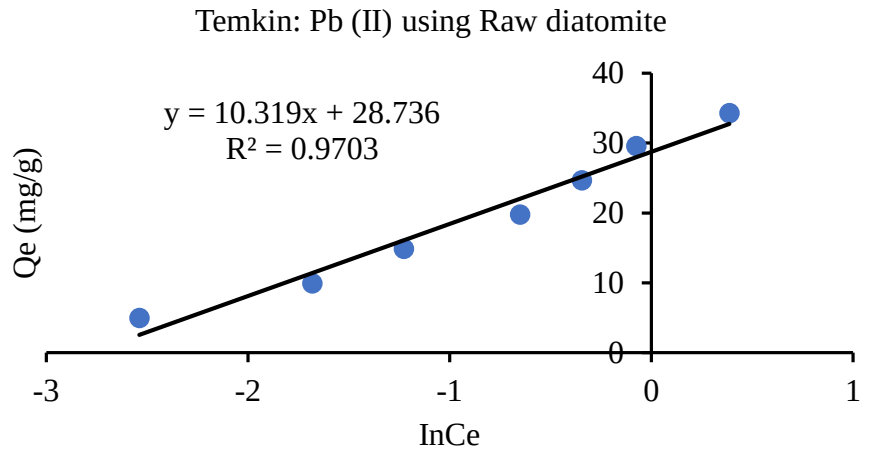

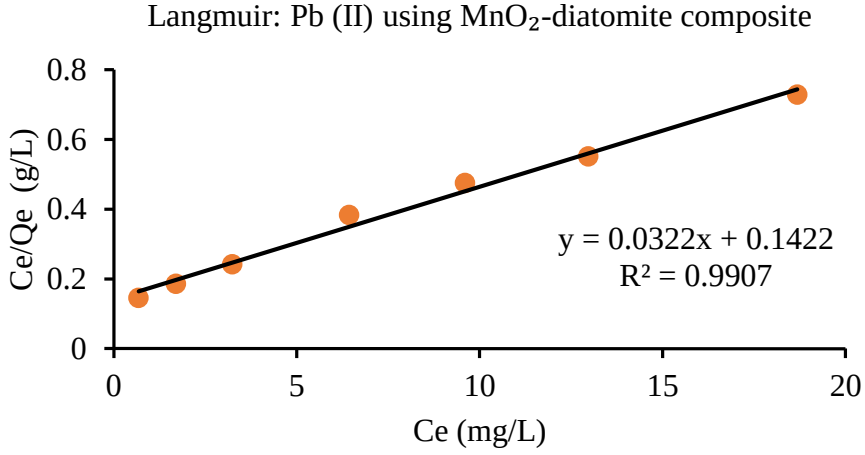

Freundlich: Pb (II) using MnO_2-diatomite composite

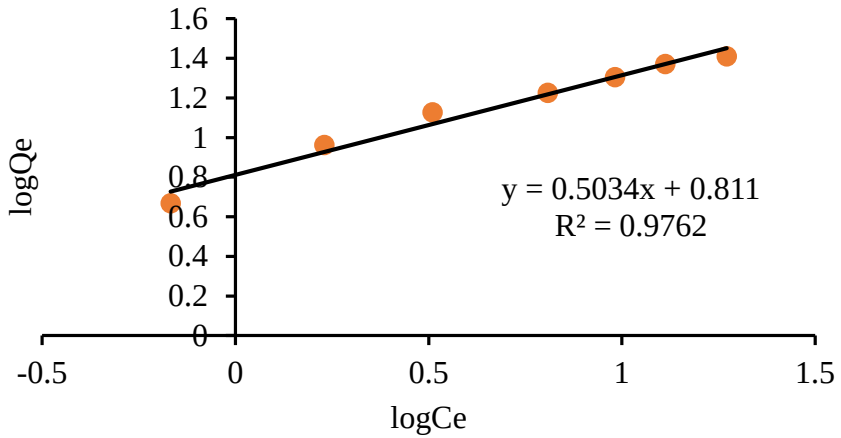

Temkin: Pb (II) using MnO_2-diatomite composite

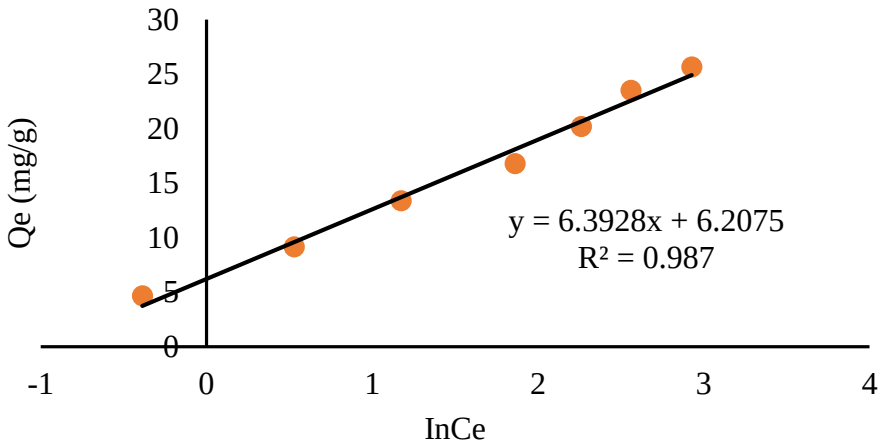

Appendix XXIV: Adsorption isotherms for Cd (II) ions adsorption using raw diatomite and MnO2-diatomite composite.

Langmuir: Cd (II) using Raw diatomite

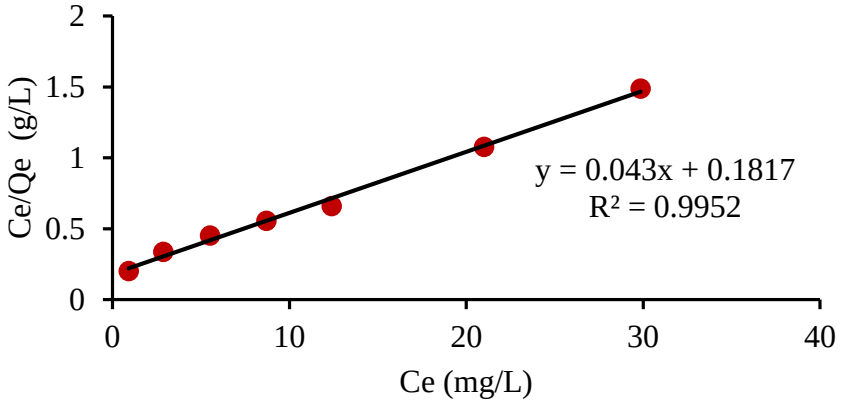

Freundlich: Cd (II) using Raw diatomite

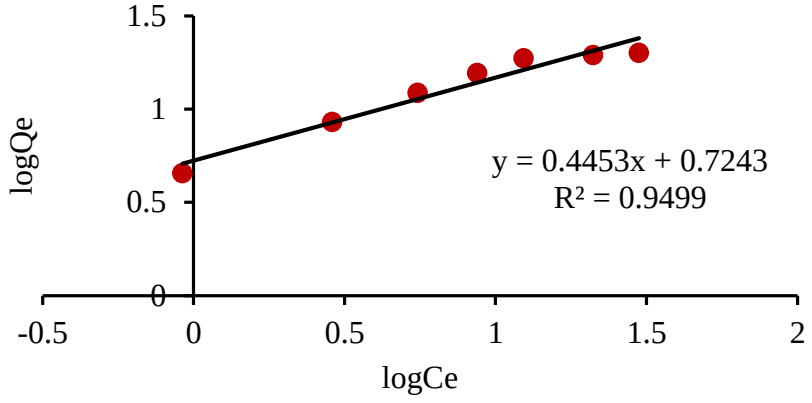

Temkin: Cd (II) using Raw diatomite

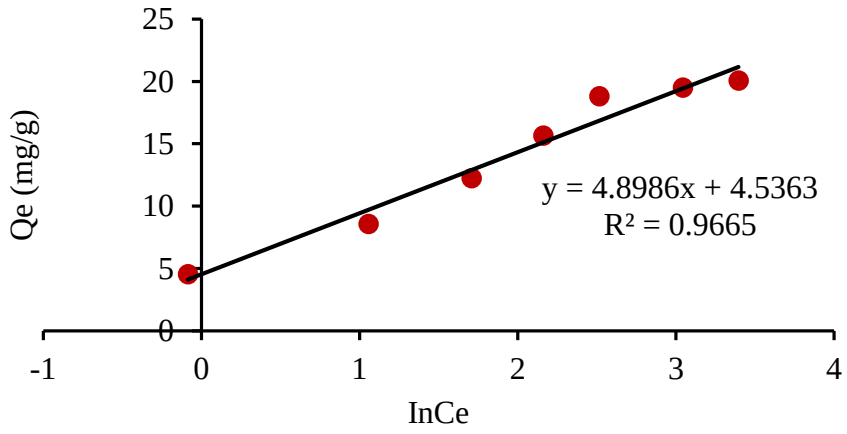

Langmuir: Cd (II) using MnO_2-diatomite composite

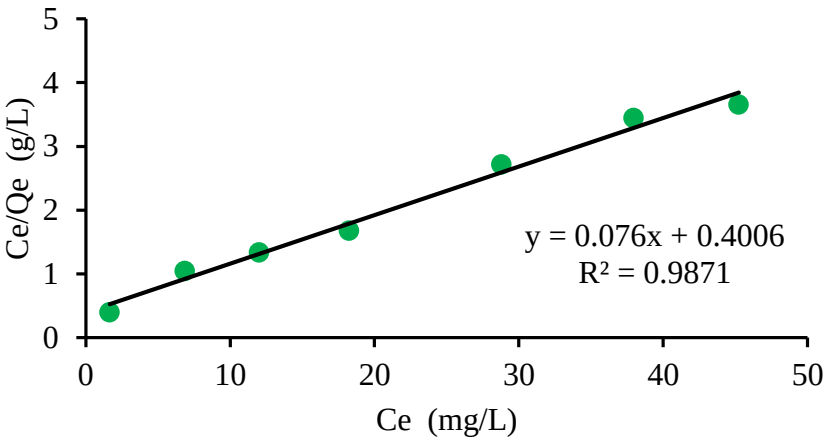

Freundlich: Cd (II) using MnO_2-diatomite composite

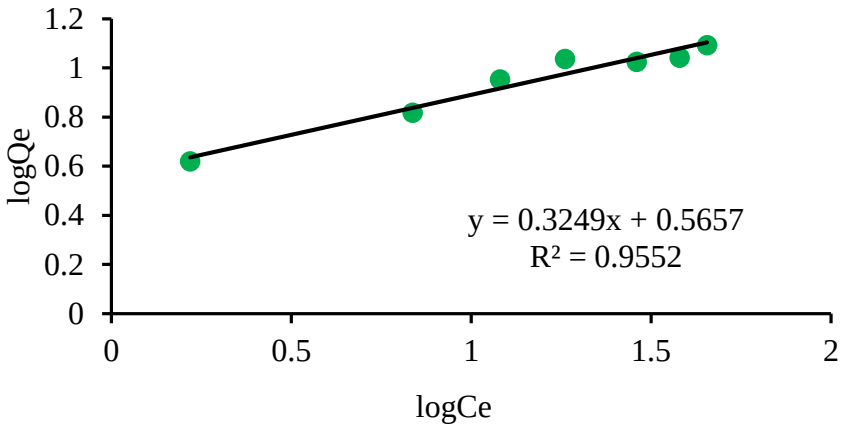

Temkin: Cd (II) using MnO_2-diatomite composite

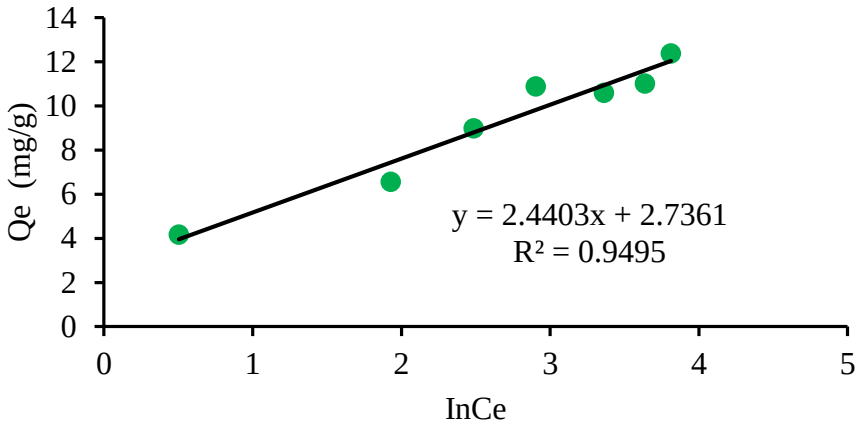

Appendix XXV: Kinetics data for Pb (II) ions adsorption using raw diatomite and MnO_2-diatomite composite

Raw diatomite									
Contact Time (minutes)						Pseudo-first order		Pseudo-second order	
	Co	Ce	qt	qe	In(qe-qt)	t	In(qe-qt)	t	t/qt
20	10	0.4076	4.7962	4.9605	-1.80606125	20	-1.80606125	20	4.16996789
40	10	0.2412	4.8794	4.9605	-2.51207232	40	-2.51207232	40	8.19772923
60	10	0.079	4.9605	4.9605	Error	60	Error	60	12.0955549
80	10	0.079	4.9605	4.9605	Error	80	Error	80	16.1274065
100	10	0.07901	4.960497	4.9605	-12.7168983	100	-12.7168983	100	20.1592703
120	10	0.07901	4.960497	4.9605	-12.5627476	120	-12.5627476	120	24.1911268
140	10	0.079	4.9605	4.9605	Error	140	Error	140	28.2229614
MnO_2-diatomite composite									
Contact Time (minutes)						Pseudo-first order		Pseudo-second order	
	Co	Ce	qt	qe	In(qe-qt)	t	In(qe-qt)	t	t/qt
20	10	1.9722	4.0139	4.9212	-0.09728212	20	-0.09728212	20	4.98268517
40	10	1.0947	4.45265	4.9212	-0.75811246	40	-0.75811246	40	8.98341437
60	10	0.1576	4.9212	4.9212	Error	60	Error	60	12.1921483
80	10	0.1576	4.9212	4.9212	Error	80	Error	80	16.2561977
100	10	0.15762	4.92119	4.9212	-11.5129255	100	-11.5129255	100	20.3202884
120	10	0.1576	4.9212	4.9212	Error	120	Error	120	24.3842965
140	10	0.15761	4.921195	4.9212	-12.2060726	140	-12.2060726	140	28.4483748

Appendix XXVI: Kinetics data for Cd (II) ions adsorption using raw diatomite and MnO_2-diatomite composite

Raw diatomite									
Contact Time (minutes)						Pseudo-first order		Pseudo-second order	
	Co	Ce	Qt	qe	In(qe-qt)	t	In(qe-qt)	t	t/qt
20	10	2.9018	3.5491	4.54635	-0.00275379	20	-0.00275379	20	5.63523147
40	10	1.70467	4.147665	4.54635	-0.91958365	40	-0.91958365	40	9.64398041
60	10	0.9182	4.5409	4.54635	-5.21213967	60	-5.21213967	60	13.2132397
80	10	0.9073	4.54635	4.54635	Error	80	Error	80	17.5965335
100	10	0.9095	4.54525	4.54635	-6.8124451	100	-6.8124451	100	22.00099
120	10	0.908	4.546	4.54635	-7.9575774	120	-7.9575774	120	26.3968324
140	10	0.9082	4.5459	4.54635	-7.70626298	140	-7.70626298	140	30.7969819
MnO_2-diatomite composite									
Contact Time (minutes)						Pseudo-first order		Pseudo-second order	
	Co	Ce	Qt	qe	In(qe-qt)	t	In(qe-qt)	t	t/qt
20	10	3.0167	3.49165	4.2249	-0.31026857	20	-0.31026857	20	5.72795097
40	10	1.85	4.075	4.2249	-1.89778687	40	-1.89778687	40	9.81595092
60	10	1.6033	4.19835	4.2249	-3.62872553	60	-3.62872553	60	14.2913287
80	10	1.5502	4.2249	4.2249	Error	80	Error	80	18.9353594
100	10	1.5502	4.2249	4.2249	Error	100	Error	100	23.6691993
120	10	1.55021	4.224895	4.2249	-12.2060726	120	-12.2060726	120	28.4030727
140	10	1.55022	4.22489	4.2249	-11.5129255	140	-11.5129255	140	33.1369574

Appendix XXVII: Pseudo-first and second order kinetic models for Pb (II) ions using raw diatomite and MnO_2-diatomite composite

Pseudo-first order: Pb (II) using raw diatomite

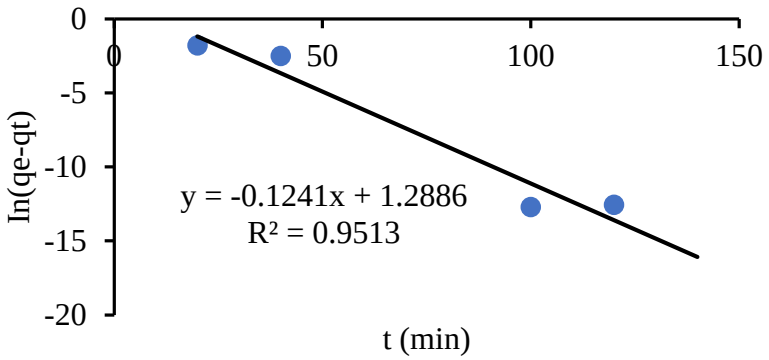

Pseudo-secon order: Pb (II) using raw diatomite

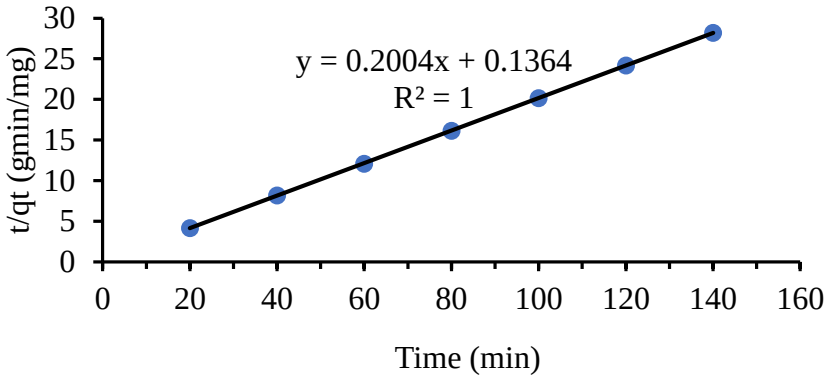

Pseudo-first order: Pb (II) using MnO_2-Diatomite composite

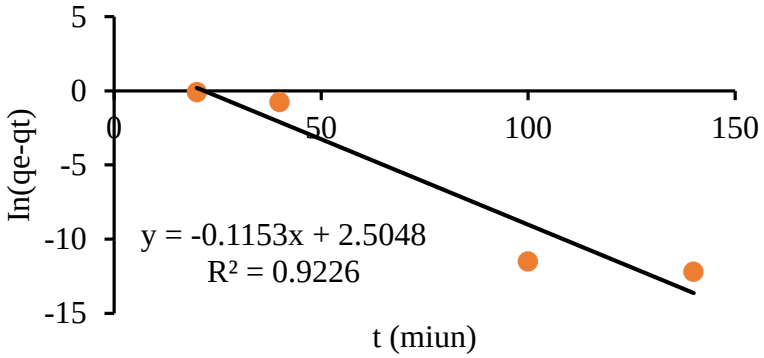

Pseudo-second order: Pb (II) using MnO_2-Diatomite composite

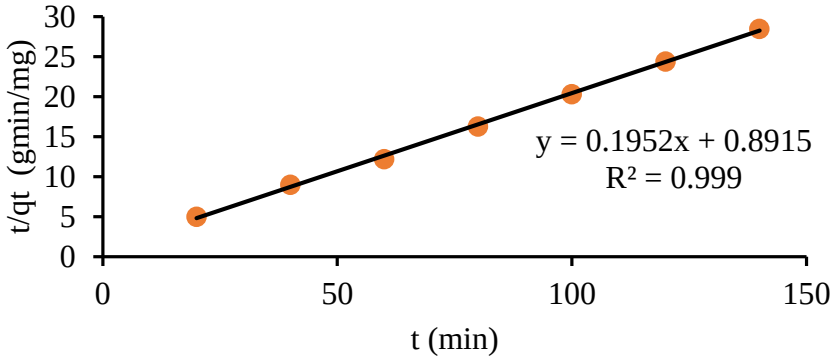

Appendix XXVIII: Pseudo-first and second order kinetic models for Cd (II) ions using raw diatomite and MnO_2-diatomite composite

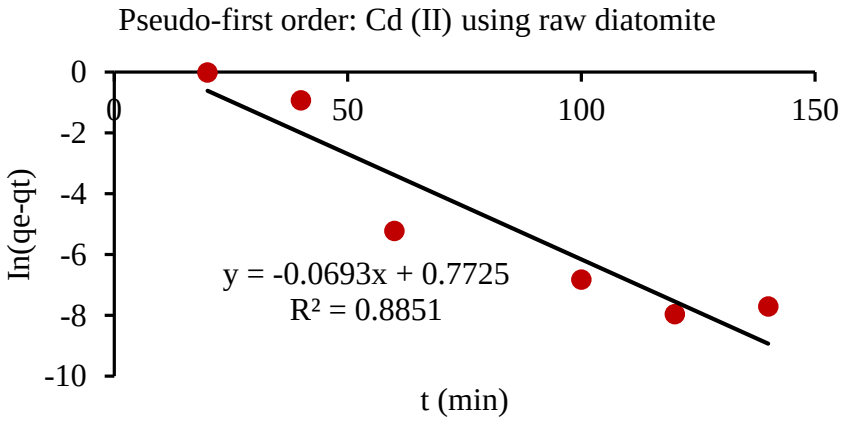

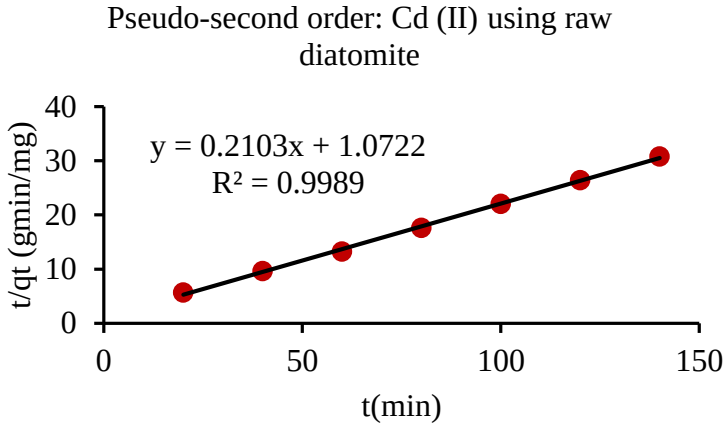

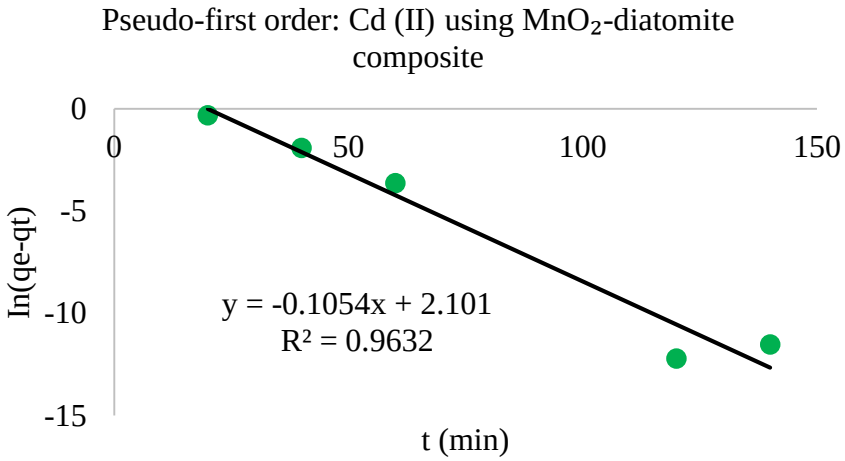

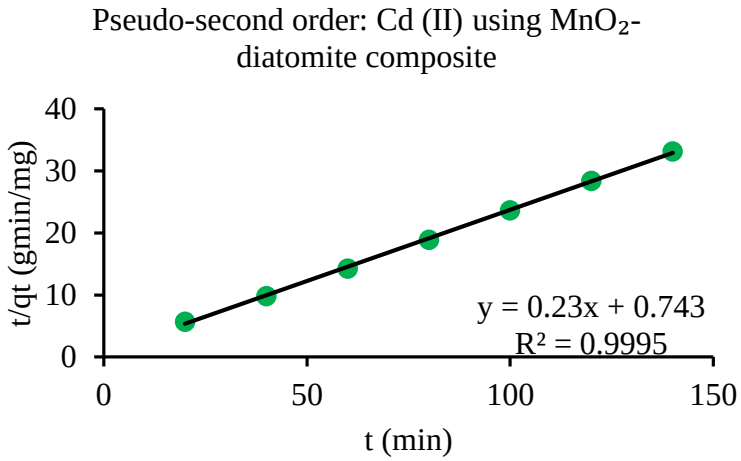

Appendix XXIX: Thermodynamic data for Pb (II) ions adsorption using raw diatomite and MnO2-diatomite composite.

Raw diatomite										
Temp (K)	Co	Ce	Cad	Kc=Cad/Ce	lnKc	1/T	lnKc	ΔG (kJ/mol)	ΔH (kJ/mol)	ΔS (J/mol/K)
298	10	0.079	9.921	125.5822785	4.832961149	0.0033557	4.83296115	-11.974	-8.4071168	11.9505436
308	10	0.09054	9.90946	109.4484206	4.695453393	0.00324675	4.69545339	-12.0237	-8.4071168	11.9505436
318	10	0.09794	9.90206	101.1043711	4.61615336	0.00314465	4.61615336	-12.2044	-8.4071168	11.9505436
328	10	0.10019	9.89981	98.81036032	4.593202461	0.00304878	4.59320246	-12.5256	-8.4071168	11.9505436
338	10	0.12366	9.87634	79.86754704	4.380369601	0.00295858	4.3803696	-12.3094	-8.4071168	11.9505436
MnO_2-diatomite composite										
Temp (°K)	Co	Ce	Cad	Kc=Cad,eq/Ce	lnKc	1/T	lnKc	ΔG (kJ/mol)	ΔH (kJ/mol)	ΔS (J/mol/K)
298	10	0.1638	9.8362	60.05006105	4.095178565	0.0033557	4.09517857	-10.1461	-45.9398384	-120.09573
308	10	0.29774	9.70226	32.58635051	3.483893505	0.00324675	3.4838935	-8.92125	-45.9398384	-120.09573
318	10	0.5273	9.4727	17.96453632	2.88839961	0.00314465	2.88839961	-7.6365	-45.9398384	-120.09573
328	10	0.73786	9.26214	12.55270648	2.529936298	0.00304878	2.5299363	-6.89912	-45.9398384	-120.09573
338	10	1.3846	8.6154	6.22230247	1.82814001	0.00295858	1.82814001	-5.13731	-45.9398384	-120.09573

Appendix XXX: Thermodynamic data for Cd (II) ions adsorption using raw diatomite and MnO_2-diatomite composite

Raw diatomite										
Temp (K)	Co	Ce	Cad	Kc=Cad/Ce	lnKc	1/T	lnKc1	ΔG (kJ/mol)	ΔH (kJ/mol)	ΔS (J/mol/K)
298	10	0.9073	9.0927	10.02171277	2.304754017	0.0033557	2.30475402	-5.71019	86.432344	304.259144
308	10	0.7364	9.2636	12.57957632	2.532074572	0.00324675	2.53207457	-6.48391	86.432344	304.259144
318	10	0.402	9.598	23.87562189	3.172857934	0.00314465	3.17285793	-8.38857	86.432344	304.259144
328	10	0.0815	9.9185	121.6993865	4.801553959	0.00304878	4.80155396	-13.0938	86.432344	304.259144
338	10	0.0167	9.9833	597.8023952	6.393260257	0.00295858	6.39326026	-17.9659	86.432344	304.259144
MnO_2-diatomite composite										
Temp (K)	Co	Ce	Cad	Kc=Cad/Ce	lnKc	1/T	lnKc2	ΔG (kJ/mol)	ΔH (kJ/mol)	ΔS (J/mol/K)
298	10	1.5502	8.4498	5.450780544	1.695758818	0.0033557	1.69575882	-4.20136	33.372396	124.75157
308	10	1.375	8.625	6.272727273	1.836211232	0.00324675	1.83621123	-4.70201	33.372396	124.75157
318	10	0.8753	9.1247	10.4246544	2.344173616	0.00314465	2.34417362	-6.19765	33.372396	124.75157
328	10	0.7242	9.2758	12.80834024	2.55009654	0.00304878	2.55009654	-6.95409	33.372396	124.75157
338	10	0.3392	9.6608	28.48113208	3.349241836	0.00295858	3.34924184	-9.41181	33.372396	124.75157

Appendix XXXI: Van't Hoff plots for Pb (II) and Cd (II) ions adsorption using raw diatomite and MnO_2-diatomite composite

Van't Hoff plot for adsorption of Pb (II) onto raw diatomite

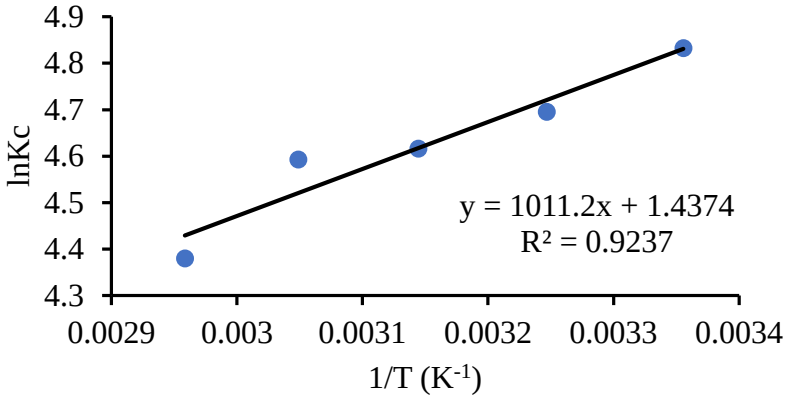

Van't Hoff plot for adsorption of Pb (II) onto MnO_2-diatomite composite

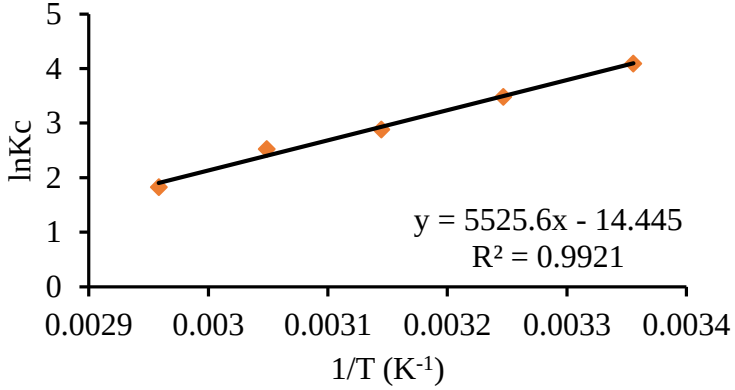

Van't Hoff plot for adsorption of Cd (II) onto raw diatomite

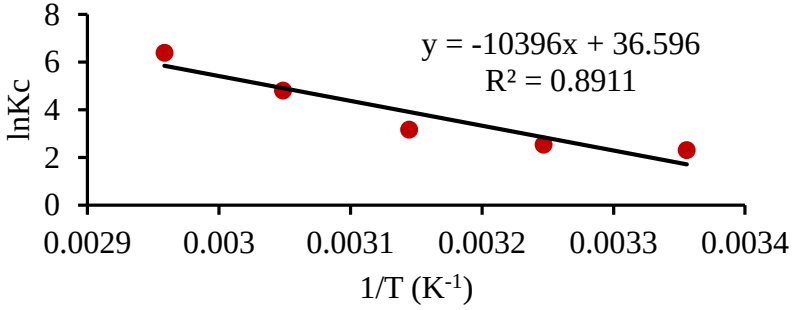

Van't Hoff plot for adsorption of Cd (II) onto MnO_2-diatomite composite

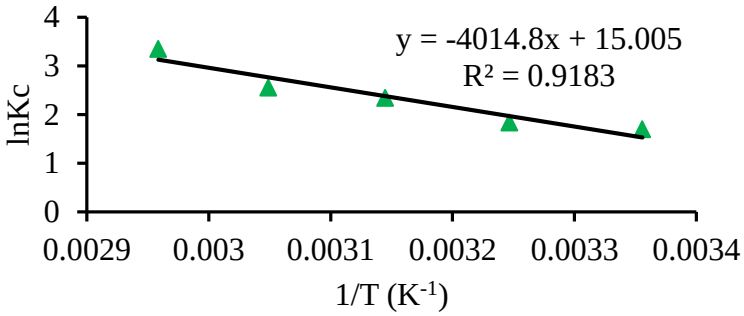

Appendix XXXII: Kinetics data for the competitive adsorption of Pb (II) and Cd (II) ions from Pb-Cd binary ion solution using raw diatomite.

Pb (II)									
						Pseudo-first order		Pseudo-second order	
Contact Time (min)	Co	Ce	qt	qe	In(qe-qt)	t	In(qe-qt)	t	t/qt
20	10	0.60368	4.69816	4.93467	-1.441764789	20	-1.4417648	20	4.256986
40	10	0.40808	4.79596	4.93467	-1.975369856	40	-1.9753699	40	8.340353
60	10	0.13066	4.93467	4.93467	Error	60	Error	60	12.15887
80	10	0.13066	4.93467	4.93467	Error	80	Error	80	16.21182
100	10	0.13066	4.934669	4.93467	-13.81551056	100	-13.815511	100	20.26478
120	10	0.13066	4.93467	4.93467	-14.50865774	120	-14.508658	120	24.31774
Cd (II)									
						Pseudo-first order		Pseudo-second order	
Contact Time (min)	Co	Ce	qt	qe	In(qe-qt)	t	In(qe-qt)	t	t/qt
20	10	3.7993	3.10035	4.426	0.281902905	20	0.281902905	20	6.45088458
40	10	2.12067	3.939665	4.426	-0.72085759	40	-0.72085759	40	10.1531475
60	10	1.29775	4.351125	4.426	-2.59193522	60	-2.59193522	60	13.7895372
80	10	1.148	4.426	4.426	Error	80	Error	80	18.0750113
100	10	1.1481	4.42595	4.426	-9.90348755	100	-9.90348755	100	22.5940194
120	10	1.148	4.426	4.426	Error	120	Error	120	27.1125169

Appendix XXXIII: Pseudo-first and Second order kinetics models for the competitive adsorption of Pb (II) and Cd (II) ions from Pb-Cd binary ion solution using raw diatomite.

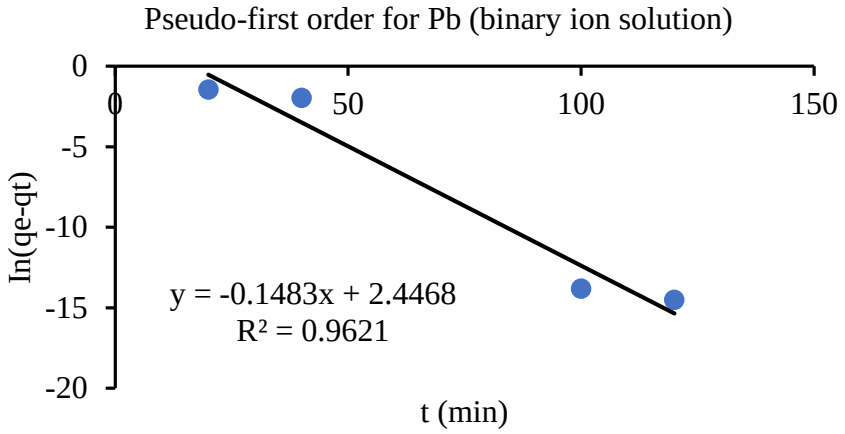

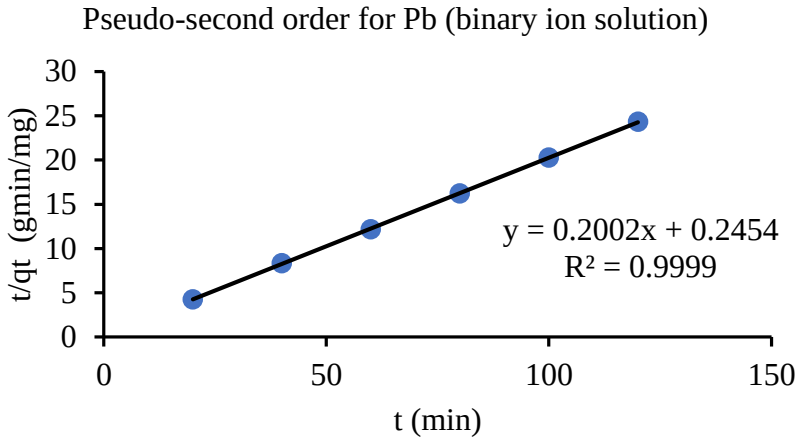

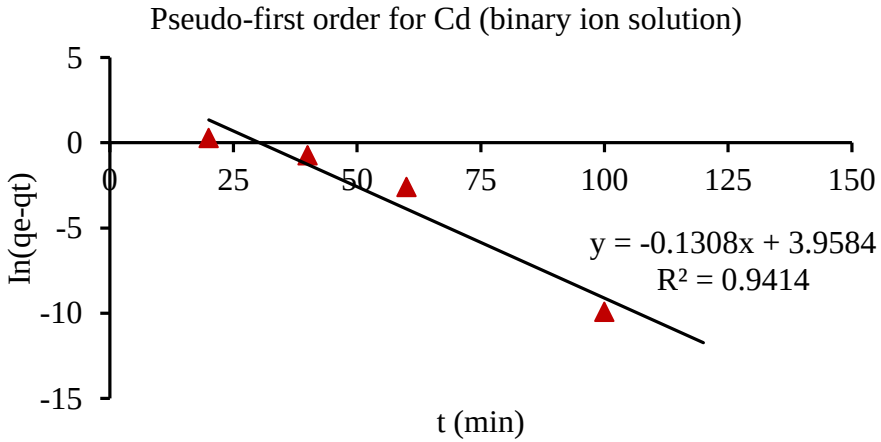

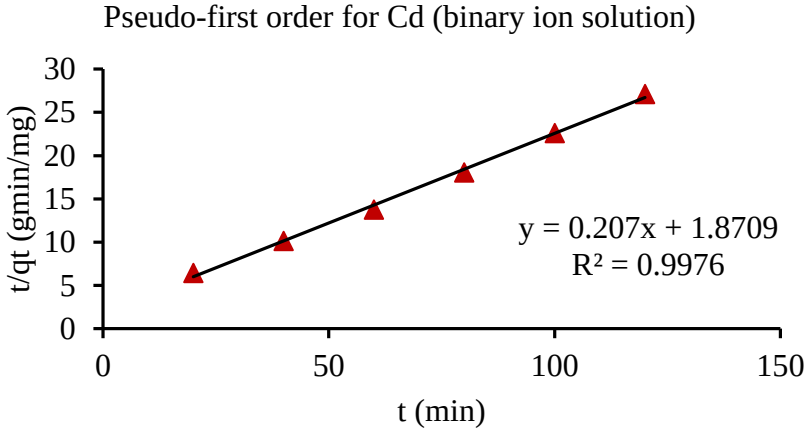

Appendix XXXIV: Thermodynamics data for the competitive adsorption of Pb (II) and Cd (II) ions from Pb-Cd binary ion solution using raw diatomite.

Pb (II)										
Temp (K)	Co	Ce	Cad	Kc=Cad/Ce	lnKc	1/T	lnKc	ΔG (kJ/mol)	ΔH (kJ/mol)	ΔS (J/mol/K)
298	10	0.13066	9.86934	75.53451707	4.324589731	0.0033557	4.32458973	-10.7145	-13.9932934	-10.952032
308	10	0.1501	9.8499	65.62225183	4.183914843	0.00324675	4.18391484	-10.7138	-13.9932934	-10.952032
318	10	0.1887	9.8113	51.99417064	3.951131609	0.00314465	3.95113161	-10.4462	-13.9932934	-10.952032
328	10	0.2242	9.7758	43.60303301	3.775126712	0.00304878	3.77512671	-10.2947	-13.9932934	-10.952032
338	10	0.24233	9.75767	40.26604217	3.695508488	0.00295858	3.69550849	-10.3849	-13.9932934	-10.952032
Cd (II)										
Temp (K)	Co	Ce	Cad	Kc=Cad/Ce	lnKc	1/T	lnKc1	ΔG (kJ/mol)	ΔH (kJ/mol)	ΔS (J/mol/K)
298	10	1.148	8.852	7.710801394	2.042622124	0.0033557	2.04262212	-5.06074	4.59922166	32.6515722
308	10	1.0405	8.9595	8.610764056	2.153013055	0.00324675	2.15301306	-5.51325	4.59922166	32.6515722
318	10	0.97854	9.02146	9.219306313	2.221299798	0.00314465	2.2212998	-5.87279	4.59922166	32.6515722
328	10	0.97373	9.02627	9.269787313	2.226760436	0.00304878	2.22676044	-6.07236	4.59922166	32.6515722
338	10	0.9299	9.0701	9.753856064	2.277662701	0.00295858	2.2776627	-6.40053	4.59922166	32.6515722

Appendix XXXV: Van't Hoff plots for the competitive adsorption of Pb (II) and Cd (II) ions from Pb-Cd binary ion solution using raw diatomite.

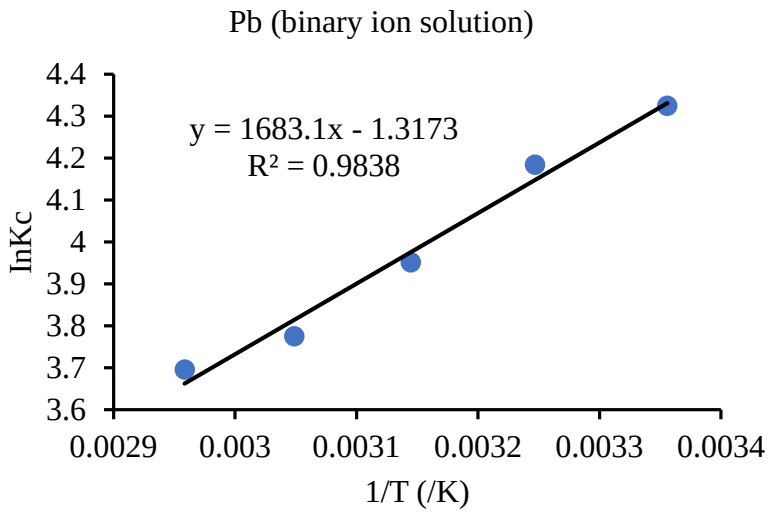

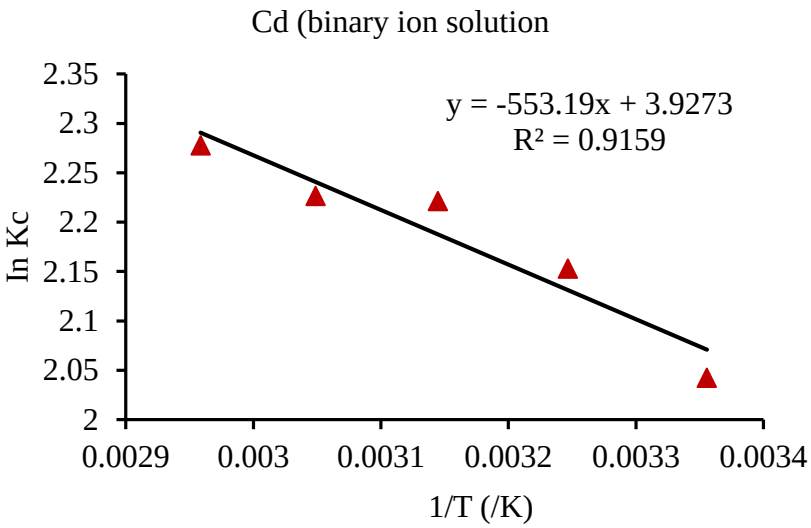

Appendix XXXVI: Chuka University Ethics Review Letter

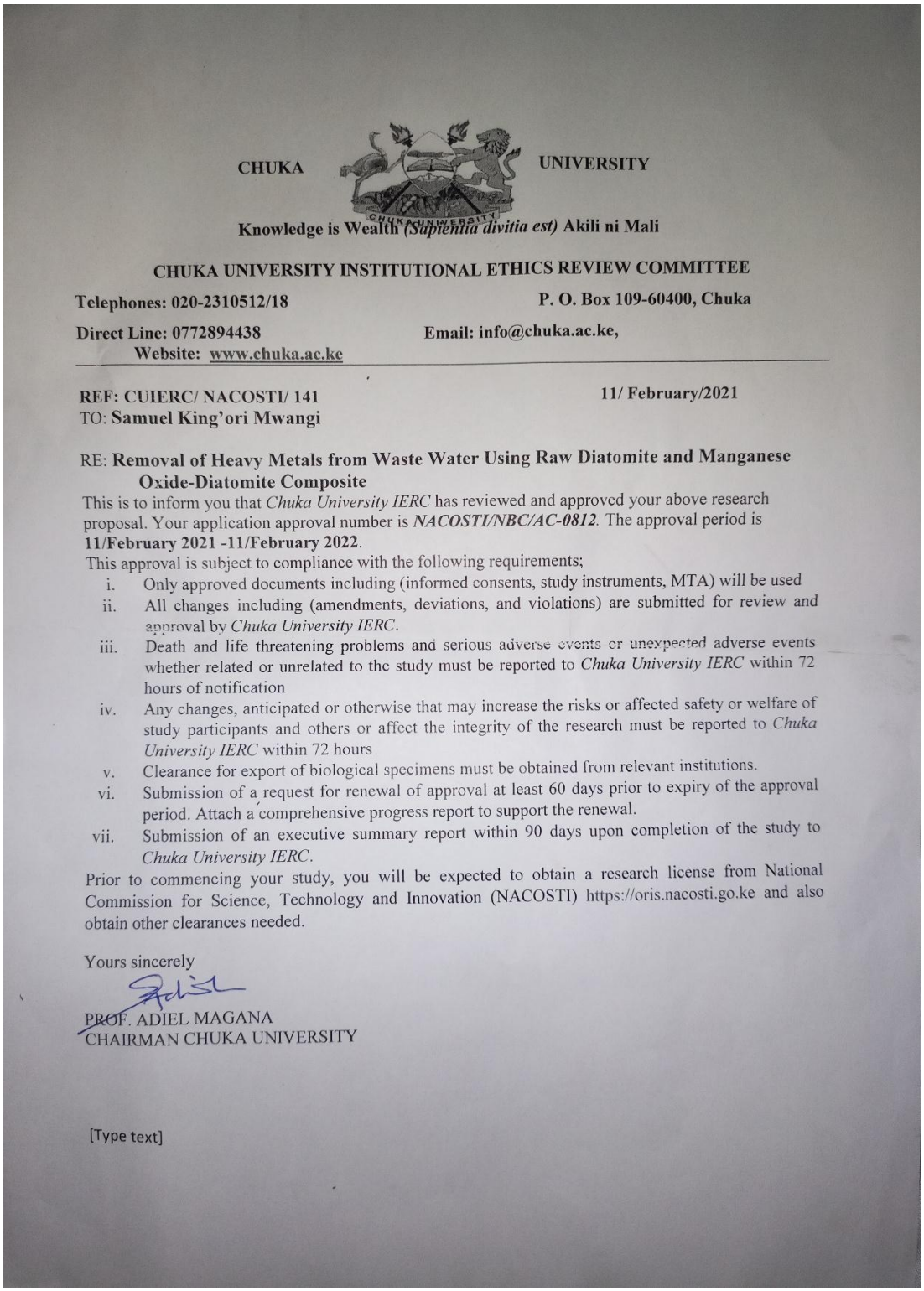

CHUKA UNIVERSITY

Knowledge is Wealth *(Sapientia divitia est)* Akili ni Mali

CHUKA UNIVERSITY INSTITUTIONAL ETHICS REVIEW COMMITTEE

Telephones: 020-2310512/18 **P. O. Box 109-60400, Chuka**

Direct Line: 0772894438 **Email: info@chuka.ac.ke,**

Website: www.chuka.ac.ke

REF: CUIERC/ NACOSTI/ 141 **11/ February/2021**

TO: **Samuel King'ori Mwangi**

RE: **Removal of Heavy Metals from Waste Water Using Raw Diatomite and Manganese Oxide-Diatomite Composite**

This is to inform you that *Chuka University IERC* has reviewed and approved your above research proposal. Your application approval number is ***NACOSTI/NBC/AC-0812***. The approval period is **11/February 2021 -11/February 2022**.

This approval is subject to compliance with the following requirements;

i. Only approved documents including (informed consents, study instruments, MTA) will be used
ii. All changes including (amendments, deviations, and violations) are submitted for review and approval by *Chuka University IERC*.
iii. Death and life threatening problems and serious adverse events or unexpected adverse events whether related or unrelated to the study must be reported to *Chuka University IERC* within 72 hours of notification
iv. Any changes, anticipated or otherwise that may increase the risks or affected safety or welfare of study participants and others or affect the integrity of the research must be reported to *Chuka University IERC* within 72 hours
v. Clearance for export of biological specimens must be obtained from relevant institutions.
vi. Submission of a request for renewal of approval at least 60 days prior to expiry of the approval period. Attach a comprehensive progress report to support the renewal.
vii. Submission of an executive summary report within 90 days upon completion of the study to *Chuka University IERC*.

Prior to commencing your study, you will be expected to obtain a research license from National Commission for Science, Technology and Innovation (NACOSTI) https://oris.nacosti.go.ke and also obtain other clearances needed.

Yours sincerely

PROF. ADIEL MAGANA
CHAIRMAN CHUKA UNIVERSITY

[Type text]

Appendix XXXVII: Research permit from the National Commission for Science Technology and Innovation (NARCOSTI).

REPUBLIC OF KENYA

NACOSTI

NATIONAL COMMISSION FOR SCIENCE,TECHNOLOGY & INNOVATION

Ref No: **641089**

Date of Issue: **19/March/2021**

RESEARCH LICENSE

This is to Certify that Mr.. SAMUEL KING'ORI MWANGI of Chuka University, has been licensed to conduct research in Tharaka-Nithi on the topic: Removal of heavy metals from wastewater using raw diatomite and manganese oxide-diatomite composite for the period ending : 19/March/2022.

License No: **NACOSTI/P/21/9646**

641089

Applicant Identification Number

Director General
NATIONAL COMMISSION FOR SCIENCE,TECHNOLOGY & INNOVATION

Verification QR Code

NOTE: This is a computer generated License. To verify the authenticity of this document, Scan the QR Code using QR scanner application.